

Copyright
by
Mark Allan Rainey
2004

**The Dissertation Committee for Mark Allan Rainey
certifies that this is the approved version of the following dissertation:**

**A Structure/Function Analysis of Macromolecular Recognition by the
Protein Kinase ERK2**

Committee:

Kevin Dalby, Supervisor

Hung-wen Liu

Andy Ellington

John Tesmer

Brent Iverson

**A Structure/Function Analysis of Macromolecular Recognition by the
Protein Kinase ERK2**

by

Mark Allan Rainey, B.S.

Dissertation

Presented to the Faculty of the Graduate School of

The University of Texas at Austin

in Partial Fulfillment

of the Requirements

for the Degree of

Doctor of Philosophy

The University of Texas at Austin

December, 2004

Dedication

To Mom and Dad

Acknowledgements

I would like to acknowledge Dr. Kevin Dalby for his help and support, Dr. Su Dharmawardhane for advice and support, and my committee members Dr. Andy Ellington, Dr. John Tesmer, Dr. Hung-wen Liu, and Dr. Brent Iverson for their discussions and review of this dissertation. I would also like to acknowledge the members of the Dalby laboratory for their support.

September 2004

A Structure/Function Analysis of Macromolecular Recognition by the Protein Kinase ERK2

Publication No. _____

Mark Allan Rainey, Ph.D.

The University of Texas at Austin, 2004

Supervisor: Kevin N. Dalby

Mitogen-activate protein kinases (MAPKs) phosphorylate protein substrates in the presence of magnesium and adenosine triphosphate in response to extracellular environmental signals to carry out signal-dependent intracellular responses. Extracellular signal-regulated protein kinase 2 (ERK2), a member of the MAPK family, mediates cellular growth, differentiation, and proliferation in response to growth factors. Understanding the mechanism by which MAPKs specifically recognize their protein substrates to carry out phosphoryl-transfer on specific residues within these macromolecules is critical for understanding the mechanism of signal transduction fidelity. Phage display was carried out against the active form of ERK2 to find novel ERK2-binding peptides. One peptide, KKKIRCIRGWTKDIRTLADSCQY, inhibited ERK2 phosphorylation of the protein substrate Ets Δ 138, exhibiting competitive and mixed inhibition towards Ets Δ 138 ($K_i = 20.7 \pm 5.5 \mu\text{M}$) and MgATP^{2-} , respectively.

Steady-state kinetics combined with a novel fluorescence anisotropy binding assay were used to quantitatively elucidate the roles of several proposed ERK2 exosites in forming a macromolecular docking complex with EtsΔ138 required for efficient phosphorylation. An ERK2–EtsΔ138 docking complex (K_d of $6.6 \pm 1.2 \mu\text{M}$) was shown to form independent of the substrate phospho-acceptor. Docking motif peptides proposed to bind ERK2 exosites could dissociate the ERK2–EtsΔ138 docking complex, however, dissociation did not occur using a peptide containing an ERK2 phospho-acceptor indicating the lack of active site interactions in the docking complex. Mutation of ERK2 residues Lys-229 and His-230 to p38 MAPK α -like residues, an enzyme that does not efficiently phosphorylate EtsΔ138, led to a 20-fold decrease in the specificity constant (k_{cat}/K_m) of EtsΔ138 phosphorylation largely due to its inability to bind EtsΔ138. This structure/function analysis offers a quantitative approach towards understanding the molecular determinants of protein substrate recognition by a protein kinase prior to phosphorylation.

Table of Contents

ABBREVIATIONS	XV
CHAPTER 1: MAPK SIGNALING	1
Signal Transduction Pathways	1
Specificity Determinants of Signal Transduction	2
Mitogen-Activated Protein Kinases	4
The Importance of Characterizing Protein-Protein Interactions	6
Elucidating Sites of MAPK Protein-Protein Interactions	7
Computational Studies to Determine Functional Differences Between Subfamilies	7
Genetic Studies Reveal Sites of Interest	9
Yeast 2-Hybrid Studies	10
Co-Crystallization of a Docking Motif Peptides and a MAPK	14
Hydrogen Exchange Mass Spectrometry	16
Footprinting.....	20
Quantifying and Characterizing Protein-Protein Interactions.....	22
Non-Quantitative Pull-Down Studies	22
Isothermal Titration Calorimetry	23
Surface Plasmon Resonance	24
Fluorescence anisotropy/polarization	25
The Function of MAPK Protein-Protein Interactions	27
Kinetic Studies of MAPK Catalysis	27
Enzymic MAPK Exosites	28
MAPK-Interacting Docking Motifs	32
The DEF Docking Motif.....	33
The DEJL Docking Motif	34
A MAPKAPK/RSK-Like Docking Motif.....	35
Docking Mediates Enzymatic Specificity	35
DEJL Motif Specificity	36
Regulation of MAPK Docking Interactions	36

Proline Binding Pocket	37
Substrate Phosphorylation	39
Highly Specific Enzymatic Interactions	40
MAPKK–MAPK Docking.....	40
MAPK–MKP Docking.....	41
Non-Enzymatic Protein-Protein Interactions with MAPKs.....	43
Conclusions.....	45
CHAPTER 2: PHAGE DISPLAY IDENTIFIES NOVEL PEPTIDES THAT BIND ERK2 AND COMPETE WITH TRANSCRIPTION FACTOR BINDING	48
OVERVIEW	48
Purpose.....	48
Approach.....	48
Results.....	50
Conclusions.....	50
INTRODUCTION	52
RESULTS AND DISCUSSION	55
Purification of Active ERK2.....	55
Biotinylation of ERK2	55
Immobilized b-ERK2 is Active	57
Biopanning Scheme for Selecting Phage that Bind b-ERK2.....	62
Titering Phage Stocks	64
Amplification of Phage Libraries.....	65
Round I: Non-Stringent Biopanning Conditions to Select Phage that Bind b- ERK2.....	65
Round II: Extending Wash Time to Select for Small k_{off} Rates	67
Round III: Decreased Receptor Concentration to Encourage Phage Competition	70
Individual Phage Preparation.....	71
Phage Attachment Assay	72
Round IV: Decreased Receptor	75

DTT Inhibits Cyclic Peptide Binding	77
EtsΔ138 Disrupts Phage Binding to b-ERK2	79
MgATP ²⁻ Inhibits Phage Binding	80
Purification of Cyclic Peptide 20a	81
Inhibition of ERK2 by Cyclic Peptide 20a	84
Inhibition is Not Specific to ERK2	88
CONCLUSIONS.....	89
EXPERIMENTAL PROCEDURES	90
Materials	90
Purification of ERK2	90
Purification of His ₆ - and GST-Tagged Proteins	92
Activation of p38 MAPKα	94
Biotinylation of ERK2	94
Kinetic Measurements of b-ERK2 in Solution	95
Kinetic Measurements of Immobilized b-ERK2	95
Large Scale Amplification and Purification of Phage	96
Biopanning Conditions	97
Small Scale Phage Amplification	97
Enzyme-Linked Immunosorbent Assay.....	98
Sequencing Single-Stranded Phage DNA.....	98
Synthesis and Purification of Peptide 20a	99
Oxidation of Peptide 20a	100
Peptide Inhibition.....	100
CHAPTER 3: A STEADY-STATE KINETIC ANALYSIS OF ERK2 EXOSITE MUTANTS AND DOCKING MOTIF MUTANTS OF ETSΔ138	102
PURPOSE	102
INTRODUCTION	103
RESULTS AND DISCUSSION	105
The Purification of Unphosphorylated ERK2.....	105

Purification of MAPKK1	107
Activation of ERK2 Using MAPKK1	108
Purification of Dual-Phosphate ERK2.....	109
Tryptic Peptide and Phosphoamino Acid Analysis of ERK2	111
Methodology Toward Understanding Exosites	114
The Common Docking (CD) and the Hydrophobic (YY) Exosites.....	115
The TT/ED Specificity-Determining Exosite	121
The Docking Groove of MAPKs	124
Specificity Determination Through Evolutionary Changes After Gene Duplication.....	127
Putative DEJL Motif on EtsΔ138	138
An EtsΔ138 Phenylalanine Docking Motif	143
CONCLUSIONS.....	146
EXPERIMENTAL PROCEDURES	152
Materials	152
Construction of Site-Specific ERK2 Mutants.....	152
Construction of Site-Specific EtsΔ138 Mutants	154
Purification of Unphosphorylated ERK2.....	156
Purification of MAPKK1G7b.....	158
EtsΔ138 Purification.....	159
Activation of ERK2 Using MAPKK1	159
Purification of Dual-Phosphate ERK2.....	161
Phosphoamino Acid Analysis.....	162
Kinetic Methods for EtsΔ138 Phosphorylation	164
ATPase Assays.....	164
SDS-PAGE Gel.....	166

EXPERIMENTAL DATA.....	167
CHAPTER 4: PHOSPHORYLATION DIFFERENTIALLY REGULATES MAPK PROTEIN-PROTEIN INTERACTIONS: A QUANTITATIVE ANALYSIS USING FLUORESCENCE ANISOTROPY	183
PURPOSE	183
INTRODUCTION	184
Fluorescence Anisotropy	186
RESULTS AND DISCUSSION	189
Choosing a Substrate Amenable to Fluorescent Labeling	189
Cysteine Mutagenesis	191
Labeling EtsΔ138 With Fluorescein	194
Fluorescence Anisotropy of EtsΔ138-F Increases When Bound to ERK2.....	197
Competition Assay	199
Docking Motif Peptides Compete For EtsΔ138 Exosites on ERK2	202
PEA-15 Can Distinguish Between Different Phosphorylation Forms of ERK2	207
CONCLUSIONS.....	209
EXPERIMENTAL PROCEDURES	213
DTNB Labeling	215
Preparation of EtsΔ138-Fluorescein (EtsΔ138-F)	216
Tryptic Digest of EtsΔ138-F	217
Preparation of ERK2.....	217
Calibrating the Polarizers: Measuring Glycogen/Ludox Scatter	218
Fluorescence Anisotropy Binding Assay.....	219
Competition Assay.....	220

EQUATION DERIVATION	222
EXPERIMENTAL DATA.....	227
CHAPTER 5: MACROMOLECULAR RECOGNITION OF A PROTEIN SUBSTRATE BY A PROTEIN KINASE	236
PURPOSE	236
INTRODUCTION	237
RESULTS AND DISCUSSION	243
Fluorescence Anisotropy Competition Assay.....	243
The His ₆ -Tag on EtsΔ138 Does Not Have a Large Affect on the Affinity for ERK2.....	244
EtsΔ138 Docking Motifs Mediate Macromolecular Substrate Recognition.....	248
The P+1 Proline Determinant Is Required For Efficient Catalysis	251
The P+1 Proline Determinant Is Not Required For the ERK2-EtsΔ138 Docking Complex and Macromolecular Recognition	258
Magnesium Chloride Decreases the Affinity of EtsΔ138 and ERK2	262
Macromolecular Substrate Recognition In the Presence of Magnesium and an ATP-Mimic	266
A Model For EtsΔ138 Substrate Recognition By ERK2	268
CONCLUSIONS.....	271
EXPERIMENTAL PROCEDURES	273
Construction of Site-Specific EtsΔ138 Mutants	273
Cleavage of the His ₆ -Tag of EtsΔ138	275
Kinetic Methods for EtsΔ138 Phosphorylation	276
Phosphoamino Acid Analysis.....	276
Fluorescence Anisotropy Binding Assay.....	277
Competition Assay	279
Isothermal Titration Calorimetry	280

EQUATION DERIVATION	281
EXPERIMENTAL DATA.....	282
BIBLIOGRAPHY	303
VITA	313

ABBREVIATIONS

5-IAF, 5'-iodoacetomido-fluorescein

ABTS, 2,2'-azine-di[3-ethylbenzthiazolinesulfonate]

ADP, adenosine diphosphate

AMP-PNP, 5'-adenylylimidodiphosphate

ATF2, activating transcription factor 2

ATP, adenosine triphosphate

b-ERK2, biotin-ERK2

BL21 (DE3), *E. coli* for protein production that lack OmpT and Lon proteases for
expression of proteins from vectors containing a T7 promoter

BSA, bovine serum albumin fraction V

CDK, cyclin-dependent kinase

CD, common docking

C. elegans, *Caenorhabditis elegans*

D domain, docking domain

D₂O, deuterated water

DEF, docking site for ERK, FXFP

DEJL, docking site for ERK/JNK, LEL

DTNB, 5,5'-dithiobis(2-nitrobenzoic acid)

DTT, dithiothreitol

EB, ERK binding domain

E. coli, *Escherichia coli*

EDTA, ethylene diamine tetraacetic acid

EGF, epidermal growth factor

EGFR, epidermal growth factor receptor

EGTA, ethylene glycol-*bis*[2-aminoethyl ether]-*N,N,N',N'*-tetraacetic acid

ELISA, enzyme-linked immunosorbent assay

ERK, extracellular signal-regulated protein kinase

E-S, enzyme-substrate

ESI, electrospray ionization

ETS, E26 transformation specific

EtsΔ138, murine (His₆-tagged)Ets1¹⁻¹³⁸

EtsΔ138-C31*, EtsΔ138NC containing Cys-31

EtsΔ138-F, EtsΔ138-C31* covalently labeled with fluorescein at Cys-31

EtsΔ138NC, EtsΔ138 No Cysteines, containing alanines at Cys-31,99,106, and 112

FXFP, Phe-X-Phe-Pro

G-factor, grating factor

GST, glutathione *S*-transferase

HEPES, *N*-(2-hydroxyethyl)-piperazine-*N'*-2-ethanesulfonic acid

I, intensity

IPTG, *isopropyl*-β-D-thiogalactopyranoside

ITC, isothermal titration calorimetry

JNK, c-jun N-terminal kinase

k_{cat} , maximum catalytic rate (s⁻¹)

k_{obs} , observed rate (s⁻¹)

K_d , equilibrium dissociation constant

$K_{d'2}$, equilibrium dissociation constant for a competitor

K_m , Henri-Michaelis-Menten constant

KCl, potassium chloride

KIM, kinase interaction motif

LB, Luria broth

LC/MS, Liquid Chromatography/Mass Spectrometry

LDH, lactate dehydrogenase

MALDI, matrix assisted laser desorption ionization

MAPK, mitogen-activated protein kinase

MAPKK, MAPK kinase

Mef2a, myocyte enhancing factor 2a

min, minutes

MKP, MAPK phosphatase

MNK, MAPK-interacting kinase

η , viscosity

NAD^+ , oxidized form of B-nicotinamide adenine dinucleotide

NADH, reduced form of B-nicotinamide adenine dinucleotide

Ni^{2+} -NTA, Nickel-nitrilo-triacetic acid

OD₆₀₀, optical density at 600 nm

ρ , rotational relaxation time

P, polarization

pIII, protein III

Pea-15, phosphoprotein enriched in astrocytes-15 kDa

PEG, polyethylene glycol 8000

PK, pyruvate kinase

PKI, peptide inhibitor of cyclic AMP-dependent protein kinase

PMSF, phenyl methyl sulfonyl fluoride

$\langle r \rangle$, anisotropy

R , gas constant ($8.314 \text{ J mol}^{-1} \text{ K}^{-1}$)

RSK, ribosomal S6 kinase

s, seconds

S, substrate

SA, specific activity

SDS-PAGE, sodium dodecylsulfate – polyacrylamide gel electrophoresis

Sec, seconds

SH2, Src homology 2

SH3, Src homology 3

SOS, son of sevenless

SPR, surface plasmon resonance

ssDNA, single stranded DNA

sulfo-NHS-LC-biotin, sulfosuccinimidyl-6-(biotinamido)hexanoate

T, temperature

TB, Terrific broth

TBS, Tris-buffered saline

TCA, tri-carboxylic acid

TEMED, N,N,N',N'-tetramethylethylenediamine

TFA, trifluoroacetic acid

TPCK, L-1-chloro-3-[4-tosylamido]-4-phenyl-2-butanone

Tris-HCl, 2-amino-2-(hydroxymethyl)-1,3-propanediol with hydrochloric acid

TU, transduced unit

UDHB, underdehydrated hydrogen bond

V, volts

V, molecular volume (italics)

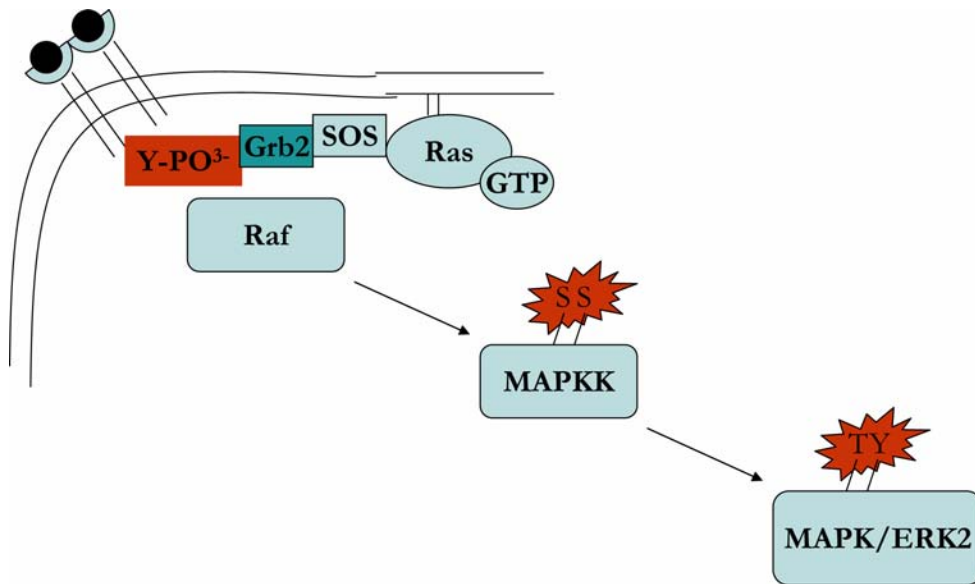
VOOH, vanadate + hydrogen peroxide (peroxyvanadate)

CHAPTER 1: MAPK SIGNALING

SIGNAL TRANSDUCTION PATHWAYS

Cells respond to both their intracellular and extracellular environment in order to adapt to changing conditions or to carry out various cellular fates such as growth, differentiation, proliferation, and apoptosis. Upon epidermal growth factor (EGF) binding to the epidermal growth factor receptor (EGFR), an intracellular signal transduction pathway is activated (Scheme 1) that allows the cell to respond to the EGF. The EGFR is a membrane spanning protein that recognizes EGF in the extracellular portion of the cell and upon binding to EGF forms homodimers which allows their intracellular tyrosine kinase domains to autophosphorylate one another on tyrosine residues. The phosphorylated tyrosine residues recruit proteins containing Src homology 2 (SH2) domains such as Grb and Shc which recognize and bind such motifs. Grb contains an SH3 domain that binds a proline-rich region of a protein called son-of-sevenless (SOS), thereby recruiting this molecule to the intracellular cell surface. SOS is a guanine nucleotide exchange factor (GEF) which activates Ras by exchanging the inactivating guanine diphosphate for the activating guanine triphosphate. Through unknown mechanisms, Raf is recruited to the membrane and activated by Ras. Raf phosphorylates mitogen-activated protein kinase kinase 1 (MAPKK1) which leads to its activation. Active MAPKK1 can then activate extracellular signal-regulated protein kinase 2 (ERK2) through dual-phosphorylation of Thr-183 and Tyr-185, residues conserved throughout the MAPK family. ERK2 phosphorylates multiple proteins within the cell which can lead to transcriptional activation of genes in response to EGF [1]. In

this fashion, an extracellular signal can lead to an intracellular response of the cell via transcriptional changes as a result of an intricate signal transduction pathway.



Scheme 1. EGF-induced signal transduction pathway. EGF binds the EGFRs on the cell surface (top left) and induces an intracellular signal transduction pathway of phosphorylation events, protein–protein interactions, nucleotide exchange, and protein localization that leads to ERK2 activation via dual-phosphorylation of a threonine (T) and tyrosine (Y) residue (bottom right).

SPECIFICITY DETERMINANTS OF SIGNAL TRANSDUCTION

Cell signaling specificity is derived from several components consisting of the type of input signal, type of cell, gene expression levels, temporal and spatial location of proteins, chemical catalytic events, and the specificity of macromolecular interactions that are dependent upon all of the aforementioned factors. The input signal is the first step towards switching a signaling transduction pathway on. In the case of EGF-

mediated ERK2 activation, the EGF is that signal that binds the EGFR on the cell surface leading to its activation and a cellular response. Other MAPK family members, such as p38 MAPK and c-jun amino-terminal kinase (JNK), are activated in response to other cellular stresses such as UV irradiation, osmotic shock, heat shock, and through cytokine signaling. ERK activation generally leads to cellular proliferation or differentiation, while JNK and p38 activation generally lead to apoptosis, an immune response, or cytokine production. Therefore, the input signal determines which signal transduction pathway(s) are activated and determines the type of cellular response.

Since different types of cells have differential gene expression, the cell type also plays a critical role in the specificity of cell signaling. For example, some cells may not express EGFRs or certain transcription factors and, therefore, would not be able to respond to EGF signaling or have a differential response, respectively. Signaling specificity also occurs through temporal and spatial location of proteins within the cell which is dependent upon the state of cell. Recruitment of proteins to the intracellular cell surface in EGFR signaling occurs by protein-protein interactions which include proteins containing SH2 and SH3 domains that specifically recognize and bind phosphorylated tyrosines and proline-rich regions, respectively. In the former situation, chemical catalysis via phosphorylation of specific residues by protein kinases can mediate the spatial location of proteins, while in the latter situation the SH3 domain does not require chemical catalysis for recruitment. Since phosphorylation events are reversible due to dephosphorylation by phosphatases, the specificity of protein localization in the case of EGF signaling is dependent upon the level of protein phosphorylation within the cell. Alternatively, the ability of Ras to recruit Raf to the cell surface is dependent upon whether Ras is bound to the triphosphate or diphosphate form of guanine indicating that the phosphorylation state of bound nucleotides is also a critical determinant of protein

localization. Therefore, spatial and temporal location of proteins is dependent upon protein-protein interactions which can be regulated by their phosphorylation state and bound-ligand state.

MITOGEN-ACTIVATED PROTEIN KINASES

Members of the mitogen-activated protein kinase (MAPK) family of proteins, including ERK, p38, and JNK, are capable of transferring the γ -phosphate of adenosine triphosphate (ATP) to the hydroxyl group on protein substrates that contain a serine or threonine immediately followed by a proline (Ser/Thr-Pro) [2]. These phosphoryl-transfer reactions are the predominant mechanism of post-translational modifications within a cell. Dual phosphorylation of MAPKs causes a conformational change of the enzyme that aligns catalytic residues in the active site and increases their ability to phosphorylate protein substrates within the cell and activate cell signaling pathways. When protein substrates are phosphorylated, the addition of a covalent negatively charged phosphate moiety may cause proteins to undergo a conformational change, localize to a new region in the cell, regulate differential protein-protein interactions, or regulate its stability within the cell. Phosphorylation of proteins is a major “means” of cell signaling and is highly regulated so that the cell can achieve its “ends”. Therefore, the MAPKs play a significant role in carrying out specific cell signaling in response to mitogens by phosphorylating its protein substrates.

MAPKs can exist in a catalytically inactive (unphosphorylated) or activated (phosphorylated) state depending on whether or not it has been dually-phosphorylated by

a MAPKK [3]. For example, dual phosphorylation of the inactive form of ERK2 by MAPKK1 induces an intramolecular conformational change leading to the alignment of catalytic residues in the active form of ERK2 [4] causing an increase in its catalytic efficiency toward protein substrates¹ [5]. Activation of ERK2 occurs by dual-phosphate incorporation into Thr-183 and Tyr-185 by MAPKK1 and is further activated by magnesium binding [6]. In the presence of saturating magnesium, active ERK2 forms a ternary complex with MgATP²⁻ and a protein substrate (EtsΔ138) through a sequential random order mechanism [7] prior to phosphate transfer from the ATP to EtsΔ138. All protein kinases bind ATP in their active site but less is known about how protein substrates bind the protein kinases in order to carry out efficient phosphorylation of the Ser, Thr, or Tyr in the active site. MAPKs are thought to phosphorylate Ser/Thr-Pro motifs, however, although many proteins contain Ser/Thr-Pro motifs only a small percentage of them are actually phosphorylated by MAPKs. Therefore, a mechanism other than Ser/Thr-Pro recognition in the active site of the active kinase must exist to facilitate the specificity of substrate phosphorylation that exists in cells. The question remains as to how protein kinases specifically recognize their cognate protein substrates within a cell.

Protein kinases recognize consensus phosphorylation sites, consisting of the phospho-acceptor and its surrounding residues, in their active site [8], however, the protein kinases also recognize protein substrates through an enzymic site (termed an exosite) that lies outside of the active site. Here, we refer to an “exosite” as a small patch of amino acids existing on the surface of the protein kinase that binds to a “docking motif” on the surface of an interacting protein such as a substrate to form a docking complex. A “docking complex” is defined as a protein-protein interaction occurring

¹ The catalytic efficiency of ERK2 is increased 600,000-fold towards the non-specific protein substrate MBP when activated by dual-phosphorylation.

between an exosite and a docking motif to form a stable tethered complex independent of other proteins and is separate from active site interactions.

The substrates of MAPKs are diverse and include transcription factors, protein kinases, and phosphatases which all play a role in intracellular signaling. MAPKs phosphorylate serine or threonine residues placing them in the kinase sub-family of serine/threonine kinases distinct from the tyrosine kinase sub-family. MAPKs also prefer a proline immediately adjacent to the phospho-acceptor, thereby, preferring to phosphorylate Ser/Thr-Pro motifs within their active site [9]. For this reason, MAPKs are referred to as proline-directed kinases. Each of the subclasses of MAPKs contain several related homologs (e.g. ERK1, 2, 3, 5 and 7) and also contain splice-variants (e.g. ERK1b) which allows for differential primary amino acid sequences, expression patterns, and ultimately leads to functional differences.

THE IMPORTANCE OF CHARACTERIZING PROTEIN-PROTEIN INTERACTIONS

Protein–protein interactions are of critical importance in many cellular events including signal transduction and the regulation of protein phosphorylation. The spatial and temporal activity of these interactions is also of critical importance to the fidelity of signal transduction. In the case of EGF signaling, protein–protein interactions are crucial for the recruitment of proteins to the membrane, ligand exchange of Ras, and are required for the MAP kinase phosphorylation cascade which ultimately leads to several proteins being phosphorylated. Of course, the downregulation of this signaling pathway through dephosphorylation is also dependent on protein–protein interactions. A critical understanding of the protein–protein interactions in cells and how they are regulated and mediate catalysis is crucial towards learning how the fidelity of signal transduction is

maintained. Disrupting protein–protein interactions in a site-specific fashion is also of interest towards developing drugs that interrupt specific signal transduction pathways.

Elucidating Sites of MAPK Protein-Protein Interactions

COMPUTATIONAL STUDIES TO DETERMINE FUNCTIONAL DIFFERENCES BETWEEN SUBFAMILIES

A computational study was carried out to predict regions of functional difference between subfamilies of MAPKs [10]. With the hypothesis that physicochemical differences between homologous residues amongst subfamilies can confer functional differences such as specificity determination, Caffrey et al. compared the primary sequences of MAPKs and searched for regions amongst subfamily members that significantly changed after gene duplication and remained conserved amongst subfamily members thereafter. In other words, MAPKs are hypothesized to be related through gene duplication. After gene duplication, a region of a protein that confers a functional difference between subfamilies will undergo a physicochemical change and conserve this change amongst the subfamily. This study computationally predicted two exosite regions of interest on ERK2 that were later shown to confer functional differences. One predicted region (Figure 1) was the TT/ED exosite of ERK2/p38 MAPK α (corresponding to residues Thr-157 and Thr-158 in ERK2 and the homologous residues Glu-160 and Asp-161 in p38 MAPK α) thought to be involved in substrate specificity determination [11]. Another predicted region was the residues Lys-229 and His-230 in ERK2 (Figure 1) which were shown to mediate MAPKK1 binding and phosphorylation of ERK2 [12] and the nonspecific protein substrate myelin basic protein (MBP) [12], phosphoprotein enriched in astrocytes-15 kDa (PEA-15) binding [13], ERK2 induced activation of

MAPK phosphatase 3 (MKP3), and Elk-1 phosphorylation [14]. Therefore, this computational study proved to be an excellent way to determine residues of MAPKs that confer functional differences amongst subfamilies, however, the functional differences that the residues confer remain largely unknown and their elucidation by further studies with proteins of interest must be pursued.

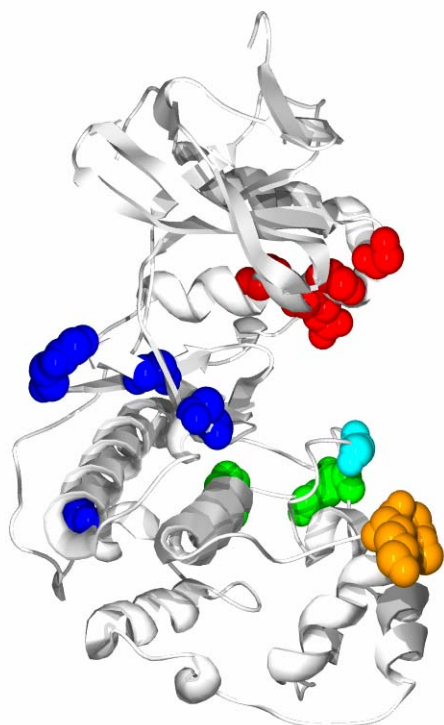


Figure 1. Structural representation of dual-phosphate ERK2 and proposed specificity determining residues. A computational study was carried out by Caffrey *et al.* to predict regions of MAPKs conferring specificity differences amongst the MAPK subfamily members [10]. Residues from Table 1 of this study comparing ERK and p38 are displayed here for ERK2 (PDB: 2ERK) in 5 regional colors: (red: His-59, Tyr-62, Gln-64, Leu-67), (blue: Tyr-111, Lys-112, Cys-125, Leu-154, Thr-157, Thr-158), (cyan: Glu-184), (green: Lys-201, Gly-202, Lys-205, and Ser-206), and (burnt orange: Lys-229, His-230).

GENETIC STUDIES REVEAL SITES OF INTEREST

Genetic studies lend a powerful approach toward finding novel docking motifs and exosites involved in MAPK protein–protein interactions. An excellent example was the identification of a gain-of-function mutation in the *Drosophila rolled* gene, a homolog of ERK, which led to the initiation of several cell signaling pathways in the absence of a mitogenic signal [15]. A single point mutation of a conserved MAPK residue was shown to disrupt interactions with a phosphatase, allowing for sustained activation in response to mitogenic stimuli indicating that this residue was critical for the ability of a phosphatase to down regulate its activity through dephosphorylation [16]. This residue was shown to be required for several MAPK protein–protein interactions including binding to activators, substrates, and phosphatases, and led to the establishment of the common docking (CD) exosite on MAPKs required for multiple protein–protein interactions [17].

Another genetic study led to the discovery of a MAPK substrate recognition motif found in ETS (E26 transformation specific) proteins that mediates phosphorylation by ERK. The genetic model system *C. elegans* was probed for mutations that led to defective vulva development and suppression of the multivulva phenotype [18]. Multiple gain-of-function mutations in LIN-1, a MAPK transcription factor substrate, led to the discovery of a conserved Phe-X-Phe-Pro (FXFP) substrate recognition motif that was conserved in some ETS protein substrates and facilitated efficient phosphorylation by a homolog of ERK. The FXFP motif was later termed a docking site for ERK, FXFP (DEF) and it was shown that the two phenylalanines in the DEF motif mediated binding to ERK and could also be substituted for tyrosines indicating the importance of the phenyl ring in mediating ERK binding [19]. These studies indicate the power of genetic studies in elucidating sites on both the MAPK and its substrates that mediate protein–

protein interactions and play a critical role in signal transduction pathways required for development.

YEAST 2-HYBRID STUDIES

The yeast 2-hybrid system is an excellent technique to study specific protein-protein interactions *in vivo* for two eukaryotic proteins of interest in the absence of other eukaryotic proteins [20]. Unfortunately, yeast proteins may act as intermediates in the protein-protein interactions. The technique utilizes the transcription factor Gal4 that can be separated into two functional domains: a DNA binding and a transcriptional activation domain. Two proteins suspected to bind one another are genetically fused to each of the Gal4 functional domains. If both fusion proteins are present within a single yeast cell and bind to one another, the DNA binding domain of Gal4 (bound to DNA) lies in close proximity to the activation domain which recruits RNA polymerase transcription of a marker gene indicating a functional protein-protein interaction between the two proteins of interest.

An excellent yeast 2-hybrid study was carried out to determine ERK2 point mutations that were unable to bind the activator MAPKK1/2 but could still bind other interacting proteins such as phosphatases and substrates [12]. This study allowed the dissection of regions of ERK2 involved in specific protein-protein interactions with MAPKK1/2 that did not mediate other protein-protein interactions. An ERK2 mutant library was created and fused to the Gal4 transcription activation domain and transformed into a yeast MAT α strain and plated on minimal agar (-Leu). The yeast transformed with the plasmid could synthesize their own leucine and survive growth conditions in the absence of leucine. The yeast were replica plated onto a lawn of MAT α strain of yeast

that were transformed with either pLexA-MAPKK1 or pLexA attached to an ERK2 interacting protein and plated on minimal agar (-Trp). The two haploid strains of yeast (MATa and MAT α) were able to mate and share their genetic information to form a diploid strain that could survive when replica plated onto minimal agar lacking both amino acids (-Leu/Trp). The LexA-MAPKK1 represents the activator of ERK2 fused to a DNA binding domain (LexA). Protein-protein interactions between MAPKK1 and the ERK2 mutant library were detected by replica plating onto minimal agar lacking three amino acids (-His/Leu/Trp). If the proteins of interest could bind one another, close proximity of the LexA DNA binding domain and the Gal4 transcriptional activation domain allowed transcription of a marker gene that allowed the yeast to produce histidine. Yeast that were not able to survive on -His/Leu/Trp agar contained ERK2 mutations that disrupted ERK2-MAPKK1 binding. Interestingly, the catalytic activity of MAPKK1 led to decreased binding of ERK2 so the catalytically inactive form of MAPKK1 (MAPKK1-K97M) was used.

Each ERK2 mutant identified to have a defect in binding MAPKK1 was shown to bind other proteins such as the C-terminal ERK2 docking motif of chicken ribosomal S6 kinase (RSK) from chicken (residues 689-752, most similar to human RSK1), the phosphatase MKP3, and the substrate MAPK-interacting kinase (MNK1) in the yeast 2-hybrid assay.

Interestingly, each of the mutants shown to disrupt protein-protein interactions with MAPKK1 were found in the C-terminus of ERK2. The mutants were found to precede (H230R) or lie within (N236K) the α_G helix of ERK2 or lie near the MAPK insert region (Y261N, S264P) found exclusively in MAPKs (insert: residues 243-273), cyclin-dependent kinases (CDKs), and glycogen synthase kinase 3 (Figure 2). A similar region of ERK2 is thought to be involved in binding PEA-15 [13] as well as Ets Δ 138

binding (Rainey, K229T/H230D mutant) indicating the importance of this region for ERK2 protein-protein interactions. Interestingly, the ERK2 CD exosite mutant (D316/319A) was shown to be defective in binding MAPKK2, RSK, MKP3, and MNK1 as previously shown [17] but was able to bind MAPKK1-K97M [12]. These results indicate that a region near the α_G helix and the MAPK insert region may contribute more toward binding MAPKK1 than the CD exosite.

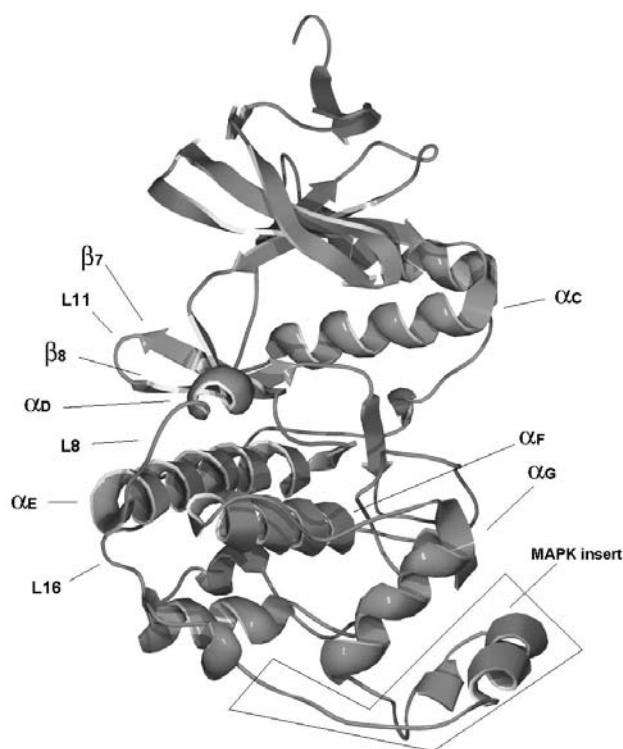


Figure 2. Structural representation of dual-phosphate ERK2. The crystal structure of the dual-phosphate form of ERK2 (PDB: 2ERK) is shown with several alpha helices (α), beta sheets (β), loops (L), and the MAPK insert region (residues 243-273) shown.

The yeast 2-hybrid system has been used to study protein-protein interactions between protein kinases and their interaction proteins including substrates, activators, and phosphatases. Some seminal research was carried out using the yeast MAPK signaling pathway to show that Ste5 could tether each of the three-tiered MAPK members Ste11 (a MAPK kinase kinase), Ste7 (a MAPK kinase), and Fus3 (a MAPK) each using different domains of Ste5 while Fus3 and a related homolog Kss1 bound to a similar Ste5 binding site [21]. Another study used p38^{hog} or SAPK (both MAPKs) fused to the Gal4 transcription factor DNA binding domain and its activator MAPKK fused to the Gal4 transactivation domain. The kinase activators MAPKK3, MAPKK6, and SAPKK1 were shown to bind p38^{hog} while only SAPKK1 was able to bind SAPK [22] indicating that the specificity of protein–protein interactions can also be determined using this technique.

The yeast 2-hybrid system has also been used to find novel proteins that bind MAPKs such as the ERK2 binding protein FLH2 pulled out of a cardiomyocyte cDNA library and shows preference toward binding active ERK2 [23]. Another ERK2 binding protein Naf1 (Nef-associated factor 1 α) was identified and found to hold ERK2 in the cytoplasm while overexpression of Naf1 decreased ERK2-dependent Elk-1 transcription [24]. JNK3 was found as a target of β -arrestin 2 which acts as a scaffold to increase the activation of JNK3 [25]. Another study showed that MKP1 could bind ERK1/2, p38 α , and JNK and helped define a docking motif on MKP1 required for ERK2 and p38 α binding but not JNK [26]. The yeast 2-hybrid system has shown to be an excellent system for studying whether or not proteins bind one another *in vivo*, it can be used to select for residues that are required for protein–protein interactions, and can also help elucidate novel binding partners.

CO-CRYSTALLIZATION OF A DOCKING MOTIF PEPTIDES AND A MAPK

Unfortunately, crystal structures are not readily available for MAPKs co-crystallized with other interacting proteins such as substrates, activating kinases, or their phosphatases. However, two crystal structures were reported recently in which docking motif peptides derived from a p38 MAPK α activator (MKK3b) and a substrate (MEF2a) are bound to the inactive form of p38 MAPK α [27]. These structures highlight a “docking groove” exosite on p38 MAPK α responsible for binding some docking motif peptides that is distinct from the active site. Both the MKK3b and the MEF2a peptide bind to the same docking groove exosite on p38 MAPK α that lies between the α_D and α_E helices and the reverse turn between the β -sheets β_7 and β_8 (Figure 3) that is distinct but near to the CD exosite [17]. Since both peptides derived from different types of MAPK-interacting proteins bind to the same exosite on the inactive p38 MAPK α it is possible that this single docking groove exosite may be responsible for other protein-protein interactions that contain a similar docking motif. Interestingly, the peptides share a basic region followed by a homologous ϕ -X- ϕ motif (where ϕ is a hydrophobic residue, usually leucine, valine, or isoleucine, and X is any residue usually basic) thought to bind MAPKs, however, the peptides bind with different orientations to one another. Peptides exhibiting a basic region near a ϕ -X- ϕ motif that bind MAPKs have been termed a docking site for ERK/JNK, LEL (DEJL motif). Point mutations on the enzyme in the peptidyl docking exosite disrupted the binding of full length MKK3b and MEF2a indicating the usefulness of the peptide/MAPK structure in determining docking exosites on MAPKs [27]. The location of the docking groove exosite on p38 MAPK α was also confirmed using deuterium hydrogen exchange mass spectrometry [28] indicating that the docking groove exosite exists in solution as well as the static crystal structure. In addition, it was shown that ERK2 DEJL motif peptides in a similar location [28]. It will

be interesting to see co-crystal structures of MAPKs and their interacting proteins to gain further insight into protein-protein interactions with MAPKs as well as insights into the catalytic activity carried out by the MAPKs, their activators, and their inactivators.

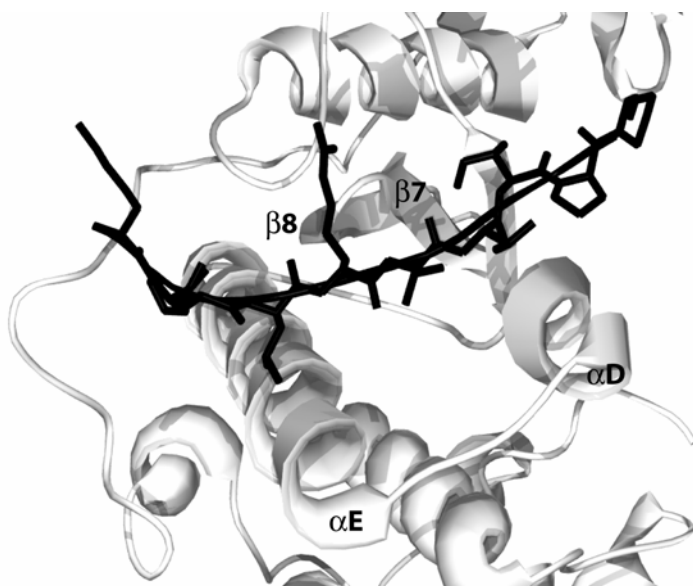


Figure 3. Structure of inactive p38 MAPK α bound to a MEF2a docking motif peptide. The crystal structure of the inactive form of p38 MAPK α (grey) bound to the docking motif peptide derived from the substrate MEF2a (black) (1LEW) is shown. The peptide binds in a groove created between the helices α_D and α_E and the β_7/β_8 reverse turn. Another peptide derived from MKK3b (not shown) binds a similar site with a different orientation with respect to its ϕ -X- ϕ motif on p38 MAPK α (1LEZ) [27].

HYDROGEN EXCHANGE MASS SPECTROMETRY

Deuterium hydrogen exchange mass spectrometry has been used to determine regions of MAPKs that are protected from hydrogen exchange in the presence of substrate docking peptides that bind MAPKs to determine enzymic exosites for the docking peptides. The amide hydrogens of the peptide backbone of proteins are constantly being exchanged with hydrogen donors from water; therefore, deuterium hydrogen exchange can be used to follow a time course of enzymic exposure to deuterated water (D₂O) by following the incorporation of the heavier deuterium into the

peptide backbone. The exchange of side chain and N-terminal amide hydrogens is not seen due to rapid back-exchange as compared to amide hydrogens. Following enzymic exposure to D₂O in the presence or absence of a deuterated docking motif peptide, the reactions were quenched/chilled at various time points, the proteins were subjected to limited proteolysis, and the masses of the proteolytic peptides were determined using liquid chromatography/mass spectrometry (LC/MS). Peptides exposed to solution in D₂O yield a higher mass than that of peptides in H₂O due to incorporation of deuterium.

Deuterium exchange of MAPKs in the presence and absence of a deuterated docking motif peptide in D₂O can yield three possible outcomes: no change, an increase, or a decrease in the mass of the enzymic peptides following proteolysis. Peptidyl regions that do not have a change in mass indicate regions of the MAPK that are unaffected by the binding of the docking motif peptide. An increase or decrease in peptidyl mass represents regions that become more or less exposed to solution, respectively. Increased exposure could indicate enzymic regions transitioning from a more buried state to a more solvent exposed state upon peptide binding due to a peptide-induced conformational change distal to the peptide binding site. A decrease in hydrogen exchange upon peptide binding might be due to the bound docking peptide directly protecting amide hydrogens from exchange or due to a peptide-induced conformational change distal to peptide binding site leading from an exposed state to a buried state. Therefore, it is often helpful to have co-crystallization experiments and other binding experiments using docking mutants to support any hypotheses.

Two substrate-derived peptides that bind MAPKs (a DEJL and DEF motif peptide) were examined for their ability to bind the inactive and active form of ERK2 as well as the inactive form of p38 MAPK α using deuterium hydrogen exchange [28]. The results suggest that the DEJL and DEF motif bind ERK in two distinct regions from one

another. The DEJL motif binds ERK and p38 MAPK α in the docking groove exosite as previously described for inactive p38 MAPK α [27]. The DEJL motif shown to bind ERK2 in the docking groove exosite (residues 311-327 in Elk-1: QKGRKPRDLELPLSPL [29]) contains a basic motif near a hydrophobic ϕ -X- ϕ . The DEJL peptide binding also increased the accessibility of the P+1 proline binding region of both p38 MAPK and ERK2 [28] as was seen in the co-crystal structure [27] indicating that DEJL motif binding in the MAPK exosite causes the disorder of the P+1 region on the opposite side of the enzyme. Unfortunately, the Elk-1 derived peptide contains a potential phosphorylation site (SP) which could potentially bind in the P+1 site. Interestingly, a RSK-derived peptide similar to, but distinct from, a DEJL peptide was also proposed to bind the docking groove exosite in ERK2 [28].

Alternatively, the DEF peptide (Elk-1 residues 387-398, PRSPAKLSFQFP) containing an FXFP motif was hypothesized to bind at a different site than the DEJL peptide locating it to the P+1 site, α_F helix, and the MAPK insert region of ERK2. Interestingly, the DEF motif peptide could only bind a pocket formed in the active ERK2 complex that was absent in the inactive form indicating that the DEF motif binds ERK2 in a phospho-dependent manner (Figure 4). Once again, the DEF peptide contained a potential phosphorylation site (SP) which could potentially bind the P+1 site on ERK2.

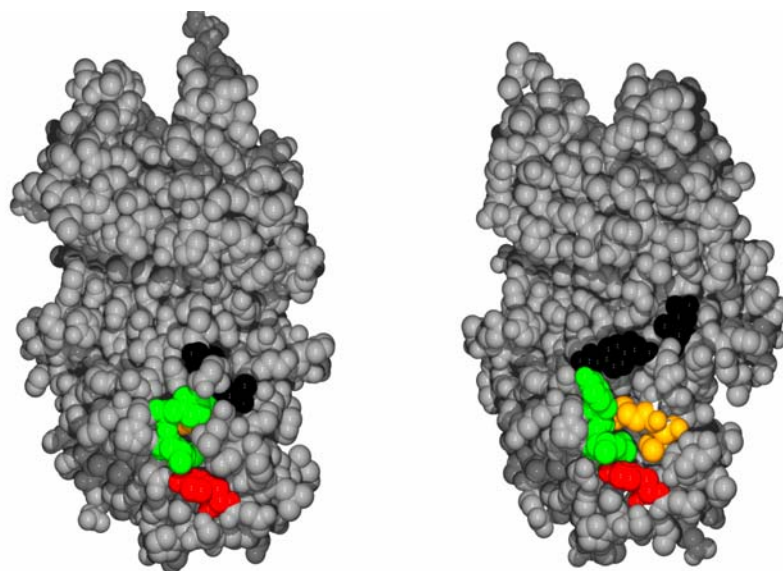


Figure 4. Exposure of a DEF binding pocket on the active form of ERK2. The unphosphorylated (PDB:1ERK, left) and the dual-phosphate/active form of ERK2 (PDB:2ERK, right) are shown with its phospho-acceptor residues Thr-183 and Tyr-185 (black). In the phosphorylated form, both Thr-183 and Tyr-185 are phosphorylated and create a conformational change of the enzyme revealing a proposed docking motif peptide binding pocket for DEF motif substrates [28]. In the inactive enzyme (left), Met-197 and Leu-198 (burnt orange) are buried and upon ERK2 phosphorylation (right) are exposed. Met-197 and Leu-198 form a DEF binding pocket in active ERK2 along with the residues Tyr-231, Leu-232, Leu-235 (green), and Tyr-161 (red). It is hypothesized that this conformational change acts as a gate that allows DEF binding of substrates such as Elk-1 to the active form of the enzyme and discriminates binding to the inactive enzyme. The proposed DEJL docking groove exosite is located at the left/middle of ERK2.

Hydrogen exchange mass spectrometry can be used to determine enzymic peptide regions that bind a specific peptide; however, individual residues involved in binding cannot be discerned using this technique. Interestingly, experiments mentioned here correlate well with co-crystallization studies of a MAPK bound to two DEJL motif peptides [27]. Hydrogen exchange has also been employed to determine regions of a

MAPK that changed accessibility upon dual-phosphorylation [30] indicating conformational changes upon phosphorylation that correlated well with existing crystal structure data. A limit to this technique is that peptidyl exposure changes may be due to direct or indirect binding so additional data indicating binding is necessary to interpret results (e.g. mutational data that indicates a lack of binding).

FOOTPRINTING

Individual residues that make up docking motifs on MAPK-binding proteins have been mapped using the biophysical technique of NMR footprinting. NMR footprinting involves the ^{15}N -labeling of a small protein and determining the NMR spectrum of the labeled protein in the presence and absence of a MAPK. When a complex is formed between the labeled protein and the MAPK, the large complex tumbles slower in solution, thereby, broadening the NMR spectrum of residues at the interface of the labeled protein and the MAPK. The docking motif of PEA-15, a small non-catalytic protein that binds ERK2, was determined using NMR footprinting [31]. The authors found several residues thought to be involved in binding the inactive form of ERK2 and used site-directed mutagenesis to confirm that the residues were required for binding ERK2 in an *in vitro* pull-down assay. Another NMR footprinting study was used to determine residues on the ERK2 binding (EB) domain of the phosphatase MKP3 required for binding ERK2 [32]. Once again, residues that showed significant NMR spectra broadening were confirmed as residues involved in ERK2 binding by site-directed mutagenesis followed by *in vitro* pull-down assays. Interestingly, this study showed that dual-phosphorylation of ERK2 did not affect binding to the EB domain of MKP3 consistent with a previous study [33] indicating that the EB domain does not recognize

the phosphorylated region of ERK2 and binding is not affected by the conformational change of ERK2 upon activation. Both of these studies indicate that NMR footprinting is a useful tool to elucidate docking motif residues located on the surface of a MAPK interacting protein.

Recently, a technique called misincorporation proton-alkyl exchange (MPAX) has been developed where footprinting of protein–protein interactions can be carried out at the individual amino acid level in the absence of heavy isotope labeling on small quantities of protein [34]. Briefly, a misincorporator tRNA (encoding for a charged cysteine) with an anticodon specific for any of the 20 amino acid codons is added with a protein of interest into *E. coli* so that low-level incorporation of a cysteine occurs at the specific amino acid codon of interest. Ultimately, the other 19 amino acids could be analyzed in this fashion by misincorporation of a cysteine. A small percentage of purified protein incorporates a single unnatural cysteine located at the amino acid site of interest. A thiol-specific alkylating reagent can react with the protein of interest if it contains a cysteine; therefore, proteins must be devoid of cysteines prior to MPAX. The technique is similar to deuterium hydrogen exchange protection in the presence of a docking peptide but exchange of the alkylating reagent occurs on the cysteine side chain and not at the amide portion of the amino acid. In this fashion, an unnatural cysteine residue will be alkylated in the absence of an interacting protein and protected from alkylation if it is bound to the interacting protein. Alkylated proteins are then cleaved with a cysteine-specific cutting reagent while the masked residues refrain from cleavage. After radiolabeling the protein, an SDS-PAGE gel can be run for each misincorporator tRNA comparing lanes in the presence and absence of the interacting protein to find different peptide fragments pertaining to differential labeling which indicates residues involved in binding the interacting protein. This technique can be used in conjunction

with mass spectrometry to find individual amino acids that are protected from solution labeling at the interface of a protein-protein interaction in the absence of heavy isotope labeling. The MPAX technique is not limited to protein size and can be carried out on microgram quantities of protein.

Quantifying and Characterizing Protein-Protein Interactions

NON-QUANTITATIVE PULL-DOWN STUDIES

Protein-protein interactions are often times interpreted by pull-down studies or immunoprecipitations where two proteins of interest are probed for their ability to interact with one another. Usually, a cellular extract is incubated with an antibody to a protein of interest or an affinity tag that is linked to a heavy bead such as sepharose or agarose. The protein of interest and its interacting proteins are extracted from the cellular milieu with a centrifugation step and then washed several times to rid of non-specific binding proteins. Other proteins bound to the protein of interest can be elucidated by running an SDS-PAGE gel followed by a Western blot with an antibody to the interacting protein of interest. A positive result indicates that the two proteins are closely associated or directly bind one another. The difficulty in interpretation is that the binding may not be a direct interaction (e.g. another intermediate protein may hold the two proteins together). Therefore, another test for direct binding is necessary. The pull-down studies are non-quantitative and do not allow an affinity of interaction to be determined. To understand protein-protein interactions on the molecular level, quantitative binding studies must be carried out to understand the specificity of interactions and how they are regulated.

ISOTHERMAL TITRATION CALORIMETRY

Isothermal titration calorimetry (ITC) has been used to determine the equilibrium dissociation constant (K_d) of MAPKs and their ligands based on the enthalpy and the stoichiometry of the binding interaction. Zhou et al. used ITC to determine the K_d of docking motif peptides that bind ERK2 (presumably inactive ERK2) [35]. When key residues of the docking motif peptides were mutated, the peptides showed an increase in the K_d indicating the importance of individual amino acids in mediating ERK2 binding. Our laboratory has used ITC to show that ATP does not bind active ERK2 in the absence of magnesium, however, a potent inhibitor of ERK2 (5-iodotubercidin) [36] was able to bind the active form of ERK2 and could be used to titrate the number of active sites in the active form of ERK2 [6]. A similar study was carried out to determine the K_d of the tight binding p38 MAPK α inhibitor SB 203580 ($K_d \sim 15$ nM) to the inactive form of p38 MAPK α [37]. Our laboratory has used ITC to discern the K_d of a protein-protein interaction between the active form of p38 MAPK α and the *N*-terminal portion of the transcription factor ATF-2 (A. Szfranska) as well as the association between the dual-phosphate form of ERK2 and a protein substrate Ets Δ 138 (M. Rainey). ITC is a quantitative study of protein-protein interactions useful for determining the stoichiometry of binding as well as the thermodynamics of MAPKs interacting with their substrates and/or products under conditions that do not allow phosphoryl-transfer to occur (as phosphorylation would disrupt equilibrium and change the binding energetics of the two partners).

SURFACE PLASMON RESONANCE

Surface plasmon resonance (SPR) allows the measurement of direct protein-protein and protein-ligand interactions as they occur so that the rates of association and dissociation can be measured and used to calculate the K_d ($k_{\text{off}}/k_{\text{on}}$) of unlabeled proteins. Unfortunately, the proteins are trapped on a solid surface and are not free in solution. Similar to ITC, conditions that do not allow phosphoryl-transfer must be employed to ensure equilibrium conditions. SPR is carried out by binding an analyte to a dextran layer attached to a gold-coated glass surface. The analyte is expected to be free to bind ligands that pass by in solution. Polarized light is reflected off the glass surface underneath the analyte and the reflected light is analyzed for an increase in refractive index due to ligand binding the analyte and an increase in the apparent molecular mass of the analyte. SPR has been utilized to determine the K_d of a JNK DEJL-motif inhibitor peptide (TI-JIP peptide: RPKRPTTLNLF) which was shown to bind to both JNK2 and JNK3 (both presumed to be the inactive forms) but did not bind the JNK substrates GST-ATF-2¹⁹⁻⁹⁶, GST-c-Jun¹⁻¹³⁵, and Elk-1³⁰⁷⁻⁴²⁸ [38]. The TI-JIP peptide displayed a low micromolar affinity (1-10 μM) which was not affected by salt (0-200 mM) or pH (7.4 ± 1.0) changes [38]. These studies indicate that the specificity of protein-protein interactions can be measured using SPR in a quantitative fashion in a variety of buffer conditions. Another group has used SPR to determine the K_d for the tight binding p38 MAPK α inhibitors SB 203580 ($K_d = 22$ nM) and RWJ 67657 ($K_d = 10$ nM) with the inactive form of the enzyme indicating that this is a useful tool for studying drug interactions as well. Although the data generated for the SB 203580 inhibitor appears consistent with similar data obtained from ITC [37] and steady-state kinetic assays [39], the data was generated using rather high surface densities of protein and gave large errors for the dissociation phase of the experiment indicating that this technique may not be

suitable for small ligands. SPR can be used to determine the rates of association and dissociation of direct interactions between MAPKs and their interacting peptides, proteins, and small molecules.

FLUORESCENCE ANISOTROPY/POLARIZATION

An alternative method to finding the K_d for interacting MAPK ligands is fluorescence anisotropy (or polarization) which utilizes a fluorescent probe attached to the ligand of interest. The advantage of anisotropy over SPR is that the assays are carried out in solution and not on a solid-state; however, fluorescence anisotropy assays require the use of a labeled ligand. Fluorescence anisotropy is carried out in a fluorometer using polarized light to excite the fluorophore of interest. The emitted light is measured both horizontal and vertical to the stimulated light and the ratio of these measured emissions gives an anisotropy value which is low for fluorophores attached to low molecular weight molecules and high for fluorophores attached to high molecular weight molecules. Anisotropy measures the molecular tumbling of the fluorophore in solution and is dependent upon temperature, viscosity, and molecular volume. By holding temperature and viscosity constant, changes in molecular volume can be measured through anisotropy changes. Usually the smaller of the two binding partners is attached to a fluorophore and a decrease in molecular tumbling of the labeled ligand is observed as an increase in anisotropy (molecular volume is inversely proportional to anisotropy) when a larger protein binds the labeled ligand. Fluorescence anisotropy has been used to determine the K_d of a fluoresceinated MAPKK1 derived peptide ($K_d = 77$ nM) and active ERK2² [40]. Interestingly, the same peptide showed an IC_{50} of 7 μ M for *in vitro* activation of ERK2

² The figure shows that it is active ERK2, no mention of which antibody was used.

but did not affect the activation of JNK3 and p38 [40], however, fluorescence anisotropy was not carried out with JNK3 and p38 to determine the specificity of the peptide for MAPKs. It would be interesting to use fluorescence anisotropy as a tool to measure specificity differences of protein substrates and their protein kinases.

A fluorescence polarization assay (similar to anisotropy) was used to determine steady-state kinetics of inactive JNK-1 phosphorylation of ATF-2 for high-throughput screening of inhibitors that disrupt the phosphorylation event [41]. This assay was set up differently than the aforementioned by adding a fluorescent phosphorylated peptide (called a tracer) that can bind to a phospho-specific antibody. The tracer peptide was similar to the ATF-2 phosphorylation site of interest. As JNK-1 phosphorylated the ATF-2 protein, the antibody could bind either the phosphorylated ATF-2 or the tracer. In the presence of increased amounts of phosphorylated ATF-2, more tracer was free in solution thereby yielding a lower polarization signal than when bound to the antibody. This assay was used to determine the K_m of both ATP and ATF-2 and was automated for studies of kinase inhibition. However, inhibitors that exhibited their own fluorescence caused false positive results and some inhibitors may also disrupt the antibody/tracer interaction causing alternate problems in the data analysis. Our lab has developed a fluorescence anisotropy assay capable of measuring the K_d of protein-protein interactions between a MAPK and an interacting protein and can be used for structure-function studies and determining the specificity of protein-protein and protein-peptide interactions. It may also prove useful for the development of inhibitors that disrupt protein-protein interactions.

The Function of MAPK Protein-Protein Interactions

KINETIC STUDIES OF MAPK CATALYSIS

Our lab has been interested in characterizing MAPK catalytic events towards their protein substrates, mainly the catalytic events of fully activated MAPKs. Kinetic studies are an excellent means of understanding the order in which substrates bind to the enzyme, the rate of the enzymatic activity of both the nucleotide and protein substrate turnover, and elucidating rate-determining steps of catalysis. We have shown that an active form of p38 MAPK α phosphorylates the transcription factor ATF-2¹⁻¹¹⁵ at two sites in a two-step distributive mechanism, whereby, the first phosphorylation occurs on the enzyme, followed by dissociation of the docking complex, and re-association for a second phosphorylation [42]. Such a mechanism indicates that a transient docking complex between the kinase and the substrate exists long enough to allow a single phosphorylation event. Other evidence of a docking complex mediating phosphorylation came from product inhibition studies with ERK2 and a protein substrate Ets Δ 138 indicating that the monophosphorylated form of Ets Δ 138 could form an unproductive docking complex with ERK2 in the absence of active site interactions [7]. This study also suggested that both the nucleotide and protein substrate could bind ERK2 in a random order mechanism while other another study suggested that the homologous protein p38 MAPK α binds the protein substrate prior to the nucleotide in an ordered sequential mechanism [39] suggesting that the order of substrate binding may differ amongst MAPKs or perhaps may even be substrate dependent [43]. We have also used transient state kinetics to demonstrate that both phosphoryl-transfer and product release are partially rate-limiting for ERK2 phosphorylation of Ets Δ 138 [44].

ENZYMIC MAPK EXOSITES

Protein kinases are thought to mediate protein–protein interactions through enzymic exosites that are spatially distinct from their active sites. While the active site mediates ATP binding and phosphoryl-transfer to the hydroxyl group of a protein substrate, the exosite is thought to mediate recognition of interacting proteins and regulate its activity, localization, and catalytic properties. A protein kinase exosite was first identified by Kallunki *et al.* who showed that JNK2 residues that lie outside of the active site mediated binding to the substrate GST-c-jun 25-fold more efficiently than the homologous protein JNK1. These results were obtained using Western blot analysis after loading equal amounts of JNK onto a GST-c-jun column and assaying for retention of the JNKs. When residues 208-230 of JNK2, located in the L13 and α_G region based on the JNK3 structure (Figure 5a, JNK3, yellow), were swapped with homologous residues from JNK1 to form a chimera, the ability of the chimera to bind the substrate c-jun³ was reduced 25-fold [45]. Alternatively, the reverse experiment allowed a JNK1 chimera with residues 208-230 from JNK2 to bind c-jun more efficiently. These results indicate that the JNK2 residues of this region mediate c-jun binding and that a similar region in JNK1 is unable to bind c-jun as efficiently. Phosphorylation of c-jun by JNK was more efficient with the JNK2 residues as well indicating that an efficient exosite may enhance

³ HA-JNK2, immunopurified from Jurkat cells treated with 50 ng/mL of anisomycin, was added to a glutathione-agarose-GST-c-jun¹⁻⁷⁹ affinity resin and found to bind 25-fold more efficiently than HA-JNK1 in an immunoprecipitation study followed by a Western blot. HA-JNK2 phosphorylated the substrate c-jun ~3-fold more “efficiently” than HA-JNK1. Substitution of homologous JNK1 residues into the 208-230 region of JNK2 caused the binding of the chimeric JNK2 to decrease 25-fold and phosphorylation to decrease 3-fold, indicating that the substituted amino acids were involved in docking and phosphorylation of c-jun. The reverse experiment allowed a JNK1 chimera containing JNK2 residues 208-230 to bind c-jun 30-fold greater than JNK1 increased c-jun phosphorylation 5-fold. No effects on the JNK/c-jun docking complex formation occurred as a result of anisomycin stimulation (it is unclear whether the chimeras are activated). Data was similar using a GST-JNK affinity resin to bind ³⁵S-labeled c-jun generated *in vitro*. The K_m of JNK1 and JNK2 towards c-Jun was determined to be 2.5 μ M and 0.4 μ M, respectively.

substrate phosphorylation. An exosite in a similar region of a homologous protein kinase was seen several years earlier in cyclic AMP-dependent protein kinase binding to a peptidyl protein kinase inhibitor (PKI) [46]. In a co-crystal structure, the *N*-terminal α -helical portion of PKI lies in the same groove as the proposed exosite for JNK2 proposed by Kallunki *et al.* Both of these early studies indicated that protein kinases could recognize protein substrates at regions distinct from the active site.

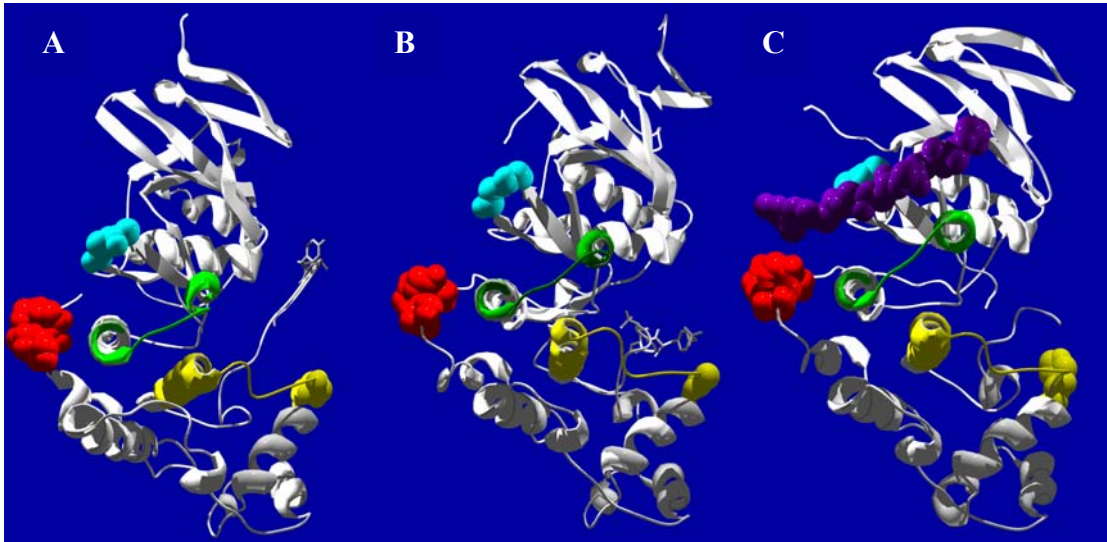


Figure 5. Structural representation of proposed exosites on JNK3, ERK2, and p38 MAPK α . The crystal structures of (a) inactive JNK3 (PDB: 1JNK), active ERK2 (PDB: 2ERK), and inactive p38 MAPK α bound to a MEF2a docking motif peptide (PDB: 1LEW) are shown. The yellow region represents the JNK docking exosite for c-jun located in the L13 and α_G helix and the homologous region in ERK2 and p38 MAPK α (JNK3: residues 246-268; ERK2: 209-231; p38: 206-228). The red region represents the CD and YY exosites located in L16 conserved amongst MAPKs (JNK3: 362-368; ERK2: 314-320; p38: 311-317). The cyan region represents the TT/ED exosite located in L11 (β_7 - β_8 reverse turn) (JNK3: 199-200; ERK2: 157-158; p38: 160-161). The green region represents the MAPK docking groove for DEJL docking peptides located in α_D -L8- α_E (JNK3: 154-165; ERK2: 111-123; p38: 114-126). The purple peptide represents the MEF2a docking motif peptide. The phosphorylation loop is shown with the Thr- and Tyr- residues highlighted (grey sticks) in JNK3 (middle right), ERK2 (middle right), and absent in inactive p38 MAPK α (broken strand).

Recently, several proposed exosites for MAPK-interacting proteins have been identified on ERK2. The CD exosite of ERK2 (Figure 5b, red), also conserved in the related MAPK family members (red), is thought to mediate both the cellular localization of ERK2⁴ [47] and the ability to bind⁵ its activators (MAPKKs), inactivators (MKPs),

⁴ As measured from the ability of overexpressed ERK2 to stay localized in the cytoplasm in the presence of overexpressed MAPKK1 in CHO cells under unstimulated conditions.

and substrates [17]. The CD exosite, composed of acidic residues, has been shown to mediate the binding of several different proteins including MKP3, MNK1, MAPKK1 [17], MSK1, and RSK2 [11]. Nearby hydrophobic residues Tyr-314 and Tyr-315 form the YY exosite in ERK2, also conserved among MAPKs, and have been suggested to mediate the localization of ERK2 [47] and MAPKK1 binding⁶ [48]. The TT/ED exosite (Figure 5, cyan) of ERK2/p38 MAPK α , is thought to regulate the specificity determination of MAPK substrates in conjunction with the CD exosite for the binding⁷ of interacting proteins such as MAPKAPKs [11]. PEA-15, is thought to bind an exosite on inactive ERK2 at the α_G helix as well as the MAP kinase insert region (243-273) (although data not shown) [31] in a similar site as that proposed to mediate ERK2–MAPKK1/2 binding [12] and JNK/c-jun binding [45].

In addition to the CD and TT/ED, other exosites have been identified in p38 MAPK α , which has 46% sequence similarity to ERK2. The α_D -L8- α_E region (Figure 5, green ribbon) was originally identified as an exosite thought to mediate MAPKAPK-2/3 binding and phosphorylation⁸, and interestingly, did not affect similar interactions with

⁵ Immunoprecipitations using lysates from NIH-3T3 cells showed that HA-MEK1 (*xenopus*), Myc-MKP3 (*rat*) and Myc-MNK1 (*hum*) could co-immunoprecipitate with WT ERK2 (*xenopus*) but not D321N ERK2. Mutation of D321N/D324N decreased binding further. S323D increased binding to MEK1. The MEK1 peptide (1-30) was able to inhibit HA-ERK2 from binding MEK1, MKP3, and to a lesser extent MNK1 (figure 2c).

⁶ Immunoprecipitations were performed using HEK293 cells co-transfected with mutants of Myc-ERK2 and HA-MAPKK1. The Y314/315A and the D316/319A E320A ERK2 mutants both showed a small decrease in the ability to co-immunoprecipitate with HA-MEK1.

⁷ TT/ED and CD site mutants (E160T/D161T to make the TT/ED domain ERK-like and D313/315/316N, respectively) were made in human HA-p38 MAPK α and co-transfected with human Myc-3pk in NIH3T3 cells. The ERK2-like p38 MAPK α and CD mutant exhibited a decreased ability to co-immunoprecipitate with 3pk. The double mutants were unable to bind indicating that both p38 MAPK α sites contribute to 3pk binding. The p38like-ERK2 (*xenopus*, T157E/T158D and S318D) mutant was able to co-immunoprecipitate with Myc-3pk and MSK2, whereas, WT ERK2 could not. In the case of MSK2 binding, the TT/ED site was more important than the CD site.

⁸ Both p38 MAPK α and p38 MAPK δ can phosphorylate the substrates ATF-2 and MBP, the former can also phosphorylate both MAPKAPK2 and 3, while the latter can not. A chimera was made in which residues 110-184 from p38 MAPK α were replaced with the homologous residues 111-184 of p38 MAPK δ leading to a total of 12 amino acid changes that lie between residues 114-127. The chimera could not co-immunoprecipitate or phosphorylate MAPKAPK2 or 3 while it maintained the ability to phosphorylate

ATF-2 and MBP [49]. Later, it was shown that point mutations within this region, I116A and Q120A, disrupted p38 MAPK α binding⁹ to the transcription factor MEF2; the former mutant could not bind a constitutively active form of MAPKK3b [27]. These results indicate that MAPKs have several exosites thought to be involved in protein-protein interactions, each of which may be the exosite for various proteins to dock *via* substrate docking motifs.

MAPK-INTERACTING DOCKING MOTIFS

Docking motifs are short peptidyl sequences located on MAPK interacting proteins that function to recognize kinase exosites to form a tethered docking complex between the two. In several cases deletion or mutation of the docking motif ameliorates the protein kinases ability to phosphorylate the substrate indicating their importance in mediating phosphorylation [50-52]. Indeed, MAPK substrates that contain both a docking motif and a consensus phosphorylation sequence surrounding the phospho-acceptor are more efficiently phosphorylated¹⁰ [51]. Several docking motifs have been identified in activators, substrates, and phosphatases including the DEJL, DEF, and RSK-like motifs which mediate MAPK protein-protein interactions and recent biochemical and structural studies have elucidated their binding sites on p38 MAPK α and ERK2 [27, 28].

ATF2 and MBP indicating that the swapped residues may be an exosite for MAPKAPK2/3 but not ATF2 or MBP.

⁹ HA-p38 MAPK α (murine) and either MEF2A or MAPKK3b(EE) were co-transfected in HEK 293 cells and immunoprecipitated using an anti-HA antibody.

¹⁰ c-Jun has a docking motif for JNK2 and two major Ser-Pro phosphorylation sites, whereas a related substrate, JunB, has a docking motif but lacks the P+1 prolines in the phosphorylation sites. Adding a proline at the P+1 positions of the two homologous JunB serines (Ser-63 and Ser-73 of c-jun) allows JunB

THE DEF DOCKING MOTIF

The DEF motif was found in a genetic study and coined by Jacobs *et al.* to describe a docking for ERK/FXFP that was composed of a consensus sequence of Phe-X-Phe-Pro (FXFP), where X represents any amino acid [19]. A DEF motif is thought to mediate ERK2 binding to several ETS family proteins. The two phenylalanine residues contribute most of the binding energy and can be substituted to tyrosines and retain functional docking. Peptides resembling a DEF motif act as general inhibitors of ERK2 function [19]. The reason for general inhibition may be due to the fact that the DEF peptide (Elk-1 residues 391-399: PRSPAKLSFQFP) contained a phosphorylation consensus sequence (SP) as well as an FXFP motif and could possibly bind the active site region of ERK2 [28]. If this were the case, general inhibition of the kinase could be due to blockade of the active site in addition to exosite binding. As mentioned earlier, a study using deuterium hydrogen exchange in the presence of the DEF peptide to predict ERK2 exosites was carried out and suggested that the peptide protected amide exchange in regions near the active site including α_F helix, α_G helix, and the MAPK insert region [28]. Therefore, the DEF peptide may dock into the active site of ERK2 causing protection from amide exchange or, alternatively, bind the α_F/α_G helix and the MAPK insert region inducing conformational changes that affect movement within the active site. Conformational changes distal to peptide binding sites have been shown for MAPKs using docking motif peptides [27]. The authors claim that the DEF motif binding pocket is occluded in inactive ERK2 [28] (K. Cox). Since the DEF motif has a phosphorylation

to be phosphorylated similar to c-jun following UV irradiation of F9 cells as measured by phospho-peptide mapping.

site (SP motif), it could be also be argued that the peptide does not bind inactive ERK2 due to P+1 exclusion of the proline from the active site of ERK2.

THE DEJL DOCKING MOTIF

The DEJL docking motif was also coined by Jacobs *et al.* to describe a docking-site for ERK/JNK LEL (DEJL) [19] composed of a consensus sequence of several basic residues followed by a ϕ -X- ϕ motif (where ϕ is a hydrophobic residue and X is any residue and usually basic). The DEJL motif is similar to the kinase interaction motif (KIM) found in phosphatases [53] and the D-domain found in MAPK substrates [29]. KIM peptides inhibit MAPKK2 binding and phosphorylation of ERK2, ERK2 phosphorylation of Elk-1, and MKP1 dephosphorylation of ERK2 [54] indicating that the KIM inhibition occurs at an exosite on ERK2 important for many different types of protein-protein interactions such as activator, substrate, and regulator binding, respectively. It was thought that the KIM may form a docking complex with the CD exosite of ERK2 since the CD site is thought to regulate similar protein-protein interactions [17]. However, a recent co-crystal structure of two DEJL-like peptides, derived from the activator MKK3b and the substrate MEF2a, bound to inactive p38 MAPK α suggest that neither peptide shows direct contact with the CD exosite and instead binds the nearby β 7- β 8 reverse turn [27]. Hydrogen exchange experiments verified the p38 MAPK α docking groove for DEJL motifs and also verify a similar binding region in the active form of ERK2 for a DEJL peptide derived from Elk-1 [28].

A MAPKAPK/RSK-LIKE DOCKING MOTIF

Another type of docking motif similar to the KIM/DEJL/D-domain motifs, found on the C-terminus of MAPKAPKs, such as RSK, contains both basic and hydrophobic residues and is critical for *in vivo* activation by ERK2 [55, 56]. The RSK docking motif mediates binding between inactive ERK2 and RSK but upon phosphorylation of RSK at a residue near to the docking motif, binding is disrupted so that active ERK2 cannot bind RSK [57]. Hydrogen exchange showed that the RSK docking peptide also bound to the docking groove exosite of ERK2 thought to bind DEJL motifs [28].

DOCKING MEDIATES ENZYMATIC SPECIFICITY

Docking motifs are thought to mediate binding to the protein kinase exosite and are found on variety of different proteins including substrates, regulators, and activators. Docking motifs that differ amongst homologous substrates may specify phosphorylation by a specific kinase. Docking motifs have been genetically switched causing a switch in substrate specificity by a kinase. For example, p38 MAPK α can phosphorylate MAPKAPK1 *in vitro* and *in vivo* in response to stress when an ~35 residue docking motif from its normal substrate MAPKAPK2 is attached to MAPKAPK1 [58] while under similar conditions p38 cannot phosphorylate MAPKAPK1. Phosphatase activity of Ptp3 towards Fus3 (MAPK) is dependent upon the non-catalytic amino-terminal docking motif of Ptp3 [59] and the amino-terminal docking motif on MAPKK1 is required for the binding and activation of ERK2 [60] indicating the importance of docking motifs in mediating phosphorylation and dephosphorylation of MAPKs in addition to determining MAPK substrate specificity.

DEJL MOTIF SPECIFICITY

The DEJL motif residues are highly variant and can be found in substrates for ERK, JNK, and p38 MAPK indicating that a DEJL motif alone does not determine the specificity of phosphorylation. Perhaps subtle differences exist in DEJL motifs which help to mediate specificity. Some substrates containing a DEJL motif are phosphorylated by several kinases indicating the lack of specificity that these domains achieve. For example, Elk-1 is a substrate for JNK, p38 MAPK, and ERK2, SAP-1 and SAP-2 are substrates for ERK and p38, and ATF-2 has been shown to be phosphorylated by p38, JNK [61], and ERK [62]. In addition, both ERK2 and p38 MAPK α have been shown to bind DEJL motifs in a homologous docking groove exosite [27, 28] although DEJL motifs specific for each MAPK were used, it will be interesting to determine the specificity of each DEJL motif for the different MAPKs.

REGULATION OF MAPK DOCKING INTERACTIONS

Docking complexes between MAPKs and their interacting proteins determine the specificity of their binding events. The ability to form a docking complex can be regulated by both phosphorylation and proteolytic cleavage. In some cases, the ability of docking motifs to bind exosites is regulated by the phosphorylation state of either the MAPK or the interacting protein [57, 63]. However, other kinetic evidence indicates that substrate phosphorylation does not affect the docking complex formation as seen by the ability of dual-phosphate ERK2 to form a docking complex with Ets Δ 138 regardless of the phosphorylation state of Ets Δ 138¹¹ [42]. Phosphorylation of ERK2 causes

¹¹ The K_m of Ets Δ 138 for activated ERK2 was similar to the K_i of phosphorylated Ets Δ 138 indicating that they bind ERK2 with similar affinities.

destabilization of the docking that occurs between cytosolic inactive ERK2 and its substrates MNK [64], RSK [57, 65], and MAPKK1 [66]. Phosphorylation of Ser-231 in the docking motif of the phosphatase PTP-SL causes a decrease in ERK2s ability to bind the phosphatase and causes ERK2 translocation into the nucleus [67]. Other protein substrates, such as GST-Elk-1³¹⁰⁻⁴²⁸ and IEX-1, can increase their affinity for ERK2 when ERK2 is phosphorylated [29, 68] indicating that phosphorylation can both positively and negatively regulate docking complex formation. Alternatively, a protein component of the anthrax toxin known as lethal factor proteolytically cleaves the *N*-terminal docking motif of MAPKKs [69] eliminating their ability to bind and activate ERK2 [60]. Therefore, docking complexes between MAPKs and their interacting proteins can be positively and negatively regulated by phosphorylation and negatively regulated by proteolysis.

PROLINE BINDING POCKET

The crystal structure of activated ERK2 reveals a proposed substrate binding pocket that is accessible to the P+1 proline of a MAPK protein substrate in its active site (Figure 6) [4]. Alternatively, the inactive structure of ERK2 indicates that the proline binding pocket is blocked by Arg-192 [70]. The P+1 proline binding region is conserved among the proline-directed MAPKs and is also conserved with an unrelated proline-directed kinase termed the cyclin-dependent kinase (CDK). Other kinases do not preferentially bind and phosphorylate substrates with a P+1 proline as different kinase families have differing phospho-acceptor recognition motif specificities [8]. The P+1 binding pocket of ERK2 consists of residues 185-192 (YVATR^WYR) in the phosphorylation lip of ERK2 that is recognized and phosphorylated by MAPKK1 for

ERK2 activation. Interestingly, one of the two phosphorylated residues on active ERK2 (phosphorylated Tyr-185, cyan, Figure 6) is responsible for forming the proline binding pocket. Upon phosphorylation and activation of ERK2, Tyr-185 forms two hydrogen bonds with Arg-192 which blocks the proline binding pocket in the inactive structure. Phosphorylation allows the phosphorylation lip to flip toward the active site to form the proline binding pocket. Val-186 and Ala-187 also bind to Arg-192 to form the proline binding pocket. The binding pocket is thought to only mediate the binding of prolines in the trans-configuration and exclude those in the cis-configuration. This is not surprising as only 5% of all prolines in protein structures are in the cis-conformation and it has been shown that the trans-configuration of the P+1 is preferred for catalysis by ERK2 [71]. Amino acids larger than proline at the P+1 position were hypothesized to be excluded due to blockage by Arg-192 and amino acids such as glycine and alanine were hypothesized to be unstructured and not amenable to catalysis [4]. It has been shown that peptides containing serines or threonines followed by a proline at the P+1 position (a MAPK recognition motif) are efficiently phosphorylated by ERK [9] and that removal of the P+1 proline leads to less efficient phosphorylation. It has also been shown that addition of prolines C-terminal to a serine phospho-acceptor to a protein substrate with a MAPK docking motif can convert a protein that was not an efficient substrate into an efficient protein substrate [51]. These results suggest that both a docking motif and a P+1 proline are required for efficient substrate phosphorylation.

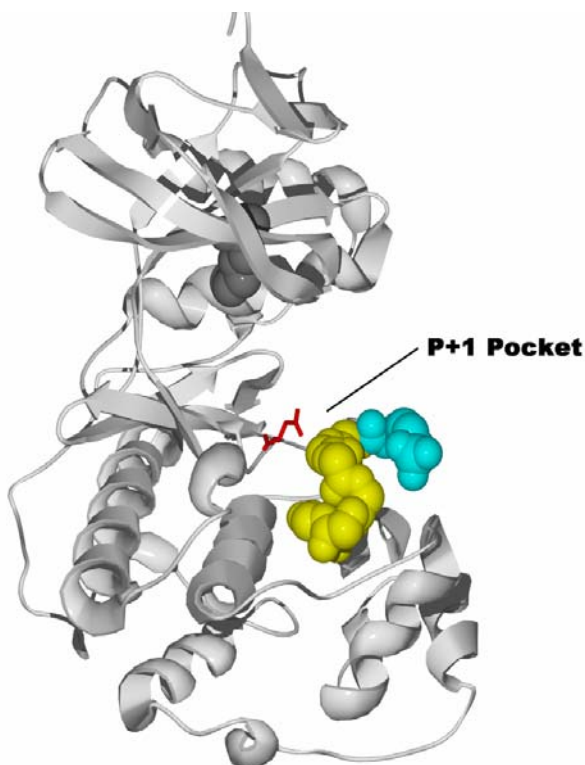


Figure 6. Structural representation of the proposed P+1 binding pocket on ERK2. A ribbon diagram of the activated dual-phosphate form of ERK2 (taken from the PDB file 2ERK) is shown with the active site Lys-52 (dark gray) and the catalytic base (Asp-147) as a reference with the proposed P+1 proline binding pocket composed of residues 185-192 (YVATR WYR, yellow/cyan). One of the phosphorylated residues of ERK2 (Tyr-185, cyan) is thought to form the proline binding pocket along with residues 186-192 (yellow). Tyr-185, Val-186, and Ala-187 bind Arg-189 in the active structure which excludes P+1 binding in the inactive ERK2 structure. The proposed catalytic base is shown in red (Asp-147).

SUBSTRATE PHOSPHORYLATION

A model has been proposed for substrate phosphorylation in which docking motifs and enzymic exosites mediate a protein-protein interaction between the protein kinase and the protein substrate followed by the phosphorylation of the substrate's

phospho-acceptor [29, 51]. It has also been suggested that these docking events are not involved in enzyme/substrate complexes [72] assuming significant non-productive binding or that docking to an inactivated kinase is not the same as docking to activated proteins. However, this hypothesis was not tested using an activated version of the MAPK containing an exosite to phosphorylate a protein substrate containing a docking motif which might lead to an alternate hypothesis. Our laboratory has characterized an activated protein kinase (ERK2) and proposed the role of the docking complex [7] in mediating the phosphorylation of a protein substrate (EtsΔ138) containing a docking motif [52].

Highly Specific Enzymatic Interactions

MAPKK–MAPK DOCKING

MAPKKs show a high degree of specificity for their cognate MAPK members during signal transduction which is crucial for the fidelity of the cellular response. High-affinity docking complexes ($K_d \sim 5$ nM)¹² are formed between the MAPK yeast homologs Ste7 (MAPKK) and Kss1/Fus3 (MAPK), however, mutation of the MAPK phospho-acceptor region decreased the apparent affinity of the complex by 10-fold [72] indicating that the enzymic active site of MAPKs may contribute to the highly specific docking complexes formed between MAPKKs and MAPKs in yeast. It was suggested

¹² The apparent K_d is based on the immunoprecipitation of *in vitro* translated proteins that were partially purified by ammonium sulfate precipitations. The immunoprecipitation was carried out “using very brief washes with ice-cold buffer”. Ste7 (1 pmol) was immunoprecipitated in the presence and absence of Kss1 or Fus3 (1 pmol). The affinity was determined by calculating the amount of complex formation based on how much Kss1 or Fus3 bound to Ste7 using the equation $K_d \sim ([A]_{eq} \times [B]_{eq})/[AB]_{eq}$. In the absence of Ste7, Kss1 and Fus3 were not immunoprecipitated and other yeast MAPKs such as Hog1 and Mpk1 as well as a mammalian MAPK (ERK2) were not precipitated under these conditions.

that these high-affinity complexes do not facilitate catalysis because dissociation of the two proteins occurs prior to the phosphorylation of the substrate upon the addition of MgATP^{2-} [72]. However, it is not mechanistically clear in this study whether MgATP^{2-} can bind to the activated kinase Ste7 in the presence of the docked MAPK substrate (Kss1 or Fus3). Our laboratory has shown that in the case of activated mammalian ERK2, MgATP^{2-} has access to the active site even in the presence of the docked protein substrate EtsΔ138 [7]. Later studies by Bardwell *et al.* show that human MAPKK1 and MAPKK2 bind to GST-ERK1 (human) and GST-ERK2 (rat) with apparent affinities in the low micromolar range ($K_d \sim 9 \mu\text{M}$ and $29 \mu\text{M}$, respectively) and that the deletion of the *N*-terminal docking motif on the MAPKKs led to a 5-10-fold decrease in affinity¹³ [73] indicating the importance of the docking motif in determining the specificity of binding. However, the contributions of the active site interactions were not addressed for the mammalian proteins. These studies indicate that docking complexes are formed between both active and inactive enzymes and their substrates and that mutation of active site residues such as phospho-acceptors can lead to weaker docking interactions. It is interesting to note that the mammalian MAPKK–MAPK docking complexes [73] are weaker than those from yeast [72].

MAPK–MKP DOCKING

Another highly specific interaction in the MAPK signaling pathway is that of the MKPs and their cognate MAPKs which is also crucial for the fidelity of the cellular response. Activation of ERK2 by dual-phosphorylation is reversible by

¹³ Radio-labeled MAPKKs were translated *in vitro*, partially purified by ammonium sulfate precipitation, and allowed to bind glutathione-agarose-GST-ERKs affinity resins that had been expressed and purified from bacteria.

dephosphorylation by the enzyme MKP3. MKP3 is an ERK2-specific phosphatase and is one of the phosphatases responsible for the regulatory control of ERK2 activity. MKP3 forms a tight docking complex with ERK2 ($K_d \sim 170$ nM) [14], and can act as a dual-specificity phosphatase to dephosphorylate both Thr-183 and Tyr-185 [74]. Tight-binding is achieved through a KIM located in the N-terminal region of MKP3 (residues 61-75) that contributes to the docking complex [35]. The KIM contains a positively charged sequence cluster that is thought to bind to the CD exosite of ERK2 due to evidence that the KIM sequence competes with other proteins thought to bind the same exosite [54]. ERK2 also stimulates para-nitrophenyl phosphate hydrolysis by MKP3 indicating that the general phosphatase activity is stimulated in the presence of its natural substrate ERK2 [33]. Other phosphatases increase their enzymatic activity when bound to their natural substrates indicating that specific binding to MAPKs through docking motifs may lead to their specific inactivation by phosphatases. MKP3 also contains a DEF motif that is required for the activation of MKP3 phosphatase activity by ERK2 [35] indicating that both a KIM and a DEF motif are involved in docking complex formation. Site-directed mutagenesis has shown that residues of ERK2 may differentially regulate the binding and activation of MKP3 (Figure 7) suggesting that the two interactions can be separated from one another.

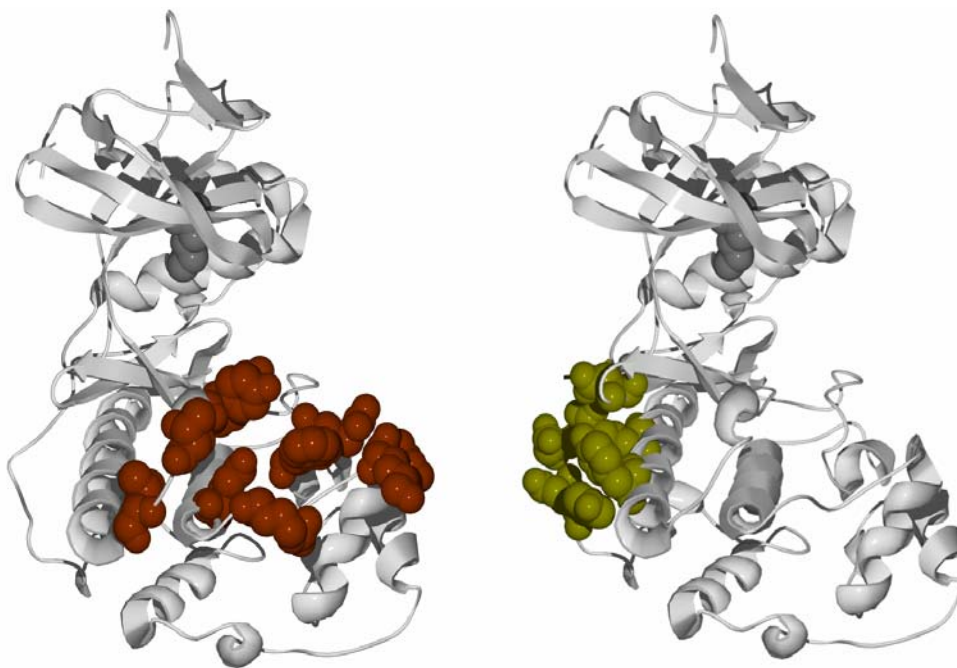


Figure 7. Structural representation of the proposed MKP3 activation and high-affinity binding exosites on ERK2. A ribbon diagram of the activated dual-phosphate form of ERK2 (PDB: 2ERK) is shown with the active site Lys-52 (dark gray) as a reference with the proposed MKP3 activation site composed of residues Tyr-111, Thr-116, Leu-119, Lys-149, Arg-189, Trp-190, Glu-218, Arg-223, Lys-229, and His-230 highlighted in brown. This region is distinct from the active site and the MKP3 high-affinity binding site composed of residues Tyr-314, Asp-316, Asp-319, Glu-79, Tyr-126, Arg-133, and Asp-160 highlighted in green. Asp-319 is the most critical residue involved in the binding of MKP3 and all of these residues are centered at the CD exosite of ERK2, a negatively charged cluster of residues.

Non-Enzymatic Protein-Protein Interactions with MAPKs

Phosphoprotein enriched in astrocytes-15 kDa (PEA-15), a protein with a death effector domain implicated in apoptosis, has a docking motif for ERK2 that does not correspond to known docking motifs [31]. Although PEA-15 binds ERK more readily than p38 and JNK, it is not a substrate of ERK2 but is a substrate of PKA [75]. PEA-15

is thought to anchor ERK2 in the cytoplasm as deletion of PEA-15 causes increased ERK2 entry into the nucleus and subsequent increase in c-fos transcription and overexpression of PEA-15 decreased the ability of ERK2 to enter the nucleus after serum stimulation resulting in decreased Elk-1 phosphorylation and subsequent decreased transcriptional activity due to its retention in the cytoplasm [75]. Furthermore, PEA-15 was shown to bind both active and inactive ERK2 indicating that phosphorylation of ERK2 does not affect PEA-15 binding. However, our laboratory has data to suggest that phosphorylation of ERK2 does alter the affinity of PEA-15 (K. Cox). The NMR structure of PEA-15 has been determined and NMR footprinting was carried out in the presence of ERK2 to find residues of PEA-15 involved in binding ERK2 and the importance of individual residues in mediating ERK2 binding were elucidated using a GST-pulldown assay [31]. PEA-15 is thought to bind ERK2 in the α_G helix and the α_{1L14} helix of the MAPK insert, specifically ERK2 residues Y213, L232, K257, and R259 were found to disrupt binding after mutagenesis to glutamic acid [13]; these ERK2 mutants were reported to have no defects in their ability to be activated by a MAPKK. The same region of ERK2 was shown to be important for ERK2–MAPKK1/2 interactions where ERK2 mutants H230R, N236K, Y261N, and S264P showed decreased interactions with MAPKK1/2 and also exhibited defects in MBP phosphorylation as determined by an increase in the K_m [12]. We also have data that suggests that ERK2 residues Lys-229 and His-230 near the α_G helix may mediate docking interactions with Ets Δ 138 (Rainey).

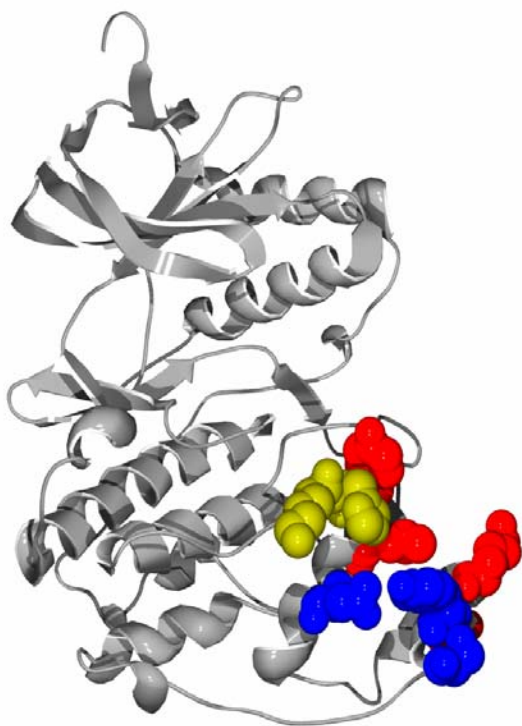


Figure 8. A structural representation of the ERK2 exosite involved in PEA-15, MAPKK1/2, and EtsΔ138 binding. A structural representation dual phosphorylated ERK2 (2ERK) is shown where the residues in red represent residues involved in PEA-15 binding, the residues in blue represent residues involved in MAPKK1/2 binding and phosphorylation of ERK2 and MBP phosphorylation (His-230, Asn-236, Tyr-261, and Ser-264), and the residues in olive represent those residues involved in EtsΔ138 binding and phosphorylation.

Conclusions

In this review of MAPK signaling, we have discussed the importance of protein–protein interactions in mediating the fidelity of signal transduction from the cell surface to an intracellular response with respect to EGF-induced signaling. Specific protein–protein interactions in this pathway and others ensure the fidelity of signaling and are driven by the ability of proteins to recognize one another. These interactions can be

regulated by conformational changes, chemical catalysis such as phosphorylation and dephosphorylation, they are temporally and spatially dependent, and cell-type and cell-state dependent. We specifically detail protein–protein interactions of the MAPK family and how these interactions can be regulated with respect to binding their upstream activating kinases (MAPKKs), their substrates, and their regulators (phosphatases, MKPs).

A variety of techniques have been used in which sites of interaction on the MAPK and its interacting proteins have been elucidated. Computational studies have been carried out by comparing sequence homology amongst MAPK subfamily and family members to determine residues conserved amongst the subfamilies that differ amongst other family members to discern residues and regions of specificity determination. Genetic studies have been critical in the elucidation of docking motifs on substrates and exosites on the MAPK that mediate protein–protein docking complexes. The yeast 2-hybrid system has been useful for detecting residues involved in specific protein interactions that are absent in others and also to identify novel MAPK binding partners. Although, no co-crystallization studies exist with a MAPK bound to a protein substrate, co-crystals have been produced in which DEJL peptide docking motifs are bound to a MAPK exosite giving insight to the regions of MAPKs that bind interacting proteins to form a docking complex. Hydrogen exchange mass spectrometry confirmed the co-crystal results and identified a novel DEF peptide exosite on a MAPK. And footprinting studies have allowed the detection of residues involved in docking MAPKs.

Quantifying protein–protein interactions is also of importance in order to better understand the specificity of interactions and how they are regulated by phosphorylation. Classic analysis of protein–protein interactions have utilized non-quantitative immunoprecipitation or pull-down studies but give little insight to the strength, duration,

and regulation of the protein–protein interactions. Therefore, we have outlined several techniques now being used to quantitate binding events with MAPKs and their substrates. ITC, SPR, and fluorescence anisotropy/polarization experiments have been used to discern the K_d values of protein–ligand, protein–peptide, and protein–protein interactions. The strength of ITC is that it measures enthalpy changes and thermodynamic parameters of the interaction but has the disadvantage of using a lot of protein. The strength of SPR is that it uses smaller amounts of protein and measures both on rates and off rates but has the disadvantage of measuring these values for a protein bound in a solid-state. Fluorescence anisotropy has the advantage of measuring protein–protein interactions in solution using relatively small amounts of protein but has the disadvantage of a fluorescently labeled protein or ligand.

All of these techniques can be used to discern sites of interaction, quantify the interactions, and used in conjunction with steady-state and pre-steady state kinetics to understand protein kinases and their interactions with other proteins. In conjunction with mutagenesis, enzymic exosites and MAPK interacting docking motifs have shown to be required for efficient protein–protein interactions to generate a docking complex and mediate the enzymic specificity of signaling, phosphorylation, and dephosphorylation events. Efficient substrate phosphorylation requires both a docking interaction as well as specific recognition of the phospho-acceptor and the P+1 proline in the active site of MAPKs. Our goal is to achieve a thorough understanding of the MAPKs and how they interact with other proteins to carry out specific cellular signaling. Once this has been achieved we can begin to design novel inhibitors to disrupt specific protein–protein interactions that will abrogate specific cellular signaling pathways.

CHAPTER 2: PHAGE DISPLAY IDENTIFIES NOVEL PEPTIDES THAT BIND ERK2 AND COMPETE WITH TRANSCRIPTION FACTOR BINDING

OVERVIEW

PURPOSE

Mitogen-activated protein kinases (MAPKs) such as extracellular signal-regulated protein kinase 2 (ERK2) phosphorylate a plethora of protein substrates within a cell. However, the mechanism by which ERK2 recognizes protein substrates prior to phosphorylation is poorly understood. It was hypothesized that ERK2 may recognize a subset of motifs or patches of amino acids on the surface of protein substrates [17]. To identify such peptide motifs, random peptides were displayed on the surface of phage and tested for their ability to bind the active form of ERK2 in a process known as biopanning [76]. DNA encoding each of the ERK2-binding phage was purified and sequenced to determine the amino acid composition of displayed peptides responsible for ERK2-binding.

APPROACH

The dual-phosphate form of ERK2 was purified, biotinylated, and immobilized in streptavidin-coated wells. Each round of phage display biopanning consisted of ERK2 immobilization, several washes to remove unbound ERK2, phage binding to ERK2, several washes to rid of unbound phage, and then the phage were eluted from biotin-

ERK2 (b-ERK2) using acidic conditions. Several rounds of phage display were carried out with an $X_2CX_{14}CX_2$ cyclic peptide library fused to the N-terminus of protein III on the surface of the phage. After several rounds of biopanning, phage clones selected for their ability to bind ERK2 were sequenced. Phage clones displaying the cyclic peptides were tested for their ability to bind b-ERK2 in the presence of a reducing agent, a small molecule substrate for ERK2 ($MgATP^{2-}$), and a protein substrate (Ets Δ 138) to test whether or not cyclization of peptides, small molecule binding, and protein substrate binding affect phage affinity for b-ERK2, respectively. One of the phage sequences was selected and a peptide with that sequence was chemically synthesized and assayed for its ability to inhibit the binding of $MgATP^{2-}$ and the protein substrate Ets Δ 138 using steady-state inhibition kinetics. The synthesized peptide was also assayed with a homologous protein kinase (p38 MAPK α) to test whether or not the peptide was specific for ERK2-binding.

RESULTS

B-ERK2 maintained its catalytic activity following immobilization and several washes as determined by its ability to phosphorylate EtsΔ138 when bound in the solid-state. The catalytic activity was dependent on the amount of plated b-ERK2. The number of eluted phage in each round of biopanning was also dependent upon the amount of plated b-ERK2. Several phage clones were identified that could bind b-ERK2 by both a phage attachment assay as well as an enzyme-linked immunosorbent assay (ELISA). Reduced phage binding to ERK2 was seen in the presence of a reducing agent, MgATP^{2-} , and EtsΔ138. A chemically synthesized peptide derived from these experiments, inhibited ERK2 phosphorylation of the protein substrate EtsΔ138, exhibiting competitive and mixed inhibition towards EtsΔ138 and MgATP^{2-} , respectively. Surprisingly, the same peptide displayed equally potent inhibition towards the phosphorylation of ATF2 by p38 MAPK α , a MAP kinase that has 46% sequence similarity to ERK2.

CONCLUSIONS

This study indicates that phage display can be used to identify peptides that bind the dual-phosphate form of ERK2. Furthermore, binding of selected phage to ERK2 was dependent upon the cyclization of the displayed peptides as detected by the reduction of binding in the presence of a reducing agent. Phage also displayed reduced binding in the presence of both a nucleotide and protein substrate indicating that either direct competition occurs between the phage and these ERK2 substrates or perhaps a conformational change occurs upon substrate binding to ERK2 that inhibits or excludes the phage from binding. Steady-state inhibition kinetics of ERK2 in the presence of a

chemically synthesized peptide indicates that the peptide directly competes with the EtsΔ138 binding site. However, the peptide shows mixed inhibition with MgATP²⁻ indicating that phage can bind to ERK2 whether or not it is bound to its nucleotide substrate. This study shows that active ERK2 can be targeted by phage display to find novel antagonists to kinase function and suggests that protein-binding sites within the MAPK family may contain conserved features that render them susceptible to ligand binding.

INTRODUCTION

Since the activation of ERK2 induced by growth factors stimulates cells to proliferate, many cancers and transforming agents utilize the MAPK cell-signaling pathway to carry out unregulated cell growth [77]. Therefore, ERK2 is an obvious target for the development of small molecule inhibitors for cancer therapeutics. However, development of antagonists specific to individual members of the protein kinase family has proven difficult due to the conservation of active site residues in the hydrophobic MgATP^{2-} binding pocket of protein kinases. Many inhibitors of protein kinases target the MgATP^{2-} binding site as seen in the case of polyhydroxylated flavones [78], isoquinolinesulfonamides [79, 80], and both pyridinyl imidazoles and triarylimidazoles [39, 81, 82] which inhibit cyclin-dependent kinase (CDK), cAMP-dependent protein kinase, and p38 $\text{MAPK}\alpha$, respectively. Unfortunately, these inhibitors often bind other enzymes that utilize MgATP^{2-} [83] and must compete with high intracellular concentrations of ATP ($3.2 \pm 1.7 \text{ mM}$) [84].

An alternative approach to kinase inhibition involves the use of peptides that resemble a consensus phosphorylation site that is recognized by an enzyme's active site [46]. Active site-directed peptide inhibitors, however, are not typically potent due to weak binding affinities and since several kinases tend to recognize similar phosphorylatable regions, they may also be fairly nonspecific. For example, both MAPKs and CDKs phosphorylate serine or threonine residues followed by a proline so a peptide inhibitor designed to inhibit a MAPK containing a Ser/Thr-Pro-like site may also inhibit a CDK. A recent approach physically linked $\text{ATP}\gamma\text{S}$ and a peptide inhibitor, both capable of binding the enzyme independently, to generate bisubstrate inhibitors that inhibit in the nanomolar range [85].

Another potentially more promising approach towards the inhibition of certain protein kinases is to block protein binding sites on the enzyme that lie distant to the active site. Some protein kinases, including members of the MAPK and CDK family, contain docking regions for proteins located outside of the active site [17, 86]. In the case of the MAPKs these regions regulate the specificity of interactions of the kinase with protein substrates, as well as with positive and negative regulators of their activity. The C-terminal region of ERK2 for example, contains acidic residues Asp-316 and Asp-319, that function as an exosite for the activator MAPKK1, the inactivator MAPK phosphatase 3, and several protein substrates including Elk-1, MAPK signal-integrating kinase 1, and ribosomal S6 kinase [11, 17]. Therefore, these putative exosites are attractive drug targets in that they may contain primary and/or secondary structure information specific to an individual kinase and its interactions with other proteins. Indeed, peptides with an Arg-X-Leu motif have been shown to disrupt substrate binding to CDK2 through such a mechanism [87].

Proteins that contain “hot-spots,” such as human growth hormone [88], integrins [89], and streptavidin [90], have evolved to bind small peptide motifs tightly. Hot spots have been proposed to be regions where intramolecular backbone hydrogen bonds are not sufficiently dehydrated. These bonds have been termed under-dehydrated hydrogen bonds (UDHBs) [91]. Thus, a UDHB on the surface of the protein may indicate a potential binding site, or hot spot, that can associate with proteins or peptides to exclude water from backbone hydrogen bond. Such hot spots have been elucidated using peptide phage display [92]. Phage display is a technique used to select phage that bind a protein of interest (referred to as a receptor of phage binding) from a large library of phage, each expressing a novel peptide on their protein coat. Each peptide is displayed as a fusion to a protein on the extracellular surface of the phage coat and can potentially be captured by

binding to the receptor protein. Each peptide is physically linked to its internal phage DNA allowing rapid identification. Using this technique, phage particles with a phenotype of interest can be selected through receptor binding and their genotype determined.

Previously, Zwick *et al.* used phage display to select peptides that bind ERK1/2 MAP kinase. However, a peptide substrate (TGPLSPGPF) was used to competitively elute the phage, presumably targeting only the phage that bind the active site [93]. The selected sequences found to bind ERK1/2 in their study, FHKPLKR and NPAHSPW, were not further characterized for their ability to bind or inhibit ERK1/2.

In this study, phage display was performed to select for novel peptides that bind an activated form of ERK2 using a disulfide-constrained peptide library fused to the phage minor coat protein III (pIII) using multiple rounds of affinity purification (biopanning) [92].

RESULTS AND DISCUSSION

PURIFICATION OF ACTIVE ERK2

A plasmid encoding both His₆-tagged ERK2 and a constitutively active form of MAPKK1 (MAPKK1G7b) [94] was transformed into BL21 cells, grown in the presence of 50 µg/mL carbenicillin, and induced with IPTG for 12 hours. During the induction and 12 hour incubation, MAPKK1G7b phosphorylated some of the ERK2 *in vivo* which was separated from the monophosphorylated and unphosphorylated forms of ERK2 in later procedures. The bacterial cells were pelleted by centrifugation and separation from the media, snap frozen, and lysed. All forms of ERK2 were purified using nickel-nitrilotriacetic acid (Ni²⁺-NTA) affinity chromatography to capture the His₆-tagged ERK2. The protein was washed and then eluted with imidazole which competes for Ni²⁺-NTA binding sites to release the Ni²⁺-NTA-bound His₆-ERK2. His₆-ERK2 was subjected to anion exchange chromatography using a Mono Q HR 5/5 column and eluted with a linear gradient of NaCl to separate non-, mono-, and the dual-phosphorylated (active) form of ERK2. When run on an SDS-PAGE gel, the active form of ERK2 can be discerned from the inactive form by a band shift toward slower mobility due to the incorporation of two phosphates (Figure 9) [7].

BIOTINYLATION OF ERK2

The dual-phosphate form of ERK2 was biotinylated so that it could be immobilized for phage display biopanning in streptavidin-coated wells. ERK2 was biotinylated on primary amine-containing side chains adding a 2:1 mol/mol ratio of

sulfosuccinimidyl-6-(biotinamido)hexanoate (sulfo-NHS-LC-biotin) to ERK2 in the presence of ATP. The sulfo-NHS-LC-biotin formed an irreversible carbamate bond with ERK2, thereby, biotinylating ERK2. ATP was added to competitively inhibit labeling of the active site lysine, Lys-52 [95], so that ERK2 could maintain its catalytic activity. Unreacted biotin was removed by buffer-exchange. To confirm the biotinylation of ERK2, a Western Blot was performed using a primary antibody to detect the biotin (Figure 9). B-ERK2 was also compared to unbiotinylated ERK2 to show that the observed catalytic rate constant (k_{obs}) of b-ERK2 was within 2-fold of unbiotinylated ERK2 (data not shown), indicating that biotinylation did not greatly affect the activity of the enzyme.

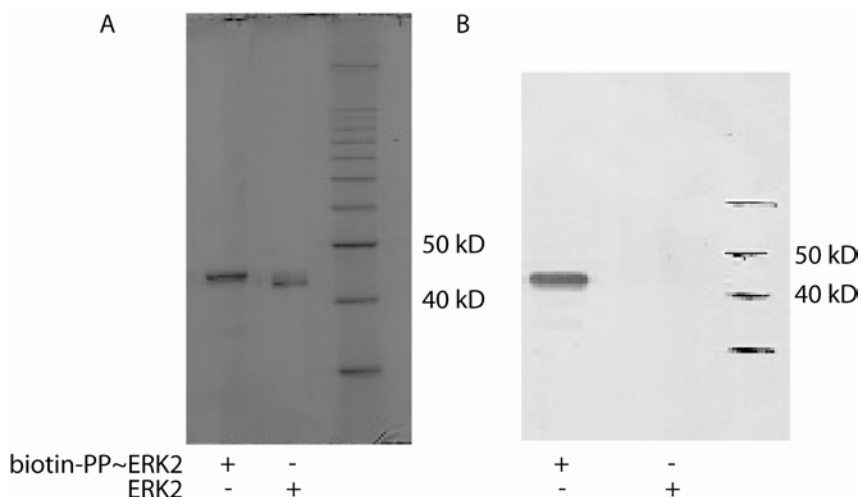
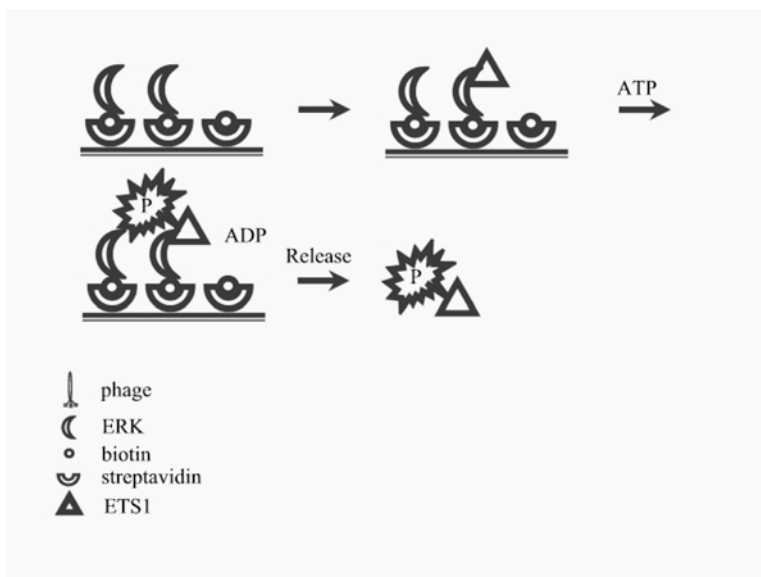


Figure 9. Western Blot of biotinylated active ERK2. (A) The dual-phosphate form of ERK2 was biotinylated (biotin-PP~ERK2) and separated on a 10% SDS-PAGE gel with inactive ERK2 that was not biotinylated. The dual-phosphate form of b-ERK2 migrated slower than inactive ERK2. The proteins were transferred from the gel to nitrocellulose using electrophoresis. (B) A Western Blot was performed on the nitrocellulose using a horseradish-peroxidase conjugated secondary rabbit anti-goat antibody (1:10,000) and primary goat anti-biotin antibody (1:10,000) as described by the manufacturer (Pierce).

IMMOBILIZED b-ERK2 IS ACTIVE

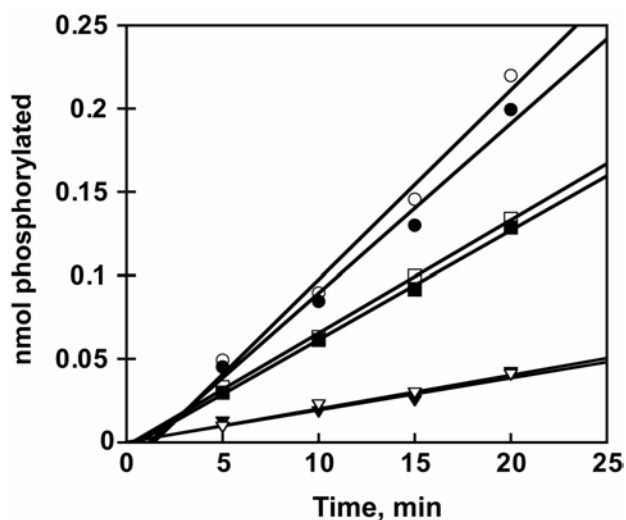
To carry out biopanning, b-ERK2 was immobilized in streptavidin-coated wells. To ensure that b-ERK2 maintained catalytic activity during biopanning and phage binding, b-ERK2 was immobilized, subjected to biopanning conditions prior to the addition of phage, and assayed for catalytic activity. Two different concentrations of b-ERK2 were captured in streptavidin-coated wells *via* high affinity biotin-streptavidin interactions, blocked with a non-specific protein bovine serum albumin (BSA), washed

several times with buffer to remove unbound b-ERK2 and BSA, then assayed by measuring initial rates of phosphate incorporation into the model protein substrate EtsΔ138 (Scheme 2, Figure 10a). Using the data from Figure 10a, the observed catalytic rate was determined by finding the slope of the line (k_{obs} immobilized $\sim 0.01 \text{ nmol min}^{-1}$ for 0.8 μg of plated b-ERK2).



Scheme 2. Catalytic activity assay of immobilized b-ERK2. B-ERK2 was immobilized in a streptavidin-coated well. The wells were washed once to remove the unbound b-ERK2 (not shown) prior to the addition of blocking buffer (not shown). The wells were washed 6× with buffer to prepare for the assay in either reducing or non-reducing conditions. Immobilized b-ERK2 assays were carried out in the streptavidin-coated wells by adding EtsΔ138 (triangle, ETS1) in assay buffer and then initiating the reaction with ATP. Over time, aliquots of the reaction were taken, spotted on P81 paper, washed, and counted to determine the number of phosphorylated EtsΔ138 molecules (P~ETS1).

A



B

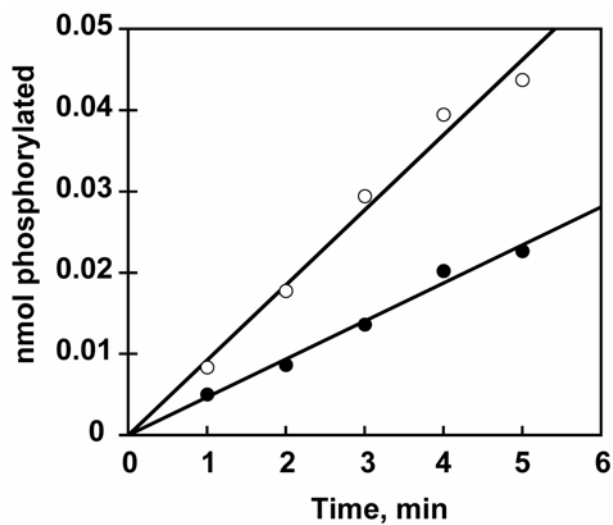


Figure 10. Immobilized b-ERK2 maintains activity during biopanning. (A) Two concentrations of plated b-ERK2 (0.8 μg , circles; 0.4 μg , squares) and unlabeled active ERK2 (0.9 μg , triangles) were immobilized in streptavidin-coated wells in buffer B0 for 1 h at 4 $^{\circ}\text{C}$, blocked with buffer B1 for 1 h, washed 6 times with buffer B0 in the presence (filled) or absence (open) of 2-mercaptoethanol. Assays were performed in a 100 μl volume using 11.3 μM Ets Δ 138, 10 mM MgCl_2 , 100 $\mu\text{g}/\text{mL}$ BSA, and 100 μM [γ - ^{32}P] ATP (500-1000 cpm pmol^{-1}) in buffer S0 at 25 $^{\circ}\text{C}$. (B) B-ERK2 (1.5 nM, open circles; 0.75 nM closed circles) were assayed as above without immobilization.

The specific activity of non-immobilized b-ERK2 was measured in solution by measuring initial rates of phosphate incorporation into EtsΔ138. The specific activity of b-ERK2 in solution was determined by finding the observed catalytic rate from the data in Figure 10b (the slope) and dividing by the mass of b-ERK2 (1587 nmol min⁻¹ mg⁻¹). Using Equation 1, the amount of active ERK2 immobilized during biopanning was determined (~ 6.3 × 10⁻⁶ mg). After converting to grams, Equation 2 was used to determine the number of molecules of active immobilized b-ERK2 (~ 9.0 × 10¹⁰) when using 0.8 μg of plated b-ERK2.

$$\text{Equation 1} \quad \frac{k_{\text{obs}} \text{ immobilized (nmol min}^{-1}\text{)}}{SA \text{ solution (nmol min}^{-1} \text{ mg}^{-1}\text{)}} = \text{immobilized active b-ERK 2 (mg)}$$

Equation 2

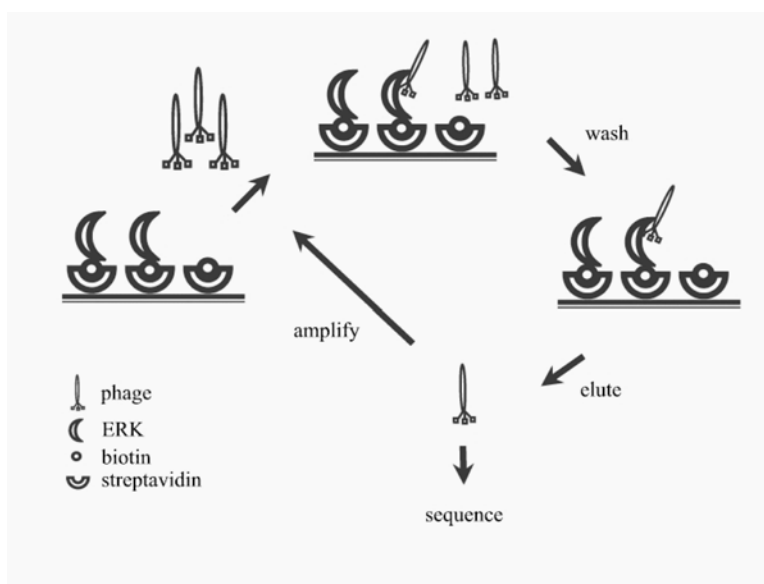
$$\frac{\text{active immobilized b-ERK 2 (g)}}{MW \text{ ERK 2 (g / mol)}} \times \frac{6.02 \times 10^{23} \text{ molecules}}{\text{mol}} = \# \text{ of immobilized molecules of b-ERK 2}$$

The catalytic activity of immobilized b-ERK2 increased when the amount of plated b-ERK2 was increased (Figure 10a) as expected due the increased chance of b-ERK2 capture in streptavidin-coated wells. In addition to the Western Blot, these results further confirm the biotinylation of b-ERK2 and demonstrate that streptavidin is capable of capturing the catalytically active receptor using biopanning conditions prior to the addition of phage. Since immobilized b-ERK2 maintains functional protein binding sites as indicated by its ability to phosphorylate a protein substrate, b-ERK2 represents an excellent receptor for phage display. These data also indicate that b-ERK2 can be

immobilized and maintain activity even after washes using non-reducing conditions. Therefore, non-reducing washes were carried out prior to phage binding (also carried out in non-reducing conditions) to maintain the cyclization of the peptide library on the phage surface.

BIOPANNING SCHEME FOR SELECTING PHAGE THAT BIND B-ERK2

Biopanning was carried out using a large library of fd-tet bacteriophage displaying a single polypeptide ($X_2CX_{14}CX_2$) fused to the *N*-terminus of the surface coat protein pIII [96]. When the phage were produced in *E. coli*, the *N*-terminus of pIII is exposed to the oxidized environment of the periplasm causing disulfide bridge formation between the two cysteines in the displayed peptides, thereby, maintaining conformational rigidity of the peptides favored for binding [97, 98]. Each round of biopanning against the phage receptor (b-ERK2) was carried out as seen in Scheme 3.



Scheme 3. Biopanning scheme for phage display against b-ERK2. (Left) The receptor for phage display (b-ERK2) was immobilized in streptavidin-coated wells for 1 h at 4 °C, unbound b-ERK2 was washed away and non-specific binding sites in the wells were blocked using BSA for 1 h at 4 °C (not shown), phage were allowed to bind the receptor (top), wells were washed to remove weak or non-binding phage (right), the bound phage were eluted with acidic conditions (bottom), and either prepared for sequencing or amplified in *E. coli* for further rounds of selection.

Following each round of biopanning, the eluted phage were amplified in *E. coli* to create multiple copies of each selected member and purified so that they could be re-introduced to subsequent rounds of selection. Each round used increased selection pressures to encourage the selection of tight binding phage over weak binders. The stringency of selection was increased using methods such as extending the washing times following phage binding (to encourage the release of phage with fast k_{off} rates prior to the elution of those with slow k_{off} rates), lowering the concentration of receptor used to capture the phage (to select for tight binding phage *via* competition for rare receptors),

decreasing the phage binding time (to select for those phage with higher k_{on} rates), and by increasing the concentration of the detergent in the washing steps (to discourage weak and non-specific binding). Phage selected in later rounds were individually purified and tested for their ability to bind b-ERK2 in a phage attachment assay and by phage ELISA to specifically select for receptor-binding phage over non-specific binders. Non-specific binding phage may bind other members in the phage library or the streptavidin-coated wells prior to elution and must be selected against to exclude these as receptor-binding phage. The genomic DNA of each receptor-binding phage was purified and sequenced to determine the primary amino acid sequence of the polypeptide displayed on the phage surface.

TITERING PHAGE STOCKS

To determine the titer of the phage (i.e. the number of phage present) serial dilutions of the phage pools were made and infected into K91BluKan *E. coli* cells to determine the number of transduced units (TUs) [76]. A TU is defined as an *E. coli* cell that is infected by phage and gains resistance to tetracycline encoded by the phage genome. An overnight culture of K91BluKan was grown in terrific broth (TB) containing kanamycin. The following day, the overnight culture was diluted, grown to late log phase in TB containing kanamycin, infected with serial dilutions of phage for 10 min at room temperature, allowed to incubate at 37 °C, and plated on Luria broth (LB)/agar plates containing kanamycin and tetracycline. A colony gaining resistance to tetracycline represented a TU.

AMPLIFICATION OF PHAGE LIBRARIES

A library containing 3.1×10^{11} TU/mL was obtained from B. Wang's laboratory and amplified in K91BluKan cells. The amplification of the original library and the eluted phage following each ensuing round of phage biopanning was carried out on a large scale. K91BluKan cells were grown to late log phase in TB containing kanamycin. After slow shaking to allow bacteria to regenerate their F-pili, phage were added and allowed to infect the bacteria. These infected cultures were added to 2 L of LB containing a small amount of tetracycline and later the concentration of tetracycline was increased and the phage were amplified overnight. Purification of phage was carried out as described [76] preceding the cesium chloride purification steps that remove trace amounts of polyethylene glycol (PEG). The purified phage were raised in Tris-buffered saline (TBS) containing glycerol, snap-frozen in liquid nitrogen, stored at -80 °C and a portion of these phage were titered.

ROUND I: NON-STRINGENT BIOPANNING CONDITIONS TO SELECT PHAGE THAT BIND B-ERK2

It is critical in early rounds to use non-stringent biopanning conditions that allow the phage an opportunity to bind the receptor since each member of the phage library is only represented by a few copies and the yields of tight binding phage are usually less than 1% [76]. In later rounds, the selected phage were amplified several-fold so that the members were not as scarce, and the stringency of selection was increased to select for tighter binding phage. Therefore, 4 µg of receptor was allowed to bind the streptavidin-coated well and biopanned in the presence of 7.9×10^{10} TU of phage in the first round of biopanning. Since 4 µg of receptor was added, and $\sim 9.0 \times 10^{10}$ active molecules of b-

ERK2 were predicted when allowing only 0.8 μ g of b-ERK2 to bind the wells (above), these conditions allowed for \sim 1:1 ratio of phage TU to b-ERK2 giving each of the phage a sufficient opportunity to bind b-ERK2. Biopanning was carried out using an acid elution of phage and eluted phage titers from wells containing b-ERK2 were 1.2-fold higher than those eluted from wells lacking the receptor (Figure 11) indicating that the presence of b-ERK2 increased phage capture. However, these results indicate that a significant portion of the eluted phage in the presence of receptor were binding non-specifically to the wells lacking receptor (non-specific binders are estimated from the number of phage eluted from wells lacking receptor). The phage eluted from the receptor-containing well were amplified, purified, and biopanned in Round II to discriminate against non-specific binding phage.

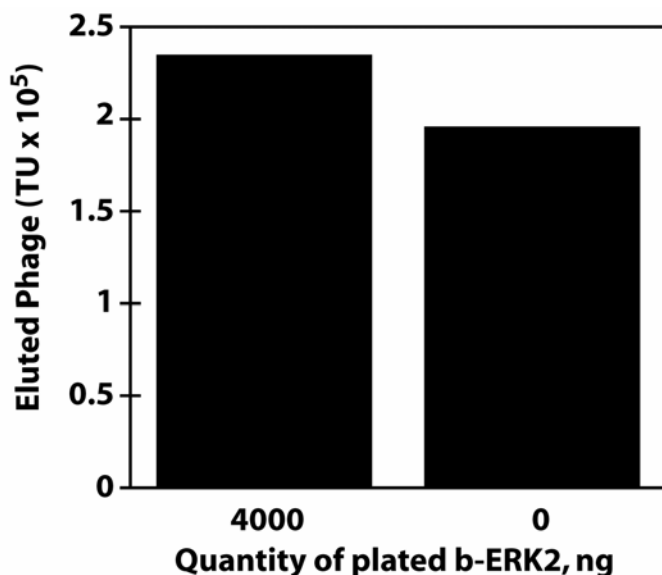


Figure 11. Eluted phage from Round I of biopanning. Streptavidin-coated wells were allowed to bind in the presence or absence of b-ERK2 in buffer B0 for 2h at 4 °C with mild shaking. The wells were washed once with buffer B0 to remove the unbound b-ERK2 prior to the addition of blocking buffer B1 for one hour at 4° C. The wells were briefly washed 6× with buffer B2. The phage (7.9×10^{10} TU) were added in buffer B2 and allowed to bind immobilized b-ERK2 for 1 h at 25 °C with mild shaking. After phage binding, 0.1 mM biotin was added for 5 min to free any streptavidin-binding phage. The wells were washed 12×1 min with buffer B2 containing 0.1% Tween-20. Phage were eluted for 10 min using 100 μ l 0.2 M glycine, pH 2.2, containing 1 mg/mL BSA and immediately buffered with 15 μ l of 1 M Tris-HCl, pH 9.1, following the elution, and titered.

ROUND II: EXTENDING WASH TIME TO SELECT FOR SMALL k_{OFF} RATES

In the second round, the stringency of selection was increased by temporally extending the washes following phage binding to enhance selection of phage with small k_{off} values. Also, several concentrations of the receptor were biopanned under identical

conditions to determine the affects of receptor concentration on phage binding. Eluted phage were shown to increase with increasing receptor concentrations (Figure 12), indicating that members of the Round II phage pool could specifically bind b-ERK2 and that increased receptor enhanced the binding opportunities for the phage. These results are consistent with immobilized b-ERK2 phosphorylation assays of EtsΔ138 that exhibited an increase in phosphorylation of EtsΔ138 with higher plated concentrations of b-ERK2 (Figure 10a). The enrichment ratio, defined as the number of eluted phage from wells containing receptor divided by the number of phage eluted from wells lacking receptor in a given round [99], increased in Round II to 63-fold above non-specific binding as compared to 1.2-fold in Round I (Table 1). Enrichment ratios above unity indicate that the phage can bind the receptor. The increase in enrichment ratio is expected to rise in early rounds and indicates an increase in selectivity for the receptor. It should also be noted that the number of non-specific phage binding to wells lacking the receptor also increased as compared to Round I, albeit, at a lesser extent than those phage eluted from wells containing receptor. These results can be explained by the fact that both b-ERK2-binding phage and non-specific binding phage were selected for in Round I and amplified prior to Round II. To discourage the selection of non-specific phage in later rounds, the amplified pool of phage should contain a large ratio of receptor-binding to non-specific binding phage to increase the chance of selecting receptor-binding phage. Therefore, the phage pool eluted from wells containing 1000 ng of plated receptor were amplified for further selection.

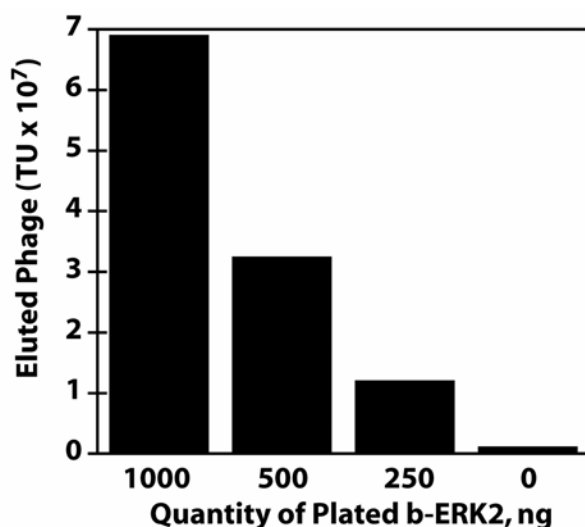


Figure 12. Eluted phage from Round II of biopanning. Streptavidin-coated wells were allowed to bind in the presence or absence of b-ERK2 in buffer B0 for 2h at 4 °C with mild shaking. The wells were washed once with buffer B0 to remove the unbound b-ERK2 prior to the addition of blocking buffer B1 for one hour at 4° C. The wells were briefly washed 6× with buffer B2. The phage (1.4×10^{11} TU) were added in buffer B2 and allowed to bind immobilized b-ERK2 for 1 h at 25 °C with mild shaking. After phage binding, 0.1 mM biotin was added for 5 min to free any streptavidin-binding phage. The wells were washed 12×10 min with buffer B2 containing 0.1% Tween-20. Phage were eluted for 10 min using 100 μ l 0.2 M glycine, pH 2.2, containing 1 mg/mL BSA and immediately buffered with 15 μ l of 1 M Tris-HCl, pH 9.1, following the elution, and titered.

Round	Plated b-ERK2 (ng)	Input Phage (TU)	Eluted Phage (TU)	Background (TU)
1	4000	7.9×10^{10}	2.3×10^5	2.0×10^5
2	1000	1.4×10^{11}	6.9×10^7	1.1×10^6
3	10	2.0×10^{11}	6.0×10^5	1.9×10^5
4	0.1	2.0×10^{10}	1.1×10^4	4.0×10^3

Table 1. Yields of eluted phage from biopanning experiments used for subsequent rounds. In the first round, an amplified version of the original X₂CX₁₄CX₂ library was used. Thereafter, eluted phage were amplified from wells containing the amount of plated receptor concentration shown here and added as input phage to subsequent rounds. The concentrations of phage were determined by titrating experiments based on the number of bacterial infections from eluted phage (Experimental Procedures).

ROUND III: DECREASED RECEPTOR CONCENTRATION TO ENCOURAGE PHAGE COMPETITION

The stringency of selection was increased in Round III by using multiple receptor concentrations during biopanning and selecting the phage eluted from wells containing b-ERK2 with titers just above non-specific phage binding [100]. As receptor concentrations were lowered and became limiting, the phage had to compete with one another for limited receptor sites creating conditions where tighter binders could be selected for. In addition, the detergent concentration was increased to 0.3% Tween-20 during washes to further discriminate against non-specific binding. In wells in which 1 and 10 ng of receptor was plated, eluted phage titers were only ~ 3-fold above non-specific binding (Figure 13). To ensure that individual phage could bind to b-ERK2 at this stage of the biopanning, individual phage selected from Round III were purified and tested for b-ERK2 binding in a phage attachment assay.

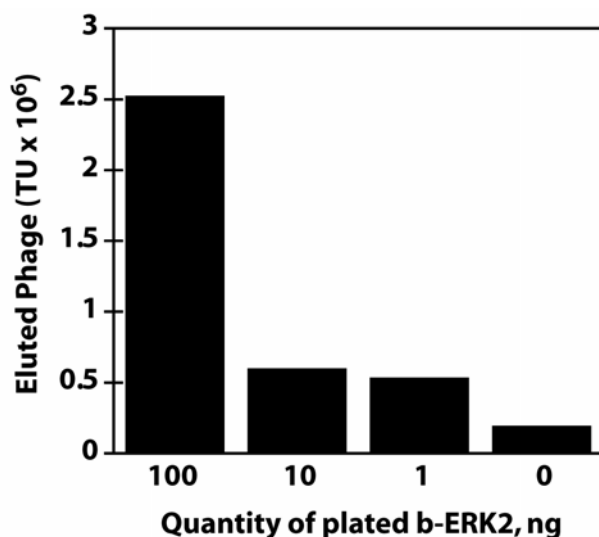


Figure 13. Eluted phage from Round III of biopanning. Streptavidin-coated wells were allowed to bind in the presence or absence of b-ERK2 in buffer B0 for 2h at 4 °C with mild shaking. The wells were washed once with buffer B0 to remove the unbound b-ERK2, prior to the addition of blocking buffer B1 for one hour at 4° C. The wells were briefly washed 6× with buffer B2. The phage (2×10^{11} TU) were added in buffer B2 and allowed to bind immobilized b-ERK2 for 1 h at 25 °C with mild shaking. The wells were washed 12×5 min with buffer B2 containing 0.3% Tween-20. Phage were eluted for 10 min using 100 μ l 0.2 M glycine, pH 2.2, containing 1 mg/mL BSA and immediately buffered with 15 μ l of 1 M Tris-HCl, pH 9.1, following the elution, and titered.

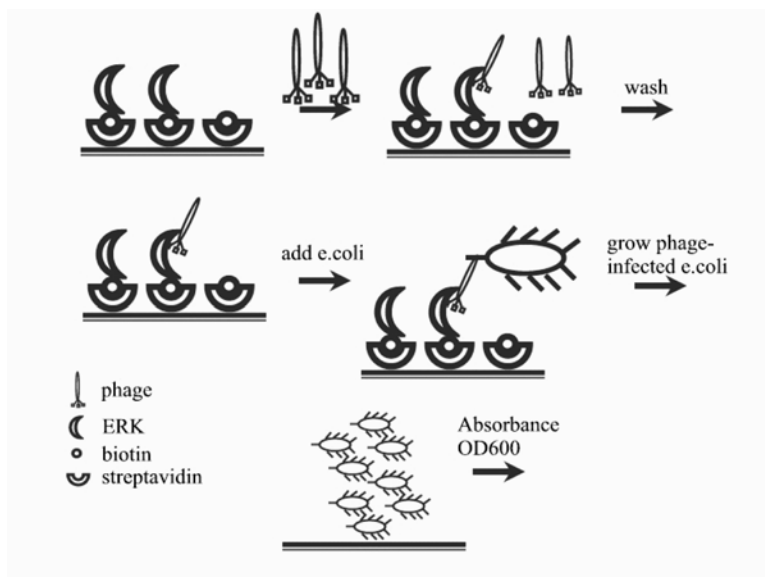
INDIVIDUAL PHAGE PREPARATION

Single colonies of bacteriophage-infected K91BluKan cells were selected from titrating plates, grown in LB containing tetracycline and kanamycin, and purified on a small scale. To purify the phage, the *E. coli* and phage suspension was centrifuged to rid of the bacterial pellet. The supernatant containing the phage was precipitated twice by the addition of PEG and NaCl and the phage were raised in TBS. This procedure usually

yielded $\sim 1 \times 10^8$ TU/ μ L. The phage were frozen and stored at -80 °C in TBS containing glycerol.

PHAGE ATTACHMENT ASSAY

Individually purified phage were selected from the Round III elution from wells containing 1 ng of plated b-ERK2 and subjected to a phage attachment assay (Scheme 4). The phage attachment assay verified whether or not a pool of an individual phage clone could bind the receptor. The phage attachment assay was similar to biopanning, except that it was carried out with a pool of a single phage clone, and instead of eluting the phage in the final step of biopanning, the immobilized phage were allowed to infect K91BluKan cells. Bacterial cells that were infected by phage were selected for by their ability to grow in LB containing tetracycline. Individual phage clones showing a positive result in the phage attachment assay in the presence of b-ERK2 and not in the absence of the receptor were identified as phage that could specifically bind b-ERK2.



Scheme 4. Phage attachment assay. Biopanning conditions were carried out using 1 ng of plated b-ERK2 and 1×10^{10} TU of a single phage clone. Instead of eluting bound phage after several washes, late log phase K91BluKan cells were added and allowed to incubate with the b-ERK2-bound phage. Phage-infected bacterial cells gained resistance to tetracycline and were allowed to grow. Control wells in the absence of b-ERK2 were tested with each phage to select against clones that could bind the wells in the absence of b-ERK2.

Of 40 phage clones tested, 11 tested positive for receptor binding which is consistent with the fact that eluted phage from this well was ~ 3 -fold above background (~ 13 expected). Single-stranded genomic DNA was purified from these clones and sequenced to reveal the sequence of the displayed peptide responsible for binding b-ERK2 (Table 2).

Clone	Amino acid sequence
1	HQCDSLHYPTSGWWATACHG
2	SWCDAMSGNLFKGQALYCVL
3	GACEGFLLPGFGRTAGQCTH
4	SYCDQLLESGSVNRPLDCMR
5	GTCPQDAVTMSMDLASRCEV
6	TTCHSRGNNGSNFPSTRACLS
7	HECRLTFSLGSQVARI-CPL
8	DTCYNGEDRRVARGTFICNR
9	*IRCIRGWTKDIRTLADSCQY*

Table 2. Phage clone peptidyl sequences from Round III that mediated binding to b-ERK2. Round III phage selected for their ability to bind b-ERK2 by a phage attachment assay were amplified, their DNA was purified using a phenol extraction, and sequenced to determine the primary amino acid sequence of the displayed peptide on the phage. (*) - indicates the sequence was selected for 3 times.

Three of the selected phage sequences were similar indicating that the selected clone bearing the peptide IRCIRGWTKDIRTLADSCQY was being selected for more often than the others. No other sequences were identical to one another and a consensus sequence was not observed. The lack of consensus sequence is possibly due to the complexity of the library since all possible combinations of amino acids cannot be represented in libraries greater than X_{6-7} . However, it could also be due to the fact that

ERK2 recognizes and binds a variety of protein surfaces, where individual amino acids make a small contribution to binding. Single phage clones eluted from wells containing more receptor (100 ng of plated b-ERK2) showed that 17/20 were able to bind b-ERK2 in a phage attachment assay, further indicating that phage selected from wells containing more receptor are more likely to bind b-ERK2 due to a greater ratio of b-ERK2-binders to non-specific binders.

ROUND IV: DECREASED RECEPTOR

A fourth round of biopanning was carried out to determine if a consensus sequence could be reached or to confirm the selection of similar phage from the previous round. Several receptor concentrations were biopanned using decreased phage binding time to select for high k_{on} rates (Figure 14). Individual phage eluted from wells containing 0.1 ng of plated receptor were subjected to a phage attachment assay and an ELISA assay and the positive clones were sequenced. Six of the thirteen positive phage clones (Table 3) contained the peptide sequence IRCIRGWTKDIRTLADSCQY (termed hereafter peptide 20) also seen in Round III (Table 2) indicated that the selection of phage bearing peptide 20 was favored under these conditions. Only one other sequence, HQCDSLHYPTSGWWATAACHG, was similar to those selected in Round III, indicating that both displayed peptides were selected under the conditions of both Round III and IV.

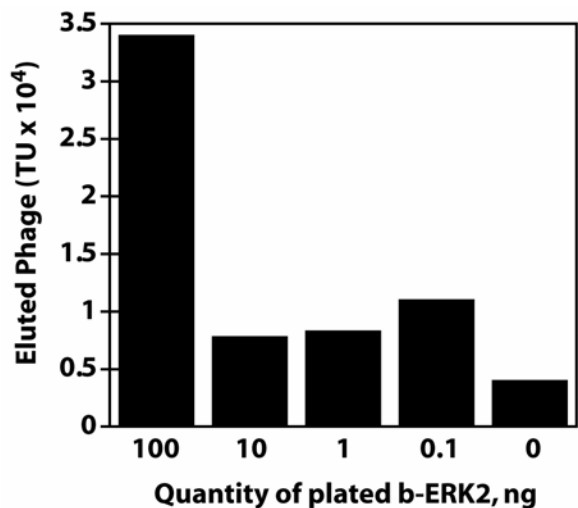


Figure 14. Eluted phage from Round IV of biopanning. Streptavidin-coated wells were allowed to bind in the presence or absence of b-ERK2 in buffer B0 for 2h at 4 °C with mild shaking. The wells were washed once with buffer B0 to remove the unbound b-ERK2, prior to the addition of blocking buffer B1 for one hour at 4° C. The wells were briefly washed 6× with buffer B2. The phage (2×10^{10} TU) were added in buffer B2 and allowed to bind immobilized b-ERK2 for 20 min at 25 °C with mild shaking. The wells were washed 12×5 min with buffer B2 containing 0.3% Tween-20. Phage were eluted for 10 min using 100 μ l 0.2 M glycine, pH 2.2, containing 1 mg/mL BSA and immediately buffered with 15 μ l of 1 M Tris-HCl, pH 9.1, following the elution, and titered.

Clone	Amino acid sequence
12	IWCNCGGMTNGLLDAVRCHS
20 ^{a,b}	IRCIRGWTKDIRTLADSCQY
32 ^a	HQCDSLHYPTSGWWATACHG
40	QHCQGIWKSCSKHSTKCCSL
52	TGCRTTWIRWGWQAETCTS
55	YSCKAWNRTVSGRIASGCLW
68	MGCVRRVTRPGLAVAEACSV
76	VFCRDVTRTPFGSFAPQCMR

Table 3. Round IV b-ERK2-binding peptides displayed on phage. Isolated phage clones selected in Round IV were tested using a phage attachment assay and phage ELISA for the ability to bind b-ERK2. The DNA of positive clones was purified and sequenced to determine the primary amino acid sequence of the displayed peptide on the phage. a, sequence also represented in phage after Round III; b, selected at a frequency 6× greater than the others.

DTT INHIBITS CYCLIC PEPTIDE BINDING

To determine whether the cyclization of the peptides on the surface of the phage were important for b-ERK2 binding, a reducing agent, dithiothreitol (DTT), was added to an ELISA using the phage clones selected from Round IV. An ELISA detects the ability of a population of an individual phage to bind the receptor [101]. The ELISA was carried out in a manner similar to biopanning, however, instead of eluting the receptor-bound phage, a horse-radish peroxidase-linked antibody specific for the phage coat was used to

detect the relative amount of receptor-bound phage using a colorimetric assay utilizing the reduction of hydrogen peroxide. Addition of DTT during the phage binding significantly reduced the ELISA signal for all of the phage clones when compared to similar experiments in the absence of DTT indicating that the reduction of intramolecular disulfide bonds in each of the phage polypeptides ameliorates binding to b-ERK2 (Figure 15) [98]. These results indicate that the disulfide constraint within the displayed peptide is critical for efficient binding to b-ERK2 and also emphasizes the importance of biopanning in non-reducing conditions when using disulfide-constrained phage libraries.

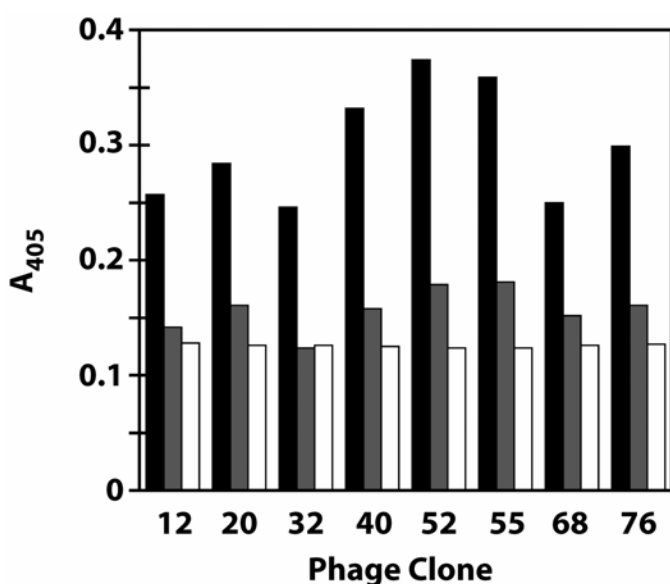


Figure 15. Phage binding to b-ERK2 decreases in the presence of a reducing agent. An ELISA was performed using $\sim 1 \times 10^8$ TU of individually purified phage clones and 500 ng of plated b-ERK2 in the presence of 0 mM (black) and 10 mM DTT (grey) during phage binding. A control was performed in the absence of b-ERK2 (white) revealing background phage binding to wells lacking DTT.

ETSΔ138 DISRUPTS PHAGE BINDING TO b-ERK2

The effects of protein-protein interactions on phage binding to b-ERK2 were studied using the transcription factor protein substrate EtsΔ138 [42] to inhibit phage binding in a competition ELISA. A competition phage ELISA was carried out with phage selected from Round IV using several concentrations of EtsΔ138 to compete with phage binding using a limited quantity of b-ERK2. The results indicate that the presence of EtsΔ138 decreased phage binding to b-ERK2 in a concentration-dependent manner (Figure 16). Conversely, the addition of BSA, a protein that does not bind ERK2, did not have a concentration-dependent effect (data not shown). The data indicates that a protein capable of binding ERK2 can release the bound phage or prevent them from binding since EtsΔ138 was added prior to the addition of the phage. Whether or not EtsΔ138 is competing with phage for a similar binding site or simply detaching phage due to a conformational change of the enzyme upon substrate binding cannot be elucidated from these experiments.

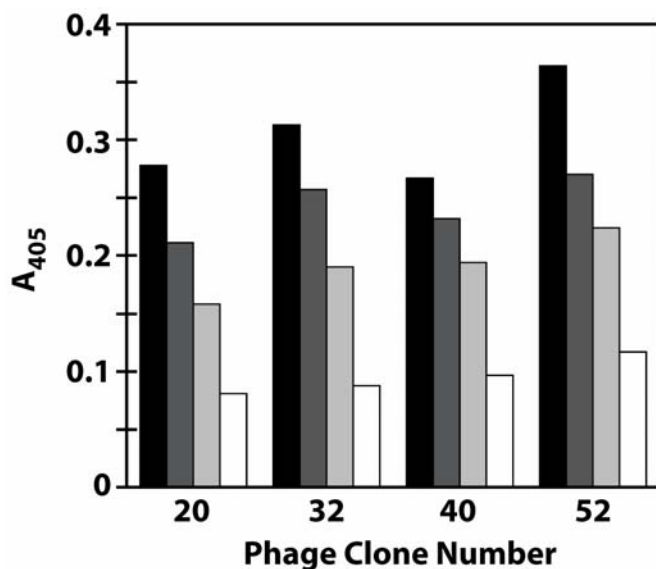


Figure 16. The transcription factor Ets Δ 138 reduces phage binding to b-ERK2 in a phage ELISA. An ELISA was performed using 500 ng of b-ERK2 and $\sim 1 \times 10^8$ TU of individually purified phage clones in the presence of 0 μ M (black), 100 μ M (dark grey), and 200 μ M (light grey) Ets Δ 138 added 10 min prior to the phage. A control was performed in the absence of b-ERK2 and in the presence of phage (white).

MgATP²⁻ INHIBITS PHAGE BINDING

The effects of a smaller non-protein ERK2 substrate on phage binding was also studied using MgATP²⁻ in a competition ELISA. MgATP²⁻ binds ERK2 in a hydrophobic pocket and is required for protein phosphorylation. In the absence of a protein substrate, ERK2 can bind MgATP²⁻ and carry out its hydrolysis to form the products ADP and inorganic phosphate. MgATP²⁻ showed the ability to inhibit phage binding in a phage ELISA in a concentration-dependent manner (Figure 17). The mechanism by which MgATP²⁻ is capable of inhibiting phage binding to b-ERK2 in a competition ELISA

cannot be elucidated by these experiments but is possibly due to competitive binding or through an indirect conformational change upon binding b-ERK2.

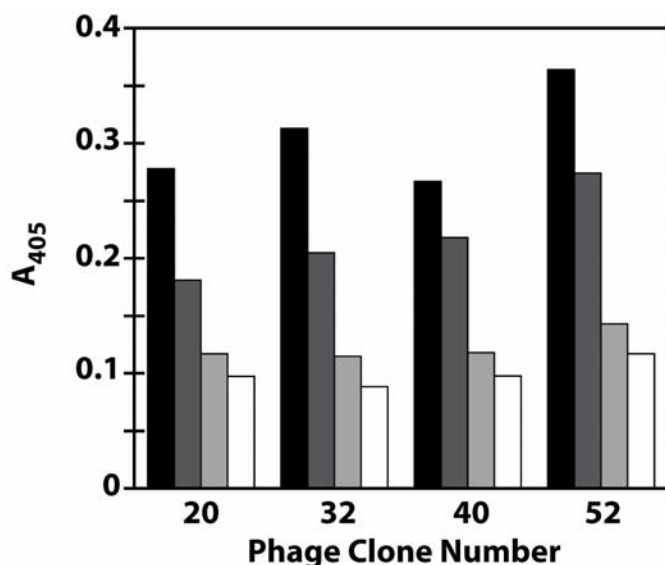


Figure 17. MgATP²⁻ reduces the phage binding to b-ERK2 in a phage ELISA. An ELISA was performed using 500 ng of b-ERK2 and $\sim 1 \times 10^8$ TU of individually purified phage clones in the presence of 0 mM ATP and 0 mM MgCl₂ (black), 5 mM ATP and 10 mM MgCl₂ (dark grey), and 10 mM ATP and 10 mM MgCl₂ (grey). A control was performed in the absence of b-ERK2 and in the presence of phage (white).

PURIFICATION OF CYCLIC PEPTIDE 20A

Since the phage displaying peptide 20 were predominantly selected in Rounds III and IV, this peptide was chemically synthesized and examined for inhibition of ERK2 catalytic activity as measured by ERK2 phosphorylation of EtsΔ138. This experiment accomplished two goals: (i) the characterization of the peptide binding ERK2 in the

absence of the phage coat proteins and (ii) an interaction study with active ERK2 in the absence of biotin to assure that the biotin moiety is not being recognized by the peptide. Unfortunately, peptide 20 was not readily soluble at neutral pH. To circumvent this problem, the peptide was synthesized with 3 lysines attached to the *N*-terminus (*N*-KKKIRCIRGWTKDIRTLADSCQY-C, termed peptide 20a hereafter) that increased the solubility of the peptide significantly. Peptide 20a was purified using reverse phase HPLC, oxidized to form a cyclic peptide with a disulfide bond formed between the cysteine residues, and re-purified using reverse phase HPLC (Figure 18). The oxidation was confirmed by mass using electrospray ionization (ESI) mass spectrometry by revealing the loss of two protons due to cyclization (Table 4).

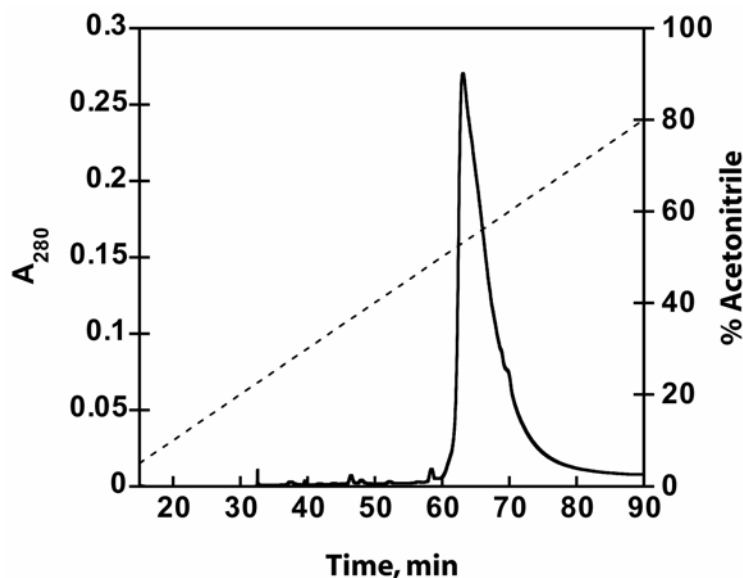


Figure 18. Cyclic peptide 20a purification. The oxidized form of peptide 20a was dissolved in equilibration buffer (0.1% trifluoroacetic acid (v/v) and 5% acetonitrile) and purified by reverse phase chromatography using an Econosil C18 10u column (Alltech), developed with a linear acetonitrile gradient of 5-80% over 75 min using a flow rate of 5 mL/min. Fractions absorbing at 280 nm were applied to MALDI and analyzed for peptide purity; the pooled fractions were further analyzed by ESI.

Peptide	Mass (Da)
Linear 20a	2782.6
Cyclic 20a	2780.4

Table 4. Mass analysis of peptide 20a in linear and the oxidized/cyclic form. A linear and an oxidized/cyclic form of peptide 20a (KKKIRCIRGWTKDIRTLADSCQY) were purified by reverse phase HPLC, lyophilized, raised in 0.1% TFA containing 50% acetonitrile and analyzed by ESI to show a loss of two protons in the oxidized/cyclic form due to the formation of an intramolecular disulfide bond.

INHIBITION OF ERK2 BY CYCLIC PEPTIDE 20A

Peptide 20a (cyclic) inhibited ERK2 phosphorylation of EtsΔ138 and a mode of inhibition was assigned for the substrates EtsΔ138 and MgATP²⁻ (Table 5). Inhibitors are classified according to whether they affect the apparent specificity constant $(k_{\text{cat}}/K_{\text{m}})^{\text{app}}$ by affecting only the apparent Henri-Michaelis-Menten constant $K_{\text{m}}^{\text{app}}$ (competitive inhibition), only the apparent observed rate constant $k_{\text{cat}}^{\text{app}}$ (uncompetitive inhibition), or both (mixed inhibition). By plotting the data in reciprocal form as $1/v$ against $1/[\text{substrate}]$ at varied concentrations of inhibitor, one can determine the mechanism of inhibition by noting whether an inhibitor affects the slope or intercept of a plot. A competitive inhibitor increases the slope while maintaining a constant y -intercept, an uncompetitive inhibitor increases the intercept while maintaining a constant slope, while a mixed inhibitor affects both the slope and intercept of such plots. A mixed inhibition pattern was seen for peptide 20a with respect to MgATP²⁻ (Figure 19a) and a competitive inhibition pattern with respect to EtsΔ138 (Figure 19b).

Table 5. Inhibition Patterns for the Phosphorylation of EtsΔ138 by ERK2^a.

Varied Substrate	Fixed substrate	Inhibitor	Mechanism	$k_{\text{obs}}, \text{s}^{-1}$	$K_m, \mu\text{M}$	$K_i^{\text{app}}, \mu\text{M}$
MgATP ²⁻ ^b	EtsΔ138 ^c	Peptide ^d	Mixed ^h	15.9 ± 0.4	91.3 ± 9.5	76.7 ± 32.9
EtsΔ138 ^e	MgATP ²⁻ ^f	Peptide ^d	Competitive ^g	15.3 ± 0.6	13.0 ± 2.2	20.7 ± 5.5

^aInitial velocities were measured using 1 nM ERK2, 20 mM MgCl₂, (62.5-2000 μM) ATP, and (6.25-200μM) EtsΔ138, 20 mM HEPES pH 7.3, 0.1 mM EDTA, 0.1 mM EGTA, 27 °C, and an ionic strength of 0.1 M (KCl).

^b62.5-2000 μM

^c25 μM

^d0-50 μM

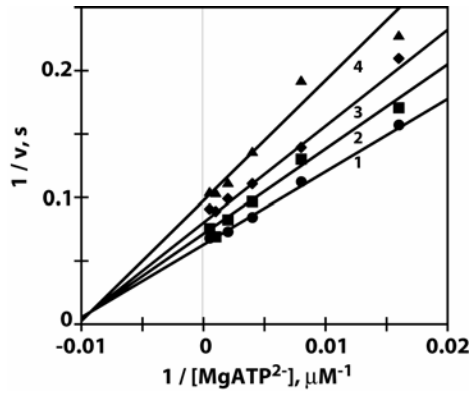
^e6.25-200 μM

^f270 μM

^g Best fit of the data according to $V = (V_{\text{max}} \times [\text{S}]) / (K_m(1 + [\text{I}] / K_i) + [\text{S}])$ for competitive inhibition using global fitting in the program Scientist.

^h Best fit of the data according to $V = (V_{\text{max}} \times [\text{S}]) / (K_m(1 + [\text{I}] / K_i) + [\text{S}](1 + [\text{I}] / K_{ii}))$ for mixed inhibition using global fitting in the program Scientist.

A



B

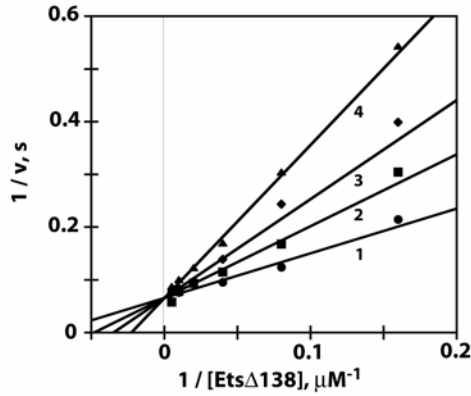
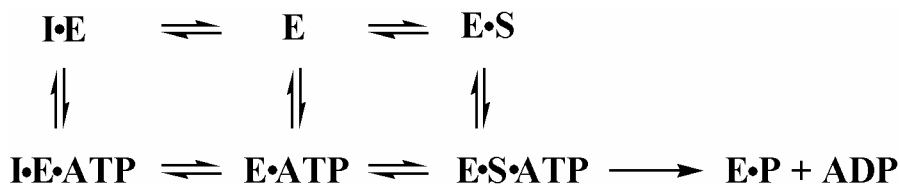


Figure 19. Cyclic peptide 20a inhibition of ERK2 with respect to MgATP^{2-} and Ets $\Delta 138$. (A) Initial velocities were measured using 1 nM ERK2, 20 mM MgCl_2 , 25 μM Ets $\Delta 138$, in the presence of several fixed concentrations of peptide 20a (1, 0 μM ; 2, 12.5 μM ; 3, 25 μM ; and 4, 50 μM), varied concentrations of ATP (62.5-2000 μM), 20 mM HEPES pH 7.3, 0.1 mM EDTA, 0.1 mM EGTA, 27°C, and an ionic strength of 0.1 M (KCl). The data were globally fit to the equation $V = (V_{\max} \times [S]) / (K_m(1 + [I]/K_i) + [S](1 + [I]/K_{ii}))$ using the program Scientist. (B) Initial velocities were measured using 1 nM ERK2, 20 mM MgCl_2 , 270 μM ATP, in the presence of several fixed concentrations of peptide 20a (1, 0 μM ; 2, 12.5 μM ; 3, 25 μM ; and 4, 50 μM), and varied concentrations of Ets $\Delta 138$ (6.25-200 μM), 20 mM HEPES pH 7.3, 0.1 mM EDTA, 0.1 mM EGTA, 27°C, and an ionic strength of 0.1 M (KCl). The data were globally fit to the equation $V = (V_{\max} \times [S]) / (K_m(1 + [I]/K_i) + [S])$ using the program Scientist.

As seen in Scheme 5, a productive complex (E·S·ATP) leading to a phosphorylated product (P) is formed when ERK2 (E) binds both MgATP²⁻ (ATP) and EtsΔ138 (S). In order to bind EtsΔ138, ERK2 cannot be bound to the peptide 20a inhibitor (I) as determined by the competitive inhibition results. Since the inhibition of ERK2 by peptide 20a is mixed with respect to MgATP²⁻, the enzyme can bind ATP in the presence and absence of the inhibitor. Therefore, peptide 20a binds a region of ERK2 that is distinct from the MgATP²⁻ binding site.



Scheme 5. Mechanism of ERK2 inhibition by peptide 20a. The mechanism of peptide 20a inhibition where (I) represents the peptide 20a inhibitor, (E) represents ERK2, (S) represents the protein substrate EtsΔ138, (ATP) represents the nucleotide substrate MgATP²⁻, (P) represents the phosphorylated EtsΔ138 product, and (ADP) represents the nucleotide product MgADP¹⁻.

The kinetic inhibition data are in accord with the experimental evidence that EtsΔ138 competed with phage 20 in a dose-dependent manner for binding to ERK2 in a competition ELISA (Figure 16). The $K_{i(\text{Ets}\Delta 138)}^{\text{app}}$, a measure of the affinity of the peptide for the enzyme, has a similar affinity to the K_m of the protein substrate EtsΔ138 [42] indicating that they not only compete for the same binding site but also bind with similar

affinities (Table 5) despite their difference in size. While it remains to be determined how peptide 20a competes with EtsΔ138 for ERK2 binding it is certainly conceivable that it binds an enzymic MAPK exosite utilized by EtsΔ138 that lies outside of the active site. This is consistent with the observation that the peptide is not a competitive inhibitor of MgATP²⁻.

INHIBITION IS NOT SPECIFIC TO ERK2

A related member of the MAPK family, p38 MAPK α , was also inhibited by peptide 20a. In this case, the kinetic data of inhibition was best fit to a competitive inhibition mechanism with respect to the protein substrate GST-ATF2-(1-115) ($k_{\text{cat}} = 0.7 \pm 0.1 \text{ s}^{-1}$, $K_m = 3.6 \pm 0.9 \text{ }\mu\text{M}$, $K_i = 5.6 \pm 1.4 \text{ }\mu\text{M}$,) (data not shown). These results indicate that peptide 20a, although selected for ERK2 binding, is not specific for ERK2 and may recognize an enzymic MAPK exosite shared amongst this family. Indeed, both MAPK family members, 46% identical, have a number of regions of similarity that the peptide may be recognizing. One region could be the semi-conserved active site region responsible for peptide substrate recognition and MgATP²⁻-binding. However, peptide 20a could bind ERK2 in the presence and absence of MgATP²⁻, indicating that the peptide may not be targeting the active site. Both MAPKs share a similar phosphorylation loop containing a phosphorylated threonine and tyrosine residue required for the activation of each enzyme. Basic residues on peptide 20a could bind this region through recognition of the negatively charged phosphate groups, thereby, inactivating the enzyme. Another region of similarity between p38 MAPK α and ERK2 is the common docking MAPK exosite composed of acidic residues responsible for binding substrates, activating kinases, and phosphatases [17]. Several basic residues in

peptide 20a could mediate the binding to this acidic region through electrostatic interactions. However, it has not yet been determined whether Ets Δ 138 and GST-ATF2-(1-115) utilize the common docking exosite on ERK2 and p38 MAPK α . It is also plausible that the peptide recognizes a novel hot spot, conserved amongst ERK2 and p38 MAPK α , mediating protein substrate docking.

CONCLUSIONS

We have shown that phage display can be used to select peptides that bind the active form of ERK2. One of the peptides selected, peptide 20a, was chemically synthesized and shown to competitively inhibit the ability of ERK2 to phosphorylate a model transcription factor substrate, Ets Δ 138. However, the selected peptide also inhibited a closely related MAPK family member p38 MAPK α . These results suggest that there may be a hot spot on ERK2 and p38 MAPK α that has evolved to bind ligands and serves as a superficial target for phage display. In nature, this same region on ERK2 may bind other ligands within the cell and mediate their recognition of ERK2.

EXPERIMENTAL PROCEDURES

MATERIALS

The X₂CX₁₄CX₂ fd-tet phage library, inserted into a fUSE5 virion, was a gift from B. Wang (Case Western Reserve University, Cleveland, OH) and the *E. coli* K91BluKan strain used for propagation of the phage was a gift from G. Smith (Washington University, St. Louis, MO). Tween-20 was obtained from J.T. Baker (Phillipsburg, NJ). Sulfo-NHS-LC-biotin, biotin, streptavidin-coated 96-well plates, antibodies, and ELISA reagents were purchased from Pierce (Rockford, IL). Kinase assays utilized Na₄ATP (Roche, Indianapolis, IN) and [γ -³²P]ATP⁴⁻ (ICN, Irvine, CA). BSA was obtained from Fisher Scientific (USA), DTT from USBio (Swampscott, MA), Tris base from EM Industries (Gibbstown, NJ), and all other reagents from Sigma. Proteins were concentrated using Centricon-10 centrifugation filter devices with a molecular weight cutoff of 10 kDa (Millipore, Bedford, MA).

PURIFICATION OF ERK2

DNA encoding rat-His₆-ERK2 and MAPKK1 R4F (a gift from M. Cobb, Southwestern, Dallas, TX) were simultaneously expressed in *E. coli* BL21 (DE3) pLysS giving rise to the dual-phosphate form of ERK2 and purified essentially as described [102]. The proteins were expressed in *E. coli* BL21 (DE3) pLysS, grown to an OD₆₀₀ of 0.6-0.8 at 30 °C in LB containing 50 µg/mL carbenicillin, and induced with 0.5 mM IPTG for 12 h. The cells (21 grams from 7.2 liters) were centrifuged at 6,000 rpm at 4 °C

in a GS3 rotor (Sorvall) and the pellet was snap-frozen. The cells were thawed, resuspended in 200 mL 50 mM Tris-HCl, pH 8.0, 0.1% 2-mercaptoethanol (v/v), 0.1 mM PMSF, 0.1 mM TPCK, 1 mM benzamidine, 2 mM EDTA, 2 mM EGTA, 1% Triton X-100 (w/v), 0.25 M NaCl, and sonicated on ice (5×30 second pulses) to maintain a temperature lower than 4 °C. The cellular debris was pelleted by spinning at 16,000 rpm for 30 min at 4 °C in an SS34 rotor (Sorvall). The supernatant was gently mixed for 1.5 h at 4 °C with 2 mL of Ni-NTA agarose beads to bind the His₆-ERK2. The beads were washed with 50 mM Tris-HCl, pH 8.0, 0.1% 2-mercaptoethanol (v/v), 0.1 mM PMSF, 0.1 mM TPCK, 1 mM benzamidine, 2 mM EDTA, 2 mM EGTA and eluted with a similar buffer containing 200 mM imidazole. Fractions containing protein were applied to a Mono Q HR 5/5 column pre-equilibrated with 20 mM Tris pH 8.0, 20 mM bis-Tris, 0.1% 2-mercaptoethanol, 0.03% Brij-30, 0.1 mM EDTA, 0.1 mM EGTA (buffer A). Protein was eluted with a mixture of buffer B (buffer A at pH 5.5) and buffer C (buffer B + 0.5 M NaCl) following the procedure below at a flow rate of 1.5 mL/min:

Minutes	Buffers (%)		
	A	B	C
0	100	0	0
15	100	0	0
30	35	65	0
35	30	70	0
40	30	50	20
90	30	0	70
120	0	0	100

Purified ERK2 was run on a gel, analyzed for a gel shift indicating dual-phosphorylation, and dialyzed overnight at 4 °C into buffer S0 (20 mM HEPES pH 7.3, 100 mM KCl, 0.1 mM EDTA, 0.1 mM EGTA, and 2 mM DTT) containing 10% glycerol, concentrated using a Centricon-10 filter, snap-frozen in liquid nitrogen, and stored at -80 °C.

PURIFICATION OF HIS₆- AND GST-TAGGED PROTEINS

DNA encoding murine His₆-EtsΔ138 in a pET28a vector (Invitrogen) was expressed and purified as described previously [42], however, DNaseI was omitted from the lysis buffer and the Mono Q HR 10/10-purified EtsΔ138 was dialyzed overnight into S0 buffer at 4 °C, concentrated to 25 mg/mL, snap-frozen in liquid nitrogen, and stored at -80 °C.

DNA encoding inactive rat-His₆-p38 MAPKα in a pET14b vector (Invitrogen) was expressed in *E. coli* BL21 (DE3) pLysS, grown in LB containing 50 µg/mL ampicillin to an OD₆₀₀ 0.6-0.8 at 30 °C, and induced for protein expression with 0.5 mM IPTG for 3h. The His₆-tagged protein was purified using Ni-NTA-affinity

chromatography as described [42], dialyzed overnight in S0 buffer containing 10% glycerol at 4 °C, concentrated to 2 mg/mL, and snap-frozen.

DNA encoding the mutant GST-MAPKK6b (S207E/T211E) fusion protein was expressed in *E. coli* BL21 (DE3) pLysS, grown to an OD₆₀₀ of 0.6-0.8 at 30 °C in LB containing 50 µg/mL ampicillin, and induced with 0.5 mM IPTG for 3 h. The cells (9 grams from 3.2 liters) were centrifuged at 6,000 rpm at 4 °C in a GS3 rotor (Sorvall) and the pellet was snap-frozen. The cells were thawed, resuspended in 50 mM Tris-HCl, pH 7.5, 0.1% 2-mercaptoethanol (v/v), 0.1 mM PMSF, 0.1 mM TPCK, 1 mM benzamidine, 2 mM EDTA, 2 mM EGTA, 1% Triton X-100 (w/v), 0.25 M NaCl, and sonicated on ice (5 × 30 second pulses) to maintain a temperature lower than 4 °C. The cellular debris was pelleted by spinning at 16,000 rpm for 15 min at 4 °C in an SS34 rotor (Sorvall). The supernatant was gently mixed for 2 h at 4 °C with 2 mL of glutathione agarose resin to bind the fusion protein. The agarose beads were washed with 30 mL of 50 mM Tris-HCl, pH 7.5, 0.1% 2-mercaptoethanol (v/v), 0.1 mM PMSF, 0.1 mM TPCK, 1 mM benzamidine, and 0.125 M NaCl. The fusion protein was eluted with 10 mL of 20 mM reduced glutathione dissolved in 50 mM Tris-HCl, pH 8.0, 0.1% BME, 0.1 mM PMSF, 0.1 mM TPCK, 1 mM benzamidine to yield 1.4 mg of total protein. The GST-MKK6b fusion protein was dialyzed at 4 °C in buffer S0 containing 10% glycerol, concentrated to 2 mg/mL, and snap-frozen.

DNA encoding GST-ATF2-(1-115) was expressed and purified as described [103], omitting protease inhibitors from the Mono Q buffers.

ACTIVATION OF p38 MAPK α

p38 MAPK α (4 μ M) and a constitutively active mutant form of its activator (GST-MAPKK6b) (0.3 μ M) were incubated with an activation buffer containing 10 mM HEPES pH 8.0, 4 mM ATP, 20 mM MgCl₂, and 2 mM DTT for 3 h to phosphorylate p38 MAPK α . Activated p38 MAPK α was purified using methods similar to activated ERK2 [7] and eluted from the Mono Q HR 10/10 at 0.42 M NaCl. The eluted protein was dialyzed overnight in buffer S0 containing 10% glycerol at 4 °C, concentrated to 2 mg/mL, snap-frozen in liquid nitrogen, and stored at -80 °C. An analogous reaction was carried out in the presence of [γ -³²P]ATP (150 cpm pmol⁻¹) to determine the mol/mol ratio of phosphate incorporated into p38 MAPK α . This was carried out by spotting portions of the reaction on P81 cellulose paper [7] or TCA precipitated, washed to rid of radiolabeled ATP, counted in a scintillation counter, and determined to be 2.8 mol/mol phosphate (only 2 mol/mol is expected for active p38 MAPK α).

BIOTINYLATION OF ERK2

Biotin was covalently linked to dual-phosphate ERK2 to form biotin-ERK2 using sulfo-NHS-LC-biotin. The NHS mixed carbonate reacts with primary amine side chains to form a stable carbamate bond with ERK2. A 2:1 mol/mol ratio of NHS-LC-biotin to ERK2 was added in buffer S0 containing 1 mM ATP on ice for 2 h. ATP was added to protect biotin incorporation into Lys-52 of ERK2, which is required for efficient catalysis [95]. Unreacted biotin was removed using a Centricon-10 filter by buffer-exchange (at least 3 \times 2 mL of buffer S0 containing 10% glycerol). Aliquots were snap-frozen in liquid nitrogen and stored at -80° C. Biotinylation was confirmed by Western Blot

analysis using a horseradish-peroxidase conjugated secondary rabbit anti-goat antibody (1:10,000) and primary goat anti-biotin antibody (1:10,000) as described by the manufacturer (Pierce). ERK2 that was not biotinylated was not detected in the Western Blot.

KINETIC MEASUREMENTS OF B-ERK2 IN SOLUTION

The specific activity of ERK2 was determined by measuring initial rates of radiolabeled phosphate incorporation into the substrate EtsΔ138 by spotting the reaction on P81 paper as previously described [42]. Reactions were performed in a 100 μl volume in the presence of 1 nM b-ERK2, 11.3 μM EtsΔ138, 10 mM MgCl₂, 100 μg/mL BSA, and 100 μM [γ -³²P] ATP (500-1000 cpm pmol⁻¹) in buffer S0 at 25 °C.

KINETIC MEASUREMENTS OF IMMOBILIZED B-ERK2

Immobilization of b-ERK2 in 96-well streptavidin-coated wells was carried out by adding the enzyme in binding buffer B0 (buffer S0 containing 0.1% 2-mercaptoethanol substituted for DTT) for 2 h at 4 °C with mild shaking. The wells were washed once with buffer B0 to remove the unbound b-ERK2, prior to the addition of blocking buffer B1 (buffer B0 containing 5 mg/mL BSA and 0.1 μg/mL streptavidin, to bind any contaminating biotin in the BSA) for one hour at 4° C. The wells were washed (6 × 5 min) with buffer S0 lacking DTT to remove residual 2-mercaptoethanol in preparation for non-reducing biopanning conditions. Immobilized b-ERK2 assays were carried out in the streptavidin-coated wells using similar conditions to the kinetic assays described above without addition of ERK2, since it is already immobilized. The number

of active b-ERK2 molecules was estimated using the observed rate constant (k_{obs}) of immobilized b-ERK2 and the specific activity (SA) of b-ERK2 in solution.

LARGE SCALE AMPLIFICATION AND PURIFICATION OF PHAGE

K91BluKan cells were grown to late log phase at 37 °C in 200 mL of TB [104] containing 100 µg/mL kanamycin. Fd-tet bacteriophage were added after slow shaking for 5 min to allow F-pili regeneration. Slow shaking was continued to allow infection for 15 min. The cultures were added to 2 L of LB containing 0.22 µg/mL tetracycline and shaken at 300 rpm for 35 min. The concentration of tetracycline was increased to 18 µg/mL and shaken overnight. Purification of phage was carried out as described [76] preceding the cesium chloride purification steps that remove trace amounts of PEG. The purified phage were raised in TBS (25 mM Tris-HCl, pH 7.5, 3 mM KCl, 137 mM NaCl) containing 15% glycerol and snap-frozen in liquid nitrogen. To determine the quantity of phage, phage were titered using serial dilutions in TBS and allowed to infect late log phase K91BluKan cells at 25 °C for 10 min, followed by a 30 minute incubation at 37 °C in 100 µl of TB containing 0.22 µg/ml tetracycline, plated on agar plates containing 40 µg/mL tetracycline and 100 µg/mL kanamycin, and grown overnight to select for phage-infected *E. coli*. The number of TUs were determined by counting the colonies that gained resistance to tetracycline *via* bacteriophage infection [76].

BIOPANNING CONDITIONS

Similar procedures described above were carried out to immobilize b-ERK2. After blocking with BSA, the wells were briefly washed 6× with phage binding buffer B2 (TBS containing 5 mg/mL BSA). The phage were added in buffer B2 and allowed to bind immobilized b-ERK2 for one hour (Rounds I-III) or 20 min (Round IV) at 25 °C with mild shaking. After phage binding in the first two rounds, 0.1 mM biotin was added for 5 min to free any streptavidin-binding phage. The wells were washed 12× with buffer B2 containing 0.1% Tween-20 in the first two rounds, increasing to 0.3 % Tween-20 in the third and fourth rounds. Washes were carried out for one minute in Round I, extended to 10 min in Round II, and 5 min in Round III and IV. Phage were eluted for 10 min using 100 µl 0.2 M glycine, pH 2.2, containing 1 mg/mL BSA and immediately buffered with 15 µl of 1 M Tris-HCl, pH 9.1, following the elution. To prepare phage for freezing, 15 µl of 100% glycerol was added prior to snap freezing in liquid nitrogen and storage at -80° C. After each round of biopanning, eluted phage were titered and amplified for further rounds using phage eluted from wells containing 4 µg, 1 µg, and 10 ng of plated b-ERK2 following Rounds I, II, and III, respectively.

SMALL SCALE PHAGE AMPLIFICATION

Individual phage were obtained by growing a single TU (phage infected colony) overnight in 3 mL of LB containing 40 µg/mL tetracycline and 100 µg/mL kanamycin. The phage were purified in 1.5 mL centrifuge tubes by subjecting 1200 µL of cleared supernatant to two overnight precipitations at 4 °C by adding 200 µL of 16.7% PEG 8000 and 3.3 M NaCl followed by extensive mixing. The precipitated phage were raised

in 100 μ L TBS containing 10% glycerol, snap-frozen in liquid nitrogen, and stored at -80 $^{\circ}$ C. Yields were $\sim 1 \times 10^8$ TU/ μ L.

ENZYME-LINKED IMMUNOSORBENT ASSAY

Similar conditions to biopanning were carried out by plating 500 ng of b-ERK2 and using $\sim 1 \times 10^8$ TU of an individually purified phage clone for binding b-ERK2 in buffer B2 for 1 h at 25 $^{\circ}$ C. Following phage binding, the wells were washed (12×5 min) with buffer B2 containing 0.1% Tween-20. Phage bound to the immobilized b-ERK2 were detected by horseradish peroxidase-conjugated anti-M13 antibody (1:5000 dilution in buffer B2 + 0.5% Tween-20) using the hydrogen donor immunopure ABTS to reduce hydrogen peroxide as described by the supplier (Pierce, Rockford). The colorimetric assay was monitored using a 96-well plate reader (Bio-Tek Instruments, Winooski, VT) following absorbance at 405 nm. ELISAs using 10 mM DTT to reduce cyclic phage peptides were carried out by adding the DTT to buffer B2 during phage binding. ELISAs using Ets Δ 138 to compete with phage binding were carried out by adding Ets Δ 138 in buffer S0 lacking DTT to buffer B2 for 10 min prior to phage addition. ELISAs using MgATP $^{2-}$ to compete with phage binding were carried out by adding MgATP $^{2-}$ in buffer B2 10 min prior to phage addition in buffer B2.

SEQUENCING SINGLE-STRANDED PHAGE DNA

Single-stranded DNA (ssDNA) was purified from individual phage. Usually 100 μ L of $\sim 1 \times 10^8$ TU/ μ L was vortexed for 30 sec with 50 μ L of phenol neutralized twice

using a 1/10 volume of Tris-HCl pH 8.0 to separate the DNA and proteins. The mixture was allowed to settle for 1 min then vortexed for 30 sec again. A centrifugation step at 12 000 rpm for 1 min was carried out at 25 °C. The upper aqueous phase containing the DNA (~100 µL) was transferred to 300 µL of an ethanol/NaOAc solution containing a 25:1 ratio of ethanol to 3 M NaOAc pH 5.2. After brief vortexing, the solution was placed at -20 °C for 1 h or overnight to precipitate the DNA. A centrifugation step at 12 000 rpm was carried out for 10 min at 4 °C, the supernatant was discarded, centrifuged again for 15 sec, and the remaining supernatant removed. The pelleted DNA was washed with 200 µL of 70% ethanol at 25 °C, vortexed briefly, and centrifuged again for 10 min at 12 000 rpm at 4 °C. The supernatant was discarded, the pellet was dried at 25 °C for 10 min, and dissolved in 50 µL of water. The DNA could be seen on a 1% agarose gel and ran between 6 and 7 kb consistent with the fd-tet bacteriophage genome. The concentration of ssDNA was determined using an absorbance at 260 nm where an absorbance of one was equal to 40 µg/mL. The ssDNA was sequenced using the primer - 96gIII (5' – CCCTCATAGTTAGCGTAACG-3').

SYNTHESIS AND PURIFICATION OF PEPTIDE 20A

The peptide NH₂-KKKIRCIRGWTKDIRTLADSCQY-COOH (peptide 20a) was synthesized using Fmoc-based solid-phase synthesis. The crude form of the peptide was dissolved in equilibration buffer (0.1% trifluoroacetic acid (v/v) and 5% acetonitrile) and purified by reverse phase chromatography using an Econosil C18 10u column (Alltech), developed with a linear acetonitrile gradient of 5-80% over 75 min using a flow rate of 5 mL/min. Fractions absorbing at 280 nm were applied to MALDI and analyzed for

peptide purity. Pure fractions were pooled and analyzed by ESI and determined to have a molecular weight of 2782.6 Da for the linear peptide.

OXIDATION OF PEPTIDE 20A

Pure linear peptide 20a was oxidized to form an intramolecular disulfide bond between the cysteine residues using iodine essentially as described [105]. The peptide was oxidized while stirring in 80% acetic acid by dropwise addition of iodine (in 100% acetic acid) until a pale yellow color appeared indicating the completion of the reaction and allowed to react for 10 further min at 25 °C. The reaction was quenched with two volumes of water and the iodine was extracted 6× with equal volumes of dichloromethane. The aqueous phase, containing the peptide, was lyophilized and re-purified using reverse phase (as described above). Analysis with ESI showed a shift to 2780.4 Da in accordance with the cyclization of the peptide and loss of 2 protons. The peptide was >90% pure as determined by reverse phase HPLC analysis. The concentration of peptide was determined by denaturation in 6 M guanidine hydrochloride using $\epsilon = 7210 \text{ M}^{-1} \text{ cm}^{-1}$ at 280 nm [106].

PEPTIDE INHIBITION

Inhibition studies were carried out using an active form of ERK2 and p38 MAPK α as described previously by measuring radiolabeled phosphate incorporation into the protein substrates Ets Δ 138 and GST-ATF2-(1-115), respectively [7, 103], in the presence and absence of the cyclic form of peptide 20a. All assays were carried out at 27

°C without a reducing agent in S1 buffer (20 mM HEPES, pH 7.3, 100 mM KCl, 0.1 mM EDTA, 0.1 mM EGTA, 20 mM MgCl₂). ERK2/EtsΔ138 assays were carried out with 1 nM ERK2 and varied peptide 20a (0-50 μM) using either (a) varied EtsΔ138 (6.25-200 μM) and fixed ATP (270 μM or 2 mM in separate experiments with similar results) or (b) fixed EtsΔ138 (25 μM) and varied ATP (62.5-2000 μM). p38 MAPKα assays were performed in S1 buffer containing 4 nM p38 MAPKα, varied GST-ATF2-(1-115) (3-15 μM), fixed ATP (2 mM), and varied peptide 20a (0-20 μM). Concentrations of all proteins were determined using either Bradford assay [107] or 6M guanidine hydrochloride denaturation [106].

CHAPTER 3: A STEADY-STATE KINETIC ANALYSIS OF ERK2 EXOSITE MUTANTS AND DOCKING MOTIF MUTANTS OF ETSΔ138

PURPOSE

This chapter describes a purification scheme for the dual-phosphate form of ERK2 [44] containing two phosphates on Thr-183 and Tyr-185 *via* MAPKK1 phosphorylation. A steady-state kinetic analysis was carried out using dual-phosphate form of ERK2 and a model protein substrate EtsΔ138 [42] that contains a single phosphorylation site. Several known exosites on ERK2, regions that confer protein–protein interactions outside of the active site, were mutated to elucidate whether or not these regions were involved forming an efficient enzyme–substrate (E–S) docking complex leading to the phosphorylation of EtsΔ138. We found two residues, Lys-229 and His-230, that may form a part of the ERK2 exosite for EtsΔ138 as mutation of these residues led to decreased binding of EtsΔ138 using fluorescence anisotropy and decreased efficiency of EtsΔ138 phosphorylation. Mutations of proposed docking motifs in the substrate EtsΔ138 were also generated and two regions of EtsΔ138 were shown to be required for efficient phosphoryl-transfer suggesting that these docking motifs are involved in forming an efficient E–S docking complex.

INTRODUCTION

Intracellular signaling in the MAPK family is highly dependent upon phosphorylation events which are the predominant form of post-translational modification within cells. Members of the MAPK family must recognize their protein substrates in an efficient manner to ensure the fidelity of specific signaling pathways. It has been proposed that MAPKs and their protein substrates form a docking complex using residues that lie outside of the active site of the enzyme [51, 103] and that this docking complex allows for efficient macromolecular recognition followed by phosphoryl transfer in the active site of the enzyme. We were interested in understanding the contributions of the MAPK exosites and the substrate docking motifs in mediating efficient phosphorylation of a protein substrate. As a model system, we chose to study the phosphorylation of EtsΔ138 [42], a protein substrate derived from a transcription factor, by a highly active form of ERK2 [7, 44].

We describe the purification and characterization of a highly pure form of the dual-phosphate ERK2 enzyme containing two covalently linked phosphates on Thr-183 and Tyr-185. The unphosphorylated form of ERK2 and a constitutively active form of its activator MAPK kinase 1 (MAPKK1) termed MAPKK1G7b were expressed in *E. coli* and purified by metal-affinity chromatography. The unphosphorylated form of ERK2 was further purified by Mono Q anion exchange. In the presence of MgATP²⁻, MAPKK1G7b transferred two γ -phosphates from ATP to ERK2 as seen by a radiolabel assay following phosphoryl-transfer. The dual-phosphate form of ERK2, containing the two covalently bound phosphates, was purified away from the MgATP²⁻ and MgADP¹⁻ using DEAE-Sepharose Fast Flow anion exchange and then separated from MAPKK1G7b using Mono Q anion exchange. Radiolabeled dual-phosphate ERK2 was

proteolytically cleaved using trypsin and a peptide containing two covalently attached phosphates was purified using reverse phase chromatography and confirmed by mass spectrometry analysis. The ERK2 peptide containing two phosphates was acid hydrolyzed into individual amino acids and analyzed by phosphoamino acid analysis and shown to contain both a phospho-threonine and a phospho-tyrosine residue. These results confirmed the activation of the unphosphorylated ERK2 by MAPKK1G7b by dual phosphate incorporation into Thr-183 and Tyr-185.

A steady-state kinetic analysis was carried out using the dual-phosphate form of ERK2 to phosphorylate its protein substrate Ets Δ 138 [7]. Several ERK2 mutants were generated in which surface-exposed residues proposed to be MAPK exosites were mutated to either alanine or the homologous residues of a related protein kinase p38 MAPK α that does not efficiently phosphorylate Ets Δ 138 to find residues that were required for the formation of the E-S complex with Ets Δ 138. The ERK2 mutants were phosphorylated by MAPKK1G7b and their steady-state kinetic parameters towards the protein substrate (Ets Δ 138) and the nucleotide substrate (ATP) were examined in order to determine the contribution of proposed ERK2 exosites towards phosphorylation of the substrate Ets Δ 138. In addition, proposed docking motifs on Ets Δ 138 were mutated to determine the steady-state kinetic parameters of the mutants in an effort to understand the contributions of docking motifs in protein phosphorylation by an active MAPK.

RESULTS AND DISCUSSION

THE PURIFICATION OF UNPHOSPHORYLATED ERK2

The inactive/unphosphorylated form of His₆-tagged ERK2 was expressed and purified from *E. coli*. The bacterial lysate was incubated in the presence of Ni²⁺-NTA-agarose beads that captured the His₆-tagged ERK2. The beads were washed and the ERK2 was eluted with imidazole by competing with the histidine tag for Ni²⁺-NTA-agarose binding. The ERK2 was applied to a Mono Q HR 10/10 anion exchange column and eluted with a linear gradient of NaCl (Figure 20). The unphosphorylated ERK2 eluted as two separate peaks occurring at ~ 0.28 and ~ 0.36 M NaCl. Only the first peak was kept for further analysis as it has a higher basal activity than the latter peak. The Mono Q-purified unphosphorylated ERK2 was run on a 10% SDS-PAGE gel to confirm the purity of the protein (Figure 21).

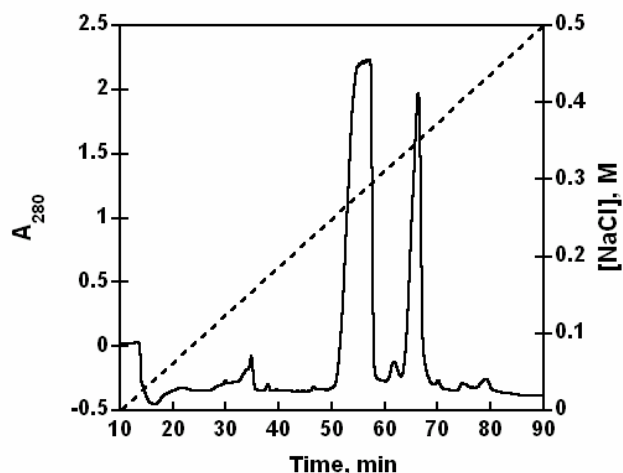


Figure 20. Unphosphorylated His₆-tagged ERK2 purified by Mono Q anion exchange. Unphosphorylated His₆-tagged ERK2 was eluted from the Ni²⁺-NTA-agarose beads with imidazole, filtered, and applied to a Mono Q HR 10/10 anion exchange column with a flow rate of 1.5 mL/min in buffer H1 and eluted with buffer H2 containing NaCl. The ERK2 eluted as two major peaks as determined by the absorbance of tyrosines and tryptophans at 280 nm. Only the first peak was collected for further analysis.

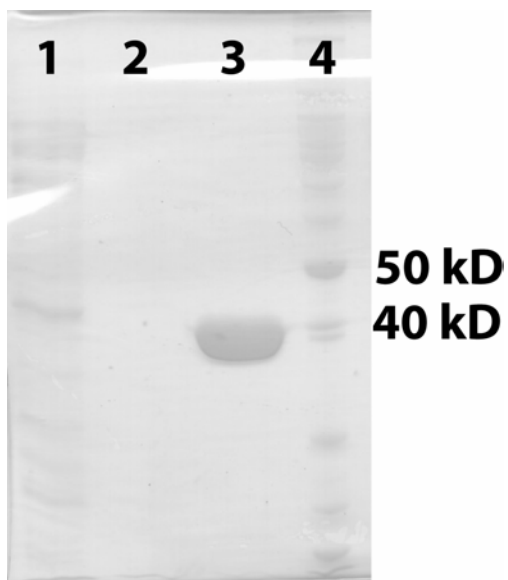


Figure 21. SDS-PAGE gel of unphosphorylated ERK2 after purification by Mono Q anion exchange. A 10% SDS-PAGE gel was loaded with a fraction of (1) Ni^{2+} -NTA column flow through, (2) Ni^{2+} -NTA column wash, (3) a pooled fraction of the first peak eluted from the Mono Q HR 10/10 anion exchange column, and (4) a 10 kD Protein Ladder. The gel was stained with Coomassie Blue stain.

PURIFICATION OF MAPKK1

Unphosphorylated ERK2 can be phosphorylated and activated by the enzyme MAPKK1 in the presence of MgATP^{2-} . To purify a constitutively active form of MAPKK1, termed MAPKK1G7b (MAPKK1/ Δ 44-51/S218D/M219D/N221D/S221D), His₆-tagged MAPKK1G7b was expressed in *E. coli* and purified in a similar fashion to the unphosphorylated ERK2 using Ni^{2+} -NTA-agarose beads to capture the His-tagged protein. The MAPKK1G7b was eluted from the Ni^{2+} -NTA-agarose beads with imidazole and applied to a 10% SDS-PAGE gel (Figure 22) to confirm the heterogeneous

purification of the ~50 kD MAPKK1G7b [44]. Fractions containing MAPKK1G7b were dialyzed into S1 buffer and frozen.

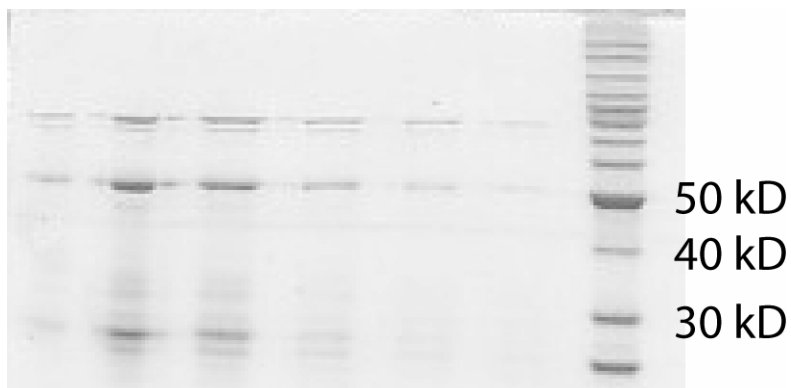


Figure 22. SDS-PAGE gel analysis of MAPKK1G7b eluted from a Ni^{2+} -NTA-agarose column. His₆-tagged MAPKK1G7b was bound to a Ni^{2+} -NTA-agarose column and eluted with 250 mM imidazole by collecting 1 mL fractions. Fractions 2-7 (left to right with a protein ladder on the right) were run on a 10% SDS-PAGE gel and stained with Coomassie Blue stain.

ACTIVATION OF ERK2 USING MAPKK1

Unphosphorylated ERK2 was activated *via* phosphorylation of residues Thr-183 and Tyr-185 by MAPKK1G7b in the presence of ATP, and MgCl_2 . The activation was carried out using radiolabeled ATP to follow phosphate incorporation into ERK2. Over the course of the activation, aliquots were spotted on P81 cellulose paper to follow phosphate incorporation into ERK2 over the course of the reaction. ERK2 bound to the P81 paper and radiolabeled phosphates incorporated into ERK2 by MAPKK1G7b were detected in the scintillation counter (Figure 23). Alternatively, aliquots of the reaction could be precipitated in TCA to give similar results. The results indicated that an average of 2 phosphates were incorporated for every molecule of ERK2, however, this data did not confirm which residues were phosphorylated.

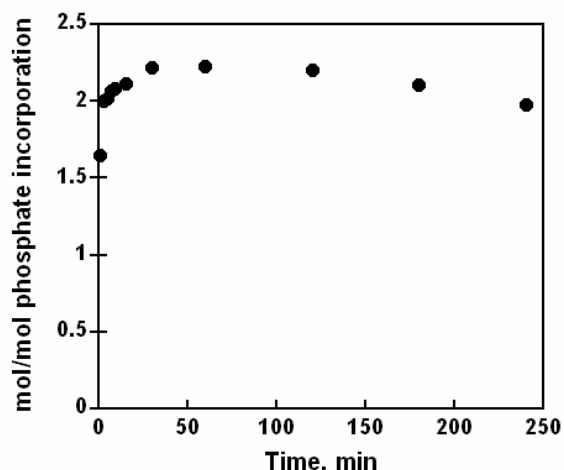


Figure 23. Phosphate incorporation into unphosphorylated ERK2 by the activator MAPKK1G7b. Unphosphorylated ERK2 (4 μ M) was phosphorylated by MAPKK1G7b (0.4 μ M) in the presence of 4 mM ATP⁴⁻ (with 125 cpm/pmol γ -³²P-ATP) and 20 mM MgCl₂ in 40 mM Hepes, pH 8.0, 100 mM KCl, 0.5 mM EGTA, and 2 mM DTT for 5 hours at 27 °C. During the reaction, aliquots were spotted on P81 cellulose paper, dried, washed 4 \times 5 min in 50 mM phosphoric acid, 1 \times 1 min in acetone, dried, and counted in scintillant fluid in a scintillation counter to determine the number of moles of phosphate per mole of ERK2.

PURIFICATION OF DUAL-PHOSPHATE ERK2

Following the activation of ERK2 by MAPKK1G7b, ERK2 was purified away from the ATP using a DEAE-Sepharose Fast Flow anion exchange column equilibrated in buffer H1 [7]. The ATP flowed through the column while the column retained ERK2. The ERK2 was eluted using a NaCl gradient. The eluted protein was subjected to a Bradford assay to determine where the protein eluted by monitoring the absorbance at 595 nm (Figure 24).

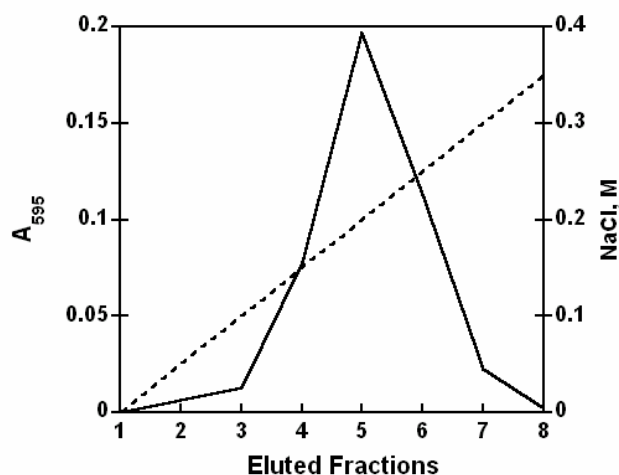


Figure 24. Elution of dual-phosphate ERK2 from the DEAE-Sepharose anion exchange column. Following the activation of ERK2, the activation solution containing MAPKK1G7b, ERK2, MgATP²⁻, and MgADP¹⁻ was applied to a DEAE-Sepharose Fast Flow anion exchange column. The column was washed with 20 column volumes of H1 buffer and eluted with 1 mL fractions using a linear gradient of NaCl (H2 buffer) in 0.05 M increments. A Bradford assay was conducted on each eluted fraction to follow the elution of the ERK2 protein using the absorbance at 595 nm.

The fractions containing the dual-phosphate ERK2 (fractions 4-6 containing ~ 0.5 mg of ERK2) were applied to a Mono Q HR 10/10 anion exchange column in 7 mL of buffer H1 to ensure a low NaCl concentration so that the dual-phosphate ERK2 could bind the column. The column was developed similar to that of unphosphorylated ERK2 (Figure 20) and the dual-phosphate ERK2 eluted at ~ 0.29 M NaCl (Figure 25). The eluted fractions were collected and dialyzed overnight in either 1 L of 50 mM Tris pH 8.6 to prepare for proteolysis by trypsin or 1 L of S1 buffer and snap frozen for steady-state kinetic assays.

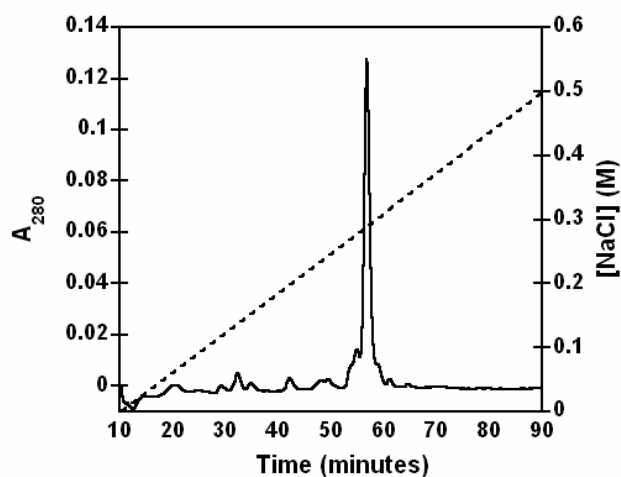


Figure 25. Purification of dual-phosphate ERK2 using Mono Q HR 10/10 anion exchange. Following elution from the DEAE column, the dual-phosphate ERK2 was diluted with buffer H1 and loaded onto a Mono Q HR 10/10 column using a 10 mL superloop and a flow rate of 1.5 mL/min. The column was developed using a linear gradient of NaCl using buffer H2. The dual-phosphate ERK2 eluted at 0.29 M NaCl.

TRYPTIC PEPTIDE AND PHOSPHOAMINO ACID ANALYSIS OF ERK2

To determine which residues were phosphorylated in the radiolabeled ERK2 protein, a tryptic peptide digest was carried out, the peptides were purified by reverse phase, the radiolabeled tryptic peptide was acid hydrolyzed, and phosphoamino acid analysis on the peptide was performed [108]. Following dialysis of the radiolabeled dual-phosphate ERK2, the protein was incubated with trypsin to proteolytically cleave the ERK2 into smaller peptides by proteolytic cleavage following the basic residues lysine and arginine. The tryptic peptide digest was purified by reverse phase HPLC using a C18 column so that individual peptides could be separated. A single radiolabeled peak was found that eluted at 25% acetonitrile indicating that only one peptide had radiolabeled

phosphates covalently attached (Figure 26). A portion of the radiolabeled peptide was analyzed by matrix assisted laser desorption ionization (MALDI) mass spectrometry which revealed a peptide of 2306.2 Da (2307.3 Da calculated) indicating that the peptide N-¹⁷¹VADPDHDHTGFLTEYVATR¹⁸⁹-C of ERK2 was phosphorylated at two positions.

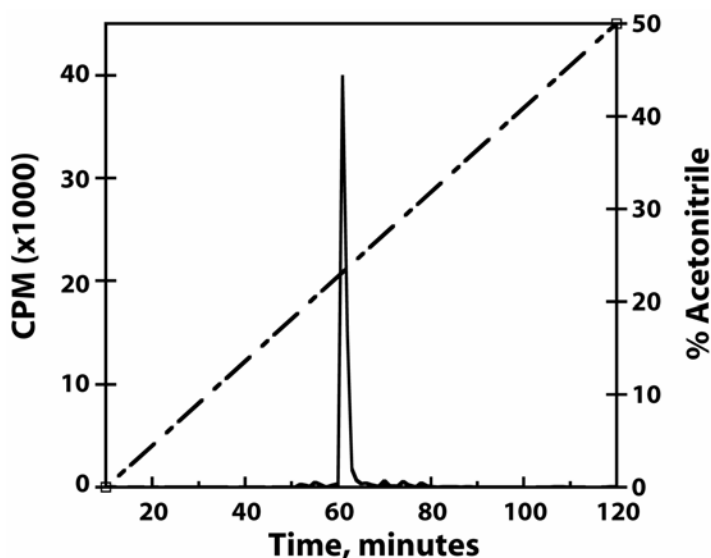


Figure 26. Tryptic peptide analysis of activated ERK2 using reverse phase HPLC following activation by MAPKK1G7b. Radiolabeled dual-phosphate ERK2 was dialyzed overnight in 50 mM Tris, pH 8.6, and cleaved with 10 μ g of trypsin for 10 hours. The tryptic digest was filtered and applied to a reverse phase C18 column in 0.1% TFA and peptides were eluted with a linear gradient of 50% acetonitrile containing 0.1% TFA. All fractions were collected and counted in a scintillation counter and radiolabeled fractions were kept for further analysis.

To determine which amino acids of the ERK2 phospho-peptide were phosphorylated, the peptide was partially hydrolyzed into its individual amino acids using hydrochloric acid. The hydrolyzed peptide was subjected to phosphoamino acid analysis by running the samples on a cellulose plate under electrophoretic conditions to separate

phospho-serine, phospho-threonine, and phospho-tyrosine (Figure 27). The results indicate that a threonine and a tyrosine (most likely Thr-183 and Tyr-185) are phosphorylated on the ERK2 peptide consisting of residues 171-189. Since there is only one tyrosine in the phosphorylated peptide, tyrosine 185 is phosphorylated. There are several threonines in the peptide and it is expected that Thr-183 is the phosphorylated residues. These results indicate that ERK2 can be phosphorylated to a 2 mol/mol ratio with phosphates incorporated into Thr-183 and Tyr-185.

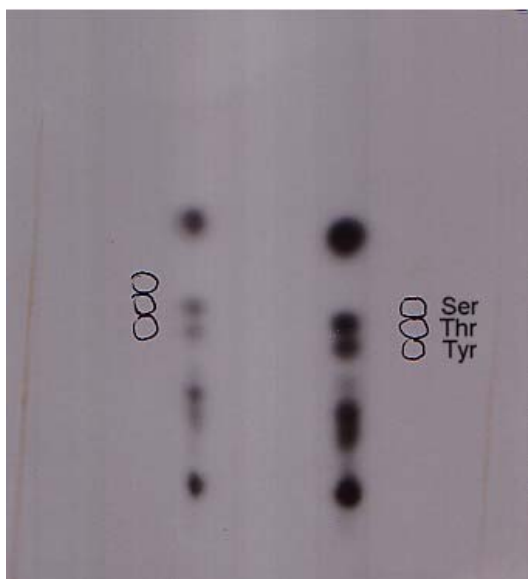


Figure 27. Phosphoamino acid analysis of the acid-hydrolyzed radiolabeled ERK2 tryptic peptide. The radiolabeled ERK2 tryptic peptide consisting of residues 171-189 was hydrolyzed using 6 M hydrochloric acid for 60 min at 110 °C and separated with pH 3.5 buffer for 2 h at 200 V. The cellulose plate was exposed to film, developed, and compared to the cold phosphoamino acid standards as shown; Ser – phospho-serine; Thr – phospho-threonine; Tyr – phospho-tyrosine. The bottom portion of the film shows the non-hydrolyzed peptide near the cathode and the upper portion of the film shows the free phosphate near the anode. The analysis is shown for 500 (left) and 1000 (right) cpm.

METHODOLOGY TOWARD UNDERSTANDING EXOSITES

MAPKs bind to their activators, inactivators, and substrates at regions that are distinct from the active site to form docking complexes that regulate the activity of MAPKs [17]. We term these regions “exosites” for enzymic sites that lie outside of the active site and facilitate MAPK protein-protein interactions. Proteins that bind MAPKs have “docking motifs” that facilitate docking complex formation with a MAPK, we hypothesize that residues that make up a docking motif on activators, inactivators, and substrates can bind to the exosite on the MAPK. One such exosite conserved amongst MAPK family members was shown to mediate protein-protein interactions with activators, inactivators, and substrates [17], indicating that proteins with docking motifs compete for MAPK exosite binding. To understand the role of exosites in mediating phosphoryl-transfer, several putative exosites on ERK2 were mutated, the mutant proteins were purified, activated by MAPKK1G7b, and characterized by studying the steady-state kinetic parameters of EtsΔ138 phosphorylation. We hypothesized that mutagenesis of an exosite required for macromolecular recognition of the protein substrate EtsΔ138 would lead to an increase in the Henri-Michaelis-Menten constant (K_m) but would not affect the steady-state rate of catalysis (k_{cat}) as compared to the WT enzyme with a functional exosite. In other words, mutations in the exosite that are required for EtsΔ138 docking would disrupt the efficient formation of the ERK2–EtsΔ138 Enzyme–Substrate (E–S) complex prior to phosphoryl-transfer and would lower the specificity constant (k_{cat}/K_m) of EtsΔ138 phosphorylation. A decrease in the specificity constant indicates the substrate is phosphorylated less efficiently.

THE COMMON DOCKING (CD) AND THE HYDROPHOBIC (YY) EXOSITES

The Common Docking (CD) exosite was identified as an acidic patch conserved throughout MAPK family members located on the surface of MAPKs, Asp-316 and Asp-319 in ERK2 (Figure 28), that mediates protein-protein interactions with activators, inactivators, and substrates [17]. The importance of the CD exosite was first identified as a gain-of-function mutation¹⁴ in an ERK2 homolog in *Drosophila* termed *rolled*^{Sem} [15]. Mutagenesis of the CD exosite disrupted the ability of ERK2 to bind and activate¹⁵ the phosphatase MKP-3 [33], and showed reduced sensitivity to dephosphorylation by the phosphatases MKP-3 [33], CL100 [16], PAC1, and MKP-2 [109]. These results suggest that the CD exosite plays a critical role in the dephosphorylation of ERK2 by several phosphatases. The CD exosite is also required for cytoplasmic retention of inactive ERK2 when overexpressed with MAPKK1 [47] but not required for dual-phosphorylation¹⁶ of ERK2 [47] or ERK1 [110]. These results suggest that the CD exosite may be involved in ERK2 binding to MAPKK1 but not required for ERK2 phosphorylation by MAPKK1. Whether or not other proteins are involved in the cytoplasmic retention of ERK2 in the presence of overexpressed MAPKK1 is unclear. However, in another report, the phosphorylation of ERK2 by MAPKK1¹⁷ and ERK2

¹⁴ The *rolled*^{Sem} mutation, D331N (corresponding to rat ERK2 D319 in the CD exosite), was found in a genetic screen for photoreceptor R7-type cell formation in the absence of an upstream signal.

¹⁵ GST-ERK2 and GST-ERK2 D319N were expressed in *E. coli*, purified, and used to immunoprecipitate His₆-tagged MKP3. D319N ERK2 showed a decrease in binding compared to ERK2. ERK2 activates the p-NPP hydrolysis activity of the phosphatase MKP3. D319N ERK2 showed a decreased ability to activate MKP3 phosphatase activity.

¹⁶ CHO cells were co-transfected with WT-GFP-ERK2 or a mutant form of GFP-ERK2 (residues 312-319 changed to alanines) along with MAPKK1 and stimulated with VOOH for 15 min to activate ERK2. Lysates were prepared and both forms of ERK2 were shown to be activated using an anti-double phosphorylated ERK2 antibody and also showed similar abilities to phosphorylate MBP.

¹⁷ Active HA-MAPKK1 (*Xenopus*) was immunoprecipitated from oestrogen-stimulated Δ B-Raf:ER cells and used to phosphorylate GST-ERK2 (*Xenopus*) and a CD exosite mutant GST-ERK2 D321N/D324N. The CD site mutant was shown to have a small decrease in the amount of phosphorylation while maintaining the ability to phosphorylate MBP and autophosphorylate itself.

phosphorylation¹⁸ of the substrate MNK1 using one concentration of MNK1 is decreased by mutating the CD exosite [17]. These results suggest that the CD exosite may not be required for activation of ERK2, however, the efficiency of ERK2 activation may be affected by CD exosite mutations. In addition, the CD exosite may be important for substrate phosphorylation. CD exosite mutants of ERK2 are active enzymes as shown by the ability of the CD exosite mutant to autophosphorylate itself and phosphorylate a non-specific substrate myelin basic protein (MBP), however, efficient substrate phosphorylation of MNK1 appears to require the CD exosite [17].

The first study to characterize kinase exosite mutation effects on the kinetics of phosphorylation appeared recently showing that single CD exosite mutants caused less than a 4-fold decrease in the specificity constant of MBP phosphorylation mostly due to an increase in K_m [14]. The same mutant displayed a 24-fold decrease in the specificity constant of Elk-1(307-428) phosphorylation with the major defect in k_{cat} . Unfortunately, these studies were carried out with inactive ERK2 phosphorylating two different substrates that contain multiple phosphorylation sites and lend no insight into the role of exosites in the dual-phosphorylated/active form of ERK2 catalyzing the phosphorylation of a specific phosphorylation site. These results indicate that CD exosite mutations can affect both the K_m and the k_{cat} for certain substrates, however, the mutations in the dual-phosphate form of ERK2 towards any substrate have not been examined.

¹⁸ Activated ERK2 CD exosite mutants, similar to above, were immunoprecipitated from oestrogen stimulated ΔB -Raf:ER cells and assayed for their ability to phosphorylate Myc-GST-MNK1 and MBP. The CD site mutant showed a 90% decrease in the ability to phosphorylate MNK1 while showing similar phosphorylation to MBP as that of WT ERK2.

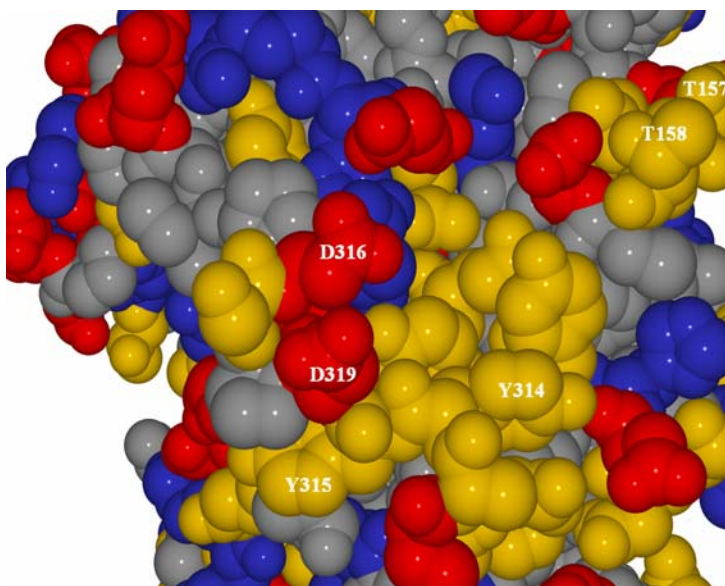


Figure 28. A surface view of potential exosites on dual-phosphate ERK2. The crystal structure of ERK2 (PDB: 2ERK) is shown highlighting acidic (red), hydrophobic (yellow), basic (blue), and neutral (gray) residues. Exosite residues thought to be involved in protein-protein interactions are labeled for the CD (D316/D319), YY (Y314/Y315), and TT/ED exosites (T157/T158).

All MAPK family members, from the budding yeast to human, contain two conserved large hydrophobic side chains (bold) that lie immediately *N*-terminal to the CD exosite (underlined): **YYD**³¹⁶, **WYD**, and **YHD**, for ERK1/2, JNK1/2, and p38 MAPK α/β , respectively. These hydrophobic residues, termed the YY exosite for ERK2, are also exposed on the surface of both the unphosphorylated [70] and dual-phosphate forms of ERK2 [4] (Figure 28) indicating that they could also interact with other proteins in concert with the nearby CD exosite. Mutation of the YY exosite in Myc-tagged ERK2 (Y314A/Y315A) decreased its ability to bind HA-tagged MAPKK1 as determined by co-immunoprecipitation from HEK 293 cells [48] indicating this region may facilitate binding to its upstream activator. When co-expressed with a constitutively active form of

MAPKK1 and immunoprecipitated, the activated Y314A/Y315A mutant was shown to have similar catalytic activity as compared to WT ERK2 towards the substrate MBP, but displayed a 25% decrease in the phosphorylation of an unknown concentration of catalytically deficient MAPKK1 suggesting that mutation of the hydrophobic YY exosite near the CD exosite may also affect the phosphorylation of some substrates. The steady-state kinetic parameters of the YY exosite mutant were not reported. Under similar conditions, both the CD exosite mutant (D316A/D319A E320A; AAA) and the 5A exosite mutant (Y314A/Y315A and AAA) had defects in both MBP and MAPKK1 phosphorylation¹⁹ [48]. These results indicate that the YY exosite may play a role in protein-protein interactions and affect the efficient phosphorylation of some substrates.

Since mutations of the CD and nearby YY exosites on ERK2 led to decreased protein-protein interactions and decreased phosphorylation of several substrates, we hypothesized that these exosites might be involved in forming a docking complex with the model protein substrate EtsΔ138 [42]. To test this hypothesis, site-directed mutants of the CD and YY exosites were generated, fully activated, and the steady-state kinetic parameters of EtsΔ138 phosphorylation were determined and compared to WT ERK2. We assumed that a 3-fold change in the specificity constant was a significant finding.

Residues in the CD and YY exosite of ERK2 were mutated to alanine to generate D316A/D319A and Y314A/Y315A, respectively. These mutants were activated and their steady-state kinetic parameters towards the phosphorylation of EtsΔ138 were measured (Table 6) and neither mutant showed more than a 2-fold decrease in the specificity constant towards EtsΔ138 phosphorylation (Figure 29) indicating that both mutants are catalytically efficient with respect to EtsΔ138 phosphorylation and ATP binding and

¹⁹ These results indicate that mutant proteins may not be fully activated at the time of immunoprecipitation or that the CD site mutation decreases MBP and MAPKK1 phosphorylation. It is difficult to determine whether or not these ERK2 mutants were fully activated or if their defects are due to docking deficiencies caused by mutations in the CD and YY sites.

indicate that mutagenesis does not affect their ability to be activated by MAPKK1G7b. These results indicate that the CD and YY exosites do not have significant contributions towards formation of the catalytically competent ERK2–EtsΔ138 docking complex. Single CD exosite mutants, D316A and D319A, were also analyzed and neither showed significant effects on the specificity constant of EtsΔ138 phosphorylation (data not shown).

Together with the aforementioned data, these results suggest that the CD and YY exosites are not required for the activation of ERK2 by a constitutively active form of MAPKK1 as previously suggested [47]. In addition, these exosites are not required for E–S formation between ERK2 and its substrates EtsΔ138 and ATP. Although this is the first kinetic evidence that suggests the CD and YY exosites on the dual-phosphate form of ERK2 do not have large effects on protein substrate phosphorylation, other reports also support these conclusions [47, 48, 110].

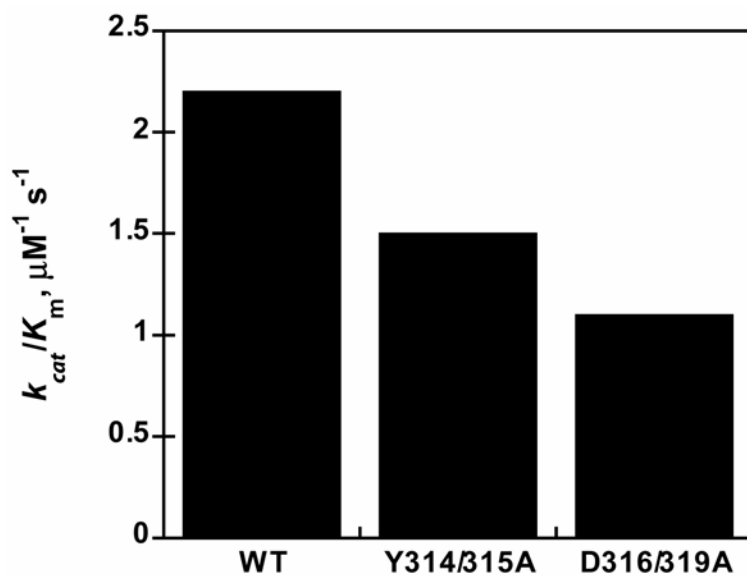


Figure 29. Specificity constant comparisons of EtsΔ138 phosphorylation by activated CD and YY exosite ERK2 mutants. The specificity constants were determined in Table 6 and plotted here to show relative differences between the WT ERK2 enzyme and the CD (D316A/D319A) and YY (Y314/Y315A) ERK2 exosite mutants.

Mutant	k_{cat}	K_m , EtsΔ138	K_m , ATP	k_{cat}/K_m (Ets)
WT	19.6 ± 0.7	8.8 ± 1.4	98.7 ± 4.4	2.2 ⁿ⁼¹²
Y111N/K112N	14.9 ± 0.1	21.3 ± 0.2	-	0.7 ⁿ⁼²
L113A	21.6 ± 3.8	7.1 ± 2.4	104.6 ± 15.7	3.0 ⁿ⁼¹
Q117A	18.1 ± 2.8	18.8 ± 3.0	108.5 ± 8.2	1.0 ⁿ⁼¹
H123A	33.3 ± 2.9	43.3 ± 4.6	132.1 ± 10.4	0.7 ⁿ⁼²
T157E/T158D	15.9 ± 2.4	15.1 ± 3.1	102.2 ± 5.3	1.1 ⁿ⁼³
K229T/H230D	7.8 ± 2.1	127.9 ± 27.3	92.3 ± 9.3	0.1 ⁿ⁼³
Y314A/Y315A	24.6 ± 2.9	16.6 ± 2.4	140.9 ± 26.4 ⁿ⁼²	1.5 ⁿ⁼³
D316A/D319A	17.6 ± 1.7	15.3 ± 3.2	129.2 ± 17.1 ⁿ⁼²	1.1 ⁿ⁼³

Table 6. The steady-state kinetic parameters for EtsΔ138 phosphorylation by dual-phosphate ERK2 mutants. These values were obtained with radiolabeled P81 assays [7]. For the determination of the K_m for EtsΔ138 saturating ATP (2 mM) was used while varying the EtsΔ138 concentration from 6.3-200 μM. For the determination of the K_m for ATP saturating EtsΔ138 concentrations (200 μM) were used while varying the ATP concentration from 31.3-1000 μM. Each value was determined using 6 initial velocities fit to the equation $k_{obs} = (k_{cat} \times [S]) / (K_m + [S])$. Assay contained 25 mM Hepes, pH 7.5, 50 mM KCl, 0.1 mM EDTA, 0.1 mM EGTA, 40 μg/mL BSA, 20 mM MgCl₂, 2 mM DTT, 1 nM ERK2, EtsΔ138, and ATP. Values are shown as a mean ± standard error. The mean k_{cat} was determined using the values obtained from both EtsΔ138 and ATP analyses and were found to be similar. Units: k_{cat} , s⁻¹; K_m , μM; k_{cat}/K_m , μM⁻¹ s⁻¹.

THE TT/ED SPECIFICITY-DETERMINING EXOSITE

A computational prediction carried out by Caffrey *et al.*, suggested several residues in ERK2 and p38 MAPKα that might be involved with substrate specificity determination based on non-conserved mutations that occurred between the two kinases after gene duplication [10]. One of the predicted specificity-determining regions from this study was the TT/ED exosite of ERK2/p38 MAPKα composed of the residues Thr-157 and Thr-158 in ERK2 and the corresponding residues Glu-160 and Asp-161 of p38 MAPKα. The location of the TT/ED exosite is shown with respect to the CD and YY exosites in Figure 28. An independent study identified the TT/ED exosite and found that

it was involved in the substrate specificity determination of ERK2 and p38 MAPK α . p38 MAPK α was shown to bind its substrate MAPKAPK-3/3pk whereas ERK2 could not, however, ERK2 could bind 3pk when its TT/ED exosite was switched from ERK2-like (TT) to p38 MAPK α -like (ED) residues to generate the p38 MAPK α -like ERK2 mutant T157E/T158D [11]. These experiments were carried out with the inactive forms of the enzymes so it is difficult to interpret the effects of the exosite on the dual-phosphate form of ERK2.

One of the residues in the TT/ED region, Glu-160 of inactive p38 MAPK α , was also shown to form a hydrogen bond in a co-crystal structure of inactive p38 MAPK α and a docking motif peptide derived from the substrate MEF2A [27]. Glu-160 and His-126 are thought to determine the directionality of this peptide in the co-crystal structure. These results indicate that the TT/ED specificity-determining exosite was computationally predicted to be a specificity-determining region, was later shown to determine substrate specificity of binding and phosphorylation of the substrate 3pk for ERK2 and p38 MAPK α , and a docking motif peptide derived from the substrate MEF2a has been shown to bind the TT/ED exosite in a co-crystal structure indicating the importance of this exosite in several protein-protein interactions. Zhang *et al.* showed that inactive ERK2 T157A and T158A mutants exhibited up to a 3-fold decrease in specificity constant towards MBP phosphorylation and a ~13-fold decrease towards Elk-1(307-428) phosphorylation indicating the involvement of the TT/ED exosite in ERK2 towards Elk-1 [14]. However, these experiments were also carried out with inactive ERK2 on two substrates that have multiple phosphorylation sites making the results difficult to interpret for the active form of ERK2.

Interestingly, the active form of ERK2 has an ~ 100 -fold higher specificity constant²⁰ towards the substrate Ets $\Delta 138$ than does the active form of p38 MAPK α (Rainey and Dalby, unpublished). Therefore, if the TT/ED exosite in ERK2 and p38 MAPK α mediate the specificity of Ets $\Delta 138$ phosphorylation, we hypothesized that a mutation of ERK2 in this region to p38 MAPK α -like residues (T157E/T158D ERK2) would have a large decrease in the specificity constant towards the substrate Ets $\Delta 138$. The T157E/T158D ERK2 mutant was activated and assayed for its ability to phosphorylate Ets $\Delta 138$ (Table 6) and had an ~ 2 -fold effect on the specificity constant of Ets $\Delta 138$ phosphorylation (Figure 30) indicating that this region does not mediate the ~ 100 -fold specificity difference seen in ERK2 and p38 MAPK α towards the phosphorylation of the substrate Ets $\Delta 138$.

²⁰ Steady state kinetic parameters of active p38 MAPK α phosphorylation of Ets $\Delta 138$: $k_{\text{cat}} = 1.8 \pm 0.3 \text{ s}^{-1}$, $K_{\text{m}} = 85.5 \pm 19.5 \text{ }\mu\text{M}$, $k_{\text{cat}}/K_{\text{m}} = 0.02$ (n=3). Dual-phosphate ERK2 phosphorylation of Ets $\Delta 138$: $k_{\text{cat}}/K_{\text{m}} = 2.2$.

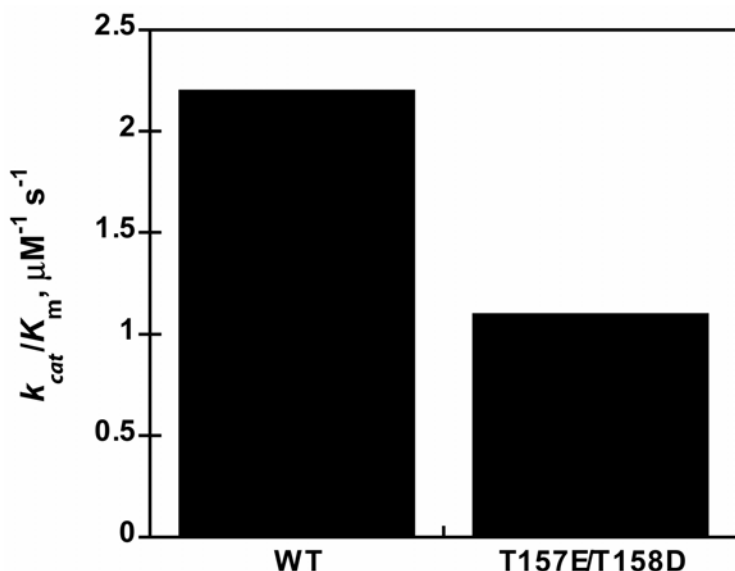


Figure 30. Specificity constant comparisons of EtsΔ138 phosphorylation by activated WT and the T157E/T158D ERK2 exosite mutant. The specificity constants were determined in Table 6 and plotted here to show relative differences between the WT enzyme and the p38-like ERK2 TT/ED (T157E/T158D) exosite mutant.

THE DOCKING GROOVE OF MAPKS

Two crystal structures were reported for the inactive form of the ERK2-related kinase p38 MAPK α bound to docking motif peptides derived from both an activating enzyme, MAPKK3b, and a substrate, MEF2A [27]. Both peptides contain a DEJL (Docking Site for ERK/JNK, LEL) motif found in MAPK substrates consisting of R/K-X₄- ϕ _A-X- ϕ _B (where X represents any amino acid and ϕ represents a hydrophobic residue: Leu, Ile, or Val). Both peptides bind in an extended conformation to the same binding groove of p38 MAPK α near to, but distinct from, the CD exosite and the active site.

These results suggest that this p38 MAPK α docking groove may represent a MAPK exosite for protein-protein interactions. The docking groove exosite identified in the co-crystal structures exists in the carboxy-terminus of p38 MAPK α between the α_D and α_E helices and the reverse turn between strands β_7 and β_8 [27]. This exosite was postulated several years earlier for p38 MAPK α 's ability to bind and phosphorylate its substrates MAPKAPK-2 and MAPKAPK-3 [49] and is distinct from the exosite hypothesized for JNK [45]. In the co-crystal structure, the p38 MAPK α residues Ile-116, Gln-120, and His-126 (homologous to the conserved ERK2 residues Leu-113, Gln-117, and His-123, respectively) line the docking groove exosite for both peptides and make either hydrophobic or hydrogen bond contacts with the DEJL peptide derived from the substrate MEF2A [27]. Mutagenic data showed that p38 MAPK α mutants I116A and Q120A failed to bind full-length MEF2A in a pull-down assay, whereas mutation of the TT/ED and CD exosite residues to alanine did not completely eliminate binding. These results suggest that I116 and Q120 are perhaps more critical than the TT/ED and CD exosites for p38 MAPK α to bind the substrate MEF2A. I116A and the CD exosite p38 MAPK α mutants could not bind MAPKK3b in similar pull-down assays indicating their importance in activator binding as well. Interestingly, phosphorylation of MEF2A was drastically reduced by p38 MAPK α mutations I116A and Q120A [27], while mutated CD and ED exosites did not have this effect. Unfortunately, the extent to which the phosphorylation was reduced by the docking mutants was not shown and it is not clear whether the results were obtained with the active or inactive form of the enzyme.

Since the residues lining the docking groove exosite on p38 MAPK α are critical for binding and phosphorylating the transcription factor MEF2a, and the fact that these residues are conserved among p38 MAPK α and ERK2, we hypothesized that mutation of these residues in ERK2 might affect E-S formation between ERK2 and Ets Δ 138 if this

exosite was involved in macromolecular recognition of EtsΔ138. Our results indicate that the dual-phosphate forms of the ERK2 mutants L113A and Q117A did not have a significant effect on the specificity constant of EtsΔ138 phosphorylation (Table 6, Figure 31). The H123A mutation, however, displayed a small 3-fold decrease in the specificity constant due to a small increase in k_{cat} and a larger increase in the K_m which may be due to the fact that K_m is a function of the steady-state rate of turnover as well as the forward and reverse rates of ES formation. These results suggest that mutation of His-123 to the smaller alanine residue may lead to a small decrease in the affinity of EtsΔ138 for ERK2, however, the affect is not large. It cannot be ruled out that the H123A mutation does not cause a global change in structure, because it lies within the α_E helix.

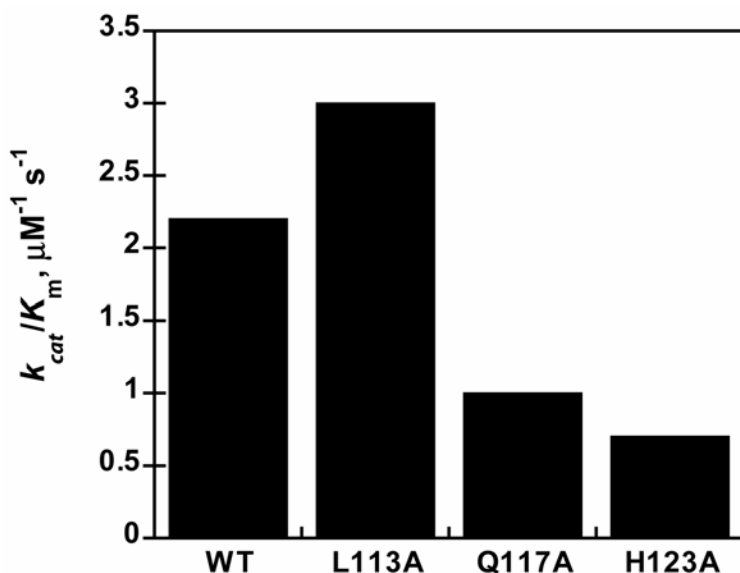


Figure 31. Specificity constant comparisons of EtsΔ138 phosphorylation by activated WT and proposed docking groove exosite mutants of ERK2. The specificity constants were determined in Table 6 and plotted here to show relative differences between the WT enzyme, L113A, Q117A, and H123A exosite mutants of ERK2. The mutations were based on conserved residues in p38 MAPK α shown to be involved in binding and phosphorylating the DEJL motif-containing proteins MEF2a and MKK3b.

SPECIFICITY DETERMINATION THROUGH EVOLUTIONARY CHANGES AFTER GENE DUPLICATION

As mentioned earlier, Caffrey *et al.* compared the amino acid sequences of p38 MAPK and ERK, two kinases related by gene duplication, and examined the residues that had undergone physicochemical changes conserved amongst subfamily ancestors (e.g. ERK1, ERK2, ERK5), but differed from the homologous residues found in p38 MAPK subfamily ancestors. Residues that scored high burst after duplication (BAD) values, or variance from the residues from which they duplicated from, were proposed to confer functional specificity differences between the two families while remaining conserved amongst subfamilies for other unknown functions [10]. Unfortunately, no experiments were carried out to test the hypothesized specificity differences. Furthermore, the proteins in which these residues confer specificity differences towards remain unknown. As mentioned earlier, the TT/ED exosite was predicted this computational study [10] prior to experimental values carried out elsewhere [11] confirming the validity of this method in determining specificity-determining exosites.

We chose two regions of ERK2 that scored high BAD values, in addition to the TT/ED exosite, and hypothesized that mutations of ERK2 residues to p38 MAPK α -like residues would decrease the specificity constant towards Ets Δ 138 if these exosites are involved in the formation of the E-S complex. One of the predicted specificity-determining exosites of ERK2, Y111N/K112N, lies near to the DEJL motif docking groove on p38 MAPK α [27] described above indicating that the computational data predicted specificity-determining residues that lie one residue *N*-terminal to residues in the docking groove exosite on p38 MAPK α . Obviously, the residues involved in the

peptide binding groove exosite of p38 MAPK α were not predicted by Caffrey *et al.* because these residues are conserved between ERK2 and p38 MAPK α .

Another computationally predicted exosite [10], K229T/H230D, was recently found to be a specificity-determinant based on a mutation made in inactive ERK2, H230R. H230 was identified from a yeast 2-hybrid study as a residue required for MAPKK1 binding and inactive H230R ERK2 had a 10-fold decrease in the specificity constant of phosphorylation towards MBP [12] indicating that this residue may be involved in substrate binding. Years earlier, a mutant was found in a genetic study (D227N in fus3p, homologous to H230 in ERK2) that showed a gain of function phenotype in the homologous yeast MAPK protein fus3p [111]. Recently, K229 and H230 were shown to be required for binding and activating the ERK2 phosphatase MKP3 [14] and their homologous residues lie in the predicted JNK2 exosite for the substrate c-jun [45] indicating that these residues may form a MAPK exosite involved in the specificity of several protein-protein interactions. This region is also distinct from the CD, YY, and docking groove exosite on ERK2. Homologous residues also lie close to a hydrophobic domain²¹ described by Knighton *et al.* reported to aid in the binding of a peptide inhibitor, PKI, to cAPK [46]. These results suggest that the computational study by Caffrey *et al.* may be very useful in determining those residues of protein kinases involved in specificity determination and may predict regions among protein kinases that are susceptible to physicochemical differences that determine the specificity of kinase interactions.

Activated Y111N/K112N ERK2 displayed a small ~3-fold decrease in the specificity constant of Ets Δ 138 phosphorylation as compared to WT ERK2 (Table 6, Figure 32) indicating that this exosite may have a small contribution toward the

²¹ cAPK residues 235-239 were shown to bind the P-11 phenylalanine of PKI in a co-crystal structure. These residues correspond to ERK2 residues 223-227, which lie near to 229/230.

formation of the E–S complex between the dual-phosphate form of ERK2 and EtsΔ138. The mutant Y111N/K112N may cause a global change due to helix misformation since these residues lie in the α_D helix. Interestingly, the K229T/H230D ERK2 mutant displayed a large decrease (~22-fold) in the specificity constant towards EtsΔ138 (Table 6, Figure 32) indicating that one or both of these residues affect E–S formation leading to phosphorylation of EtsΔ138. Since residues K229 and H230 lie in the L13 loop between α_F and α_G it is considered unlikely that mutations in these residues cause global structural change. To give perspective to the large effects of this mutation on phosphorylation of EtsΔ138, mutagenesis of the active site residue proposed to be involved with the phosphoryl-transfer of the phosphate from ATP to the protein substrate (K149A), led to a ~73-fold decrease in the specificity constant of EtsΔ138 phosphorylation²² mostly due to a defect in k_{cat} .

The decrease in the specificity constant of the K229T/H230D ERK2 mutant towards EtsΔ138 was not due to incomplete activation as ~ 2 mol/mol phosphates were shown to be incorporated by MAPKK1G7b in a radiolabeled assay (data not shown) and only one radiolabeled peptide was observed following trypsinization of the activated protein (Figure 33). The mass of the radiolabeled peptide was confirmed by mass spectrometry to mostly contain the predicted activation loop peptide corresponding to ERK2 residues 178-196 containing two phosphates (Figure 34).

²² This is based on dual-phosphate K149A ERK2 steady-state kinetic parameters of EtsΔ138 phosphorylation where $k_{cat} = 1.1 \pm 0.2 \text{ sec}^{-1}$ (n=4), $K_m^{\text{Ets}\Delta 138} = 42.8 \pm 25.6 \text{ }\mu\text{M}$ (n=2); $K_m^{\text{ATP}} = 64.1 \pm 9.1 \text{ }\mu\text{M}$ (n=2), $(k_{cat}/K_m)^{\text{Ets}\Delta 138} = 0.03 \text{ }\mu\text{M}^{-1} \text{ sec}^{-1}$.

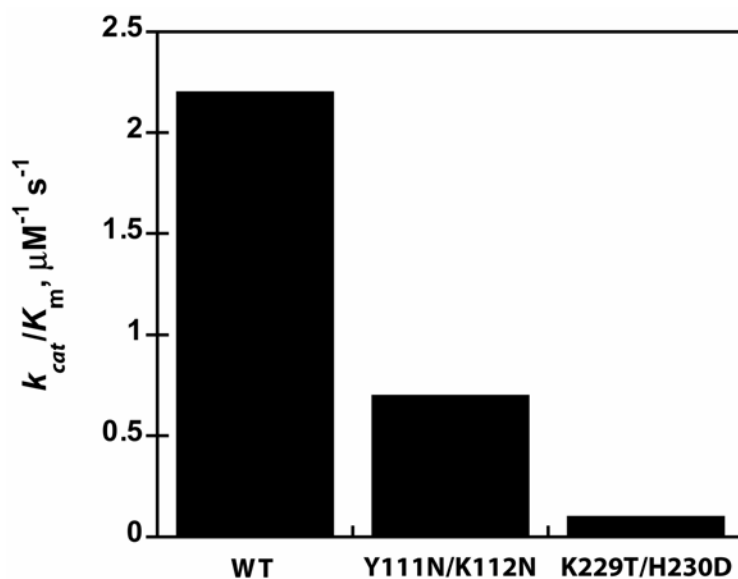


Figure 32. Specificity constant comparisons of Ets Δ 138 phosphorylation by activated WT and proposed specificity determining exosites of ERK2. The specificity constants were determined in Table 6 and plotted here to show relative differences between the WT enzyme and two computationally predicted regions thought to confer specificity differences between ERK2 and p38 MAPK α . Two regions were selected and ERK2 residues were mutated to p38 MAPK α -like residues: Y111N/K112N and K229T/H230D.

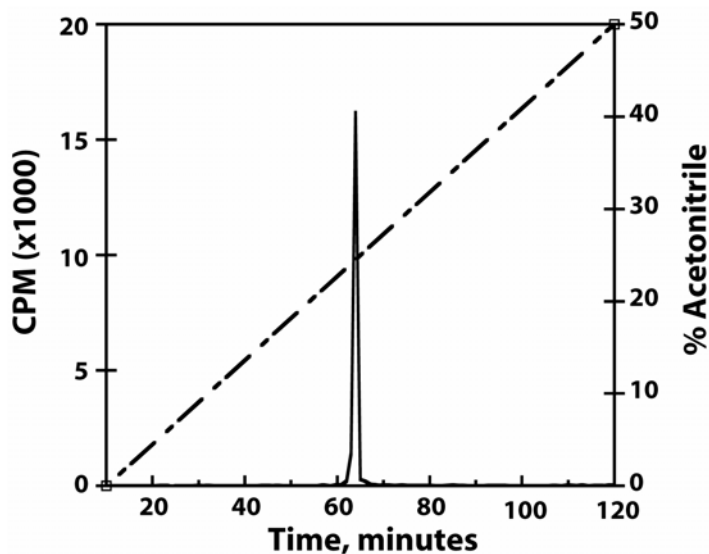


Figure 33. Tryptic peptide analysis of activated K229T/H230D ERK2 using reverse phase HPLC following activation by MAPKK1G7b. Radiolabeled active K229T/H230D ERK2 was dialyzed into 50 mM Tris, pH 8.6, overnight and cleaved with 10 μ g of trypsin for 10 hours. The tryptic digest was filtered and applied to a reverse phase C18 column in 0.1% TFA and peptides were eluted with a linear gradient of 50% acetonitrile containing 0.1% TFA. All fractions were collected and counted in a scintillation counter and radiolabeled fractions were kept for further mass analysis.

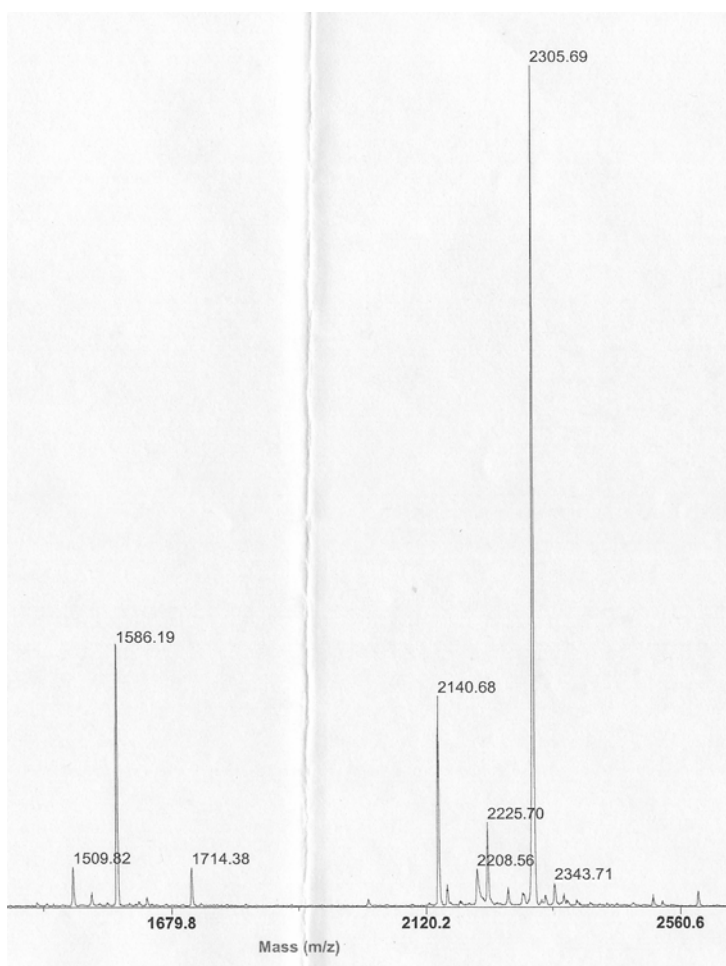
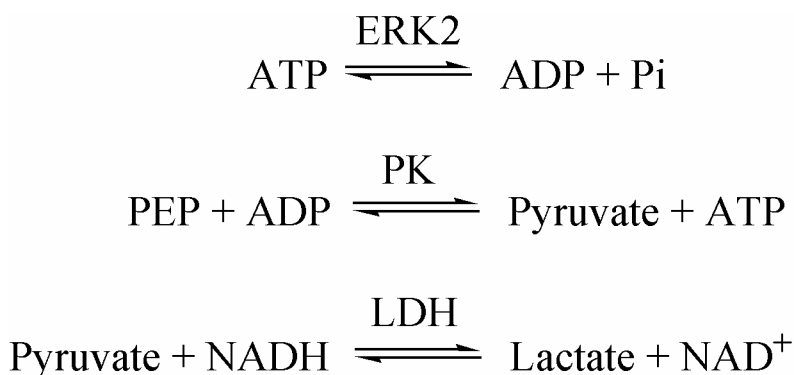


Figure 34. Mass spectrometry of the K229T/H230D phospho-peptide. The radiolabeled peptide from Figure 33 was analyzed by mass spectrometry. The peptide mass is shown as a mass:charge ratio (m/z). Peptide masses from left to right: (predicted in the format $\text{ERK2}^{\text{residue-residue}}$, actual mass shown in Da from mass spectrometry, calculated mass in Da) ERK2^{261-72} , 1509.82, 1508.7; unknown, 1586.19; unknown, 1714.38; ERK2^{1-20} , 2140.68, 2139.4; $\text{ERK2}^{178-196}$ (monophosphate) 2225.70, 2224.2, and $\text{ERK2}^{178-196}$ (dual-phosphate) 2305.69, 2304.2. The unknown 1586.19 Da peptide is near to the predicted mass of monophosphorylated peptide corresponding to ERK2^{61-72} (predicted 1588.7 Da). This is unlikely since all calculated values shown are lower than the actual mass (on average ~ 1.4 Da), whereas, in this situation, the predicted value was 2.5 Da higher.

To further characterize the K229T/H230D ERK2 exosite mutant, the steady-state kinetics of ERK2 phosphorylation of EtsΔ138 were measured with respect to ATP. Initial rates were measured for phosphate incorporation into EtsΔ138 using several concentrations of ATP while holding the EtsΔ138 at a high concentration (not saturating) so that the K_m^{app} of ATP could be elucidated. If the protein concentration is not saturating, the K_m^{app} will appear slightly smaller than the K_m . However, the mutant was shown to be similar to WT indicating that the mutation that affected the k_{cat} of EtsΔ138 did not drastically affect the ability of ATP to bind efficiently.

Since the k_{cat} of the mutant was lower than WT, we also measured the ATPase activity of the mutant enzyme to gain insight into whether or not the active site turnover of ATP was affected. To measure the ATPase activity in the absence of the protein substrate EtsΔ138, ERK2 was added to a solution containing the substrate ATP and a coupled-enzyme milieu containing phosphoenol pyruvate, pyruvate kinase, NADH, and lactate dehydrogenase [112]. The coupled-enzymes allowed the indirect measurement of the slower ATP hydrolysis reaction mediated by ERK2 by coupling the rate of ADP formation to the production of the oxidized form of NADH (Scheme 6).



Scheme 6. The coupled-reaction for ATPase measurement. ATP is converted to ADP and inorganic phosphate (Pi) by ERK2. ADP is rapidly phosphorylated by pyruvate kinase (PK) in the presence of the phospho-donor phosphoenol pyruvate (PEP) yielding pyruvate and ATP. Pyruvate was reduced to lactate by lactate dehydrogenase (LDH) in the presence of the reduced form of β -nicotinamide adenine dinucleotide (NADH) to yield the oxidized form of NAD^+ . The reaction was monitored at 340 nm for the disappearance of NADH upon formation of the colorless NAD^+ .

In the ATPase assay, ERK2 hydrolyzed ATP to form ADP and inorganic phosphate. The pyruvate kinase (PK) phosphorylated ADP in the presence of the phospho-donor phosphoenol pyruvate (PEP) to form ATP and pyruvate. Pyruvate was reduced to lactate by lactate dehydrogenase (LDH) in the presence of the reduced form of NADH to form the oxidized NAD^+ . The coupled reactions were monitored by following the rate of NADH oxidation which was proportional to the rate of ATP hydrolysis by ERK2 since the ATP hydrolysis was the rate-limiting reaction. The K229T/H230D ERK2 mutant had a similar ATPase activity to that of WT ERK2 at several concentrations of enzyme (Figure 35) indicating that the mutant could hydrolyze ATP as efficiently as the WT protein. These results further indicate that the defects in the steady

state kinetics of the phosphorylation of EtsΔ138 are a result of defects in the protein-protein interaction outside of the active site.

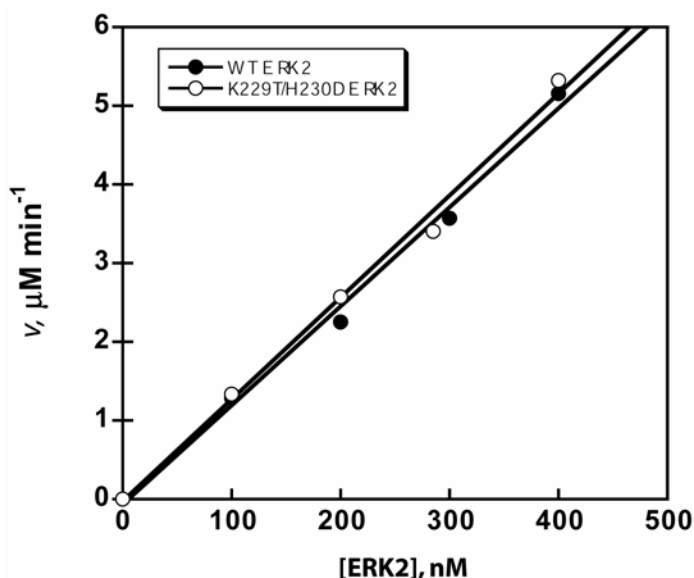


Figure 35. The ATPase activity of WT and K229T/H230D ERK2 are similar. WT and K229T/H230D ERK2 were incubated in the presence of ATP and a coupled-enzyme milieu (Scheme 6) to measure the rate of ATP hydrolysis occurring in the active site.

We have developed a fluorescence anisotropy assay to measure the equilibrium dissociation constant (K_d) between ERK2 and a fluorescent form of EtsΔ138. The K_d for the inactive K229T/H230D ERK2 mutant was significantly higher than the inactive form of WT ERK2 further indicating a deficiency in the mutant's ability to bind EtsΔ138 (Figure 36). These results suggest that the steady-state kinetic defects of K229T/H230D ERK2 stem from its inability to facilitate efficient macromolecular recognition of EtsΔ138 and form an efficient E-S docking complex while the ATPase activity and the K_m of ATP in the presence of EtsΔ138 remain similar to that of WT. Since dual-

phosphate ERK2 exhibits ~2000-fold higher ATPase activity than unphosphorylated ERK2 with respect to k_{cat} [5], we hypothesize that the catalytic residues and the phosphorylation loop of the K229T/H230D are in the proper orientation and do not affect the binding of EtsΔ138 even though these residues lie near the phosphorylated Thr-183 and Tyr-185 of ERK2 in the crystal structure [4]. The decrease in this mutants ability to bind EtsΔ138 could be due to the large physicochemical differences in the side chains at this position of ERK2 and p38 MAPK α and implies that this is an ERK2 exosite that not only determines the ability of activators (MAPKK1) [12] and inactivators (MKP3) [14] to bind but also determines substrate specificity and macromolecular recognition of the substrate EtsΔ138 and Elk-1 [14].

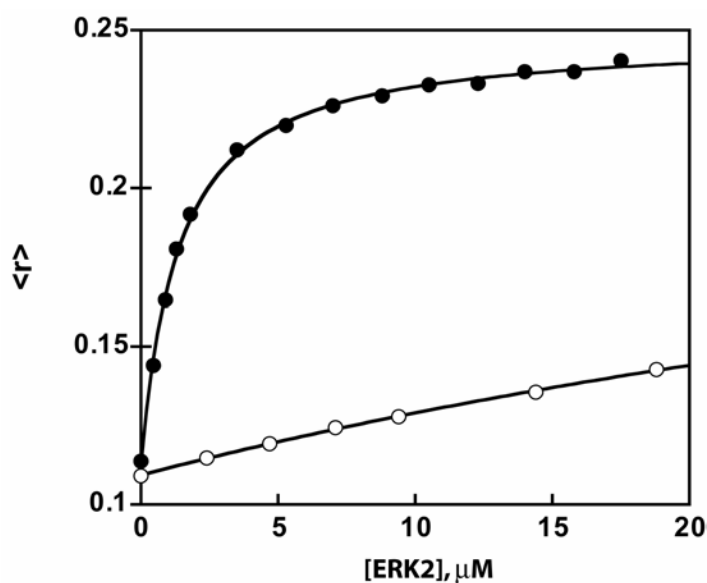


Figure 36. Fluorescence anisotropy of WT and K229T/H230D ERK2 binding to Ets Δ 138-Fluorescein. Fluorescence anisotropy was carried out using several concentrations of inactive WT (closed circles) and inactive K229T/H230D ERK2 (open circles) in the presence of 100 nM Ets Δ 138-Fluorescein. Assay conditions were 25 mM Hepes, pH 7.5, 50 mM KCl, 0.1 mM EDTA, 0.1 mM EGTA, 2% glycerol, 40 $\mu\text{g/mL}$ BSA, and 2 mM DTT; slit widths were 5 nm, integration time was 300 msec, data points represent the average of 12 data points taken for a single sample. Each reaction was excited with both vertically- and horizontally-polarized light at 492 nm and the emission was measured both vertically and horizontally to the excited light at 515 nm. The data were fit as described (Chapter 4) and the equilibrium dissociation constants determined to be $0.7 \pm 0.1 \mu\text{M}$ and $37.7 \pm 1.0 \mu\text{M}$ for WT and K229T/H230D, respectively. Although both endpoints fit to a similar value from the data shown, the K_d of K229T/H230D assumes that this value is correct.

PUTATIVE DEJL MOTIF ON ETSΔ138

To find regions on the substrate EtsΔ138 that mediate macromolecular recognition of ERK2, we mutated individual residues in a putative DEJL motif and made an *N*-terminal deletion mutant that deleted this region and tested the mutant substrates for defects in their steady-state kinetic parameters of phosphorylation by ERK2. The amino-terminus of EtsΔ138 contains a putative DEJL motif which have been shown to mediate binding to MAPKs. The putative DEJL motif was determined by primary amino acid sequence comparison to conserved DEJL motifs found in the ERK2 interacting proteins MAPKK1 and Elk-1 (Figure 37) [19, 29]. The putative DEJL motif has both the conserved lysine and leucine residues found in DEJL motifs and lies amino-terminal to the phospho-acceptor site (Thr³⁸) in EtsΔ138 similar to other known DEJL motifs. Peptides derived from Elk-1 and MAPKK1 DEJL motifs (Figure 37) inhibit ERK2 phosphorylation of the transcription factor Elk-1, MAPKK2 binding to ERK2, and MKP-1 dephosphorylation of ERK2 [54]. These results suggest that the DEJL peptides bind and inhibit ERK2, presumably, by binding the MAPK exosite involved in binding activators, regulators, and substrates. It has been suggested that DEJL motif peptides bind to the CD exosite of ERK2 which has been shown to interact with several proteins [17], however, the co-crystal structure of the inactive form of p38 MAPKα binds two DEJL peptides in the docking groove exosite near to, but distinct from, the CD exosite [27]. The Elk-1 DEJL motif has also been shown to recruit ERK2 to phosphorylate an Elk-1 consensus sequence peptide more efficiently [113] indicating the usefulness of docking motifs in increasing the catalytic efficiency of phosphorylation. We have also shown that the Elk-1 DEJL motif peptide is a competitive inhibitor towards EtsΔ138

phosphorylation, indicating that EtsΔ138 may form a docking complex *via* a DEJL motif on an ERK2 exosite (Chapter 4).

Sequence	Protein
- KTEK -VD LELF PSP-	EtsΔ138
- KGRKPRDLEL PLSPS-	Elk-1
MP KKK PT IQL NPAPDG-	MAPKK1

Figure 37. Sequence alignment comparing known DEJL motifs with a putative EtsΔ138 DEJL motif. The *N*-terminal portion of EtsΔ138 (residues 15-27 shown) contains residues that align well with known DEJL motifs that mediate ERK2 exosite recognition of activators, substrates, and phosphatases. The Elk-1 and MAPKK1 peptides have shown to inhibit ERK2 phosphorylation of Elk-1 indicating that this putative region in EtsΔ138 may be a docking motif that directs the phosphorylation of Thr-38.

We hypothesized that the putative DEJL motif of EtsΔ138 might be mediating macromolecular recognition of ERK2 since a similar region on Elk-1 recruits ERK2 and JNK to phosphorylate its multiple Ser/Thr-Pro phosphorylation sites [19, 29]. The amino-terminus of EtsΔ138 is very flexible and unstructured, as determined by the multiple conformations seen in the NMR structure of a truncated version of this protein [114]. An amino-terminal truncation of EtsΔ138 has been generated that lacked the putative DEJL motif (Ets²⁹⁻¹³⁸) and was shown to bind ERK2 using affinity chromatography [52], however, the authors did not report the kinetic parameters for its phosphorylation by ERK2. These results indicate that the amino-terminus is not absolutely required for EtsΔ138 to bind to ERK2, but its contribution to binding and phosphorylation was unknown.

Therefore, we constructed an amino-terminal deletion of EtsΔ138 lacking the first 23 amino acids (EtsΔ24-138) that contained the putative DEJL motif to study the effects

of the deletion on the steady-state kinetic parameters of EtsΔ138 phosphorylation. The truncation led to a 10-fold increase in the K_m^{app} as compared to WT EtsΔ138 with no effects on the apparent catalytic rate constant of the enzyme (Table 7, Figure 38). These results are expected for a substrate docking motif required for E–S formation through a docking complex, but not required for efficient chemical transfer of phosphate from ATP to the protein substrates phosphorylation site. EtsΔ24-138 did not affect the K_m^{app} of the nucleotide substrate (Table 7), indicating that ATP binding to ERK2 is not affected by the truncated substrate. These results indicate that the amino-terminus of EtsΔ138 is required for efficient phosphorylation of the protein substrate, but interestingly, was not found to be required for binding ERK2 from a calf thymus nuclear extract [52]. Perhaps the binding experiment did not require a high ERK2–EtsΔ138²⁹⁻¹³⁸ affinity or another possibility is that other proteins such as scaffold proteins may have enhanced their interactions. Additional data indicating the importance of the *N*-terminus of EtsΔ138 in mediating the ERK2–EtsΔ138 docking complex was generated using a fluorescence anisotropy competition assay to measure the K_d of the mutant protein and ERK2. The data indicate that the K_d for EtsΔ24-138 is ~ 13-fold higher than that of EtsΔ138²³ in line with the steady-state kinetic results (~ 15-fold increase in K_m). However, it is not clear which individual residues contribute to the binding of ERK2 or if the *N*-terminus is simply required for structural support during formation of the E–S docking complex leading to phosphoryl-transfer.

²³ The K_d of EtsΔ²⁴⁻¹³⁸ was determined to be $82.8 \pm 3.2 \mu\text{M}$ ($n = 2$) in a fluorescence anisotropy competition assay, whereas WT was determined to be $6.6 \pm 1.2 \mu\text{M}$ ($n = 3$); in the absence of both nucleotide and magnesium chloride (Chapter 5).

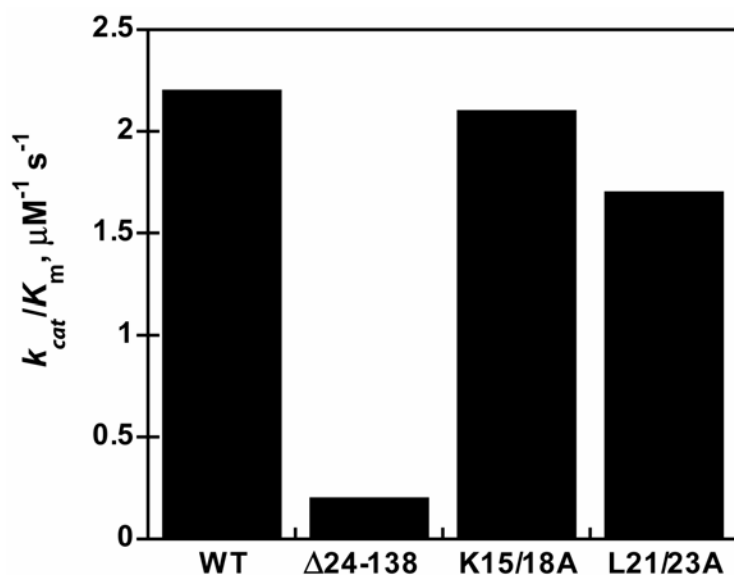


Figure 38. Specificity constant comparisons of dual-phosphate WT ERK2 phosphorylation of Ets Δ 138 containing mutations of the putative DEJL motif. The specificity constants were determined in Table 7 and plotted here to show relative differences between the WT Ets Δ 138 and the putative DEJL motif mutants of Ets Δ 138. An *N*-terminal mutant missing the first 23 amino acids of Ets Δ 138 (Ets Δ 24-138, abbreviation Δ 24-138) lacks the putative DEJL motif. K15A/K18A and L21A/L23A Ets Δ 138 are mutants of both the conserved lysines and leucines in the putative DEJL motif.

Mutant	k_{cat}	K_m , EtsΔ138	K_m , ATP	k_{cat}/K_m (Ets)
WT	19.6 ± 0.7	8.8 ± 1.4	98.7 ± 4.4	2.2 ⁿ⁼¹²
Δ24-138	20.5 ± 1.7	127.6 ± 19.4	117.3 ± 13.4 ^{app}	0.2 ⁿ⁼¹
K15A	17.3 ± 0.9	10.4 ± 2.3	-	1.7 ⁿ⁼⁴
K18A	18.4 ± 0.5	8.0 ± 0.9	-	2.3 ⁿ⁼¹
L21A	19.2 ± 1.0	12.0 ± 2.5	-	1.6 ⁿ⁼¹
L23A	18.3 ± 0.6	12.3 ± 1.7	-	1.5 ⁿ⁼¹
K15A/K18A	22.5 ± 3.4	10.8 ± 2.0	-	2.1 ⁿ⁼²
L21A/L23A	22.0 ± 0.4	13.3 ± 0.8	-	1.7 ⁿ⁼²

Table 7. The steady-state kinetic parameters for EtsΔ138 mutants phosphorylated by dual-phosphate ERK2. These values were obtained with radiolabeled P81 assays [7]. For the determination of the K_m for EtsΔ138 saturating ATP (2 mM) was used while varying the EtsΔ138 concentration from 6.3-200 μM. For the determination of the K_m for ATP saturating EtsΔ138 concentrations (200 μM) were used while varying the ATP concentration from 31.3-1000 μM. Each value was determined using 6 initial velocities fit to the equation $k_{obs} = (k_{cat} \times [S]) / (K_m + [S])$. Assay contained were 25 mM Hepes, pH 7.5, 50 mM KCl, 0.1 mM EDTA, 0.1 mM EGTA, 40 μg/mL BSA, 20 mM MgCl₂, 2 mM DTT, 1 nM ERK2, EtsΔ138, and ATP. Values are shown as a mean ± standard error. The mean k_{cat} was determined using the values obtained from both EtsΔ138 and ATP analyses and were found to be similar. Units: k_{cat} , s⁻¹; K_m , μM; k_{cat}/K_m , μM⁻¹ s⁻¹.

To elucidate the contribution of individual residues in the putative DEJL motif towards phosphorylation, we carried out alanine mutagenesis on the lysine and leucine residues corresponding to those conserved in DEJL motifs (Figure 37). We hypothesized that if these residues are involved in E-S formation, the specificity constant would decrease due to an increase in the K_m for the mutants. We found that neither the single mutants nor double mutants (K15A/K18A and L21A/L23A EtsΔ138, Table 7, Figure 38), had adverse effects on the specificity constant. These results indicate that there may be

other residues in the initial 23 amino acids of the protein²⁴ that are contributing to the formation of the E–S complex or that the structural integrity of this *N*-terminal region is important for docking. In addition, a *C*-terminal deletion of EtsΔ138 (Ets1¹⁻⁵²) was reported to have a K_m of 190 μM [52], indicating that both the *N*- and *C*-terminal region of EtsΔ138 are required for efficient E–S formation leading to phosphoryl-transfer.

AN ETSΔ138 PHENYLALANINE DOCKING MOTIF

Some ERK2 substrates have been shown to contain docking motifs containing two phenylalanine residues separated by a single amino acid that allows efficient macromolecular recognition by ERK2. The “docking site for ERK, FXFP” (DEF) motif was first identified as a gain-of-function mutation in the *lin-1* ETS gene leading to a vulvaless phenotype in *C. elegans* due to a lack of negative regulation by an ERK2 homolog (MPK-1) [18]. The two phenylalanine residues in the FXFP motif are the most important determinants for ERK2-binding [19], however, replacement of these residues with tyrosines does not disrupt the function of the DEF motif [115]. These results indicate the importance of the phenyl ring in DEF motif binding to ERK2. Many substrates utilize a DEF motif for ERK2 docking such as IEX-1 [68], SAP-1 [116], c-Fos [117], c-Myc, N-Myc of the immediate early gene family, transcription factors Elk-1 and GATA-2, MKP-1, KSR-1 [19], and PDE4D3 cAMP-specific phosphodiesterase [118]. A docking motif on EtsΔ138 was discovered in which a *C*-terminal LxLxxxF¹²⁰ motif

²⁴ The *N*-terminus of EtsΔ138 may contain an additional DEJL-like motif: M¹-K-A-A-V-D-L-K-P-T-L-T-I-I¹⁴. Mutation of the underlined DEJL-like residues may elucidate the *N*-terminal docking motif. Two mutants VDL/ADA and LTI/ATA could be tested. Another *N*-terminal mutant leaving the K¹⁵XXKXXLXL²³ motif to indicate that the binding site is *N*-terminal to this motif could also be carried out.

enhances efficient phosphorylation by ERK2; the phenylalanine contributes the bulk of the binding energy as measured by a large increase in K_m when mutated to alanine [52]. It has not been determined whether or not a tyrosine can be substituted for the phenylalanine in EtsΔ138. The EtsΔ138 C-terminal docking motif appears to be a hybrid of the known ERK2 docking motifs (DEJL and DEF), where it contains both the hydrophobic portion of the DEJL motif (LEL residues) followed by one Phe residue (DEF-like).

Since DEF motifs usually contain two Phe residues and EtsΔ138 lacks an FXFP motif, we searched the NMR structure for another nearby Phe residue and found that Phe-88 lies within 9Å of Phe-120 (Figure 39) [114], but distant by 32 amino acids in the primary amino acid sequence. Mutagenesis of Phe-88 to an alanine (F88A) had an ~3-fold effect on ERK2 phosphorylation as measured by its steady-state kinetic parameters (Table 8, Figure 40), whereas, mutation of Phe-120 (F120A) [52] led to an ~24-fold increase in K_m for EtsΔ138 phosphorylation (Table 8, Figure 40). Mutation of both phenylalanines, F88A/F120A, did not lead to further abrogations in the K_m than the F120A mutation (Table 8, Figure 40), further indicating the importance of Phe-120 and lack of a strong binding contribution by Phe-88 in forming the E-S complex with ERK2. As expected for a docking motif residue involved in E-S formation with ERK2 and not catalysis, F120 does not affect the K_m^{app} for ATP binding to ERK2 (Table 8). These results indicate that a single phenylalanine (Phe-120) on EtsΔ138, and not Phe-88, contributes a significant amount of binding energy towards E-S formation with ERK2.



Figure 39. Structural representation of EtsΔ138 and the phenylalanine docking motif. A ribbon structure of EtsΔ138 is shown (1BQV) with the phosphorylation site Thr-38 (red), the Phe-120 (blue) involved in formation of the ERK2-EtsΔ138 docking complex, and Phe-88 (green).

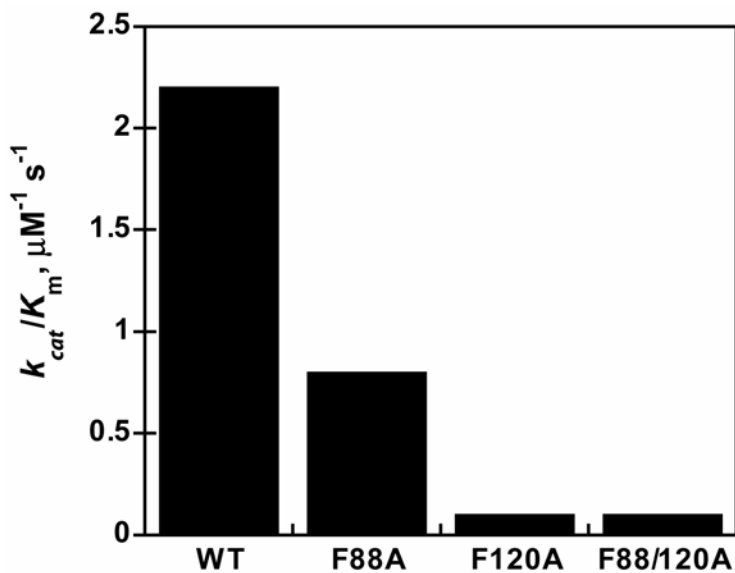


Figure 40. Specificity constant comparisons of activated WT ERK2 phosphorylation of EtsΔ138 phenylalanine mutants. The specificity constants were determined in Table 8 and plotted here to show relative differences between the WT EtsΔ138 and phenylalanine mutants.

Mutant	k_{cat}	K_m, EtsΔ138	K_m, ATP	$k_{\text{cat}}/K_m(\text{Ets})$
WT	19.6 ± 0.7	8.8 ± 1.4	98.7 ± 4.4	2.2 ⁿ⁼¹²
F88A	16.5 ± 0.8	19.5 ± 3.3	-	0.8 ⁿ⁼¹
F120A	18.6 ± 3.6	210.2 ± 26.4	96.1 ± 7.9	0.1 ⁿ⁼²
F88A/F120A	15.2 ± 5.6	264.9 ± 132.9	-	0.1 ⁿ⁼¹

Table 8. The steady-state kinetic parameters for EtsΔ138 phenylalanine mutants phosphorylated by dual-phosphate ERK2. These values were obtained with radiolabeled P81 assays [7]. For the determination of the K_m for EtsΔ138 saturating ATP (2 mM) was used while varying the EtsΔ138 concentration from 6.3-200 μM. For the determination of the K_m for ATP saturating EtsΔ138 concentrations (200 μM) were used while varying the ATP concentration from 31.3-1000 μM. Each value was determined using 6 initial velocities fit to the equation $k_{\text{obs}} = (k_{\text{cat}} \times [\text{S}]) / (K_m + [\text{S}])$. Assay conditions were 25 mM Hepes, pH 7.5, 50 mM KCl, 0.1 mM EDTA, 0.1 mM EGTA, 40 μg/mL BSA, 20 mM MgCl₂, 2 mM DTT, 1 nM ERK2, EtsΔ138, and ATP. Values are shown as a mean ± standard error. The mean k_{cat} was determined using the values obtained from both EtsΔ138 and ATP analyses and were found to be similar. Units: k_{cat} , s⁻¹; K_m , μM; k_{cat}/K_m , μM⁻¹ s⁻¹.

CONCLUSIONS

MAPKs bind and phosphorylate a wide variety of proteins within the cell including kinases, transcription factors, and phosphatases that regulate cell-signaling pathways. Understanding how protein kinases recognize their protein substrates, catalyze the phosphorylation of those substrates, and regulate cell signaling is crucial to understanding the basis of a cells response to various input signals.

We studied the steady-state kinetics of a particular protein kinase of the MAPK family, ERK2, in its dual-phosphate/activated form under conditions where residues on the surface of either ERK2 or the protein substrate EtsΔ138 had been mutated to understand the role of individual amino acids in carrying out phosphorylation. Several

putative exosites on the surface of MAPKs have been elucidated as contributing to specific protein-protein interactions with either an upstream kinase, a phosphatase, or its substrates outside of the catalytic cleft of MAPKs. Most of these studies have been carried out using non-quantitative methods with the inactive form of the enzyme and with substrates that have multiple phosphorylation sites. Here, we carried out a study using the active form of the protein kinase ERK2 since it has an enhanced catalytic rate of ~ 50,000-fold over the inactive enzyme [5] and is likely the most physiological relevant species that phosphorylates substrates within the cell.

Regions of ERK2 that mediate macromolecular recognition of protein substrates remain largely unknown. The CD exosite for MAPKs was shown to be a common binding site for several MAPK binding interactions including activators, substrates, and phosphatases [17]. However, the CD exosite does not appear to be required for activation of ERK2 by MAPKK1 and is not required for efficient phosphorylation of the substrate EtsΔ138. Mutation of the CD exosite residues Asp-316 and Asp-319 to alanine (D316A and D319A) did not significantly alter the steady-state kinetic parameters of EtsΔ138 phosphorylation by ERK2. These results indicate that although the common docking exosite might be required for efficient binding to MAPKK1 it is not essential for ERK2 activation by dual-phosphorylation. A nearby region termed the hydrophobic (YY) exosite on ERK2 consisting of Tyr-314 and Tyr-315 was shown to be required for efficient phosphorylation by MAPKK1 [48] but was not required for efficient EtsΔ138 phosphorylation. These results suggest that another region on ERK2 besides the CD and YY exosite is required for its protein–protein interaction with EtsΔ138.

The docking groove exosite of p38 MAPKα lies near to the CD and YY exosite and has been shown to bind DEJL motifs found in MAPK-interacting proteins as revealed by a crystal structure of the inactive form of p38 MAPKα with two DEJL-

derived peptides [27]. A similar exosite on the dual-phosphate form of ERK2, including the loop that spans from the α_D helix to the α_E helix and the $\beta 7$ - $\beta 8$ reverse turn, was hypothesized to bind a DEJL peptide derived from the MAPK protein substrate Elk-1 [28]. Therefore, a homologous exosite conserved in both ERK2 and p38 MAPK α may also be involved in binding activators, substrates, and phosphatases. The homologous residues on the inactive form of p38 MAPK α that made contacts with the DEJL peptide of MEF2a and MKK3b in co-crystallization experiments [27] were mutated to alanine to produce the ERK2 mutants L113A, Q117A, and H123A. These mutants were activated by MAPKK1 and H123A was shown to have small 3-fold decrease in the specificity constant, while L113A and Q117A remained largely unchanged. While His-123 may play a small role in forming the E-S complex formed between ERK2 and Ets Δ 138, this mutation may also induce a global conformational change since this residue lies in the α_F helix and not on a loop. These results indicate that these residues within the docking groove exosite of dual-phosphate ERK2 do not play a large role in directing E-S formation between ERK2 and Ets Δ 138.

MAPK members are thought to be related through gene duplication from a single gene and their novel protein functions have been obtained through physicochemical changes in residues involved in novel protein-protein interactions [10]. ERK and p38 MAPK α were compared and shown to have regions in which there were physicochemical differences between the two MAPK members following gene duplication whereas these same residues were conserved amongst the two subfamilies [10] indicating that specificity differences may exist in these regions. We have shown that Ets Δ 138 is a more efficient substrate for ERK2 than it is for p38 MAPK α . Therefore, in mutating ERK2 residues to the homologous p38 MAPK α -like residues that differ in physicochemical properties, we hypothesized that we could find an enzymic exosite on ERK2 that

mediated E-S formation with EtsΔ138 by finding p38-like ERK2 mutants that phosphorylated EtsΔ138 less efficiently.

The TT/ED exosite was shown to confer specificity differences for the ability of p38 MAPK α , but not ERK2, to bind and phosphorylate the substrate 3pk [11]. We mutated this region in ERK2 to form the T157E/T158D ERK2 mutant and showed that this mutation did not have a large affect on EtsΔ138 steady-state kinetic parameters. Similar mutations were made to generate Y111N/K112N and K229T/H230D ERK2 and were shown to have a ~3 and ~22-fold decrease in the specificity constant. While the Y111N/K112N may cause global conformational changes since these residues lie in the α_D helix, it is unlikely that the K229T/H230D mutation causes global conformational changes due to the fact that it lies in a loop (L13) between the α_F and α_G helicies. The K229T/H230D ERK2 mutant was shown to contain 2 phosphates upon activation by MAPKK1G7b in the phosphorylation loop indicating that it was bis-phosphorylated similar to WT ERK2. The dual-phosphate K229T/H230D ERK2 mutant was also shown to have a similar ATPase activity as that of WT ERK2 indicating that the mutant does not have large conformational changes within its active site. It was also shown that the inactive K229T/H230D had a >40-fold increase in the K_d as compared to the WT enzyme for its ability to bind a fluorescent form of EtsΔ138 indicating that this exosite may be responsible for ERK2 binding to EtsΔ138 to form the E-S complex required for efficient phosphoryl-transfer.

The substrate EtsΔ138 was also analyzed by mutagenesis studies to find docking motifs that were required for efficient phosphorylation by the dual-phosphate form of ERK2. The *N*-terminus of EtsΔ138 contained a putative DEJL motif that has been shown to bind the docking groove exosite on inactive p38 MAPK α [27] and a similar site on dual-phosphate ERK2 [28]. We made an *N*-terminal deletion of EtsΔ138 lacking the

putative DEJL motif and showed that this region was required for efficient phosphoryl-transfer. Upon mutating individual residues of the putative DEJL motif, we found that neither the conserved lysines nor the leucines in the DEJL motif were required for efficient phosphoryl-transfer indicating that the *N*-terminal region may be required for structural support of the phosphorylation reaction or may contain another docking motif that has yet to be elucidated.

A previously determined docking motif in the *C*-terminus of EtsΔ138 consists of an LxLxxxF¹²⁰ motif [52] which appears to be a hybrid of the DEJL motif and a DEF motif. It was confirmed that Phe-120 is required for efficient phosphorylation by ERK2 due to a large increase in K_m when mutated to alanine. Since DEF motifs contain two phenylalanines we also mutated a nearby phenylalanine and found that Phe-88 was not required for efficient phosphoryl-transfer. These results suggest that the EtsΔ138 substrate contains a *C*-terminal docking site required for forming the E–S docking complex which appears to be a hybrid form of the DEJL and DEF motif docking sites.

This study has shown that steady-state kinetics of the active form of ERK2 and its protein substrate EtsΔ138 containing a single phosphorylation site can be carried out using mutant forms of either the enzyme or the substrate to determine residues that are involved in efficient E–S formation leading to efficient phosphoryl transfer. We have shown that the *N*-terminal 23 residues of EtsΔ138 are required for efficient phosphoryl-transfer in addition to the Phe-120 docking site in the *C*-terminus. Several exosites on ERK2 (CD, YY, TT/ED, and docking groove residues) were mutated to elucidate whether or not these residues were required for efficient phosphorylation of EtsΔ138 and shown to have negligible effects. However, mutation of residues 229 and 230 in ERK2 to p38 MAPKα-like residues caused a significant reduction in the efficiency of phosphorylation of EtsΔ138 mostly due to an increase in K_m . The dissociation constant

for ERK2 binding of this mutant was also shown to increase significantly indicating that this mutation largely affected binding and not the rate of phosphoryl-transfer. These data are consistent with residues 229 and 230 binding involved in forming a docking complex with ERK2 indicating this region as an exosite required for Ets Δ 138 binding and efficient phosphorylation.

EXPERIMENTAL PROCEDURES

MATERIALS

All oligonucleotides were synthesized by Genosys. Ni^{2+} -NTA was purchased from Qiagen.

CONSTRUCTION OF SITE-SPECIFIC ERK2 MUTANTS

A bacterial expression vector, NpT7-5 encoding a hexa-histidine tag followed by cDNA encoding the rat ERK2 (NpT7-5 His₆-ERK2, a gift of N. Ahn, University of Colorado, Boulder, Colorado), was modified by PCR using site-directed mutagenesis to construct K229T/H230D, D316A, D319A, D316A/D319A, and Y314A/Y315A ERK2. The NpT7-5 His₆-ERK2 vector was digested with SacII and HindIII and ligated into a SacII-HindIII digested pBluescript (pBS) vector using T4 DNA ligase to create pBS-ERK2. The mutations were produced by a two-step PCR reaction using the following conditions: 94 °C for 5 min to denature the complementary strands; 30 cycles of 55 °C for 30 sec to anneal the primers, extension for 1 min at 72 °C, followed by a denaturation step at 94 °C for 45 sec; complementary strands were extended a final 10 min at 72 °C. The first round of PCR generated two overlapping products, fragment A and B, from two separate reactions using pBS-ERK2 as template. Fragment A was amplified using an outer forward primer that contained an EcoRI restriction site (underlined) (5'-TAT GTT GAA TTC CAA GGG TTA TAC-3') and an inner reverse primer containing the mutation (*italics*) for K229T/H230D (5'-CTG GTC AAG GTA GTC *GGT TCC* TGG GAA GAT-3'), D316A (5'-ACT TGG *GGC* ATA ATA CTG CTC C-3'), D319A (5'-GC

AAT GGG CTC *GGC* ACT TGG-3'), or Y314A/Y315A (5'-ACT TGG GTC *AGC AGC* CTG CTC CAG G-3'). Fragment B was amplified with an inner forward primer containing the mutation for K229T/H230D (5'-ATC TTC CCA *GGA ACC* GAC TAC CTT GAC CAG-3'), D316A (5'-G GAG CAG TAT TAT *GCC* CCA AGT-3'), D319A (5'-CCA AGT *GCC* GAG CCC ATT GC-3'), or Y314A/Y315A (5'-C CTG GAG CAG *GCT GCT* GAC CCA AGT-3') and an outer reverse primer containing the beginning of the HindIII restriction site in ERK2 (5'-GGT CGA CGG TAT CGA TAA GC-3'). Fragments A and B were purified and used as templates for a second round of PCR using only the outer primers. The product was digested with EcoRI and HindIII and ligated into EcoRI-HindIII digested pBS-ERK2. The pBS-ERK2 mutants were digested with SacII and HindIII and subcloned into SacII-HindIII digested NpT7-5 His₆-ERK2. Mutants containing two mutations were made using single mutant DNA as template and incorporating a second mutation.

Construction of Y111N/K112N, L113A, Q117A, H123A, and T157E/T158D ERK2 mutants were carried out similar to above using different outside primers. Fragment A was amplified with an outer forward primer that lies 5' to the SacII restriction site (5'-GAA TTG TAA TAC GAC TCA CTA TAG-3') and an inner reverse primer containing the mutation for Y111N/K112N (5'-GT CTT CAA GAG *GTT GTT* AAG ATC TGT CT-3'), L113A (5'-CTG TGT CTT CAA *GGC* CTT GTA AAG ATC-3'), Q117A (5'-TT GCT GAG GTG *CGC* TGT CTT CAA GAG-3'), H123A (5'-G AAA ATA GCA GAT *GGC* ATC ATT GCT GAG G -3'), or T157E/T158D (5'-CTT GAG ATC ACA *ATC TTC* GTT CAG CAG GAG-3'). Fragment B was amplified with an inner forward primer containing the mutation for Y111N/K112N (5'-AG ACA GAT CTT *AAC AAC* CTC TTG AAG AC-3'), L113A (5'-GAT CTT TAC AAG *GCC* TTG AAG ACA CAG C-3'), Q117A (5'-CTC TTG AAG ACA *GCG* CAC CTC AGC AA-3'),

H123A (5'-C CTC AGC AAT GAT *GCC* ATC TGC TAT TTT C-3'), or T157E/T158D (5'-CTC CTG CTG AAC *GAA GAT* TGT GAT CTC AAG-3') and an outer reverse primer containing an EcoRI restriction site (5'-GTA TAA CCC TTG GAA TTC AAC ATA-3'). Fragments A and B were purified and used as templates for a second round of PCR using only the outer primers. The product was digested with SacII and EcoRI and ligated into SacII-EcoRI digested pBS-ERK2. The pBS-ERK2 mutants were digested with SacII and HindIII and subcloned into SacII-HindIII digested NpT7-5 His₆-ERK2. All mutations were verified by sequencing the DNA at UT core facilities using an Applied Biosystems automatic DNA sequencer.

CONSTRUCTION OF SITE-SPECIFIC ETSΔ138 MUTANTS

A pET-28a bacterial expression vector encoding a hexa-histidine tag followed by the cDNA encoding murine Ets1 residues 1-138 (pET-28a EtsΔ138, a gift of L. P. McIntosh, University of British Columbia, Vancouver) was modified by PCR using site-directed mutagenesis to construct an *N*-terminal truncation mutant containing Ets1 residues 24-138 with an initial methionine (pET-28a EtsΔ24-138) and the EtsΔ138 mutants K15A, K18A, L21A, L23A, F88A, and F120A. To construct the pET-28a EtsΔ24-138 *N*-terminal truncation mutant, pET-28a EtsΔ138 was PCR amplified with a forward primer containing an NdeI site (encoding the initial methionine) followed by the codon encoding Phe-24 (5'-GG GAA TTC CAT ATG TTC CCT TCC CCG GAC ATG-3') and an outer reverse primer (5'-GCT AGT TAT TGC TCA GCG GTG G-3') using PCR conditions described for ERK2 mutants. The *N*-terminal mutant PCR product was digested with NdeI and HindIII and ligated into NdeI-HindIII digested pET-28a. All proteins produced from pET-28a have an *N*-terminal sequence of M-G-S-S-H-H-H-H-H-

H-S-S-G-L-V-P-R-G-S-H- prior to the initial methionine encoded by the Ets Δ 138 cDNA giving Ets Δ 24-138 an approximate mass of 15, 391 Da whereas Ets Δ 138 has a mass of 17, 681 Da (lacking the initial methionine) [7].

For the Ets Δ 138 point mutations, fragment A was PCR amplified with an outer forward primer (5'-GGT GAT GCC GGC CAC GAT GC) and an inner reverse primer containing the mutation for K15A (5'-TTC TGT *GGC* GAT GAT GGT GAG AGT-3'), K18A (5'-AAG CTC GAG ATC CAC *GGC* TTC TGT-3'), L21A (5'-CTC *GGC* ATC CAC TTT TTC TGT C-3'), L23A (5'-GTC CGG GGA AGG GAA *GGC* CTC-3'), F88A (5'-C TTT CAG GCT AGC CTC ATT CAC A-3'), or F120A (5'-AT ATC CCC AAC *AGC* GTC TGG AGC CA-3'). Fragment B was amplified with an inner forward primer containing the mutation for K15A (5'-ACT CTC ACC ATC ATC *GCC* ACA GAA-3'), K18A (5'-ACA GAA *GCC* GTG GAT CTC GAG CTT-3'), L21A (5'-G ACA GAA AAA GTG GAT *GCC* GAG-3'), L23A (5'-GAG *GCC* TTC CCT TCC CCG GAC-3'), F88A (5'-T GTG AAT GAG *GCT* AGC CTG AAA G-3'), or F120A (5'-TG GCT CCA GAC *GCT* GTT GGG GAT AT-3') and an outer reverse primer (5'-GCT AGT TAT TGC TCA GCG GTG G-3'). Fragments A and B were purified and used as templates for a second round of PCR using the outer primers. Mutants containing two mutations were made using single mutant DNA as template and incorporating a second mutation. The mutant PCR products were digested with NdeI and HindIII and ligated into NdeI-HindIII digested pET28a. All mutations were verified by sequencing the DNA at UT core facilities using an Applied Biosystems automatic DNA sequencer.

PURIFICATION OF UNPHOSPHORYLATED ERK2

The inactive/unphosphorylated form of ERK2 and its mutants were expressed and purified from *E. coli* [7]. The DNA vector NpT7-5 ERK2 encoding a His₆-tagged ERK2 (N. Ahn, Boulder, CO) was electroporated into BL21 (DE3) *E. coli* cells and plated on Luria Broth (LB)/agar plates containing 50 µg/mL ampicillin. A single colony was grown overnight in 25 mL of LB containing freshly added ampicillin (50 µg/mL) in an autoclaved 125 mL Erlenmeyer flask at 30 °C. The next morning, 4 mL of the overnight culture was transferred to 4 flasks each containing 800 mL of autoclaved LB (3.2 L total) containing freshly added ampicillin (50 µg/mL). The bacteria was grown to mid-log phase growth so that the optical density at 600 nm (OD₆₀₀) was ~0.6-0.8 and induced for protein expression with 0.5 mM IPTG for 5 hours. The cells were cleared of the media by centrifugation for 10 min, 6,000 rpm, at 4 °C. The supernatant was decanted and the pellet was scraped from the bottom of the centrifuge tubes, weighed, snap frozen in liquid nitrogen, and stored at -80 °C.

The bacterial pellet (~10 g) containing the ERK2 protein was raised in 200 mL of lysis buffer (50 mM Tris pH 8.0, 0.1% 2-mercaptoethanol, 0.03% Brij-35, 5 mM imidazole, 1% Triton X-100, 500 mM NaCl, 1 mM benzamidine, 0.1 mM TPCK, 0.1 mM PMSF) and kept on an ice water bath at a temperature below 4 °C to inhibit protease activity. The cells were sonicated in small volume batches in a 50 mL glass beaker 5 × 20 sec to break open the cells while ensuring that the lysate remained below 4 °C. The sonicated lysate was centrifuged for 30 min, 16,000 rpm, at 4 °C in an SS-34 rotor. The His₆-tagged ERK2 remaining in the supernatant was rotated slowly for at least one hour at 4 °C in the presence of 15 mL of Ni²⁺-NTA-agarose beads equilibrated in lysis buffer. The Ni²⁺-NTA-agarose-bound His₆-tagged ERK2 was applied to a plastic Econo-column (Bio-Rad) and allowed to drain while the beads remain in the column, washed with 10

column volumes of wash buffer (50 mM Tris pH 8.0, 0.1% 2-mercaptoethanol, 0.03% Brij-35, 10 mM imidazole, 1 mM benzamidine, 0.1 mM TPCK, 0.1 mM PMSF), and eluted with 50 mL of elution buffer (50 mM Tris pH 8.0, 0.1% 2-mercaptoethanol, 0.03% Brij-35, 250 mM imidazole, 0.1 mM EDTA, 0.1 mM EGTA, 1 mM benzamidine, 0.1 mM TPCK, 0.1 mM PMSF). The His₆-tagged ERK2 elutes due to imidazole binding and competing for the histidine binding sites on the Ni²⁺-NTA-agarose beads.

The eluant containing the His₆-tagged ERK2 was filtered with a 0.45 µm filter and measured for protein concentration by Bradford assay to determine the approximate amount of protein present (usually, 1 mL of Ni²⁺-NTA-agarose beads could bind 5-10 mg of ERK2). The ERK2 was applied to a Mono Q HR 10/10 anion exchange column equilibrated with H1 buffer (20 mM Tris, pH 8.0, 0.1% 2-mercaptoethanol, 0.03% Brij-35, 0.1 mM EDTA, 0.1 mM EGTA) and allowed to equilibrate for 10 min using a flow rate of 1.5 mL/min. The ERK2 was eluted with a linear gradient of NaCl (0-0.5 M) for 80 min using H2 buffer (H1 buffer containing 0.5 M NaCl). The unphosphorylated ERK2 eluted as two separate peaks occurring at ~0.28 and ~0.36 M NaCl. Only the first peak was kept for further analysis as it has a higher basal activity than the latter peak. The Mono Q-purified unphosphorylated ERK2 was run on a 10% SDS-PAGE gel to confirm the purity of the protein, pooled, and dialyzed overnight in storage (S1) buffer (25 mM Hepes, pH 7.5, 50 mM KCl, 2 mM DTT, 10% glycerol). The protein concentration was determined using the Gill and Von Hippel method [119] by denaturing the protein in 6 M guanidine hydrochloride and measuring the absorbance of tryptophans and tyrosines at 280 nm. The concentration of protein was determined using Beer's law (Equation 3)

Equation 3 $A = C \times \epsilon \times \lambda$

where A is the absorbance at 280 nm, C is the concentration of protein in M^{-1} , ϵ is the extinction coefficient or molar absorptivity ($44\,825\,M^{-1}\,cm^{-1}$) [5], and λ is the length that the wavelength of light has to traverse in centimeters (usually 1 cm). Amino acid analysis of purified dual-phosphate ERK2 was also performed yielding an extinction coefficient of $52\,067\,M^{-1}\,cm^{-1}$ [44]. The protein was snap frozen in liquid nitrogen in aliquots of $\sim 2\,mg/mL$ and stored at $-80\,^{\circ}C$. Precipitation of the unphosphorylated protein often occurred following dialysis. It was found that dilution of the unphosphorylated ERK2 into the dialysis buffer at $\sim 1:1$ ratio prior to dialysis could alleviate precipitation if a high concentration of ERK2 was not required in further experiments. If precipitation occurred, even during the thawing process before experiments, the protein was allowed to warm to room temperature and found to be suitable.

PURIFICATION OF MAPKK1G7B

DNA encoding His₆-tagged MAPKK1G7b, a constitutively active form of MAPKK1 (MAPKK1/ Δ 44-51/S218D/M219D/N221D/S221D) in the plasmid pRSETa (N. Ahn, Boulder, CO), was electroporated into BL21 (DE3) *E. coli* cells and selected on LB/agar plates containing 50 $\mu g/mL$ ampicillin. The bacterial cells were grown similar to the unphosphorylated ERK2 and the His₆-tagged MAPKK1G7b was purified by affinity chromatography using Ni²⁺-NTA-agarose beads similar to the methods carried out for unphosphorylated ERK2 (Purification of Unphosphorylated ERK2). The yield of

MAPKK1G7b production was much poorer than that of ERK2, therefore, only 2 mL of Ni^{2+} -NTA-agarose beads were used for 3.2 L of culture. The Ni^{2+} -NTA-agarose column was washed with 10 volumes of wash buffer, eluted with 3 volumes of elution buffer, and collected in 1 mL fractions. Eluted fractions containing protein were applied to a 10% SDS-PAGE gel to confirm the heterogeneous purification of the ~50 kD MAPKK1G7b [44]. Fractions containing MAPKK1G7b were dialyzed into S1 buffer, snap frozen in liquid nitrogen, and stored at -80 °C. Mono Q-purified MAPKK1B7b can also be obtained [44].

ETSΔ138 PURIFICATION

EtsΔ138 and its mutants were purified essentially as described [42] with the exception that proteins were dialyzed into 1.25 mM Hepes, pH 7.5, 2.5 mM KCl, and 2 mM DTT.

ACTIVATION OF ERK2 USING MAPKK1

Unphosphorylated ERK2 was activated *via* phosphorylation of residues Thr-183 and Tyr-185 by MAPKK1G7b in the presence of radiolabeled or cold ATP, and MgCl_2 . The radiolabeled activation was carried out by incubating 4 μM ERK2 and 0.4 μM MAPKK1G7b in a volume of 3 mL in activation buffer (40 mM Hepes, pH 8.0, 100 mM KCl, 4 mM ATP (with 125 cpm/pmol $\gamma^{32}\text{P}$ -ATP, 5 μL of $\gamma^{32}\text{P}$ -ATP stock), 20 mM MgCl_2 , 0.5 mM EGTA, and 2 mM DTT) for 5 hours at 27 °C.

Over the course of the activation, 10 μL aliquots were spotted on P81 cellulose paper to follow phosphate incorporation into ERK2 over the course of the reaction. ERK2 bound to the P81 paper and radiolabeled phosphates incorporated by MAPKK1G7b were detected in the scintillation counter. The P81 papers were dried at room temperature for at least 10 min, washed 4×5 min with 500 mL of 50 mM phosphoric acid ($\text{H}_3\text{PO}_4^{1-}$), 1×1 min in acetone, and dried briefly in a 100 $^\circ\text{C}$ oven. The papers were individually placed into 1.5 mL centrifuge tubes with scintillant fluid and counted in the scintillation counter. Alternatively, aliquots were precipitated on ice for 10 min in 1 mL of 20% TCA containing 10 μg of BSA (to enable visualization of the pellet), centrifuged at 14,000 rpm at 4 $^\circ\text{C}$ for 10 min, the pellet was washed briefly with 3×1 mL with 10% ice-cold TCA in a similar fashion, dried, and counted in scintillant fluid to give similar results to the P81 paper assay indicating that the TCA precipitation and P81 paper assay were equivalent.

The specific activity of the reaction was determined by diluting 5 μL of the reaction in 5 mL of water and determining the concentration of ATP using the absorbance at 259 nm ($\epsilon = 15,400 \text{ M}^{-1} \text{ cm}^{-1}$) and counting 10 μL of the 1:1000 dilution in scintillation fluid. The specific activity was determined by dividing the counts per minute of the sample by the volume counted and the concentration of the ATP in the diluted sample. By knowing the specific activity of the reaction and the molar quantity of the total ERK2 on each piece of P81 paper, an estimate of the counts per spotted aliquot was determined for the completion of the reaction with 2 mol/mol phosphate. For this reaction, 1.2 nmol of ERK2 were activated, therefore, 40 pmol of ERK2 was spotted on each piece of P81 paper. If two moles of phosphate were incorporated into ERK2 using a specific activity of 125 cpm/pmol, one would expect $\sim 10,000$ cpm at the completion of the reaction. Each spotted aliquot yielded a value in counts per minute per aliquot, this

number was converted to the number of moles of phosphate per aliquot using the specific activity of the reaction, then dividing by the mole quantity of ERK2 per aliquot yielded the mol/mol ratio of phosphate to ERK2. This mol/mol ratio was plotted against time. The activation assay indicated that MAPKK1G7b was capable of phosphorylating ERK2 by incorporating ~2 mol of phosphate into each molecule of ERK2.

WT ERK2 and its mutants were also activated by MAPKK1-G7b in cold assays lacking radiolabeled ATP [7]. Assay conditions for the activation were 0.4 μ M MAPKK1-G7b, 4 μ M ERK2, 20-50 mM Hepes pH 7.5, 50 mM KCl, 0.5 mM EGTA, 20 mM $MgCl_2$, 2 mM DTT at 27 °C for 3-5 h and in the presence of 4 mM unlabeled ATP.

PURIFICATION OF DUAL-PHOSPHATE ERK2

Following the activation of ERK2 by MAPKK1G7b, ERK2 was purified away from the ATP using a DEAE-Sepharose Fast Flow anion exchange column (Amersham Biosciences) equilibrated in buffer H1 [7]. The activation solution was applied with an equal volume of buffer H1 to a 0.5 mL DEAE-Sepharose Fast Flow column. The column was washed with 10 mL of buffer H1 and eluted with 1 mL fractions using a linear gradient of buffer H1 containing 0-0.5 M NaCl in 0.05 M increments. The eluted protein was subjected to a Bradford assay to determine where the protein eluted by monitoring the absorbance at 595 nm.

The fractions containing the dual-phosphate ERK2 were applied to a Mono Q HR 10/10 anion exchange column in buffer H1 to ensure a low NaCl concentration so that the dual-phosphate ERK2 could bind the column. The column was developed similar to that of unphosphorylated ERK2 and the dual-phosphate ERK2 eluted at ~ 0.29 M NaCl. The eluted fractions were collected and dialyzed overnight in either 1 L of 50 mM Tris pH 8.6

to prepare for proteolysis by trypsin (radiolabeled protein) or 1 L of S1 buffer and snap frozen for steady-state kinetic assays.

PHOSPHOAMINO ACID ANALYSIS

Mono Q-purified radiolabeled ERK2 was dialyzed into 50 mM Tris-HCl, pH 8.6, 250 µg of ERK2 was incubated with 5 µg of sequencing grade trypsin (Roche) in a 200 µL volume at 37 °C for 4 h to proteolytically cleave the ERK2 following basic residues (lysine and arginine). Another 5 µg of trypsin was added for 6 h and the digests were frozen at -20 °C overnight. The tryptic peptide digest was thawed, filtered with a 0.2 µm filter, raised in 0.1% trifluoroacetic acid (TFA) and applied to a 250 mm × 4 mm reverse phase C18 column (Separations Group, Hesperia, CA) equilibrated with 0.1% TFA at a flow rate of 0.7 mL/min. Following a 10 min equilibration period the peptide was eluted using a linear gradient of 50% acetonitrile containing 0.1% TFA over 110 min. Fractions were collected every minute and counted in the scintillation counter in the absence of scintillant fluid. The radioactivity of each fraction was plotted versus time with the acetonitrile gradient shown. Only one radiolabeled peptide eluted at 25% acetonitrile indicating that only one tryptic peptide had phosphates covalently attached. This radiolabeled peak was pooled and separated into two centrifuge tubes so that one could be analyzed by mass spectrometry to determine the mass of the peptide and the other for phosphoamino acid analysis to determine which residue or residues were phosphorylated within that peptide. The radiolabeled peptide purified from reverse phase HPLC was precipitated using a speed-vac centrifuge. The peptide was raised in 50% acetonitrile and precipitated using the speed-vac twice to eliminate the TFA. The precipitated peptide was raised in a small volume (~20 µL) of 50% acetonitrile and analyzed by MALDI mass

spectrometry by spotting equal portions of the peptide and α -cyano-4-hydroxycinnamic acid [44]. The mass revealed a peptide of 2306.2 Da (2307.3 Da calculated) as expected indicating that the peptide N- 171 VADPDHDHTGFLTEYVATR 189 -C was phosphorylated at two positions.

The phospho-peptide was lyophilized and raised in 6 M hydrochloric acid for 60 min at 110 °C to partially hydrolyze the peptide into its individual amino acids. The hydrolyzed peptide was lyophilized in a speed-vac centrifuge and raised to 1000 cpm/ μ L in the pH 3.5 buffer (5% glacial acetic acid (v/v) and 0.5% pyridine in water, pH adjustment is not recommended) used for amino acid separation. The samples were spotted in 0.5 μ L aliquots, dried prior to each additional spot, on a 20 \times 20 cm cellulose glass-backed plate without fluorescent indicators (Sigma). Each spot contained 500-1000 cpm of a sample in addition to 1 μ g of each cold phosphoamino acid standard for phospho-serine, phospho-threonine, and phospho-tyrosine spotted as 2 \times 0.5 μ L of a mixture containing 1 mg/mL of each standard in water. Outside lanes contained 0.5 μ L of both 5 mg/mL ϵ -dinitrophenyl (DNP)-lysine (yellow) and 1 mg/mL xylene cyanol FF (blue) solubilized in pH 3.5 buffer and allowed the direct visualization of the electrophoresis. The pH 3.5 buffer was carefully applied to the cellulose plate so that the spotted reactions were not mobile and electrophoresed at 200 V for \sim 2 h. The plates were dried, stained with 0.25% ninhydrin in acetone to expose the cold phosphoamino acid standards, exposed to film for 24 hours, and developed.

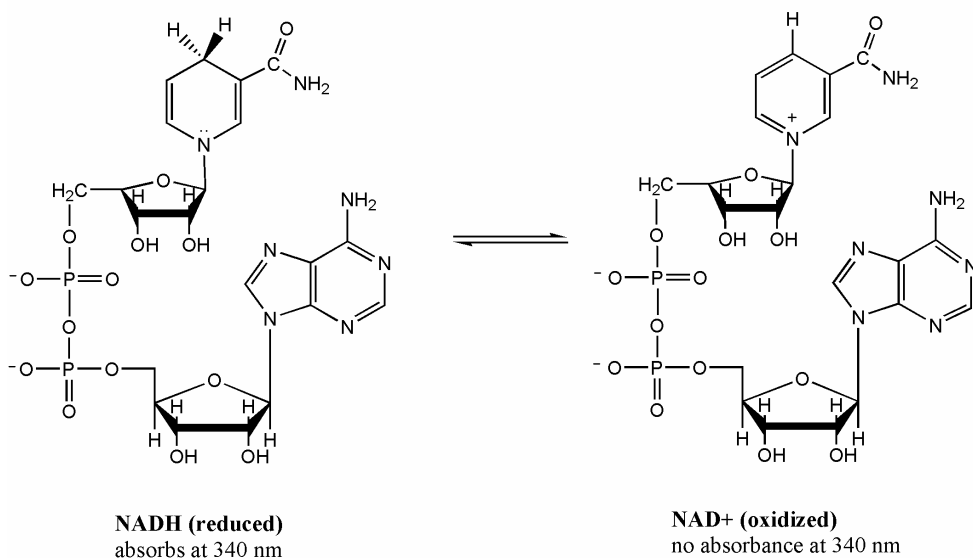
KINETIC METHODS FOR ETSΔ138 PHOSPHORYLATION

Protein kinase assays were conducted as described previously by spotting 5 μ L aliquots of a 50 μ L reaction on P81 cellulose paper [7]. Assays contained 1 nM ERK2 (for some mutants a higher concentration was used), 25 mM Hepes pH 7.5, 50 mM KCl, 20 mM MgCl₂, 0.1 mM EDTA, 0.1 mM EGTA, 40 μ g/mL BSA, and 2 mM DTT, while keeping ATP constant (2 mM) and varying EtsΔ138 (6.3-200 μ M) or while keeping EtsΔ138 constant (150 or 200 μ M) and varying ATP (31.3-1000 μ M). Initial rates were measured at each given concentration using at least 5 data points that lie in a straight line and saturation curves were fit to the Henri-Michaelis-Menten equation using Kaleidagraph (Synergy Software). Assays with F120A and F88A/F120A EtsΔ138 were carried out using 5 nM ERK2. ERK2 mutants K149A and K229T/H230D were assayed using 15 nM and 2 nM ERK2, respectively.

ATPASE ASSAYS

The ATPase activity of WT and K229T/H230D ERK2 were examined using an enzyme-coupled spectrophotometric assay [112]. All reactions were performed in 25 mM Hepes pH 7.5, 50 mM KCl, 20 mM MgCl₂, 2 mM DTT, 0.1 mM EDTA, 0.1 mM EGTA, 40 μ g/mL BSA, various concentrations of ERK2 (100-400 nM), 960 μ M ATP⁴⁻, 1 mM Phospho(enol) Pyruvate (PEP), 1.4 units Pyruvate Kinase (PK), 0.2 mM β -Nicotinamide Adenine Dinucleotide (reduced form) (NADH), 3 units L-Lactate Dehydrogenase (LDH) in a total volume of 200 μ L at 27 °C. PK and LDH were buffer exchanged 3 \times 400 μ L in MMix buffer (50 mM Hepes, pH 7.5, 100 mM KCl, 0.2 mM EDTA, 0.2 mM EGTA, 50 mM MgCl₂, 3 mM DTT, 80 μ g/mL BSA) using a Microcon

YM-10 centrifugal filter device (Amicon-#42406). PEP and NADH were raised in MMix buffer immediately prior to the assays. Reactions were made by adding the appropriate concentrations of PK, LDH, PEP, and NADH in 80 μL MMix buffer, 40 μL of ERK2 in ERK2 dilution buffer (25 mM Hepes, pH 7.5, 50 mM KCl, 0.1 mM EDTA, 0.1 mM EGTA, 2 mM DTT, 40 $\mu\text{g/mL}$ BSA), 40 μL of Ets Δ 138 dilution buffer (1.25 mM Hepes, pH 7.5, 2.5 mM KCl 0.05 mM EDTA, 0.05 mM EGTA, 2 mM DTT) although no Ets Δ 138 is added, and 40 μL of ATP, pH 7.5. Each reaction was initiated by the addition of ATP after incubation for 5 min at 27 $^{\circ}\text{C}$. The rate of ATP hydrolysis to form ADP and P_i was monitored by measuring the decrease in NADH absorbance at 340 nm as NAD^+ is formed using a molar extinction coefficient of $6220 \text{ M}^{-1} \text{ cm}^{-1}$ at 340 nm (Scheme 7). A blank containing the buffer and ATP was used in the absence of NADH and the enzymes.



Scheme 7. Structures of NADH and NAD⁺. The ATPase activity of ERK2 was followed by UV absorbance by following the disappearance of NADH as NAD⁺ was formed.

SDS-PAGE GEL

The SDS-PAGE gels were prepared by making a stacking gel on top of a separating gel. The separating gel was poured first by adding a small aliquot to a final concentration of 0.1% ammonium persulfate and 0.1% N,N,N',N'-tetramethylethylenediamine (TEMED) just prior to pouring the gel to a 10 mL solution containing 10% acrylamide/bis-acrylamide (29:1), 37.5 mM Tris, pH 8.8, and 0.1% lauryl sulfate (sodium dodecylsulfate, SDS). A stacking gel was prepared by adding a small aliquot to a final concentration of 0.25% ammonium persulfate and 0.16% TEMED just prior to pouring the gel to a 6 mL solution containing 5% acrylamide/bis-acrylamide (29:1), 12.5 mM Tris, pH 6.8, 0.25% SDS. Samples were boiled at 100 °C for 5 min in 1x protein loading buffer (a stock of 2x protein loading buffer contained 100 mM Tris-HCl, pH 6.8, 4% SDS, 0.2% bromophenol blue, 20% glycerol, with 1 mM 2-mercaptoethanol added fresh before use). The gels were run in protein electrophoresis buffer containing 25 mM Tris base, 200 mM glycine, 0.1% SDS (w/v) for 50 min at 200 V.

EXPERIMENTAL DATA

WT ERK2

~2 mol/mol phosphate incorporated

[EtsΔ138], μM	$k_{\text{obs}}, \text{s}^{-1}$											
200	16.5	15.4	17.5	21.3	19.9	23.0	18.2		16.5	16.8	20.2	20.5
100	12.9	13.7	16.8	18.3	20.5	23.4	17.7	19.3	19.7	15.4	19.9	18.4
50	10.2		12.6	21.0	19.1	21.2	15.3	17.5	16.4	17.0	18.5	18.3
25	9.3	13.1	16.7	15.9	17.3	17.6	16.1	11.6	13.3	12.0	17.2	17.6
12.5	5.5	11.6	12.1	14.0	13.3	14.0	11.5	8.6	12.6	9.2	15.5	14.8
6.3	3.6	9.1	9.9	9.8	8.1	9.1	8.0	5.6	10.4	5.2	8.5	8.9

[EtsΔ138], μM	$k_{\text{obs}}, \text{s}^{-1}$
200	18.0
100	17.8
50	16.2
25	13.5
12.5	9.2

2/25/04

Y111N/K112N ERK2

~ 2.2 mol/mol phosphate incorporated

[EtsΔ138], μM	k_{obs}, s^{-1}	
200	12.1	13.4
100	11.0	12.6
50	9.6	10.1
25	7.6	8.3
12.5	4.9	5.6
6.3	2.6	3.3

7/13/02 – 50 mM Hepes, pH 7.3, 120 mM KCl, 0.01 mM EDTA/EGTA, 1 $\mu\text{g/mL}$ BSA, 10 mM MgCl_2 , 2 mM ATP, 2.8 mM DTT

9/16/02 – 25 mM Hepes, pH 7.3, 100 mM KCl, 0.1 mM EDTA/EGTA, 1 $\mu\text{g/mL}$ BSA, 10 mM MgCl_2 , 2 mM ATP, 2 mM DTT

L113A ERK2

~ 2 mol/mol phosphate incorporated

[EtsΔ138], μM	k_{obs}, s⁻¹
200	21.2
100	23.3
50	21.8
25	20.9
12.5	17.0
6.3	8.5

10/25/02 – 50 mM Hepes, pH 8.2, 50 mM KCl, 40 μg/mL BSA, 20 mM MgCl₂, 2 mM ATP, 2 mM DTT

L113A ERK2

[ATP], μM	k_{obs}, s⁻¹
1000	17.2
500	16.2
250	12.4
125	9.8
62.5	8.0
31.25	4.4

10/25/02 – 50 mM Hepes, pH 8.2, 50 mM KCl, 40 μg/mL BSA, 20 mM MgCl₂, 200 μM EtsΔ138, 2 mM DTT

Q117A ERK2

~ 2.3 mol/mol phosphate incorporated

[EtsΔ138], μM	k_{obs}, s^{-1}
200	17.9
100	16.6
50	16.2
25	11.1
12.5	7.6
6.3	4.9

10/25/02 - 50 mM Hepes, pH 8.2, 50 mM KCl, 40 $\mu\text{g/mL}$ BSA, 20 mM MgCl_2 , 2 mM ATP, 2 mM DTT

Q117A ERK2

[ATP], μM	k_{obs}, s^{-1}
1000	14.4
500	13.6
250	10.7
125	8.7
62.5	5.9
31.5	3.7

10/25/02 - 50 mM Hepes, pH 8.2, 50 mM KCl, 40 $\mu\text{g/mL}$ BSA, 20 mM MgCl_2 , 200 μM EtsΔ138, 2 mM DTT

H123A ERK2

~ 2.1 mol/mol phosphate incorporation

[EtsΔ138], μM	k_{obs}, s⁻¹	
200	27.3	27.9
100	24.8	26.5
50	20.5	18.6
25	12.2	12.5
12.5	6.7	7.2
6.3	3.6	4.2

11/13/02 - 50 mM Hepes, pH 8.2, 50 mM KCl, 40 μg/mL BSA, 20 mM MgCl₂, 2 mM ATP, 2 mM DTT

H123A ERK2

[ATP], μM	k_{obs}, s⁻¹
1000	26.2
500	24.3
250	19.2
125	14.7
62.5	10.2
31.3	5.0

11/13/02 - 50 mM Hepes, pH 8.2, 50 mM KCl, 40 μg/mL BSA, 20 mM MgCl₂, 200 μM EtsΔ138, 2 mM DTT

T157E/T158D ERK2

~ 2.3 mol/mol phosphate incorporated

[EtsΔ138], μM	$k_{\text{obs}}, \text{s}^{-1}$		
200	12.2	11.2	19.8
100	12.1	9.7	18.6
50	10.7	9.5	16.5
25	9.1	7.6	13.4
12.5	5.5	6.8	8.7
6.3	2.9	4.7	4.3

6/28/02 and 7/9/02 - 50 mM Hepes, pH 7.3, 100 mM KCl, 0.01 mM EDTA/EGTA, 8 $\mu\text{g/mL}$ BSA, 10 mM MgCl_2 , 2 mM ATP, 0.8 mM DTT

5/31/03 - 25 mM Hepes, pH 7.5, 50 mM KCl, 0.1 mM EDTA/EGTA, 40 $\mu\text{g/mL}$ BSA, 20 mM MgCl_2 , 2 mM ATP, 2 mM DTT

T157E/T158D ERK2, 5/31/03

[ATP], μM	$k_{\text{obs}}, \text{s}^{-1}$
1000	18.5
500	16.7
250	14.0
125	11.2
62.5	7.5
31.3	5.1

5/31/03 – 25 mM Hepes, pH 7.5, 50 mM KCl, 0.1 mM EDTA/EGTA, 40 $\mu\text{g/mL}$ BSA, 20 mM MgCl_2 , 200 μM EtsΔ138, 2 mM DTT

K229T/H230D ERK2

~ 2 mol/mol phosphate incorporated

[EtsΔ138], μM	$k_{\text{obs}}, \text{s}^{-1}$
200	3.0
100	2.4
50	1.5
25	0.9
12.5	0.6
6.3	0.6

8/6/02 – 5 nM K229T/H230D, 50 mM Hepes, pH 7.3, 100 mM KCl, 0.01 mM EDTA/EGTA, 10 mM MgCl_2 , 2 mM ATP, 2.8 mM DTT

[EtsΔ138], μM	$k_{\text{obs}}, \text{s}^{-1}$	
200	6.1	6.1
150	5.0	5.2
100	4.0	4.1
75	3.1	3.4
50	2.4	2.3
25	2.1	1.8

6/25/04 (ii) – 2.5 nM K229/H230D, 25 mM Hepes, pH 7.5, 50 mM KCl, 0.1 mM EDTA/EGTA, 20 mM MgCl_2 , 2 mM ATP, 2 mM DTT, 40 $\mu\text{g/mL}$ BSA

K229T/H230D ERK2

[ATP], μM	$k_{\text{obs}}, \text{s}^{-1}$
1045.0	2.7
522.5	2.7
261.3	2.3
130.6	1.8
65.3	1.2
32.7	0.8

8/6/02 – 5 nM K229T/H230D, 50 mM Hepes, pH 7.3, 100 mM KCl, 0.01 mM EDTA/EGTA, 10 mM MgCl_2 , 2 mM ATP, 2.8 mM DTT

Y314A/Y315A ERK2, 5/17/02, 9/11/02 WTC, 5/29/03 (ii)

~ 1.8 mol/mol phosphate incorporation

[EtsΔ138], μM	k_{obs}, s⁻¹			
200	28.7	29.2	18.4	17.9
100	25.4	24.5	19.5	18.5
50	21.7	22.6	15.0	14.5
25	19.1	20.1	15.3	11.9
12.5	11.8	14.2	9.4	8.0
6.3	6.6	7.3	7.7	4.0

5/17/02 – 22 mM Hepes, pH 7.3, 60 mM KCl, 10 mM MgCl₂, 2 mM ATP

5/29/03 (ii) – 25 mM Hepes, pH 7.5, 50 mM KCl, 0.1 mM EDTA/EGTA, 2 mM DTT, 20 mM MgCl₂, 40 μg/mL BSA, 2 mM ATP

Y314A/Y315A ERK2

[ATP], μM	k_{obs}, s⁻¹	
1032	21.0	
516	19.5	
258	14.5	
129	10.8	
64.5	6.9	
32.3	4.2	
1000		17.8
500		16.5
250		13.9
125		10.1
62.5		7.0
31.3		4.6

6/3/03 – 25 mM Hepes, pH 7.5, 50 mM KCl, 0.1 mM EDTA/EGTA, 40 μg/mL BSA, 20 mM MgCl₂, 2 mM DTT, 200 μM EtsΔ138

7/25/02 – 50 mM Hepes pH 7.3, 100 mM KCl, 10 μM ED/EGTA, 10 mM MgCl₂, 2.4 mM DTT, 200 μM EtsΔ138

D316A/D319A

~ 1.5 mol/mol phosphate incorporated

[EtsΔ138], μM	k_{obs}, s^{-1}		
200	26.4	14.0	13.1
100	22.9	-	14.7
50	19.6	11.5	13.2
25	15.4	11.5	11.3
12.5	12.7	3.6	7.8
6.3	9.2	3.5	5.9

5/17/03 – 22 mM Hepes, pH 7.3, 60 mM KCl, 10 mM MgCl₂, 2 mM ATP

5/29/03 (ii) – 25 mM Hepes, pH 7.5, 50 mM KCl, 0.1 mM EDTA/EGTA, 2 mM DTT, 20 mM MgCl₂, 40 μg/mL BSA, 2 mM ATP

D316A/D319A

[ATP], μM	k_{obs}, s^{-1}	
1032	17.6	
516	14.9	
258	12.5	
129	9.3	
64.5	6.1	
32.3	3.7	
1000		13.7
500		13.1
250		10.5
125		8.1
62.5		5.6
31.25		3.4

7/25/02 – 50 mM Hepes, pH 7.3, 100 mM KCl, 10 μM EDTA/EGTA, 10 mM MgCl₂, 2.4 mM DTT, 200 μM EtsΔ138

6/3/03 – 25 mM Hepes, pH 7.5, 50 mM KCl, 0.1 mM EDTA/EGTA, 2 mM DTT, 20 mM MgCl₂, 40 ug/mL BSA, 200 μM EtsΔ138

Anisotropy data

Inactive ERK2, 2/3/04, 4/13/04, 4/16/04

ERK2, μ M	Anisotropy, $\langle r \rangle$		
0	0.1136	0.11166	0.11386
0.45	0.14389	0.1477	0.14032
0.9	0.16458	0.16731	0.16217
1.3	0.1806	0.18107	0.17619
1.8	0.1916	0.19139	0.186
3.5	0.212	0.21436	0.21088
5.3	0.21977	0.22314	0.2198
7	0.226	0.22857	0.22607
8.8	0.2292	0.23217	0.23262
10.5	0.23257		
12.3	0.23309		
14	0.23676		
15.8	0.23682		
17.5	0.24027		

Assay conditions: 100 nM Ets Δ 138–Fluorescein (Cys-31 labeled Ets Δ 138-C31*), 25 mM Hepes, pH 7.5, 50 mM KCl, 0.1 mM EDTA, 0.1 mM EGTA, 40 μ g/mL BSA, 2 mM DTT, 2% glycerol

Inactive K229T/H230D ERK2, 1/31/04

K229T/H230D, μM	Anisotropy, $\langle r \rangle$	
0	0.10916	0.10899
2.4	0.11499	0.11443
4.7	0.11956	0.11888
7.1	0.12443	0.12407
9.4	0.12809	0.12737
14.4	0.13547	0.1356
18.8	0.14324	0.14223

Assay conditions: 100 nM Ets Δ 138–Fluorescein (Cys-31 labeled Ets Δ 138-C31* containing only one cysteine), 25 mM Hepes, pH 7.5, 50 mM KCl, 0.1 mM EDTA, 0.1 mM EGTA, 40 μ g/mL BSA, 2 mM DTT, 2% glycerol

EtsΔ24-138, 11/9/01

[EtsΔ24-138], μM	k_{obs}, s⁻¹
171.0	11.9
85.5	7.7
42.8	5.3
21.4	3.1
10.7	1.8
5.3	1.0

EtsΔ24-138

[ATP], μM	k_{obs}, s⁻¹
1032	10.7
516	9.5
258	8.4
129	5.7
64.5	4.6
32.3	2.5

7/23/02 – 50 mM Hepes, pH 7.3, 100 mM KCl, 10 μM EDTA/EGTA, 10 mM MgCl₂, 8 μg/mL BSA, 3.2 mM DTT, 200 μM EtsΔ24-138 (non-saturating)

K15A EtsΔ138, 1/14/02, 3/7/02, and 6/4/02 (ii)

[K15A], μM	$k_{\text{obs}}, \text{s}^{-1}$			
200	18.2	19.0		
100	18.9	15.1		
50	17.8	14.0		
25	14.9	10.4		
12.5	13.0	-		
6.25	7.8	4.7		
160.0			13.8	14.6
80.0			12.3	12.4
40.0			12.6	13.6
20.0			10.7	11.7
10.0			7.2	8.7
5.0			4.7	4.7

6/4/02 (ii) – 25 mM Hepes, pH 7.3, 120 mM KCl, 10 mM MgCl_2 , 8 $\mu\text{g/mL}$ BSA, 2.4 mM DTT, 0.1 nM ERK2, 2 mM ATP

K18A, L21A, and L23A EtsΔ138, 11/2/01

	$k_{\text{obs}}, \text{s}^{-1}$		
[EtsΔ138], μM	K18A	L21A	L23A
200	18.0	18.7	16.6
100	16.3	16.7	16.5
50	16.4	15.3	15.0
25	14.2	12.3	12.4
12.5	10.7	11.5	9.8
6.3	8.3	5.5	5.1

K15A/K18A EtsΔ138, 1/14/02 and 5/31/02

[K15A/K18A], μM	$k_{\text{obs}}, \text{s}^{-1}$	
170.0	17.6	
85.0	16.6	
42.5	15.2	
21.3	12.3	
10.6	9.4	
5.3	5.1	
100.0		23.4
50.0		22.6
25.0		21.0
12.5		14.0
6.3		12.0

L21A/L23A EtsΔ138, 1/14/02 and 5/31/02

[L21A/L23A], μM	$k_{\text{obs}}, \text{s}^{-1}$	
200	21.0	20.2
100	19.0	18.5
50	18.2	18.2
25	14.8	13.9
12.5	9.5	10.8
6.25	7.3	7.1

F88A EtsΔ138

[F88A], μM	k_{obs}, s^{-1}
200.0	14.8
100.0	14.3
50.0	11.4
25.0	9.2
12.5	7.4
6.3	3.1

8/2/02 – 50 mM Hepes, pH 7.3, 100 mM KCl, 10 μM EDTA/EGTA, 8 $\mu\text{g/mL}$ BSA, 10 mM MgCl_2 , 2 mM ATP, 1 nM ERK2, 3.2 mM DTT

F120A EtsΔ38

[F120A], μM	k_{obs}, s^{-1}	
200	7.8	10.2
100	5.2	6.6
50	3.4	3.8
25	1.8	2.1
12.5	0.8	1.3
6.3	0.2	0.7

5/17/02 – 25 mM Hepes, pH 7.3, 60 mM KCl, 10 mM MgCl_2 , 2 mM ATP, 5 nM ERK2
 5/31/02 – 25 mM Hepes, pH 8.0, 120 mM KCl, 0.1 mM EDTA/EGTA, 8 $\mu\text{g/mL}$ BSA, 10 mM MgCl_2 , 2 mM ATP, 2.4 mM DTT, 5 nM ERK2

F120A EtsΔ138

[ATP], μM	k_{obs}, s^{-1}
1032.0	5.5
516.0	5.2
258.0	4.2
129.0	3.6
64.5	2.4
32.3	1.5

6/23/02 – 50 mM Hepes, pH 7.3, 100 mM KCl, 10 μM EDTA/EGTA, 10 mM MgCl_2 , 8 $\mu\text{g/mL}$ BSA, 3.2 mM DTT, 200 μM F120A EtsΔ138 (non-saturating)

F88A/F120A

[F88A/F120A], μM	k_{obs}, s^{-1}	
200	5.6	7.0
100	4.3	4.1
50	2.5	2.4
25	1.5	1.3
12.5	0.7	0.6
6.3	0.3	0.3

5/17/02 – 25 mM Hepes, pH 7.3, 60 mM KCl, 10 mM MgCl_2 , 2 mM ATP, 5 nM ERK2

5/31/02 – 25 mM Hepes, pH 8.0, 120 mM KCl, 0.1 mM EDTA/EGTA, 8 $\mu\text{g/mL}$ BSA, 10 mM MgCl_2 , 2 mM ATP, 2.4 mM DTT, 5 nM ERK2

CHAPTER 4: PHOSPHORYLATION DIFFERENTIALLY REGULATES MAPK PROTEIN-PROTEIN INTERACTIONS: A QUANTITATIVE ANALYSIS USING FLUORESCENCE ANISOTROPY

PURPOSE

This chapter describes the development of a fluorescence anisotropy assay that measures the equilibrium dissociation constant (K_d) of the docking complex formed between ERK2 and its protein substrate EtsΔ138. Three cysteines within EtsΔ138 were mutated to alanine and the remaining cysteine was covalently attached to a fluorescein moiety to generate fluorescent EtsΔ138 (EtsΔ138-F). The fluorescence anisotropy, a measure of molecular rotation, of the unbound fluorescent EtsΔ138 EtsΔ138-F was low and increased upon binding ERK2 due to decreased molecular rotation of the ERK2-bound EtsΔ138-F. By measuring the fluorescence anisotropy of EtsΔ138-F at several concentrations of ERK2 we were able to determine the dissociation constant for the ERK2–EtsΔ138-F complex. Unlabeled competitors that bind ERK2 and disrupt its ability to bind EtsΔ138-F were added to disrupt formation of the fluorescent complex so that the K_d s of unlabeled competitors could be determined. This quantitative binding assay allows the K_d of peptides, proteins, and presumably small molecules that disrupt the ERK2–EtsΔ138-F docking complex to be determined. This assay will be useful in elucidating target candidates for the disruption of a specific protein–protein interaction and possibly lead to the discovery of drugs that disrupt ERK2 phosphorylation of a specific subset of targets by inhibiting specific protein–protein interactions.

INTRODUCTION

Extracellular signal-regulated protein kinase 2 (ERK2, EC 2.7.1.37) is an enzyme capable of transferring the γ -phosphate of adenosine triphosphate (ATP) to the hydroxyl group of Thr-38 on one of its protein substrates Ets Δ 138 [42], thereby, phosphorylating Ets Δ 138. The NMR structure for the C-terminal portion of Ets Δ 138 has been solved for residues 29-138 [114] of the transcription factor Ets-1 (Accession: P27577) [120]. The dual-phosphate form of ERK2 efficiently phosphorylates Ets Δ 138 with a $k_{\text{cat}}/K_{\text{m}}$ of $1.0\text{--}2.5 \times 10^6 \text{ M}^{-1} \text{ s}^{-1}$ [6, 52] under conditions where ATP and MgCl_2 are saturating. In quiescent cells, ERK2 is located in the cytoplasm and upon cell stimulation is phosphorylated and localized to the nucleus [102] where it can phosphorylate nuclear transcription factors such as Ets-1 that lead to cell morphology changes.

Steady-state [7] and pre-steady state kinetics [44] of Ets Δ 138 phosphorylation have been carried out in the presence of the dual-phosphate form of ERK2 to understand the catalytic events of the enzyme–substrate pair. Ets Δ 138 is a model protein substrate for ERK2 because it is a physiologically relevant protein substrate²⁵ [121], yields a high amount and purity of protein when expressed in bacteria [42], contains only one phosphorylation site (Thr³⁸-Pro³⁹), contains a docking motif that enhances the efficiency of its phosphorylation [52], and its NMR structure has been solved [114]. Analytical techniques to directly measure the equilibrium dissociation constant (K_{d}) of the ERK2–Ets Δ 138 interaction have not been developed and are critical for studying molecular recognition determinants of the enzyme–substrate (E–S) pair under various conditions such as different phosphorylation states of the enzyme, phosphorylation states of the substrate, and under conditions where alternate substrates and enzymes are utilized. An

²⁵ Phosphorylation of Ets-1 leads to an increase in its transactivation capabilities.

analytical binding assay will make it possible to understand the rates of association and dissociation of the E-S or enzyme-product pair and determinants that affect these events, thereby, allowing a better understanding of the enzyme and its functions. We have developed a fluorescence anisotropy assay that allows the direct measurement of the K_d of the ERK2-EtsΔ138 docking interaction and facilitates the ability to carry out structure-function analyses.

The fluorescence anisotropy assay was carried by covalently labeling the smaller of the two proteins (EtsΔ138 ~ 18 kD) with a fluorescein moiety²⁶ to generate EtsΔ138-Fluorescein (EtsΔ138-F). The fluorescence anisotropy of EtsΔ138-F, a measure of the rate of molecular tumbling of a fluorescent molecule, was shown to increase in the presence of ERK2 due to an increase in molecular volume of the fluorescent substrate upon complexation with ERK2 to form an ERK2-EtsΔ138-F docking complex. Hyperbolic binding curves were generated which allowed for the determination of the K_d for the ERK2-EtsΔ138-F docking complex. Results indicate that both the unphosphorylated and phosphorylated forms of ERK2 form a docking complex with EtsΔ138-F with relatively similar affinities. The ERK2-EtsΔ138-F docking complex was disrupted by the addition of non-fluorescent proteins and peptides that competed for an ERK2 binding site for EtsΔ138 (an enzymic binding termed an exosite) and allowed for the determination of the K_d for the unlabeled competitors and ERK2. The fluorescence anisotropy and competition assay described here will facilitate further structure-function analyses on this enzyme-substrate pair and allow further insight into

²⁶ Fluorescein was chosen as it has a long excitation and emission wavelength which helps to avoid light scattering which is inversely proportional to the fourth power of wavelength. Fluorescein has a high absorption coefficient, a high quantum yield of fluorescence, it can be detected at very low concentrations, and has an excited-state lifetime of 4 ns which is the time required for significant rotation of macromolecules less than 100 kD.

the determinants of molecular recognition required for a protein kinase to phosphorylate a protein substrate.

FLUORESCENCE ANISOTROPY

Fluorescence anisotropy/polarization uses the molecular rotation rates of fluorescent molecules or their ability to tumble in solution to measure ligand-receptor complexation and dissociation. Fluorescence anisotropy/polarization has been used to study DNA–Protein, Protein–Protein, and Antibody–Ligand interactions. This technique exploits the fact that small molecules tumble quickly in solution and larger molecules tumble slowly. A fluorescently-labeled molecule that is excited with plane-polarized light can emit light that is either in the same plane or in a different plane than that with which it was excited. The plane of the emitted light is determined by the rotational relaxation time which is proportional to molecular volume and viscosity and inversely proportional to temperature. Anisotropy experiments were carried out by holding the temperature and viscosity of the solution constant while measuring changes in the molecular volume of fluorophore-bound protein upon addition of a macromolecule (protein) that binds the fluorophore-bound protein.

Fluorescence polarization was first described in 1926 by Perrin, who showed that a large fluorescently labeled molecule excited with plane-polarized light remained stationary between its excitation and emission states and, therefore, emitted light into the same plane as that in which it was excited. Smaller molecules excited with plane-polarized light that rotate or tumble through solution quickly during the excited state do not emit light back into the same plane. Therefore, molecules of different size give

different polarization values. Polarization is proportional to the rotational relaxation time of a molecule which is defined as the time it takes to rotate through an angle of 68.5° (often referred to as the magic angle). Rotational relaxation time (ρ) is proportional to the viscosity (η) of the solution and the molecular volume of the fluorophore (V) and inversely proportional to the absolute temperature (T) of the solution; where R is the gas constant 8.314 J mol⁻¹ K⁻¹ (Equation 4).

Equation 4 Debye rotational relaxation time (ρ) = $\frac{3\eta V}{RT}$

Therefore, if temperature and viscosity are held constant and the molecular volume of the labeled molecule changes by binding to another non-labeled molecule, then the polarization of the molecule changes due to an increase in the rotational relaxation time. These changes in polarization due to varying complex size allow protein–protein interactions to be measured using fluorescence polarization/anisotropy.

To measure polarization/anisotropy, a fluorescent molecule is excited with a vertical plane of light (defined as 0°) and the intensity of the emitted light in both the vertical plane (0°) and the horizontal plane (90°) are measured. The measured intensity (I) is denoted as I_{VV} or I_{VH} (where the first subscript describes the plane of excitation light and the second describes the plane of emitted light). Polarization and anisotropy are mathematically similar and are often used interchangeably.

Equation 5 and Equation 6 are used to calculate polarization and anisotropy, respectively. Both equations share similar numerators, however, the denominator for polarization describes the natural light intensity whereas anisotropy describes total light intensity.

$$\text{Equation 5} \quad \text{Polarization (P)} = \frac{(I_{VV} - I_{VH})}{(I_{VV} + I_{VH})}$$

$$\text{Equation 6} \quad \text{Anisotropy } \langle r \rangle = \frac{(I_{VV} - I_{VH})}{(I_{VV} + 2 \times I_{VH})}$$

When the fluorometer contains monochromators, the monochromator grating factor (G factor) is included into the polarization and anisotropy equations to “correct for the wavelength response to polarization of the emission optics and detectors” (Jobin Yvon Horiba users manual). The G factor also describes the “ratio of relative transmission efficiencies (intensities) of the emission channel for horizontally and vertically polarized light.” Mathematically, the G factor is defined as $G = I_{HV}/I_{HH}$. The G factor is dependent on wavelength so it must be measured at each wavelength for experiments that involve scanning the emission monochromator. For experiments that do not involve scanning, as described below, the G factor can be measured before or during each experiment. Equation 7 and Equation 8 describe polarization and anisotropy in a fluorometer which includes the G factor.

$$\text{Equation 7} \quad (\text{P}) \text{ in spectrophotometer} = \frac{(I_{VV} - G \times I_{VH})}{(I_{VV} + G \times I_{VH})}$$

$$\text{Equation 8} \quad \langle r \rangle \text{ in spectrophotometer} = \frac{(I_{VV} - G \times I_{VH})}{(I_{VV} + 2 \times G \times I_{VH})}$$

To determine the polarization/anisotropy change of a binding interaction, usually the anisotropy of the smaller of the two molecules of interest is followed. This allows for a larger change in anisotropy between the bound and unbound state as compared to labeling the larger molecule (since the change in anisotropy is proportional to the change in molecular volume). The anisotropy of the fluorescent molecule complexed with a larger molecule is expected to increase as the size of the fluorescent complex increases. This is due to an increase in the molecular volume which increases the rotational relaxation time and, therefore, increases the polarization/anisotropy. Experiments were carried out by holding the fluorescent molecule at a constant concentration while the larger molecule is titrated in to determine the steady-state equilibrium dissociation constant of the complex.

RESULTS AND DISCUSSION

CHOOSING A SUBSTRATE AMENABLE TO FLUORESCENT LABELING

The recombinant protein EtsΔ138 is a model protein substrate for studying the mechanism of phosphorylation by the dual-phosphate form of ERK2 [7, 42]. To study the protein-protein interactions between ERK2 and EtsΔ138 under conditions that do not involve phosphoryl-transfer, we developed a fluorescence anisotropy binding assay. EtsΔ138 has four cysteines (Figure 41) making it sub-optimal for fluorescent labeling on a single cysteine, however, removal of three of the cysteines by site-directed mutagenesis

generated an excellent substrate for fluorescent labeling using sulfhydryl chemistry. Since the change in fluorescence anisotropy upon binding a ligand is proportional to the change in molecular volume of the fluorescent species, we attached the fluorescent label to the smaller protein Ets Δ 138 (18 kD) so that binding the larger protein kinase ERK2 (42 kD) to form the docking complex would lead to the maximal change in anisotropy.

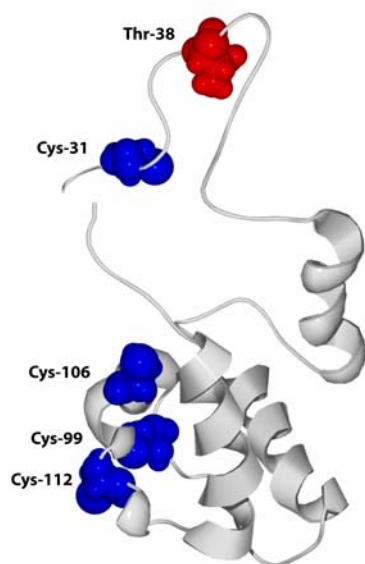


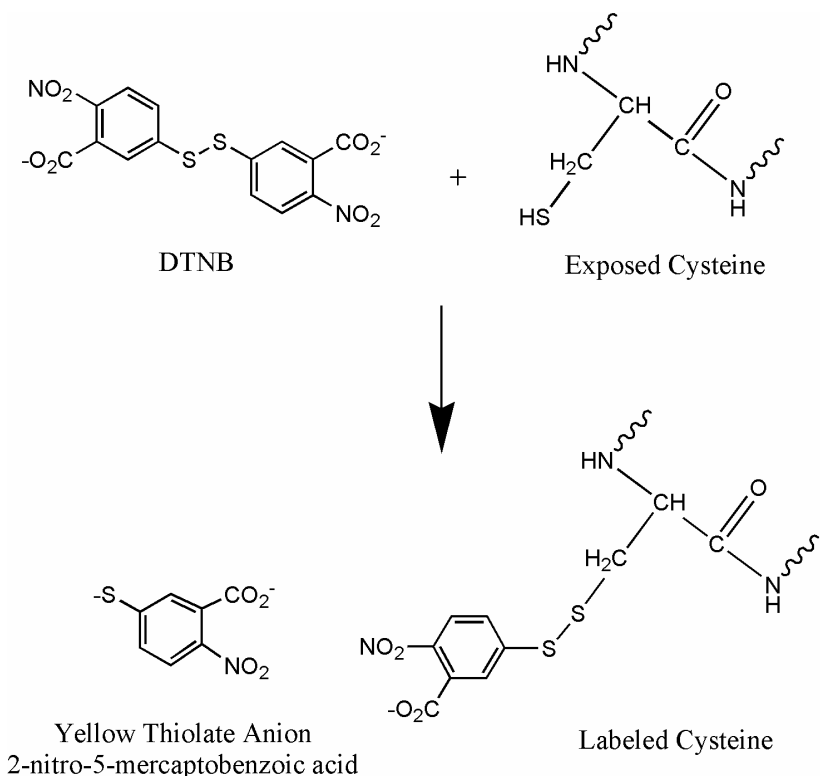
Figure 41. Structural representation of the ERK2 substrate Ets Δ 138. The four cysteines in Ets Δ 138 (1BQV) are highlighted in blue and shown with respect to the location of the phospho-acceptor residue (Thr-38). Each of the four cysteines is near the surface of the NMR structure (1BQV) with greater than 10% accessibility to the solution (as determined in DeepView/Swiss-PdbViewer (GlaxoSmithKline)). The structure was generated using DeepView/Swiss-PdbViewer and rendered in POV-Ray version 3.1.

CYSTEINE MUTAGENESIS

To label a protein with a fluorophore at a single site using sulfhydryl chemistry, we needed to generate an Ets Δ 138 protein containing only one surface exposed cysteine. To discern whether or not Ets Δ 138 was a feasible substrate for ERK2 in the absence of cysteines, each of the four cysteines (Cys-31, Cys-99, Cys-106, and Cys-112) were mutated to alanine using site-directed PCR mutagenesis. Ets Δ 138 lacking all four cysteines was termed Ets Δ 138 No Cysteines (Ets Δ 138NC).

We hypothesized that 5,5'-dithiobis(2-nitrobenzoic acid) (DTNB) would react to form thiolate anions with the surface exposed cysteines of Ets Δ 138 (containing 4

cysteines) but not with EtsΔ138NC (Scheme 8). Reactive surface exposed cysteines were quantified by comparing the molar ratio of thiolate anion formation and the molar ratio of protein in the reaction.



Scheme 8. Labeling of surface exposed cysteines on EtsΔ138. Surface exposed cysteines on EtsΔ138 and EtsΔ138 mutants lacking cysteines were reacted with DTNB to determine the number of surface exposed reactive cysteines. Sulfhydryl chemistry between the side chain of cysteines and DTNB form a labeled cysteine moiety and produce a thiolate anion that can be followed by its yellow color. The molar amount of thiolate anion formation was compared to the molar amount of EtsΔ138 protein to determine the molar ratio of reactive cysteines per molecule of EtsΔ138.

The reaction was monitored using a spectrophotometer to follow the formation of the yellow thiolate anion. EtsΔ138NC was shown to contain no cysteines while EtsΔ138

contained 3 reactive cysteines (Table 9). These results indicate that the cysteines were removed in the EtsΔ138NC construct and that one of the four cysteines in EtsΔ138 was not surface exposed for DTNB labeling. Phosphorylation of EtsΔ138NC by dual-phosphate ERK2 was carried out and shown to have similar steady-state kinetic parameters to that of EtsΔ138 (Figure 42) indicating that the cysteine residues are not essential for binding or phosphorylation by dual-phosphate ERK2.

	Cysteines ^a	Exposed Cysteines ^b	Mass ^c	Labeled Mass ^d
EtsΔ138 ^e	4	3.0	17 664	N/A
EtsΔ138NC	0	0.05	17 534	17 535
EtsΔ138-C31*	1	1	17 566	17 955
EtsΔ138-C99*	1	N/A	17 566	17 955

Table 9. Characterization of the surface exposed cysteines of EtsΔ138 and its cysteine and their mass before and after labeling with fluorescein. The number of cysteines present in each mutant protein was determined by the amino acid sequence^a. The number of surface exposed cysteines were determined by DTNB labeling^b. The mass of each protein (units: Daltons) was determined by electrospray ionization mass spectrometry before^c and after^d labeling with 5-IAF (fluorescein). Fluorescein incorporation into each protein was characterized by a 389 Da increase in mass (386 Da expected). Each EtsΔ138 contained an Ser26Ala mutation^e [44]. The expected mass for labeled and unlabeled EtsΔ138, EtsΔ138 NC, EtsΔ138-C31*, and EtsΔ138-C99* were within 2 Da on average.

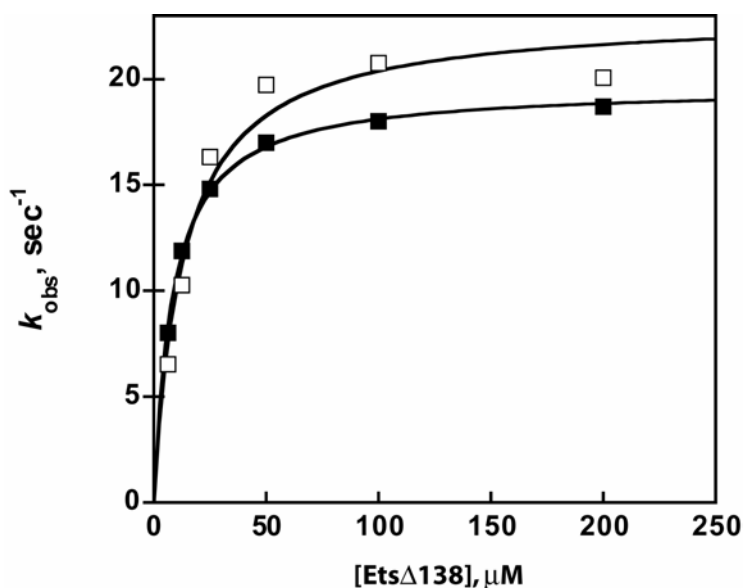
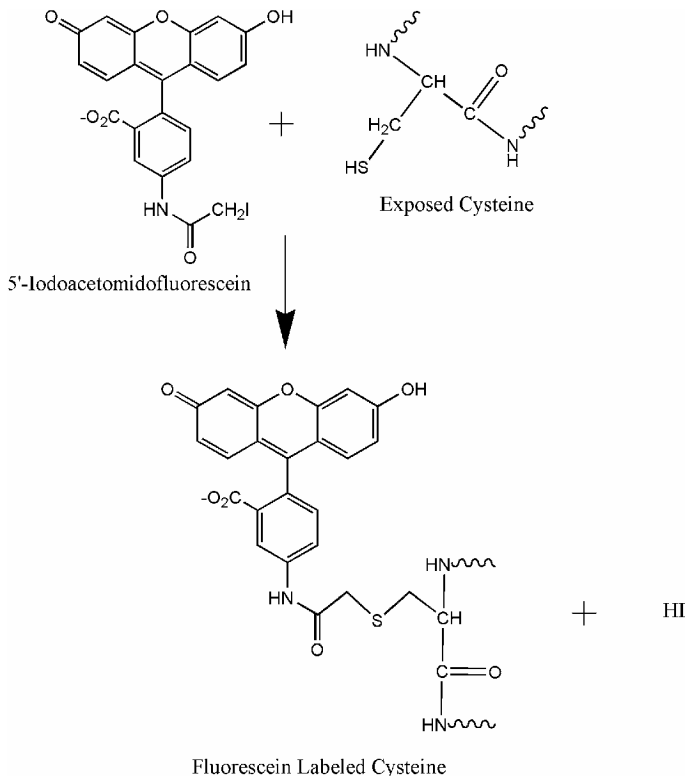


Figure 42. Steady-state kinetics of EtsΔ138NC phosphorylation by dual-phosphate ERK2. An EtsΔ138 mutant was generated that lacked cysteines (EtsΔ138NC, open squares). This mutant showed similar steady-state kinetic parameters to EtsΔ138 (closed squares) indicating that the cysteines are not required for substrate phosphorylation by ERK2. Varying concentrations of EtsΔ138 were examined for initial rates of phosphate incorporation into Thr-38 by ERK2. The observed initial rates (k_{obs}) were plotted against the concentration of substrate and the data were fit to the equation $k_{\text{obs}} = (k_{\text{cat}} \times [S]) / ([S] + K_m)$ to derive the steady-state parameters for EtsΔ138NC: $k_{\text{cat}} = 23.1 \pm 1.3 \text{ s}^{-1}$ and $K_m = 13.1 \pm 2.9 \text{ μM}$ and EtsΔ138: $k_{\text{cat}} = 19.6 \pm 0.7 \text{ s}^{-1}$ and $K_m = 8.8 \pm 1.4 \text{ μM}$. Assay conditions were 50 mM Hepes, pH 8.2, 50 mM KCl, 20 mM MgCl₂, 2 mM DTT, 40 μg/mL BSA, 2 mM ATP.

LABELING ETSΔ138 WITH FLUORESCCEIN

An EtsΔ138 mutant was generated that contained a single cysteine at position 31 (termed EtsΔ138-C31*) so that it could be labeled with a fluorophore. EtsΔ138-C31* was shown to contain one reactive cysteine when mixed with DTNB indicating that Cys-31 could be labeled with a fluorophore (Table 9). The fluorophore 5-iodoacetomido-

fluorescein (5-IAF) reacted with EtsΔ138-C31* to generate the fluorescently labeled EtsΔ138-Fluorescein (EtsΔ138-F) protein (Scheme 9).



Scheme 9. Fluorescein-labeling of a surface exposed cysteine. EtsΔ138 mutants containing a single exposed cysteine (EtsΔ138-C31* and EtsΔ138-C99*) were mixed with 5-iodoacetamidofluorescein (5-IAF) to generate EtsΔ138-F with a fluorescein moiety attached to the sulfhydryl group of either the Cys-31 or Cys-99 side chain.

The reaction was quenched, unreacted 5-IAF was removed, and the EtsΔ138-F was further purified on a Mono Q HR 5/5 anion exchange column. As expected, the EtsΔ138-C31* co-eluted with fluorescein indicating an EtsΔ138-F complex had formed (Figure

43). Similar labeling was achieved with EtsΔ138-C99* containing a single cysteines at position 99 (K. Cox).

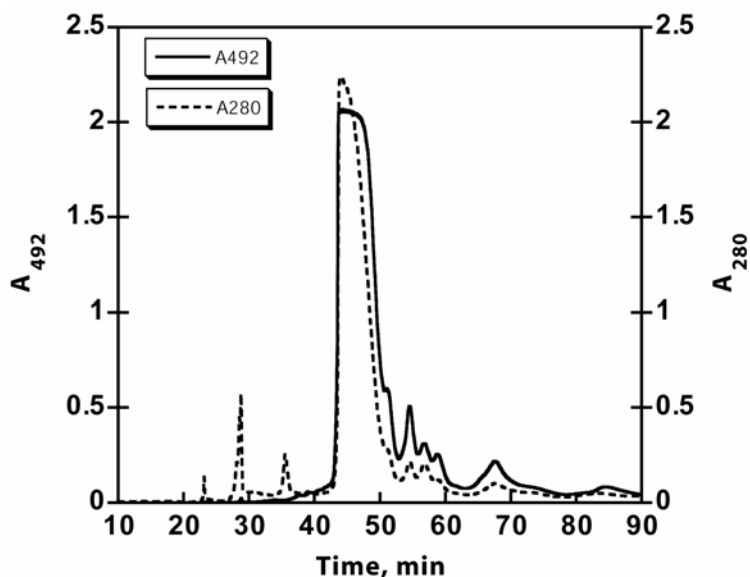


Figure 43. Mono Q HR 5/5 anion exchange purification of fluorescein-labeled EtsΔ138-C31* (EtsΔ138-F). EtsΔ138-C31* was mixed with a 15-fold molar excess of 5-IAF and labeled on Cys-31 to generate EtsΔ138-F. The unreacted 5-IAF was removed using a PD-10 desalting column and the fluorescent protein was applied to a Mono Q HR 5/5 anion exchange column. The protein was eluted with a linear gradient of NaCl (not shown) and the eluted protein was monitored for the presence of protein (tryptophan and tyrosine absorbance: A₂₈₀) as well as for the presence of fluorescein (A₄₉₂). The EtsΔ138-C31* and the fluorescein co-eluted indicating the complex EtsΔ138-F had formed.

The mass of the unlabeled EtsΔ138-C31* was 17 566 Da (expected 17 568 Da) while the mass of the EtsΔ138-F complex was 17 955 Da (expected 17 953 Da) indicating the covalent attachment of fluorescein in the EtsΔ138-F complex (K. Cox). No unlabeled EtsΔ138-C31* was detected in the EtsΔ138-F indicating complete labeling

(although mol/mol ratio of fluorescein to EtsΔ138-C31* using spectrophotometry suggests ~77% labeled). Similarly the mass of the unlabeled EtsΔ138-C99* was 17 566 Da (expected 17 568 Da) and the labeled EtsΔ138-C99*-F had a mass of 17 955 Da (expected 17 953 Da) (K. Cox). A similar labeling procedure was carried out with EtsΔ138NC, however, no labeling was detected²⁷ (K. Cox) (Table 9).

To ensure that the fluorescein moiety was covalently attached to Cys-31 in EtsΔ138-F, a tryptic digest was carried out followed by the purification of a single fluorescent tryptic peptide. The mass of the fluorescent peptide was 2 974 Da (expected 2 974 Da) indicating the fluorescent labeling of the tryptic peptide corresponding to V¹⁹DLELFPAPDMEC³¹ADVPLLTPSSK⁴² that contained a single cysteine at position 31 labeled with fluorescein. The EtsΔ138-F protein had an excitation and emission maxima of 491 and 515.5 nm, respectively, indicating its similarity to the spectral properties of fluorescein.

FLUORESCENCE ANISOTROPY OF ETSΔ138-F INCREASES WHEN BOUND TO ERK2

EtsΔ138-F generated a fluorescence anisotropy signal of $\langle r \rangle = 0.11$ and was expected to increase upon binding a larger ligand. Upon addition of both unphosphorylated and dual-phosphorylated ERK2, the anisotropy signal of EtsΔ138-F increased indicating that the EtsΔ138-F was able to bind both the inactive and active form of ERK2 (Figure 44). The increase in anisotropy was due to an increase in the molecular volume of the EtsΔ138-F since both temperature and viscosity were held

²⁷ The mass of EtsΔ138NC was 17 534 Da (expected 17536 Da) and after an attempt to label EtsΔ138NC the mass was still 17 535 (expected 17 921 Da for labeled EtsΔ138NC-F) indicating that no fluorescein was incorporated.

constant in the assay. The data were fit to Equation 9 to yield a K_d of $0.7 \pm 0.1 \mu\text{M}$ and $5.3 \pm 0.1 \mu\text{M}$ for unphosphorylated and dual-phosphorylated ERK2²⁸, respectively, indicating that both forms of ERK2 bind with similar affinity irrespective of its phosphorylation state. The difference in the anisotropy change between the phosphorylated and unphosphorylated ERK2 may be due to a difference in molecular shape of the different phosphate forms of ERK2. It is interesting that the amplitude of the anisotropy change for the inactive ERK2 is twice that of the active ERK2 indicating that EtsΔ138-F may bind a dimer of inactive ERK2 and only a monomer of active ERK2.

²⁸ EtsΔ138-C99*-F gave a similar K_d value of $4.7 \pm 0.6 \mu\text{M}$ for dual-phosphate ERK2 indicating that location of the fluorophore does not affect the K_d (K. Cox). Phosphorylation of EtsΔ138-C31*-Fluorescein did not have a significant affect on dual-phosphate ERK2 affinity ($K_d = 4.1 \pm 0.5 \mu\text{M}$) (K.Cox).

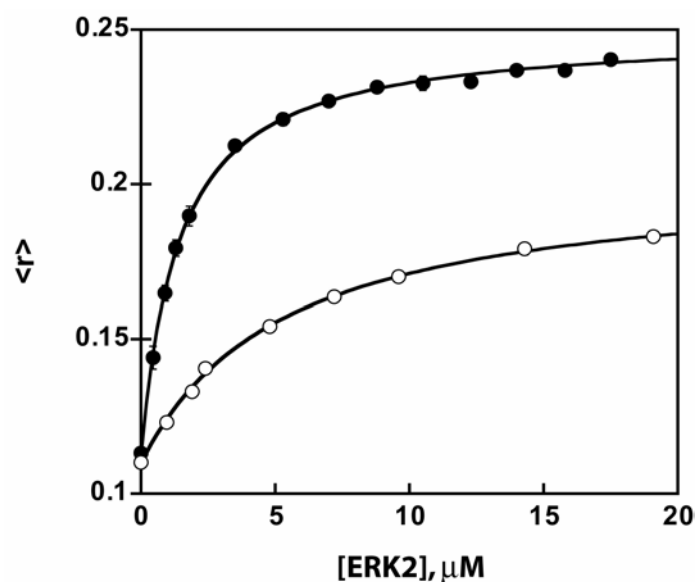
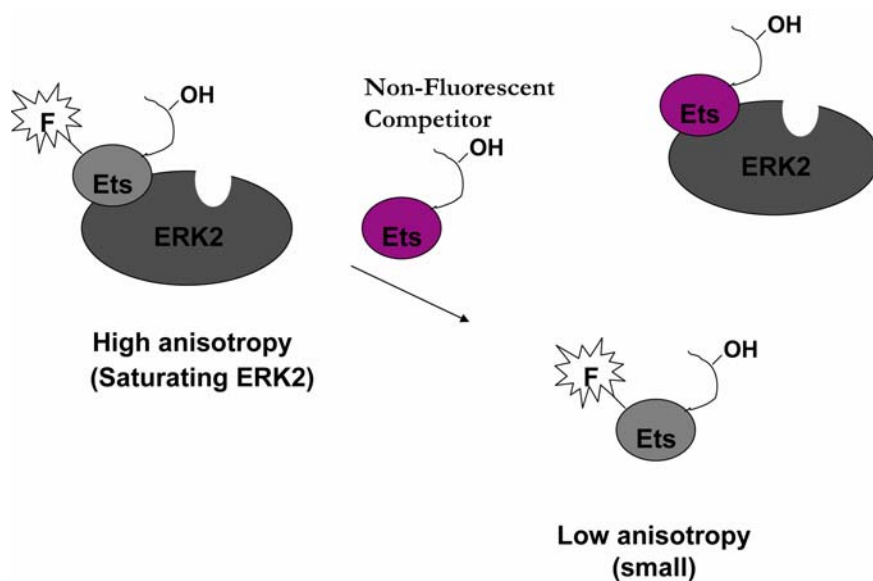


Figure 44. The fluorescence anisotropy of Ets Δ 138-F increases when bound to ERK2. Fluorescence anisotropy values ($\langle r \rangle$) were measured using 100 nM Ets Δ 138-F with varying amounts of inactive (closed) and active (open) ERK2 in 25 mM Hepes, pH 7.5, 50 mM KCl, 0.1 mM EDTA, 0.1 mM EGTA, 2% glycerol, 40 $\mu\text{g/mL}$ BSA, and 2 mM DTT. Each reaction was excited with both vertically- and horizontally-polarized light at 492 nm and the emission was measured both vertically and horizontally to the excited light at 515 nm. Anisotropy values were calculated using Equation 8. The data were plotted using KaleidaGraph and fit to Equation 9 to obtain a K_d of $0.7 \pm 0.1 \mu\text{M}$ and $2.7 \pm 0.1 \mu\text{M}$ for unphosphorylated and dual-phosphorylated ERK2, respectively. Error bars indicate the standard deviation from the mean for the inactive ($n=3$) and active ($n=2$) ERK2. Slits were set at 5 nm. Integration time was 300 msec. The G-factor did not vary between samples (0.75-0.76).

COMPETITION ASSAY

A fluorescence anisotropy competition assay (Scheme 10) was used to determine the K_d for non-fluorescent Ets Δ 138. The fluorescence anisotropy of an ERK2–Ets Δ 138-F

complex was monitored in the presence of several concentrations of non-fluorescent EtsΔ138. For the competition assay, we make the assumption that the unlabeled competitor binds an EtsΔ138-F exosite on ERK2 that competes with the ability of EtsΔ138-F to form a docking complex with ERK2. Therefore, increasing the concentration of the competitor decreases the amount of EtsΔ138-F bound to ERK2 and leads to a smaller anisotropy value as compared to the ERK2–EtsΔ138-F docking complex. We show that unlabeled EtsΔ138 acts as a competitor and disrupts both unphosphorylated and dual-phosphorylated forms of the ERK2–EtsΔ138-F complex (Figure 45). The data was simultaneously fitted to Equation 10 and Equation 11 using the pre-determined K_d for the ERK2-EtsΔ138-F complex for both ERK2 phospho-forms (derived from Figure 44) to solve for the K_d of the non-fluorescent ERK2–EtsΔ138 complex ($K_{d,2}$) for both unphosphorylated ($K_d = 2.5 \pm 1.3 \mu\text{M}$) and dual-phosphorylated ($K_d = 6.6 \pm 1.2 \mu\text{M}$) ERK2. Interestingly, the value of K_d for the fluorescent EtsΔ138-F and the unlabeled EtsΔ138 were similar indicating that the fluorophore on Cys-31 does not affect the affinity of EtsΔ138-F for ERK2. Bovine serum albumin, the main protein in mammalian blood tissue that binds several proteins, was used as a nonspecific protein competitor and did not dissociate the ERK2–EtsΔ138-F docking complex with concentrations up to 200 μM (K. Cox, data not shown). Using the competition assay, a single fluorescent protein, EtsΔ138-F, can be used to determine the value of K_d for non-fluorescent proteins that compete with EtsΔ138-F for a similar ERK2 exosite.



Scheme 10. Fluorescence anisotropy competition assay. A docking complex was formed between ERK2 (dark gray) and EtsΔ138-F (light gray) that yields a high anisotropy value. Upon addition of a non-fluorescent competitor that binds ERK2, EtsΔ138-F dissociates from ERK2, thereby, yielding a lower anisotropy value. Using several concentrations of the non-fluorescent competitor and the known K_d for the ERK2–EtsΔ138-F docking complex, the value of K_d of the non-fluorescent ERK2–EtsΔ138 docking complex was determined. We make the assumption that the competitor binds an ERK2 exosite for EtsΔ138-F.

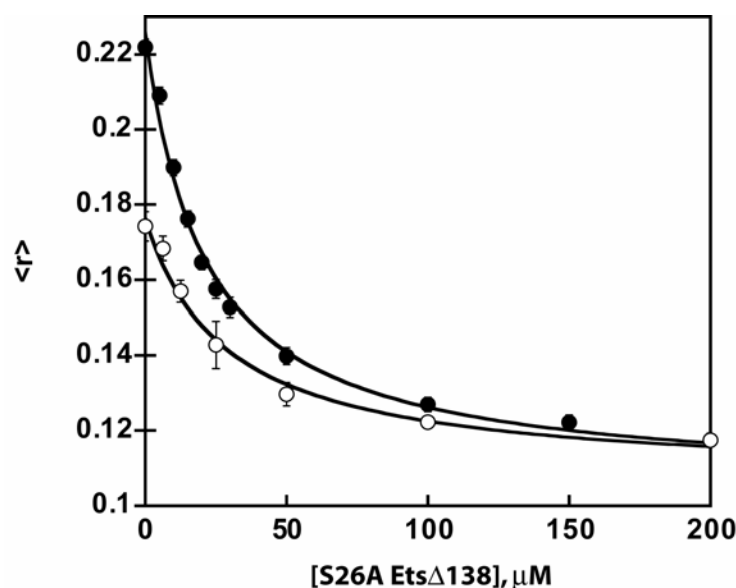


Figure 45. A fluorescence anisotropy competition assay to determine the K_d of non-fluorescent ERK2 ligands. A docking complex was formed using ERK2 (9.55 μM) and EtsΔ138-F (100 nM) and the anisotropy of the fluorescent complex was monitored in the presence of several concentrations of non-fluorescent EtsΔ138. Non-fluorescent EtsΔ138 competed for ERK2 binding and decreased the ERK2–EtsΔ138-F concentration which decreased the anisotropy. Both the unphosphorylated (closed circles) and the dual-phosphorylated (open circles) ERK2 were analyzed. The data were simultaneously fit to Equation 10 and Equation 11 using pre-determined K_d values for the ERK2-EtsΔ138-F docking complex. The K_d for EtsΔ138 and inactive ERK2 was $2.5 \pm 1.3 \mu\text{M}$ ($n=1$) and that of active ERK2 was $6.6 \pm 1.2 \mu\text{M}$ ($n=3$). Data points are shown as mean \pm SD. K_d are depicted as mean \pm SE.

DOCKING MOTIF PEPTIDES COMPETE FOR ETSΔ138 EXOSITES ON ERK2

MAPK docking motifs exist on proteins that interact with MAPKs and mediate binding to specific MAPKs or a subset of MAPKs. These docking motif peptides have been shown to bind MAPKs and disrupt the protein-protein interactions and catalytic events between MAPKs and their activators, substrates, and inactivators. One such

docking motif is termed a docking for ERK/FXFP (DEF) motif and contains a consensus sequence of Phe-X-Phe-Pro (FXFP), where X represents any amino acid [19]. A DEF motif is thought to mediate ERK2 binding to the ETS family of proteins, however, EtsΔ138 does not contain a DEF motif. Peptides resembling a DEF motif act as general inhibitors of ERK2 catalysis [19]. A recent study using amide exchange proposed that a DEF motif peptide derived from the ERK2 substrate Elk-1 can bind only the dual-phosphate form of ERK2 in a region near the α_F helix, α_G helix, and the MAPK insert region that is not available in the inactive protein [28].

Another docking motif is termed the kinase interaction motif (KIM) [53] (also referred to as both a docking-site for ERK and JNK LEL (DEJL) [19] and a D-domain [29]) which contains both basic and small hydrophobic residues in the consensus sequence R/K-X₄- ϕ_A -X- ϕ_B where ϕ is a hydrophobic residue such as leucine, isoleucine, or valine. Peptides containing a KIM inhibit MAPKK2 binding and phosphorylation of ERK2, ERK2 phosphorylation of Elk-1, and MKP1 dephosphorylation of ERK2 [54] indicating that the KIM inhibition occurs at an exosite on ERK2 important for many different types of protein-protein interactions such as activator, substrate, and inactivator binding. It was originally proposed that the KIM of MAPKK1 may form a docking complex with the common docking (CD) exosite on ERK2 since this region is thought to regulate similar protein-protein interactions [17]. However, a recent co-crystal structure of two DEJL motif peptides, derived from the activator MAPKK3b and the substrate MEF2a, bound to inactive p38 MAPK α suggest that neither peptide shows direct contact with the CD exosite and instead binds a region between the β_7 - β_8 reverse turn and the α_D - α_E helix [27]. Hydrogen exchange experiments also verify this MAPK binding region for a similar DEJL motif peptide (derived from Elk-1) binding to both the active and inactive forms of p38 MAPK α as well as the dual-phosphate form of ERK2 [28].

A DEJL and a DEF motif peptide derived from the ERK2 substrate Elk1 (Elk1-DEJL: *N*-QKGKPRDLELPLSPSLR-C [122] and Elk1-DEF: *N*-AKLSFQFPS-C [19]) were used as competitors in our fluorescent anisotropy assay to test whether the docking motif peptides could bind the EtsΔ138-F exosite on ERK2 and disrupt the ERK2–EtsΔ138-F docking complex. The proposed docking exosite on the dual-phosphate form of ERK2 for the Elk1-DEJL and Elk1-DEF peptides have been proposed [28]. Here, we show that both peptides were capable of disrupting the dual-phosphate ERK2–EtsΔ138-F complex as seen by the decrease in anisotropy with increased peptide concentration (Figure 46a). The Elk1-DEJL peptide ($K_d = 5.1 \pm 2.0 \mu\text{M}$) had a greater affinity than the Elk1-DEF peptide ($19.3 \pm 2.4 \mu\text{M}$) for the dual-phosphate form of ERK2. However, the unphosphorylated ERK2 was unable to bind the Elk1-DEF peptide ($K_d = 1.0 \pm 0.2 \text{ mM}$; K. Cox) while maintaining a similar affinity for the Elk1-DEJL peptide ($K_d = 2.6 \pm 0.7 \mu\text{M}$; K. Cox) (Figure 46b). These results suggest that the different phospho-forms of ERK2 can discriminate against one type of docking motif peptide (Elk1-DEF) but cannot discriminate against another docking motif peptide (Elk1-DEJL). There are conformational changes that occur when ERK2 is phosphorylated [4] which may account for the specificity of binding for the Elk1-DEF peptide [28] but not the Elk1-DEJL peptide which has been proposed to bind an exosite on ERK2 that does not undergo a conformational change upon phosphorylation [28]. The fact that both the Elk1-DEF and Elk1-DEJL peptides disrupt the docking complex between ERK2 and EtsΔ138-F indicates that the exosites proposed to bind these peptides on ERK2 [28] may be utilized for EtsΔ138 binding.

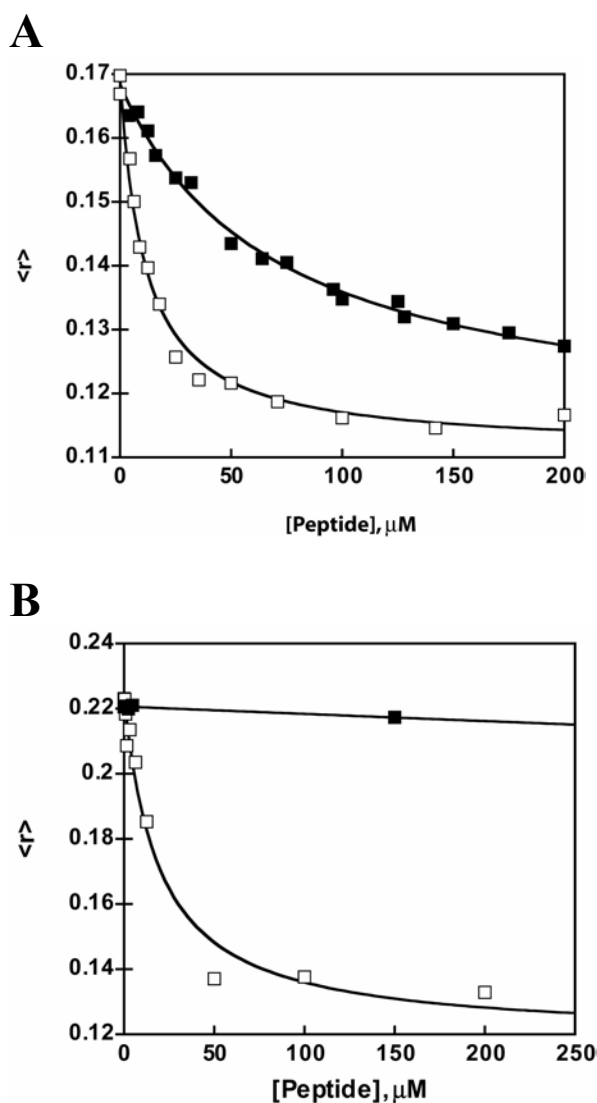


Figure 46. A fluorescence anisotropy competition assay to determine the K_d of docking motif peptides. A docking complex was formed using (A) dual-phosphate ERK2 (9.55 μM) or (B) unphosphorylated ERK2 (5 μM) with 100 nM Ets Δ 138-F and the anisotropy of the fluorescent complex was monitored in the presence of several concentrations of the Elk1-DEJL (open squares) and Elk1-DEF (closed squares) peptides. Both peptides competed for Ets Δ 138 exosites on the dual-phosphate ERK2 as seen by the decrease in fluorescence anisotropy (A), whereas the Elk1-DEF could not bind unphosphorylated ERK2 (B). The data were simultaneously fit to Equation 10 and Equation 11 using pre-determined K_d values for the ERK2-Ets Δ 138-F docking complex.

Since the Elk1-DEJL peptide is thought to bind the docking groove exosite on ERK2, similar to the docking motif peptides used in the co-crystallization study with the inactive form of p38 MAPK α [27], we were interested in studying the specificity of docking motif peptides towards MAPKs. The docking motif peptides that bind in the docking groove exosite of p38 MAPK α [27] were derived from an upstream activator (MAPKK3b) and a substrate (Mef2a). Neither MAPKK3b nor Mef2a are thought to interact with ERK2, however, the docking motifs for these proteins contain basic amino acids and a hydrophobic ϕ_A -X- ϕ_B motif that are similar to DEJL motifs that bind ERK2. Both the MAPKK3b and Mef2a peptide were able to bind the dual-phosphate ERK2 exosite for Ets Δ 138 and compete for Ets Δ 138-F binding as revealed by their ability to disrupt the ERK2–Ets Δ 138-F complex in a competition anisotropy assay (Figure 47). These results suggest that docking motif peptides of MAPK-interacting proteins may regulate binding to more than one MAPK and that other factors and perhaps additional docking motif interactions may regulate the specificity of MAPK protein-protein interactions.

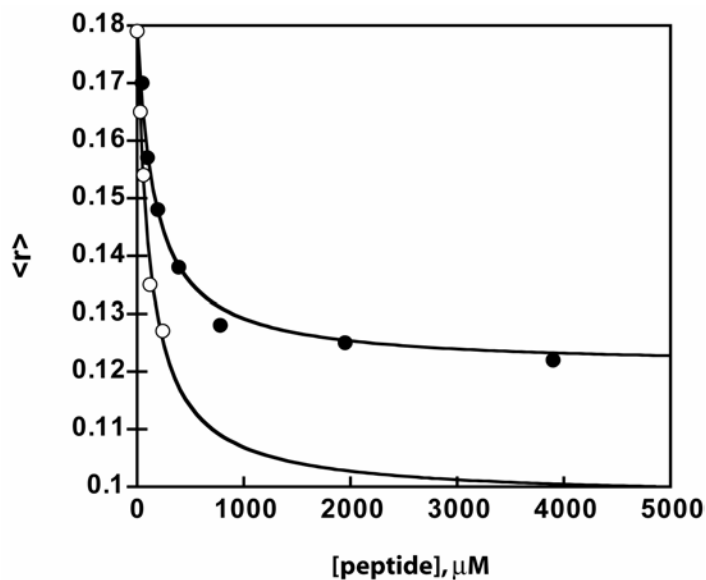


Figure 47. A fluorescence anisotropy competition assay to determine the K_d of p38 MAPK α docking motif peptides and ERK2. A docking complex was formed using dual-phosphate ERK2 (9.55 μM) and Ets Δ 138-F (100 nM) and the anisotropy of the fluorescent complex was monitored in the presence of several concentrations of the Mef2a (closed) and the MAPKK3b (open) docking motif peptides. Both peptides competed for Ets Δ 138 exosites on the dual-phosphate ERK2 as seen by the decrease in fluorescence anisotropy. The data were simultaneously fit to Equation 10 and Equation 11 using pre-determined K_d values for the ERK2-Ets Δ 138-F docking complex to obtain a K_d for the Mef2a ($54.0 \pm 7.2 \mu\text{M}$) and MAPKK3b ($35.9 \pm 10.4 \mu\text{M}$) peptides.

PEA-15 CAN DISTINGUISH BETWEEN DIFFERENT PHOSPHORYLATION FORMS OF ERK2

Phosphoprotein enriched in astrocytes-15 kDa (PEA-15) [123] is a protein with a death effector domain [124] that binds ERK2 [31] and has been shown to inhibit apoptosis and potentiate Ras-mediated ERK signaling implicating the importance of

PEA-15 in oncogenesis [124]. PEA-15 binds ERK more readily than p38 and JNK and is not a substrate or regulator of ERK2 activity. Deletion of PEA-15 caused an increase in ERK2 entry into the nucleus and a subsequent increase in c-fos transcription [75] indicating that PEA-15 is important for anchoring ERK2 in the cytoplasm. Overexpression of PEA-15 decreased the ability of ERK2 to enter the nucleus after serum stimulation resulting in decreased Elk-1 phosphorylation and subsequent decreased transcriptional activity [75]. Furthermore, PEA-15 was shown to bind both active and inactive ERK2, however, binding affinities for the dual-phosphorylated and unphosphorylated forms of ERK2 were not discussed.

The NMR structure of PEA-15 is known and NMR “footprinting” was used in the presence of ERK2 to find residues of PEA-15 that had significantly broadened NMR peaks upon introduction to ERK2 indicating residues involved in the docking complex [31]. PEA-15 is thought to bind ERK2 in the α G helix and the α 1L14 helix of the MAPK insert, specifically residues Y213, L232, K257, and R259 which were found to disrupt ERK2 binding after mutagenesis to glutamic acid [13]; the ERK2 mutants did not have defects in their ability to be activated by MAPKK1. This region is the same region elucidated by ERK2–MAPKK1/2 interactions where it was also shown that ERK2 mutants H230R, N236K, Y261N, and S264P had the largest affect on MBP phosphorylation as determined by an increase in the K_m [12] and is also a region thought to mediate ERK2 binding to Ets Δ 138 (Chapter 3).

A fluorescence anisotropy competition assay was carried out where unphosphorylated PEA-15 was labeled with fluorescein and allowed to bind both the active and inactive forms of ERK2. It was found that PEA-15 had a much higher affinity for the unphosphorylated form of ERK2 ($K_d = 12 \pm 3$ nM; K. Cox) in comparison to the dual-phosphate form of ERK2 ($K_d = 706 \pm 122$ nM; K. Cox). These results suggest that

PEA-15 can distinguish between the active and inactive forms of ERK2 and may regulate cell signaling differences in astrocytes and other cells expressing PEA-15.

CONCLUSIONS

A direct binding assay had not been established to determine the equilibrium dissociation constants for ERK2 and its interacting proteins. Here we have developed a fluorescence anisotropy assay and a competition assay that allows the equilibrium dissociation constant of ERK2-interacting proteins and peptides to be determined. The protein substrate EtsΔ138 was mutated so that it lacked each of its 4 cysteines and was shown to have similar steady-state kinetics of ERK2 phosphorylation as that of WT EtsΔ138 (Figure 42) indicating that the lack of cysteines did not affect its ability to be phosphorylated by dual-phosphate ERK2. One cysteine was incorporated into EtsΔ138 at either position 31 or 99 to generate EtsΔ138-C31* and EtsΔ138-C99*, respectively, and covalently labeled with a fluorescein moiety at a single cysteine site. An EtsΔ138 construct lacking cysteines was not susceptible to DTNB or fluorescent labeling while the EtsΔ138-C31* and EtsΔ138-C99* were, indicating that the label was incorporated into a single cysteines. To further confirm the labeling of a specific site, the fluorescent EtsΔ138-F construct was purified, digested with trypsin, the tryptic peptides were purified on a reverse phase HPLC column, and shown to be labeled on a peptide that contained either Cys-31 or Cys-99 by determining the mass of the single fluorescent peptides using mass spectrometry.

The fluorescence anisotropy signal of EtsΔ138-F increased in the presence of ERK2 indicating that a docking complex was formed between ERK2 and EtsΔ138-F.

The binding affinities for EtsΔ138-F labeled at Cys-31 or Cys-99 did not differ indicating that the position of the fluorophore on EtsΔ138 did not affect their affinity for ERK2. Both unphosphorylated and dual-phosphorylated ERK2 were able to bind EtsΔ138 with similar affinities (within 3-fold of one another) indicating that the ERK2–EtsΔ138-F docking complex can exist with both the catalytically inactive and active form of ERK2 (Figure 44). By adding ERK2 directly to the EtsΔ138-F, equilibrium dissociation constants were discerned for the ERK2-EtsΔ138-F complex. However, true dissociation constants for unlabeled proteins were desired.

To elucidate the K_d s for unlabeled proteins and peptides, a fluorescence anisotropy competition assay was developed. In this assay, a fluorescent docking complex was formed between ERK2 and EtsΔ138-F and allowed to dissociate in the presence of a competitor that could bind ERK2 (Scheme 10). Various amounts of unlabeled EtsΔ138 competitors caused a decrease in the anisotropy due to dissociation of the ERK2–EtsΔ138-F complex and increasing free EtsΔ138-F in solution. The competition assay was used to determine the K_d for unlabeled EtsΔ138 (Figure 45) and shown to be similar to the K_d for the labeled EtsΔ138-F indicating that the label did not alter the binding affinity for ERK2.

The competition assay was also used to determine the affinity of docking motif peptides that bind ERK2. Both the Elk1-DEJL motif peptide and the Elk1-DEF motif peptide have been shown to bind two different exosites on the dual-phosphate form of ERK2 [28], however, their binding affinities were not established. Here, we show that both the Elk1-DEJL and Elk1-DEF peptides displace EtsΔ138-F from dual-phosphate ERK2, however, while the Elk1-DEJL peptide could also displace EtsΔ138-F from unphosphorylated ERK2, the Elk1-DEF peptide could not. These results suggest that the Elk1-DEJL peptide binds to ERK2 with a slightly higher affinity than the Elk1-DEF

peptide and that the Elk1-DEF peptide can only bind the dual-phosphate form of ERK2. It has been hypothesized that a conformational change occurs on the dual-phosphate form of ERK2 that exposes the ERK2 exosite that binds the DEF motif, whereas, this exosite is buried in the unphosphorylated form of ERK2 [28]. This may be a means for ERK2 to differentially bind DEF-containing substrates only when it is activated allowing it to avoid DEF-mediated contacts when inactivated.

The competition anisotropy assay was also used to determine the affinity of PEA-15 and ERK2, a protein that is neither an activator, inactivator, nor a substrate of ERK2. PEA-15 has a nuclear export sequence and can anchor ERK2 in the cytoplasm preventing its nuclear presence [75]. We show that the unphosphorylated form of ERK2 binds PEA-15 much tighter than phosphorylated ERK2. These results suggest that PEA-15 can selectively bind different phospho-forms of ERK2 and may help to mediate signaling specificity within the cell. Perhaps PEA-15 can remove unphosphorylated ERK2 from the nucleus more efficiently than dual-phosphorylated ERK2. PEA-15 itself is regulated by phosphorylation by at least two different protein kinases including protein kinase C [123] and calcium/calmodulin kinase II [125] and can exist in an unphosphorylated, monophosphorylated, or dual-phosphorylated form. It will be interesting to examine whether or not phosphorylation of PEA-15 regulates its ability to bind ERK2.

The fluorescence anisotropy assay described here will prove to be a valuable assay in studying ERK2 interactions with its protein substrates. Here we have shown that it can be used to study the affinities of different phospho-forms of both the labeled protein substrate and the larger ERK2 molecule. Different phospho-forms of an unlabeled competitor of the interaction could also be used. We were also able to determine the K_{ds} of peptides that bind to MAPK exosites so that information regarding the specificity of interactions can be elucidated. We found that some peptides bind both

phospho-forms of ERK2 while others do not and that some peptides thought to be specific for another MAPK (p38 MAPK α) can also bind ERK2. This assay could also be used for high-throughput screening of small molecules that disrupt the ERK2–Ets Δ 138-F interaction so that small molecules that disrupt a specific protein–protein interaction could be determined very quickly as long as the chemical library being screened does not contain molecules that resemble the spectral properties of fluorescein. This assay and other assays that determine the binding affinities of protein–protein interactions are valuable for studying the regulation of protein–protein interactions, specificity of cellular signaling pathways, and for carrying out structure–function analyses of binding events.

EXPERIMENTAL PROCEDURES

MATERIALS

All proteins were produced in the *Escherichia coli* strain BL21 (DE3) purchased from Novagen (Madison, WI). 5'-Iodoacetamidofluorescein (5-IAF) was purchased from Molecular Probes (Eugene, OR). The Mono Q HR 10/10 and HR 5/5 anion exchange columns and PD-10 desalting columns were purchased from Amersham Biosciences (Piscataway, NJ) and run on a Waters (Milford, MA) HPLC system (600E/650E) with an absorbance detector (2487).

ANALYTICAL INSTRUMENTS

The concentrations of ERK2 and EtsΔ138 were determined by UV absorbance using a Cary Model 50 spectrophotometer purchased from Varian (Walnut Creek, CA). Mass spectrometry of EtsΔ138 proteins peptides were carried out as described [7]. Fluorescence anisotropy measurements were made at 27 °C using a Fluorolog Model FL3-11 fluorometer (Jobin Yvon, Edison, NJ) using three-window fluorescence grade quartz cuvettes with a 1.0 cm path length and 55 μL aqueous volume purchased from Hellma (Plainview, NY). The program Instrument Control Center (Jobin Yvon, Edison, NJ) was used to collect fluorescence anisotropy data and the programs KaleidaGraph (Reading, PA) and Scientist (North Andover, MA) were used to plot and fit the data, respectively.

SITE-DIRECTED MUTAGENESIS OF ETSΔ138

A pET-28a bacterial expression vector encoding a hexa-histidine tag followed by a thrombin cleavage site and the cDNA encoding murine Ets1 residues 1-138 (pET-28a EtsΔ138, a gift of L. P. McIntosh, University of British Columbia, Vancouver) was modified by PCR to construct the C31A, C99A, C106A, C112A EtsΔ138 mutants in an S26A EtsΔ138 background [44]. A two-step PCR reaction was carried out using the following conditions: 94 °C for 5 min to denature the complementary strands; 30 cycles of 55 °C for 30 sec to anneal the primers, extension for 1 min at 72 °C, followed by a denaturation step at 94 °C for 45 sec; complementary strands were extended a final 10 min at 72 °C. The first round of mutagenic PCR generated two overlapping products, fragment A and B, from two separate reactions using pET-28a EtsΔ138 as a template. Fragment A was PCR amplified with an outer forward primer (5'-GGT GAT GCC GGC CAC GAT GC) and an inner reverse primer containing the mutation (underlined) for C31A (5'- GG GAC ATC TGC GGC TTC CAT GTC CG-3'), C99A (5'-GC TCC ACT CAT GGC GAA CTT CTG GA-3'), C106A (5'-TTT ACC CAG GGC GGC CAG TGC TGC TC-3'), and C112A (5'-AG CTC GAG GAA GGC TTC TTT ACC CA-3'). Fragment B was amplified with an inner forward primer containing the mutation for C31A (5'- CG GAC ATG GAA GCC GCA GAT GTC CC-3'), C99A (5'-TC CAG AAG TTC GCC ATG AGT GGA GC-3'), C106A (5'-GA GCA GCA CTG GCC GCC CTG GGT AAA-3'), C112A (5'-TG GGT AAA GAA GCC TTC CTC GAG CT-3') and an outer reverse primer (5'-GCT AGT TAT TGC TCA GCG GTG G-3'). PCR fragments A and B were purified and used as templates for a second round of PCR using the outer primers. Mutants containing two mutations were made using single mutant DNA as template and incorporating a second mutation. The mutant PCR products were digested with NdeI and HindIII and ligated into NdeI-HindIII digested pET28a. EtsΔ138-C31*

containing a single cysteine at position 31 was generated by mutating Cys-99, 106, and 112 to alanine. Cys-31 was mutated to alanine in the EtsΔ138-C31* construct to generate EtsΔ138NC containing no cysteines. EtsΔ138-99* containing a single cysteine at position 99 was generated by mutating Cys-31, 106, and 112 to alanine. All mutations were verified by sequencing the DNA at UT core facilities using an Applied Biosystems automatic DNA sequencer. All proteins produced from pET-28a have an *N*-terminal sequence of M-G-S-S-H-H-H-H-H-H-S-S-G-L-V-P-R-G-S-H- prior to the methionine encoded by the EtsΔ138 giving a mass of 17, 664 Da for EtsΔ138 (the initial methionine is cleaved [42], all EtsΔ138 constructs have an S26A mutation [44] with the exception of T38A/P39A which has Ser-26).

DTNB LABELING

EtsΔ138 mutants were dialyzed into 20 mM Hepes, pH 8.1, 50 mM KCl, and 2 mM EDTA so that the DTT in the storage buffer would not interfere with the DTNB labeling. The concentration of protein was determined using guanidine hydrochloride [119] and an extinction coefficient of $\epsilon_{280} = 23\,231.5\text{ M}^{-1}\text{ cm}^{-1}$ [42] for each of the mutants. A fresh stock solution of 4 mM DTNB was prepared in 50 mM NaAc and stored at 4 °C. A reaction containing 20 μM protein, 400 μM DTNB, 20 mM Hepes, pH 8.1, 50 mM KCl, and 2 mM EDTA was mixed, incubated 5 min at 25 °C, and measured for optical absorbance at 412 nm. The concentration of thiolate anion formation due to DTNB reacting with free sulfhydryl groups on cysteines was determined using the extinction coefficient for the reagent ($\epsilon_{412} = 13\,600\text{ M}^{-1}\text{ cm}^{-1}$). The concentration of thiolate anion formation was compared to the protein concentration to determine the molar ratio of surface exposed cysteines per molecule of EtsΔ138.

PREPARATION OF ETSΔ138-FLUORESC EIN (ETSΔ138-F)

EtsΔ138-C31* containing only one cysteine at position 31 was purified essentially as described [42] and dialyzed into 1.25 mM Hepes, pH 7.5, 2.5 mM KCl, and 2 mM DTT. The concentration was determined using the absorbance at 280 nm using $\epsilon_{280} = 23\,231\text{ cm}^{-1}\text{ M}^{-1}$ [42] in 6 M guanidine hydrochloride [119]. EtsΔ138-C31* was covalently linked to a fluorescein moiety through a thioether linkage at cysteine 31. EtsΔ138-C31* (7.8 mg) was buffer exchanged to remove the reducing agent DTT using a pre-equilibrated PD-10 desalting column or by dialysis into L1 buffer (25 mM Hepes, pH 7.3, containing 50 mM KCl). The eluant was collected in 1 mL fractions and probed for protein using a Bradford assay. A fresh stock of 10 mM 5'-iodoacetamidofluorescein (5-IAF) was made in dimethylformamide and kept in the dark. The concentration of fluorescein was determined using the absorbance at 492 nm using $\epsilon_{492} = 78\,000\text{ cm}^{-1}\text{ M}^{-1}$ and measuring an absorbance below 0.05 (Molecular Probes) in L1 buffer; the quantum yield and absorption of fluorescein is pH sensitive, $\text{pK}_a \sim 6.5$ [126]. The 5-IAF was added dropwise to the EtsΔ138-C31* in a 12 mL reaction of L1 buffer and 7.8 mg of EtsΔ138-C31* and incubated in the dark for 2 h at 23 °C with a 15-fold molar excess of 5-IAF. The reaction was quenched by adding 2 mM free thiols using 2-mercaptoethanol. Unreacted 5-IAF was separated from the EtsΔ138-C31*-Fluorescein (EtsΔ138-F) using a PD-10 desalting column. The labeled protein was further purified by anion exchange chromatography using a Mono Q HR 5/5 column as described [42] and dialyzed in the dark into 25 mM Hepes, pH 7.5, 50 mM KCl, and 2 mM DTT, concentrated to 40 μM , and snap frozen in liquid nitrogen. The concentration of EtsΔ138-F used in assays was determined by using the fluorescein absorbance (A_{492}) in dialysis buffer. By comparing

the molar fluorescein concentration to the corrected molar EtsΔ138 concentration in the EtsΔ138-F ($A_{280 \text{ protein}} = A_{280 \text{ measured}} - (A_{494}/5)$ Molecular Probes), the molar ratio of the labeling procedure was obtained (~77% mol/mol fluorescein incorporated).

TRYPTIC DIGEST OF ETSΔ138-F

A tryptic digest was carried out on 1 mg of EtsΔ138-F to confirm the labeling site as Cys-31. Overnight dialysis was carried out in 50 mM Tris pH 8.65, followed by cleavage with 5 μg of sequencing grade trypsin for 4 h, and another 5 μg for 6 hours. The tryptic digest was filtered with 0.2 μm nylon membrane filter (Pall), applied to a 250 mm × 4 mm Vydac RP C18 column (218TP54) and eluted with a linear gradient of aqueous acetonitrile (99.9% v/v) containing 0.1% trifluoroacetic acid (TFA; 0.1%) at a flow rate of 0.7 mL min⁻¹ and collecting 0.7 mL fractions. Two peptides eluted at 48% and 49% acetonitrile. The molecular mass and purity of both peptides were verified by electrospray ionization mass spectrometry to give a mass of 2973.6 (C31-labeled) and 3333.3 Da (unknown).

PREPARATION OF ERK2

The unphosphorylated and dual phosphorylated forms of ERK2 were purified as described [44], dialyzed into S1 buffer (25 mM Hepes, pH 7.5, 50 mM KCl, 2 mM DTT, and 10% glycerol), concentrated in a Centricon YM-10 filter device (Millipore, Bedford, MA) at 4 °C, and snap frozen in 95.5 μM aliquots, and stored at -80 °C. The concentration of ERK2 was determined by absorbance at 280 nm using $\epsilon_{280} = 44\,825 \text{ cm}^2 \text{ M}^{-1}$ [5] in 6 M guanidine hydrochloride [5].

CALIBRATING THE POLARIZERS: MEASURING GLYCOGEN/LUDOX SCATTER

A small amount of glycogen/Ludox diluted in water was used to test that the polarizers in the fluorometer were working properly. The method described here measures the scatter of light by glycogen/Ludox and not anisotropy. Glycogen/Ludox was sufficiently diluted in water so that a reading of $1-1.5 \times 10^6$ cps was obtained with the polarizers both aligned at the vertical position (in-line polarizers decrease the light intensity), 370 nm excitation, 370 nm emission, 300 msec integration time, and the excitation and emission slits (bandpass) set at 1.7-3.0 nm. Once the concentration of the scattering agent was determined, the anisotropy or polarization should be $r \geq 0.97$ or $P \geq 0.98$, respectively. If this is not the case, polarizer alignment was carried out in which the fluorometer automatically sets the slit widths and aligns the polarizers so that the anisotropy was greater than 0.98.

The fluorometer should be set up so that arc lamp sends the excitation light into the each of the following in order: excitation monochromator, excitation polarizer, sample cuvette, emission polarizer, emission monochromator, and finally to the photomultiplier tube. Slits are usually set at 1.7-3.0 nm during the calibration. Once calibrated, it was determined that $I_{VV} = 1.15 \times 10^6$ cps and $I_{VH} = 14900$ cps, therefore, the anisotropy and polarization were calculated to be $\langle r \rangle \sim 0.96$ and $\langle P \rangle \sim 0.97$, respectively. If the anisotropy was lower than 0.96, the concentration of the scattering sample was adjusted and the polarizers were checked for proper alignment.

FLUORESCENCE ANISOTROPY BINDING ASSAY

The binding of EtsΔ138-F to ERK2 was monitored using fluorescence anisotropy. Fluorescence anisotropy, r , is defined in Equation 8 where I_{VH} is the intensity of the horizontal emission (second subscript) of the fluorescein moiety stimulated with vertically polarized light (first subscript), and G is the monochromator grating factor (I_{HV}/I_{HH}) to correct for emission components.

Equation 8

$$r = \frac{I_{VV} - (G \times I_{VH})}{I_{VV} + (2 \times G \times I_{VH})}$$

Various amounts of ERK2 were added to EtsΔ138-F, the fluorescence anisotropy of EtsΔ138-F signal increased and neared a saturating value indicating saturation of EtsΔ138-F binding to ERK2. All binding assays were carried out using 100 nM Fluorescein-EtsΔ138 (as measured by fluorescein concentration) in 25 mM Hepes, pH 7.5, 50 mM KCl, 0.1 mM EDTA, 0.1 mM EGTA, 40 μg/mL BSA, 2 mM DTT, 2% glycerol, and various concentrations of ERK2 in a 60 μL volume. Assays were made by adding a 5x concentration of ERK2 in 12 μL of S1 buffer, a 10x concentration of EtsΔ138-F in 6 μL of S1 buffer lacking glycerol, 30 μL of Master Mix buffer (35 mM Hepes, pH 7.5, 70 mM KCl, 80 μg/mL BSA, 0.2 mM EDTA, 0.2 mM EGTA, and 2 mM DTT), followed by 12 μL of Competition buffer (1.25 mM Hepes, pH 7.5, 2.5 mM KCl, and 2 mM DTT) to make a final volume of 60 μL.

Discontinuous assays were carried out by incubating separate reactions for 7 min at 27 °C, exciting the fluorescein moiety with both vertically and horizontally polarized light at 492 nm, and measuring the emission of polarized light at both the vertical and horizontal positions at 515 nm. Excitation and emission slit widths were set to 5 nm the integration time for each reading was 0.300 sec. The anisotropy of each assay point was

measured every 15 sec for 3 min and the average anisotropy was calculated from the 12 data points. The G factor was near 0.75-0.76.

Anisotropy data were fit to Equation 9 to determine the equilibrium dissociation constant (K_d), where r_f and r_b are the anisotropy values of the free and bound EtsΔ138-F, respectively, and $[E_T]$ and $[S_T]$ are the total ERK2 and EtsΔ138-F concentration.

Equation 9 ²⁹

$$\langle r \rangle = r_f + (r_b - r_f) \frac{K_d + [E_T] + [S_T] - \sqrt{(K_d + [E_T] + [S_T])^2 - 4[E_T][S_T]}}{2[S_T]}$$

COMPETITION ASSAY

Unlabeled EtsΔ138 and docking motif peptides that bind ERK2 were used to compete with an EtsΔ138-F exosite on ERK2, the data was simultaneously fit to Equation 10 and Equation 11 using the program Scientist to determine the equilibrium dissociation constant ($K_{d'2}$) of the unlabeled competitor and ERK2, where K_d is the equilibrium dissociation constant for EtsΔ138-F and ERK2 in the absence of competitor, $[C]$ is the concentration of the unlabeled competitor, and $[EC]$ is the concentration of the ERK2–EtsΔ138 or the ERK2–peptide docking complex.

Equation 10 ²⁹

$$\langle r \rangle = r_f + \frac{(r_b - r_f)}{K_d \frac{[C] + K_{d'2}}{K_{d'2} \times [E_T]} + 1}$$

Equation 11

$$K_{d'2} = \frac{[E_T] \times [C]}{[EC]}$$

²⁹ Derivation of Equation 9 and reference to the derivation of Equation 10 in section below (Equation Derivation). If fluorescence yield of the bound and free forms of the labeled protein differ, as in the case of EtsΔ138-Fluorescein labeled at Cys-31 (the bound form has a fluorescence yield that is 50% of the unbound form), see “Equation Derivation” below.

Assays were made similar to above with the addition of ERK2 (5x), Master Mix buffer, the competitor (5x) in Competition buffer, followed by EtsΔ138-F (10x). Peptides were raised in water and brought to pH 7.5 by the addition of sodium hydroxide. The concentration of each peptide was determined by amino acid analysis. The docking motif peptides used were Elk1-DEF: *N*-AKLSFQFPS-*C*, 1024 Da [19], Elk1-DEJL: *N*-QKGKPRDLELPLSPSL-*C*, 1934 Da [122], Mef2a: *N*-RKPDLRVVIPPS-*C*, 1377 Da [27], and MAPKK3b: *N*-SKGKSKRKKDLRISCNSK-*C*, 2064 Da [27]. The molecular weight of each peptide was determined by MALDI mass spectrometry.

EQUATION DERIVATION

The binding reaction is defined as in Equation 12 where E represents the enzyme ERK2, S represents the substrate EtsΔ138-F, and ES represents the Enzyme–Substrate complex formed between the two proteins.



The definition of the association and dissociation binding constants is shown in Equation 13 and Equation 14 while the relationship between the two is shown in Equation 15.

$$\text{Equation 13} \quad K_a = \frac{[ES]}{[E][S]}$$

$$\text{Equation 14} \quad K_d = \frac{[E][S]}{[ES]}$$

$$\text{Equation 15} \quad K_d = \frac{1}{K_a}$$

In the binding reaction the free substrate concentration [S] in the reaction where the subscript T represents the total concentration of any given species can be represented as seen in Equation 16.

$$\text{Equation 16} \quad [S] = [S_T] - [ES]$$

The total enzyme concentration [E_T] is expressed as seen in Equation 17.

$$\text{Equation 17} \quad [E_T] = [E] + [ES]$$

Equation 15 can be rearranged to give Equation 18.

$$\text{Equation 18} \quad [E] = \frac{[ES]}{K_a[S]}$$

Substitution of Equation 18 into Equation 17 and then substitution of Equation 16 into the resulting equation yields Equation 19.

$$\text{Equation 19} \quad [E_T] = \frac{[ES]}{K_a([S_T] - [ES])} + [ES]$$

Solving for [ES] using the quadratic equation gives Equation 20.

$$\text{Equation 20} \quad [ES] = \frac{1 + K_a[E_T] + K_a[S_T] - \sqrt{(1 + K_a[E_T] + K_a[S_T])^2 - 4K_a^2[E_T][S_T]}}{2K_a}$$

Using Equation 15, Equation 20 can be arranged to Equation 21.

$$\text{Equation 21} \quad [ES] = \frac{K_d + [E_T] + [S_T] - \sqrt{(K_d + [E_T] + [S_T])^2 - 4[E_T][S_T]}}{2}$$

Equation 21 gives the concentration of the complex [ES] at any given concentration of ERK2 [E] in terms of the total enzyme and substrate concentration added to the reaction. The concentration of the [ES] complex also depends on K_d . Since the amount of total substrate and enzyme is known in the reaction and the amount of [ES] is unknown, we can relate the anisotropy signal to the amount of [ES] in order to be able to solve for the unknown K_d .

The binding density of the docking complex (v) is given in Equation 22.

$$\text{Equation 22} \quad v = \frac{[ES]}{[S_T]}$$

The observed anisotropy $\langle r \rangle$ of EtsΔ138-F is given by Equation 23 where the maximum anisotropy (r_b) occurs when the fluorescent substrate is “bound” to the enzyme and the minimum anisotropy (r_f) is seen when the fluorescent substrate is tumbling “free” in solution.

$$\text{Equation 23} \quad \langle r \rangle = r_f + (r_b - r_f)v$$

Substituting Equation 22 into Equation 23 and then Equation 21 into the resulting equation gives Equation 9 which was used to fit the anisotropy data for the titration of ERK2 into EtsΔ138-F.

$$\text{Equation 9} \quad \langle r \rangle = r_f + (r_b - r_f) \frac{K_d + [E_T] + [S_T] - \sqrt{(K_d + [E_T] + [S_T])^2 - 4[E_T][S_T]}}{2[S_T]}$$

Equation 10 for the competition fluorescence anisotropy assay was derived as in [127].

If the fluorescence yield of the bound and free forms of the fluorescein-labeled protein differ, as in the case of the EtsΔ138-Fluorescein labeled at Cysteine-31 when mixed with ERK2, the dissociation constants were determined by fitting the average anisotropy values to Equation 24 using Kaleidgraph 3.6 (Synergy software)

$$\text{Equation 24} \quad r = \frac{\frac{(K_d + [S_t] + [E_t]) - \sqrt{(-K_d - [S_t] - [E_t])^2 - 4[E_t][S_t]}}{2[S_t]}(r_b R - r_f) + r_f}{1 + \frac{(K_d + [S_t] + [E_t]) - \sqrt{(-K_d - [S_t] - [E_t])^2 - 4[E_t][S_t]}}{2[S_t]}(R - 1)}$$

where r_f and r_b are the anisotropies of the free and bound fluorescein-labeled protein, R is the ratio of fluorescent yields of the bound form and the free form, $[S_t]$ and $[E_t]$ are the total concentration of the fluorescein-labeled protein and ERK2, and K_d is the dissociation constant. R was also calculated from the anisotropy experiments by measuring the polarized intensities for the free and bound form of the fluorophore, according to Equation 25

$$\text{Equation 25} \quad R = \frac{(I_V - 2GI_H)_b}{(I_V + 2GI_H)_f}$$

where I_V and I_H are the intensity of the emission at polarizations both parallel and perpendicular to the excitation source and G is a factor to correct for instrumental differences in detecting emission components. For competition experiments where the fluorescence yield of the bound and free forms of the fluorescein-labeled protein differ, the average anisotropy values were calculated and fit using Equation 26-Equation 30 in Scientist (Micromath).

$$\text{Equation 26} \quad r = \frac{\frac{[ES]}{[S_t]}(r_b R - r_f) + r}{1 + \frac{[ES]}{[S_t]}(R - 1)}$$

$$\text{Equation 27} \quad [ES] = \frac{[E_f][S_f]}{K_d + [E_f]}$$

$$\text{Equation 28} \quad K_{d'2} = \frac{[E_f][C_f]}{[EC]}$$

$$\text{Equation 29} \quad C_t = C_f + EC$$

$$\text{Equation 30} \quad E_t = E_f + EC$$

EXPERIMENTAL DATA

EtsΔ138NC, 2/28/03

[EtsΔ138NC], μM	k_{obs}, s⁻¹
200.0	20.1
100.0	20.8
50.0	19.7
25.0	16.3
12.5	10.3
6.3	6.5

EtsΔ138, average n=12

EtsΔ138, μM	k_{obs}, s⁻¹
200.0	18.7
100.0	18.0
50.0	17.0
25.0	14.8
12.5	11.9
6.3	8.0

Anisotropy Data

Active ERK2, 1/26/04, 2/26/04

[ERK2], μM	<r>
0	0.110
2.4	0.140
4.8	0.154
7.2	0.164
9.6	0.170
14.3	0.179
19.1	0.183

[ERK2], μM	<r>
0	0.110
0.96	0.123
1.91	0.133
2.4	0.141
4.8	0.154
7.2	0.163
9.6	0.170
19.1	0.183

Assay: 100 nM EtsΔ138-F, 25 mM Hepes, pH 7.5, 50 mM KCl, 0.1 mM EDTA, 0.1 mM EGTA, 2% glycerol, 40 μg/mL BSA, and 2 mM DTT

Inactive ERK2, 2/3/04, 4/13/04, 4/16/04

[ERK2], μM	<r>		
0.0	0.114	0.112	0.114
0.5	0.144	0.148	0.140
0.9	0.165	0.167	0.162
1.3	0.181	0.181	0.176
1.8	0.192	0.191	0.186
3.5	0.212	0.214	0.211
5.3	0.220	0.223	0.220
7.0	0.226	0.229	0.226
8.8	0.229	0.232	0.233
10.5	0.233		
12.3	0.233		
14.0	0.237		
15.8	0.237		
17.5	0.240		

Assay: 100 nM EtsΔ138-F, 25 mM Hepes, pH 7.5, 50 mM KCl, 0.1 mM EDTA, 0.1 mM EGTA, 2% glycerol, 40 μg/mL BSA, and 2 mM DTT

Competition Data

Competition with unphosphorylated ERK2, 4/13/04

[EtsΔ138], μM	<r>
0	0.222
5	0.209
10	0.190
15	0.176
20	0.165
25	0.158
30	0.153
50	0.140
100	0.127
150	0.122

Assay: 100 nM EtsΔ138-F, 9.55 μM unphosphorylated ERK2, 25 mM Hepes, pH 7.5, 50 mM KCl, 0.1 mM EDTA, 0.1 mM EGTA, 2% glycerol, 40 μg/mL BSA, and 2 mM DTT

Competition with dual-phosphate ERK2, 1/26/04, 3/3/04, 4/22/04

[EtsΔ138], μM	<r>		
0	0.170	0.178	0.175
6.25		0.171	0.166
12.5	0.154	0.160	0.157
25	0.136	0.148	0.144
50	0.127	0.133	0.129
100	0.121	0.124	0.122
200	0.118	0.115	0.119

Assay: 100 nM EtsΔ138-F, 9.55 μM dual-phosphate ERK2, 25 mM Hepes, pH 7.5, 50 mM KCl, 0.1 mM EDTA, 0.1 mM EGTA, 2% glycerol, 40 μg/mL BSA, and 2 mM DTT

Competition with Elk1-DEJL peptide, dual-phosphate ERK2, 5/18/04, 5/20/04

[Elk1-DEJL], μM	<r>
0.0	0.167
4.4	0.157
8.9	0.143
17.8	0.134
35.5	0.122
71.0	0.119
142.0	0.115
0	0.170
6.25	0.150
12.5	0.140
25	0.126
50	0.122
100	0.116
200	0.117
500	0.115

Assay: 100 nM EtsΔ138-F, 9.55 μM dual-phosphate ERK2, 25 mM Hepes, pH 7.5, 50 mM KCl, 0.1 mM EDTA, 0.1 mM EGTA, 2% glycerol, 40 μg/mL BSA, and 2 mM DTT

Competition with Elk1-DEF peptide, dual-phosphate ERK2, 5/18/04, 5/20/04

[Elk1-DEF], μM	<r>
0	0.167
4	0.164
8	0.164
16	0.157
32	0.153
64	0.141
96	0.136
128	0.132
0	0.170
12.5	0.161
25	0.154
50	0.143
75	0.141
100	0.135
125	0.134
150	0.131
175	0.129
200	0.127

Assay: 100 nM EtsΔ138-F, 9.55 μM dual-phosphate ERK2, 25 mM Hepes, pH 7.5, 50 mM KCl, 0.1 mM EDTA, 0.1 mM EGTA, 2% glycerol, 40 μg/mL BSA, and 2 mM DTT

Competition with Mef2a peptide, dual-phosphate ERK2, 7/20/04

[Mef2a peptide], μM	<r>
0	0.179
0	0.179
48.75	0.17
97.5	0.157
195	0.148
390	0.138
780	0.128
1950	0.125
3900	0.122
18720	0.125

Assay: 100 nM Ets Δ 138-F, 9.55 μM dual-phosphate ERK2, 25 mM Hepes, pH 7.5, 50 mM KCl, 0.1 mM EDTA, 0.1 mM EGTA, 2% glycerol, 40 $\mu\text{g/mL}$ BSA, and 2 mM DTT
 $r_f = 0.212 \pm 0.002$, $r_b = 0.121 \pm 0.001$, K_d fit to 2.7 μM , $K_{d \text{ Mef2a}} = 54.9 \pm 7.2 \mu\text{M}$

Competition with MAPKK3b peptide, dual-phosphate ERK2, 7/20/04

[MAPKK3b peptide], μM	<r>
0	0.179
0	0.179
30	0.165
60	0.154
120	0.135
240	0.127
480*	0.128
1200*	0.133
2400*	0.146
11280*	0.176

Assay: 100 nM Ets Δ 138-F, 9.55 μM dual-phosphate ERK2, 25 mM Hepes, pH 7.5, 50 mM KCl, 0.1 mM EDTA, 0.1 mM EGTA, 2% glycerol, 40 $\mu\text{g/mL}$ BSA, and 2 mM DTT
 $r_f = 0.222 \pm 0.005$, $r_b = 0.102 \pm 0.009$, K_d fit to 2.7 μM , $K_d_{\text{MKK3b}} = 35.9 \pm 10.4 \mu\text{M}$
excluding the data points with * due to increasing anisotropy values at high peptide concentration, fitting the data to $r_f = 0.11$ does not have a large affect on the K_d

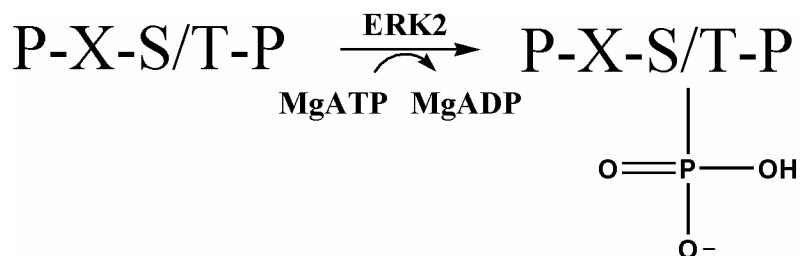
CHAPTER 5: MACROMOLECULAR RECOGNITION OF A PROTEIN SUBSTRATE BY A PROTEIN KINASE

PURPOSE

This chapter extends on the use of mutagenesis, fluorescence anisotropy, and steady-state kinetics to describe a model for macromolecular substrate recognition of EtsΔ138 by ERK2. We show that a region that lies *N*-terminal to the phospho-acceptor in EtsΔ138 is required for efficient docking complex formation and for efficient phosphorylation by ERK2. A *C*-terminal docking motif is also required for efficient binding and phosphorylation by ERK2. Several lines of evidence suggest that the phospho-acceptor region of EtsΔ138 (including the phospho-acceptor and the P+1 proline determinant for MAPK substrates) does not contribute to the formation of docking complex. However, the P+1 proline is required for efficient catalysis of the phospho-acceptor and the fidelity of the phosphorylated residue. We also show that large concentrations of magnesium chloride decreases the affinity of the docking complex that can partially be rescued in the presence of an ATP analog (AMP-PNP) that binds the active site. However, in the presence of AMP-PNP and magnesium, conditions that mimic phosphorylation conditions, the phospho-acceptor does not form a strong interaction in the active site of the enzyme indicating that the docking interactions occurring outside of the active site are a major determinant of macromolecular substrate specificity.

INTRODUCTION

More than 500 human genes have been predicted to encode protein kinases [128] which are capable of phosphorylating protein substrates by transferring the gamma-phosphate of adenosine triphosphate (ATP) to a hydroxyl acceptor on a serine, threonine, or tyrosine residue (Scheme 11). Kinases are spatially and temporally activated in response to cellular signaling allowing them to phosphorylate a specific subset of proteins in the presence of MgATP^{2-} leading to a cellular response. An efficient response relies upon the fidelity of the kinase to recognize specific macromolecules and phosphorylation sites within the macromolecular substrates; however, the molecular mechanism of protein substrate recognition by protein kinases remains unclear.



Scheme 11. The phosphorylation of a peptide substrate by a serine/threonine kinase. Phosphorylation of a protein substrate occurs on a hydroxyl-containing side chain such as a serine, threonine, or tyrosine. ERK2, a serine/threonine kinase, catalyzes the transfer of the γ -phosphate from ATP to the peptide substrate (P-X-S/T-P where P is proline, X is any amino acid) on either a Ser (S) or Thr (T) residue in the presence of MgATP^{2-} ; a tyrosine kinase can phosphorylate tyrosine residues (not shown). Phosphorylation generates two products: a phosphorylated peptide/protein substrate and MgADP^{1-} .

Serine/Threonine-specific kinases such as Protein Kinase A (PKA) [8, 129, 130], Protein Kinase B (PKB)/AKT [131], ERK1/2 [132-134], cdc2 [135], Cyclin-Dependent Kinase (CDK) 5, Casein Kinase (CK) I δ and γ , Phosphorylase Kinase, Calcium/Calmodulin Kinase II [133], CKII [136], and others [137] have been hypothesized to recognize and phosphorylate their substrates based on small recognition motifs (Scheme 12) that include the sequence of amino acids that surround the phosphorylation site (P-site). Since members within a kinase sub-family phosphorylate similar recognition motifs but phosphorylate distinct protein substrates, macromolecular substrate recognition must occur by some alternate means distinct from active site

interactions. For example, both mitogen-activated protein kinase (MAPK) and CDK families are proline-directed kinases in that they phosphorylate surface exposed Ser-Pro or Thr-Pro recognition motifs, yet they preferentially recognize distinct macromolecular substrates. On average, human proteins of ~ 40 kD whose structures are known contain ~1.6 Ser-Pro or Thr-Pro sites that are surface exposed, however, not all of these potential phosphorylation sites are phosphorylated³⁰. Clearly, kinases could benefit from other factors beyond active site recognition of recognition motifs to determine substrate specificity.

³⁰ The Protein Data Base was searched for human proteins of ~40 kD (350-375 amino acids, n=40 proteins) that were intracellular proteins. The primary sequence was scanned for Ser-Pro and Thr-Pro motifs and these were checked for surface exposure using Swiss-PDB Viewer (GlaxoSmithKline). A phosphorylation motif was considered surface exposed if one of the two residues of either a Ser-Pro or Thr-Pro motif was more than 10% exposed.

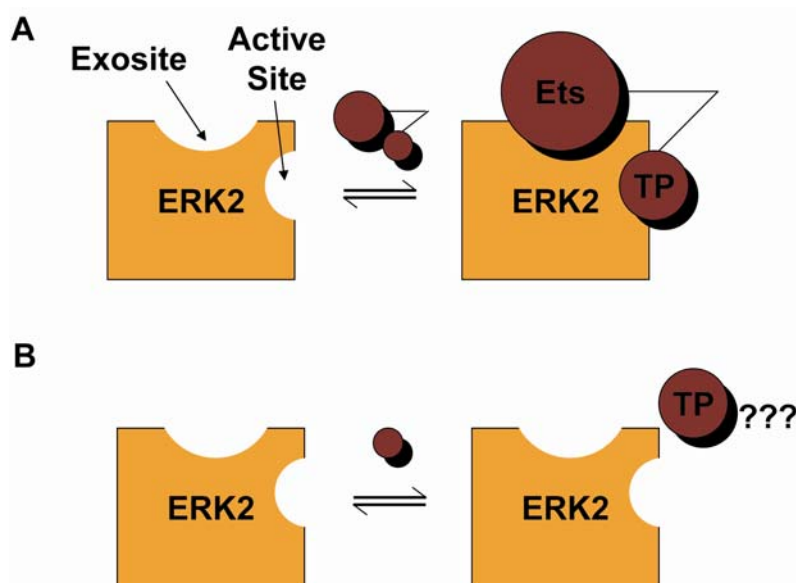
	+	+	X	S/T					Basophilic
									PKA
+	X	+	X	X	S/T				PKB
		P	X	S/T	P				Proline-Directed
									ERK1/2
			X	S/T	P	X	+		CDK
-	X	X	S/T						Acidophilic
									CKI
	X	X	S/T	X	X	X	-		CKII
			S/T	X	X	X	-		GSK3

Scheme 12. Recognition motif substrate specificity of several serine/threonine protein kinases. Ser-Thr (S/T) protein kinases have been shown to preferentially phosphorylate serine or threonine residues (***) surrounded by amino acids with specific physicochemical properties. The phosphorylation site and the surrounding residues make up the recognition motif. Three classes of S/T protein kinases have been established whose active sites recognize basic (+), proline, or acidic residues (-) within recognition motifs.

Substrate specificity can be described by the specificity constant ($k_{\text{cat}}/K_{\text{m}}$) which is the apparent second-order rate constant for an enzyme–substrate reaction. The specificity constant relates the velocity of the reaction to the concentration of free enzyme at any substrate concentration and can be used to determine specificity differences between two competing substrates. MAPK *peptide* substrates have a lower specificity constant than *protein* substrates [138] indicating that peptides are not as efficiently phosphorylated as proteins usually due to the higher affinity of protein substrates for MAPKs as compared

to peptide substrates. Increased enzymatic activity toward protein substrates over peptide substrates has also been seen in other macromolecule modification enzymes such as proteases [139] and phosphatases [140]. This may be explained by the lack of conformational freedom seen in proteins versus that of free peptides reducing the entropic cost of protein-protein interactions with respect to fewer conformational states [139].

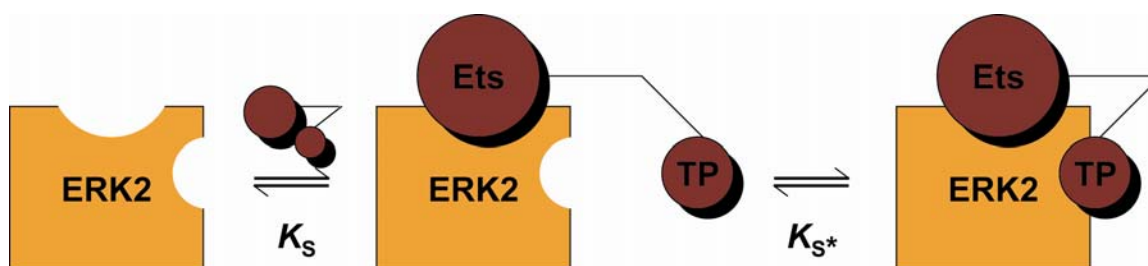
An alternate explanation may be due to larger protein substrates containing docking motifs, small peptide fragments or individual residues, which facilitate enzymic binding and thereby enhance enzymic activity towards the protein substrate. Several MAPKs appear to bind protein substrates using small motifs that lie outside of their active site [17] and this docking interaction is thought to increase the efficiency of protein substrate phosphorylation by enhancing the affinity of kinase–substrate interactions [61]. Enzymic regions of the MAPK that bind docking motifs outside and distinct from the active site to mediate docking interactions are termed enzymic exosites (Scheme 13) and it is hypothesized that these exosites determine macromolecular substrate recognition independent of active site binding and enzymic catalysis. Indeed, the addition of a small docking motifs to a MAPK recognition motif peptide has been shown to enhance the efficiency of recognition motif phosphorylation by decreasing the apparent affinity (K_m) thereby increasing the specificity constant [115]. Other enzymes that modify macromolecular substrates have taken advantage of their size to spatially separate macromolecular substrate recognition and catalysis. For example, prothrombinase undergoes a bimolecular mechanism in which an enzymic exosite binds the substrate prethrombin followed by intramolecular recognition of the scissile bond in the active site [141].



Scheme 13. Protein and peptide substrate recognition by a protein kinase. (A) The protein kinase ERK2 is shown containing both an exosite for protein substrate docking and an active site for catalysis. A protein substrate (Ets) is shown containing both a docking motif (located on the larger circular domain) and a recognition motif containing the threonine phospho-acceptor (TP: Thr-Pro). The protein substrate is thought to form a docking complex with ERK2 where the docking motif of the substrate binds the ERK2 exosite (A). The docking complex (ERK2–Ets) is hypothesized to aid active site recognition of the phosphorylation site. (B) A peptide substrate containing only the recognition motif, including the phosphorylation site, in the absence of a docking motif is shown in which the phosphorylation site is not efficiently recognized by ERK2.

We were interested in understanding the relative contributions of the exosite and active site interactions in macromolecular substrate recognition and the catalytic mechanism of the dual-phosphate form of ERK2 [44, 102] with a protein substrate Ets Δ 138 [42, 114]. Surprisingly we found evidence for a two-step process suggestive of (1) macromolecular substrate recognition of Ets Δ 138 and (2) phospho-acceptor selection. We propose that primary macromolecular substrate recognition by ERK2 is achieved by exosite recognition of a docking motif to form an ERK2–Ets Δ 138 tethered complex (K_s ,

Scheme 14) and a secondary form of intramolecular substrate recognition occurs through enzymic active site interactions with the recognition motif of the substrate (K_{S^*} , Scheme 14). Together, macromolecular substrate recognition through exosite/docking motif and active site/recognition motif interactions act in concert to ensure the efficient post-translational covalent phosphate modification of a specific phospho-acceptor within a specific protein substrate to prevent cross-talk and aberrant cell signaling.



Scheme 14. A proposed two-step docking mechanism for Ets Δ 138 recognition by ERK2. A docking complex forms between Ets Δ 138 (Ets) and ERK2 via the exosite on ERK2 and the docking motif of Ets (middle). The formation of the docking complex is referred to as macromolecular substrate recognition. Intramolecular recognition of the recognition motif occurs as the phosphorylation site enters the active site of the kinase (right). An equilibrium dissociation constant is shown for both the intermolecular (K_S) and the intramolecular (K_{S^*}) steps.

RESULTS AND DISCUSSION

FLUORESCENCE ANISOTROPY COMPETITION ASSAY

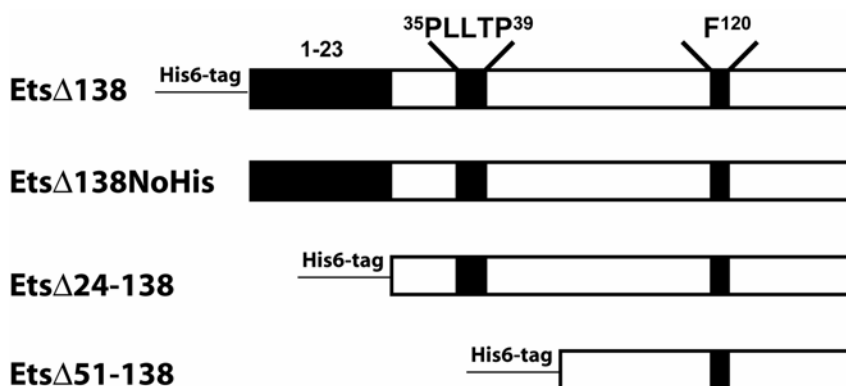
A novel fluorescence anisotropy binding assay was generated (Chapter 4) to study the mechanism by which ERK2 recognizes the protein substrate Ets Δ 138. A binary fluorescent docking complex was formed between ERK2 and Ets Δ 138-Fluorescein

(EtsΔ138-F) to generate an ERK2–EtsΔ138-F docking complex which dissociated upon the addition of unlabeled EtsΔ138 or an EtsΔ138 mutant. As the smaller EtsΔ138-F dissociated from the larger docking complex, its fluorescence anisotropy decreased indicating that the EtsΔ138-F was free in solution. The equilibrium dissociation constant (K_d) of the unlabeled EtsΔ138 proteins were measured by their ability to dissociate the binary fluorescent complex through competition with an ERK2 exosite required for EtsΔ138 binding.

THE HIS₆-TAG ON ETSΔ138 DOES NOT HAVE A LARGE AFFECT ON THE AFFINITY FOR ERK2

To test whether or not the His₆-tag used to purify EtsΔ138 affected the affinity of the ERK2–EtsΔ138-F docking complex, we cleaved the His₆-tag off of EtsΔ138, purified the EtsΔ138 lacking the His₆-tag (EtsΔ138NoHis, Scheme 15), and measured the K_d of EtsΔ138NoHis and EtsΔ138 (containing a His₆-tag) using a fluorescence anisotropy competition assay. His₆-tagged EtsΔ138 was purified using Ni²⁺-NTA metal-affinity chromatography followed by Mono Q HR 10/10 anion exchange chromatography [42]. The purified protein was subjected to proteolysis with thrombin and cleavage occurred following the proline-arginine pair following the His₆-tag. The EtsΔ138NoHis was purified on the Mono Q HR 10/10 anion exchange column and eluted at 0.17 M NaCl (Figure 48a). An SDS-PAGE gel shows a large shift towards a smaller protein indicating that the cleavage of the His₆-tag had occurred (Figure 48b). The purified EtsΔ138NoHis was run on a reverse phase HPLC C18 column (Figure 49a) and mass spectrometry of the EtsΔ138NoHis was performed to confirm the cleavage as indicated by a mass of 15 912

Da (expected 15 914 Da) (Figure 49b)³¹. The EtsΔ138NoHis was used as a competitor in a fluorescence anisotropy competition assay with dual-phosphate ERK2 and EtsΔ138-F and yielded a K_d of $10.0 \pm 0.1 \mu\text{M}$ (Figure 50) for ERK2 similar to EtsΔ138 ($K_d = 6.6 \pm 1.2 \mu\text{M}$) indicating that the His₆-tag did not have a large affect on the formation of the docking complex between ERK2 and EtsΔ138.



Scheme 15. Schematic of EtsΔ138 and truncation mutants. EtsΔ138 is composed of 138 residues of the *N*-terminus of the Ets-1 gene and contains a single phosphorylation site at Thr-38 within a MAPK recognition motif (PLLTP). To facilitate purification of EtsΔ138 and its mutants a His₆-tag was placed *N*-terminal to EtsΔ138. The His₆-tag was cleaved to generate EtsΔ138NoHis. Two *N*-terminal truncations were generated in which the first 23 and 50 amino acids, respectively, were deleted to generate EtsΔ24-138 and EtsΔ51-138. The docking motif residue Phe-120, required for efficient binding to ERK2 [52], is shown in the *C*-terminal portion of EtsΔ138.

³¹ The mass was calculated based on the sequence of EtsΔ138 with a Ser26Ala mutation and cleaved with thrombin after the His₆-tag and the proline-arginine pair.

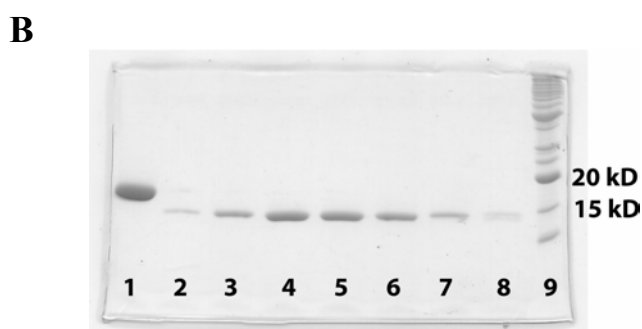
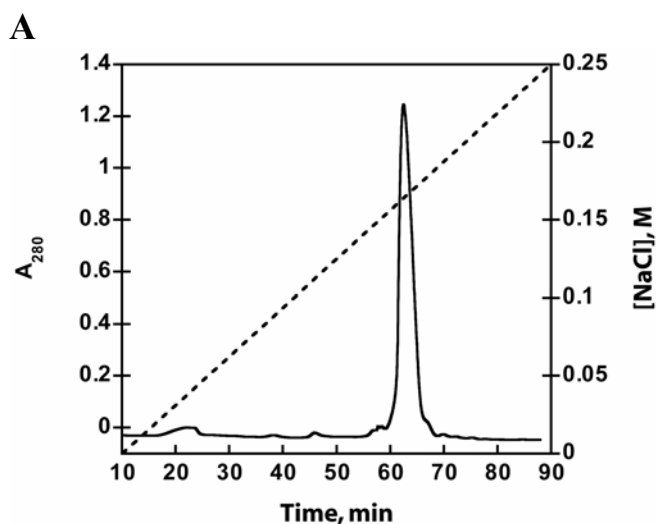


Figure 48. Purification of EtsΔ138NoHis. EtsΔ138 (containing a His₆-tag) was cleaved with thrombin and applied to a (A) Mono Q HR 10/10 anion exchange column equilibrated in 20 mM Hepes, pH 8.0, 0.1% 2-mercaptoethanol (v/v), 0.03% Brij-35 (w/v), 0.1 mM EDTA, and 0.1 mM EGTA and eluted with NaCl as shown using a flow rate of 1.5 mL min⁻¹. A 5 μg portion of the reaction lacking thrombin (lane 1) was run on a 15% SDS-PAGE gel along with the cleaved fractions purified from the Mono Q (lane 2-8; representing 61'-67' of the Mono Q trace) and a protein ladder (lane 9). Lanes 3-7 containing EtsΔ138NoHis were kept for further analysis. The gel was stained with Coomassie blue stain.

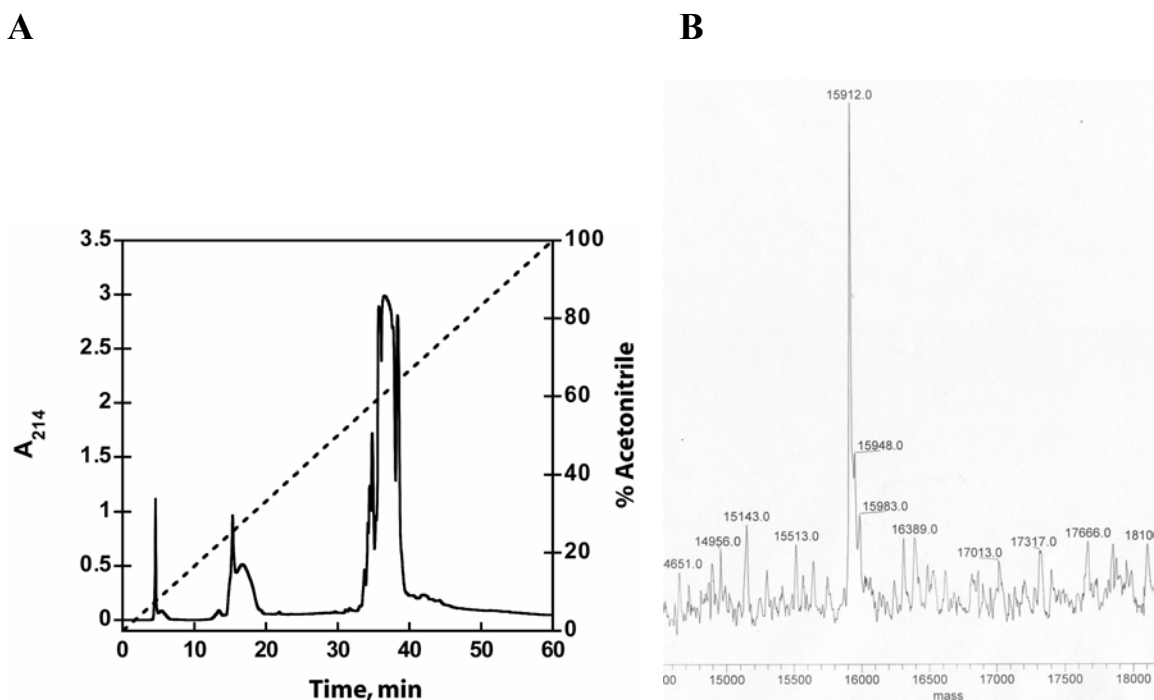


Figure 49. Mass spectrometry analysis of Ets Δ 138NoHis. (A) Purified Ets Δ 138NoHis was applied to a reverse phase C18 column equilibrated in 0.1% trifluoroacetic acid and eluted with an acetonitrile gradient in equilibration buffer as shown at a flow rate of 0.7 mL min⁻¹. (B) Both peaks were collected, the fractions from each peak were pooled separately, lyophilized, raised in 50% acetonitrile, lyophilized again, and analyzed by electrospray ionization mass spectrometry to reveal that the second peak contained Ets Δ 138NoHis that lacked a His₆-tag. The first peak in (A) was also analyzed by electrospray mass spectrometry, however, no significant protein or peptide was detected and may be due to solvent exchange.

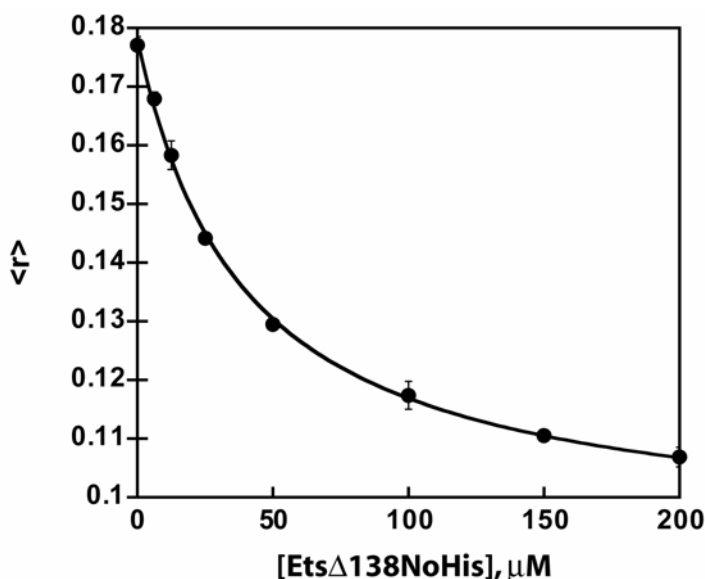


Figure 50. A fluorescence anisotropy competition assay to determine the K_d of EtsΔ138NoHis. A docking complex was formed using dual-phosphate ERK2 (9.55 μM) and EtsΔ138-F (100 nM) and the anisotropy of the fluorescent complex was monitored in the presence of several concentrations of non-fluorescent EtsΔ138NoHis. EtsΔ138NoHis competed for ERK2 binding and decreased the ERK2–EtsΔ138-F docking complex concentration which decreased the anisotropy. The data were simultaneously fit to Equation 10 and Equation 11 using the pre-determined K_d value for the ERK2–EtsΔ138-F docking complex ($K_d = 2.7 \mu\text{M}$). The K_d for EtsΔ138NoHis and dual-phosphate ERK2 was $10.0 \pm 0.1 \mu\text{M}$ ($n=2$). Data points are shown as mean \pm SD. K_d is depicted as mean \pm SE.

ETSΔ138 DOCKING MOTIFS MEDIATE MACROMOLECULAR SUBSTRATE RECOGNITION

We found that efficient macromolecular substrate recognition of EtsΔ138 by dual-phosphate ERK2 was dependent upon a region found in both the *N*- and *C*-terminal portions of EtsΔ138. An *N*-terminal truncation of residues 1-23 and 1-50 on EtsΔ138 (Scheme 15) led to a 13- and 19-fold increase, respectively, in the K_d when compared to EtsΔ138 (Table 10) indicating that a region in the first 23 amino acids of EtsΔ138 was

required for forming an efficient docking complex with ERK2. Interestingly, the additional mutation of residues 24-50 in Ets Δ 51-138 led to less than a two-fold increase in the K_d as compared to the mutant lacking residues 1-23 in Ets Δ 24-138 indicating that the recognition motif of Ets Δ 138, located in residues 35-39 of Ets Δ 138 (Scheme 15), may not contribute a large amount towards Ets Δ 138 binding ERK2.

EtsΔ138 Mutant	r_f	r_b	K_d , μM
WT	0.111 ± 0.002	0.209 ± 0.004	$6.6 \pm 1.2^{n=3}$
NoHis	0.096 ± 0.001	0.220 ± 0.003	$10.0 \pm 0.1^{n=2}$
Δ24-138	0.11*	0.209 ± 0.001	$82.8 \pm 3.2^{n=2}$
Δ51-138	0.11*	0.203 ± 0.001	$128.6 \pm 6.8^{n=1}$
F120A	0.11*	0.211 ± 0.001	$67.8 \pm 3.1^{n=2}$
P39A	0.114 ± 0.001	0.199 ± 0.001	$8.0 \pm 0.5^{n=1}$
P39D	0.114 ± 0.001	0.198 ± 0.001	$8.5 \pm 1.0^{n=1}$
P39G	0.112 ± 0.002	0.197 ± 0.003	$7.9 \pm 0.5^{n=2}$
P39R	0.114 ± 0.002	0.202 ± 0.005	$4.9 \pm 0.8^{n=2}$
P39V	0.109 ± 0.000	0.195 ± 0.003	$8.8 \pm 0.3^{n=2}$
T38A/P39A	0.112 ± 0.002	0.209 ± 0.004	$11.0 \pm 0.8^{n=3}$

Table 10. EtsΔ138 docking motif and proline-determinant mutant's equilibrium dissociation constants as measured by a fluorescence anisotropy competition assay. Fluorescent anisotropy competition assays were carried out by allowing several concentrations of unlabeled EtsΔ138 mutants (6.25-200 μM) to compete with 100 nM EtsΔ138-F forming a complex with 9.55 μM ERK2. A decrease in anisotropy occurred upon introduction of non-fluorescent mutant competitors and the equilibrium dissociation curves were simultaneously fit to Equation 10 and Equation 11. The K_d for the fluorescent complex was fixed at 2.7 μM . Since the EtsΔ24-138, EtsΔ51-138, and F120A mutants were particularly poor binders, the r_f was fixed at 0.110 (the anisotropy of the free EtsΔ138-F) assuming that these mutants completely dissociate EtsΔ138-F at high concentrations of competitor. All data are shown as a mean \pm SE. The number of experiments for each competitor are shown.

Mutation of the proposed docking motif residue Phe-120 to alanine in the C-terminal portion of EtsΔ138 led to a 10-fold increase in the K_d as compared to EtsΔ138 indicating that a docking motif exists in the globular C-terminal portion of EtsΔ138 (a similar mutation decreased the specificity constant of EtsΔ138 phosphorylation by ERK2 [52]). We hypothesized that the N-terminal 23 residues and the C-terminal docking motif mediate efficient EtsΔ138 docking onto ERK2 exosites. The specificity constant of

phosphorylation for both Ets Δ 24-138 and the F120A docking motif mutant [52] were also less than Ets Δ 138 due to an increase in the K_m (Chapter 3) and not a result of a deficiency in its steady-state rate of catalysis. The steady-state kinetics and equilibrium binding assays of ERK2–Ets Δ 138 interactions indicate that docking motifs enhance the specificity constant of substrate phosphorylation by increasing the affinity of the docking complex and do not appear to affect the steady-state rate of catalysis. These results are indicative of a loss of a docking motif required for enzymic exosite recognition at a protein–protein interface outside of the enzymic active site.

THE P+1 PROLINE DETERMINANT IS REQUIRED FOR EFFICIENT CATALYSIS

ERK2 is defined as a proline-directed kinase capable of phosphorylating the alcohol group on a serine or threonine residue that lies in the consensus sequence -Pro-X-Ser/Thr-Pro- [132, 134], where X can be any amino acid. The Ser/Thr phosphorylation site is referred to as the P-site while the residues that lie *n* residues *N*- and *C*-terminal to this site are termed P-*n* and P+*n*, respectively, where *n* is any integer. Steady-state kinetic studies of ERK2 phosphorylation of a synthetic peptide derived from epidermal growth factor receptor (EGFR) were carried out in the early 1990's [9]. Mutation of the conserved P-2, P+1, and P-2/P+1 prolines to alanine in the EGFR peptide led to a 10-, 100-, and 1000-fold decrease in V_{max} (however another Figure suggests only 5 and 10-fold decrease) [9] suggesting that the proline-determinants surrounding the phospho-acceptor determine the catalytic rate of phosphorylation. Since these studies were carried out with a peptide substrate, we were interested in studying the role of the P+1 proline determinant in the recognition motif of a protein substrate with a docking motif.

Another study suggested that the P+1 proline-determinant of the substrate can enter a competent proline binding pocket in the active form of ERK2 [4] that is absent in the inactive form due to Val-187 and Arg-192 blocking this site [70]. As mentioned previously, MAPK protein substrates containing docking motifs are more efficiently phosphorylated than peptide substrates [42, 138], therefore, we sought to determine the role of the proline-determinant in mediating phosphorylation of the protein substrate EtsΔ138 which contains a MAPK docking motif.

We carried out a steady-state kinetic analysis of EtsΔ138 in the presence and absence of the prolines surrounding the P-site in the recognition motif. Since EtsΔ138 does not contain a P-2 proline normally found in the ERK recognition motif, we mutated the prolines at the P-3 and P+1 position ($P^{35}\text{-L-L-T-P}^{39}$) to alanines to generate P35A, P39A, and the double mutant P35/39A EtsΔ138 (Figure 51). The P35A mutation did not have an adverse affect on the specificity constant (Figure 52, Table 11) which is consistent with results that there are MAPK substrates that lack the P-2 proline [142, 143]. Although, Pro-35 did not contribute to the specificity constant of EtsΔ138, it cannot be ruled out that this is the case for all MAPK substrates. A study carried out using peptide phosphorylation suggested that the P-2 proline enhanced the V_{\max} of peptide phosphorylation over a peptide that has a P-3 proline; however, it was only a 3-fold difference [132]. These results suggest that a proline at the P-3 position is not required for efficient phosphorylation of EtsΔ138.

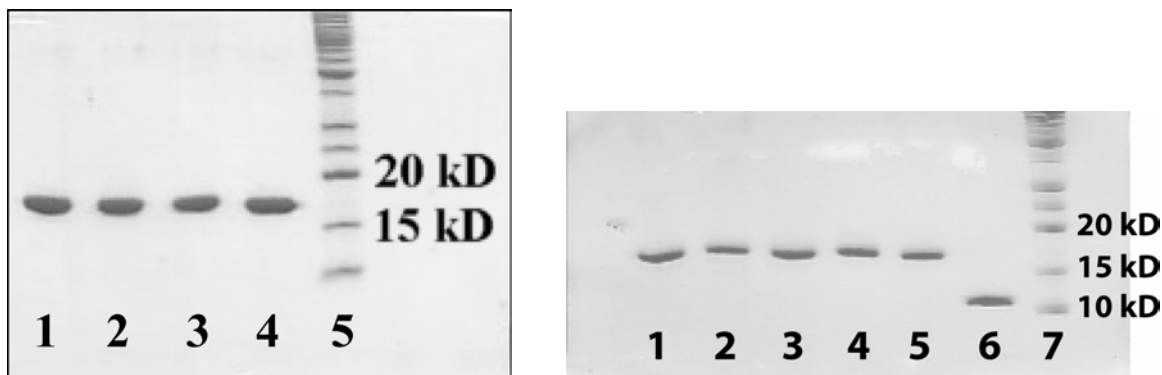


Figure 51. SDS-PAGE gel of EtsΔ138 proline mutants. (A) A 15% SDS-PAGE gel was prepared and loaded with 2 μg of (1) WT, (2) P35A, (3) P39A, (4) P35/39A EtsΔ138, and a (5) protein ladder. (B) A similar gel was prepared and loaded with 1 μg of (1) P39R, (2) P39K, (3) P39D, (4) P39E, (5) T38A/P39A, (6) EtsΔ51-138, and a (7) protein ladder.

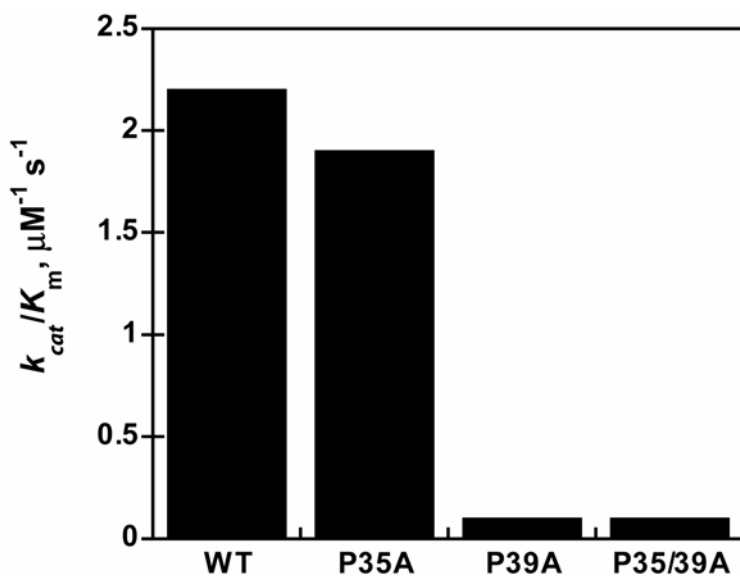


Figure 52. Specificity constant comparisons of dual-phosphate ERK2 phosphorylation of EtsΔ138 proline mutants. The specificity constants were determined in Table 11 and plotted here to show relative specificity constant differences between EtsΔ138 and the proline mutants.

Mutant	k_{cat}	K_m , EtsΔ138	K_m , ATP	$k_{\text{cat}}/K_m(\text{Ets})$
WT	19.6 ± 0.7	8.8 ± 1.4	98.7 ± 4.4	2.2 ⁿ⁼¹²
P35A	16.5 ± 0.9	8.7 ± 1.2		1.9 ⁿ⁼⁴
P39A*	4.9 ± 1.2	45.8 ± 8.7		0.1 ⁿ⁼³
P39A	3.9 ± 0.2	38.4 ± 4.5*	75.1 ± 2.4	0.1 ⁿ⁼⁶
P35/39A	2.6 ± 0.1	39.8 ± 6.8		0.1 ⁿ⁼⁴
P39V	1.1 ± 0.2	73.8 ± 10.8		0.01 ⁿ⁼²
P39G	0.7 ± 0.1	34.3 ± 0.6		0.02 ⁿ⁼²
P39R	0.12 ± 0.02	48.3 ± 2.0		0.002 ⁿ⁼³
P39K	0.07 ± 0.05	56.9 ± 8.8		0.001 ⁿ⁼²
P39D	0.05 ± 0.01	56.0 ± 9.6		0.001 ⁿ⁼⁵
P39E	0.06 ± 0.01	91.7 ± 31.7		0.001 ⁿ⁼²

Table 11. The steady-state kinetic parameters for EtsΔ138 proline mutants phosphorylated by dual-phosphate ERK2. These values were obtained with radiolabeled P81 assays [42]. For the determination of the K_m for EtsΔ138 saturating ATP (2 mM) was used while varying the EtsΔ138 concentration from 6.3-200 μM . For the determination of the K_m for ATP saturating EtsΔ138 concentrations (150-200 μM) were used while varying the ATP concentration from 31.3-1000 μM . Each value was determined using 6 initial velocities fit to the equation $k_{\text{obs}} = (k_{\text{cat}} \times [\text{S}]) / (K_m + [\text{S}])$. Assay conditions were 25 mM Hepes, pH 7.5, 50 mM KCl, 0.1 mM EDTA, 0.1 mM EGTA, 40 $\mu\text{g/mL}$ BSA, 20 mM MgCl_2 , 2 mM DTT, ERK2, and ATP. Values are shown as a mean \pm standard error. The mean k_{cat} was determined using the values obtained from both EtsΔ138 and ATP analyses and were found to be similar. Units: k_{cat} , s^{-1} ; K_m , μM ; k_{cat}/K_m , $\mu\text{M}^{-1} \text{s}^{-1}$. * - denotes that the EtsΔ138 had Ser-26 while all other EtsΔ138 constructs contained a Ser26Ala [44].

In contrast, the P39A mutation at the P+1 position of EtsΔ138 exhibited a 5-fold decrease in k_{cat} and 4-fold increase in K_m for EtsΔ138 while showing little defects in the ability to bind ATP (Figure 52, Table 11). These data suggest that the P+1 proline is required for efficient phosphoryl-transfer. The P+1 proline may be required for a conformational change leading to the activation of the enzyme and catalysis or may act to stabilize the transition state leading to catalysis. It is clear that the lack of proline at

position 39 decreases the catalytic rate of the enzyme indicating that the proline is required for proper chemistry of phosphoryl-transfer in the active site. Interestingly, in the absence of a P+1 proline, Ets Δ 138 is still able to undergo phosphorylation, albeit at a slower rate. The P39A mutation does not change the specificity of the phosphorylation site as seen by a single phosphorylated peak following limited phosphorylation and a tryptic digest analysis (Figure 53A), followed by phosphoamino acid analysis of the phosphorylated peptide (Figure 53B) to indicate that a threonine is phosphorylated [42]. Mutation of Thr-38 to alanine eliminated the phospho-threonine in the phosphoamino acid analysis (data not shown).

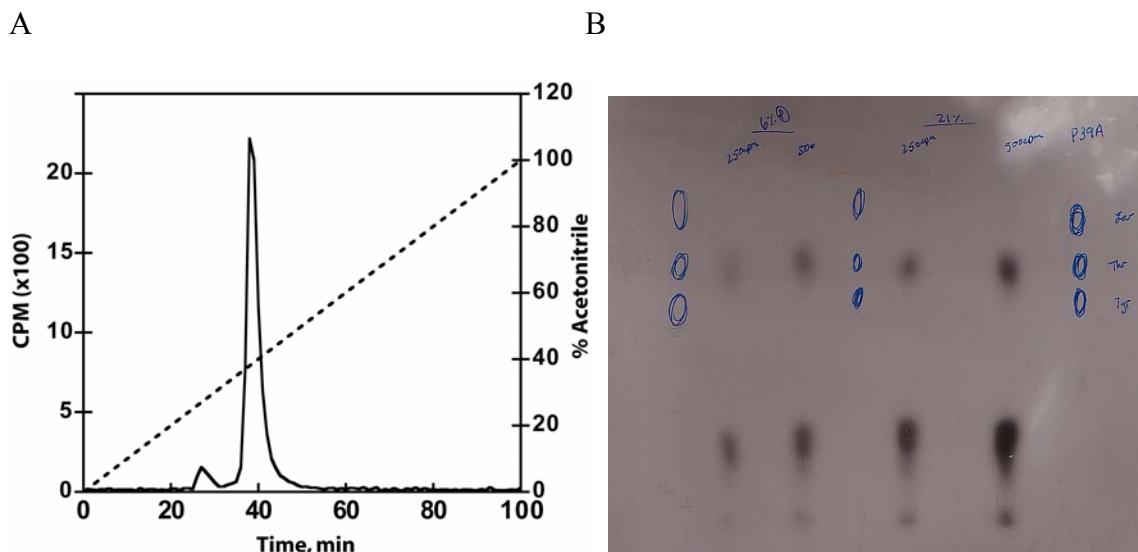


Figure 53. Tryptic peptide digest and phosphoamino acid analysis of radiolabeled P39A EtsΔ138 phosphorylated by active ERK2. P39A EtsΔ138 was phosphorylated under initial rate conditions by ERK2 so that 6% and 21% of the total substrate was phosphorylated. The products were purified, cleaved with trypsin, and (A) run on a reverse phase C18 column to locate the radiolabeled peptide (only the 21% product is shown, the 6% product was similar). (B) The major radiolabeled tryptic peak from both initial rate conditions were collected, hydrolyzed with acid, and subjected to phosphoamino acid analysis to determine which residue was phosphorylated; both 250 (left) and 500 cpm (right) were loaded for each initial rate conditions. These experiments were carried out with P39A EtsΔ138 that contained Ser-26 which is normally mutated to alanine to prevent phosphorylation of this secondary site. Both the 6% and 21% phosphorylated P39A EtsΔ138 indicate that a threonine is phosphorylated (presumed to be Thr-38 as mutation of Thr-38 to alanine eliminated the phospho-threonine spot).

The efficiency of phosphorylation of the double mutant (P35/39A) was not significantly different from the P39A mutant (Figure 52, Table 11) further indicating the lack of importance of Pro-35 in mediating phosphorylation of EtsΔ138 and the importance of Pro-39 in mediating efficient catalysis. The 5-fold decrease in the k_{cat} of

the P39A EtsΔ138 mutant is in stark contrast to phosphorylation studies of the EGF peptide that showed a 100-fold decrease in the rate of phosphorylation when mutating the P+1 proline to alanine. These results suggest that a protein substrate containing a docking motif may be phosphorylated even in the absence of a Pro-X-Ser/Thr-Pro recognition motif.

To further understand the role of the proline-determinant in MAPK recognition of a protein substrate, we mutated the proline determinant at position 39 of EtsΔ138 to long chain polar residues as well as other small hydrophobic residues besides alanine to test whether or not EtsΔ138 could be phosphorylated by ERK2 with residues other than alanine and proline at the P+1 position. Mutation of the P+1 proline to long chain polar residues led to a significant decrease in the efficiency of EtsΔ138 phosphorylation as indicated by a decrease in k_{cat} and an increase in the K_m of the mutants (Table 11). In addition, the site-specificity of phosphorylation in the P39K and P39D mutants was lost as seen by the phosphorylation of both serine and threonine residues as determined by phosphoamino acid analysis (data not shown).

Mutation of the P+1 proline to glycine and valine showed an ~ 20-fold decrease in k_{cat} (Table 11) indicating that small nonpolar residues are tolerated more than large polar residues but much less than a proline or alanine. These results suggest that the P+1 proline directs or guides the residue to be phosphorylated and that an alanine at the P+1 position can be tolerated albeit ~ 22-fold less efficiently by comparing the specificity constant to EtsΔ138.

The importance of the P+1 proline in a protein substrate may be less important in directing the phosphorylation of a protein substrate containing a docking motif than previously seen with alanine mutagenesis in a peptide substrate. It was previously thought that proteins must contain a proline at the P+1 position to be phosphorylated by

ERK2 although our study suggests that an alanine at the P+1 position can be phosphorylated ~ 22-fold less efficiently at sub-saturating concentrations of substrate and ~5-fold less efficiently at saturating concentrations.

It is interesting to note that the EGF-peptide studies showed that mutation of the P-1 site to proline decreased the V_{\max} by ~ 20-fold [9]. However, ATF2 was shown to be an *in vivo* substrate of ERK2 with the consensus phosphorylation sequence Thr69-Pro-Thr71-Pro where only the latter Thr-71 is phosphorylated by ERK2 [62]. These results suggest that a proline directly preceding the phosphorylation site is tolerated *in vivo* and that a substrate phosphorylated ~ 20-fold less efficiently at saturating conditions can be an *in vivo* substrate suggesting that ERK2 substrates lacking a P+1 proline may also exist.

THE P+1 PROLINE DETERMINANT IS NOT REQUIRED FOR THE ERK2-ETSΔ138 DOCKING COMPLEX AND MACROMOLECULAR RECOGNITION

The EtsΔ24-138 mutant contains an ERK2 recognition motif including the phospho-acceptor Thr-38 and shows less than a two-fold increase in affinity as compared to a protein that lacks this region (EtsΔ51-138) (Table 10). These results suggest that the recognition motif contributes little to the formation of the docking complex. We synthesized a peptide that was selected as the optimal peptide substrate of ERK1 (N-TGPLSPGPF-C) [133], a protein with 83% homology that phosphorylates similar recognition motifs as that of ERK2, and found that this peptide could only displace 20% of the ERK2-EtsΔ138-F docking complex at a high concentration of 3.2 mM ($K_d \sim 4.7 \pm 0.2$ mM) indicating that this ERK recognition motif either binds very poorly to ERK2 or does not compete with EtsΔ138 binding and can bind ERK2 while it is bound to EtsΔ138-F. Further support that the recognition motif does not mediate macromolecular

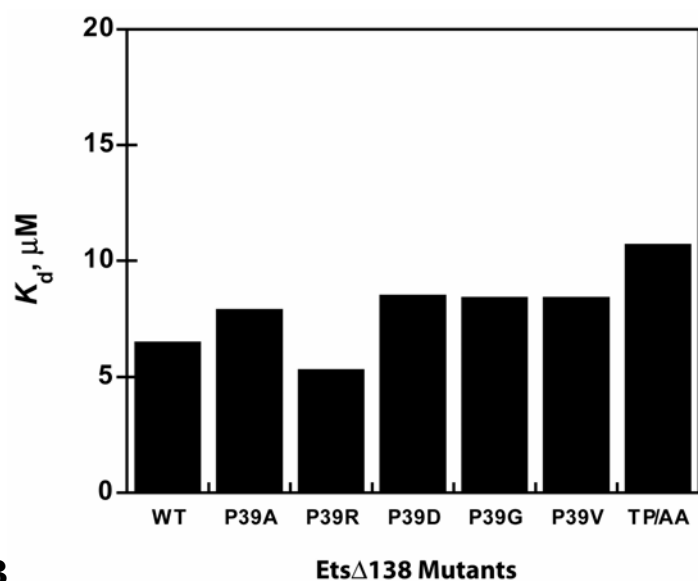
recognition of EtsΔ138 is that the phosphorylated product (EtsΔ138~P) binds ERK2 with similar affinity as that of the unphosphorylated substrate and shows competitive inhibition with respect to EtsΔ138 binding to ERK2 but does not compete with the alternate substrate MgATP²⁻ in the active site [7]. These results were further confirmed by fluorescence anisotropy assays using the phosphorylated EtsΔ138 substrate (K. Cox)³² indicating that a docking complex can exist when the recognition motif is phosphorylated.

Based on crystal structure data of the inactive and active form of ERK2, it has been proposed that a competent proline binding pocket exists in dual-phosphate ERK2 [4] that is absent in unphosphorylated ERK2 due to Val-187 and Arg-192 blocking this site [70]. It was suggested that the P+1 proline of a MAPK substrate could bind in this pocket in the active form of ERK2 but not the inactive form. However, we have shown that both dual-phosphate ERK2 and unphosphorylated ERK2 bind EtsΔ138 with similar affinity (Chapter 4) indicating that the formation of the proline-binding pocket in dual-phosphate ERK2 does not have a large affect on the affinity for the substrate EtsΔ138. To understand whether or not the P+1 proline facilitates ERK2 macromolecular substrate recognition of EtsΔ138, we used the P+1 mutants in a fluorescence competition assay to see whether or not different residues at the P+1 position affected the K_d of the docking complex. We hypothesized that the proline mutations would not affect the K_d if the docking complex occurred primarily through exosite interactions on ERK2 and excluded the enzymic active site and the recognition motif in the substrate EtsΔ138. All of the P+1 proline mutants exhibited less than a 2-fold affect on the K_d of the docking complex with ERK2 (Table 10, Figure 54a) indicating that EtsΔ138 docking motifs mediate macromolecular substrate recognition independent of the P+1 proline. Mutation of both

³² Fluorescence anisotropy was carried out using EtsΔ138~P (containing only one cysteine at position 31) labeled with fluorescein and titrated with ERK2 to yield a K_d of 4.1 μM (K. Cox).

the P+1 proline and the phospho-acceptor to alanine (T38A/P39A) caused less than a 2-fold increase in the K_d (Table 10, Figure 54a) indicating that neither the phospho-acceptor nor the P+1 proline is required for macromolecular substrate recognition. Conversely, mutation of the P+1 proline had a dramatic affect on k_{cat} (Figure 54b). These results indicate that the P+1 proline does not facilitate macromolecular substrate recognition of EtsΔ138 and, hence, formation of the docking complex, but is required for the dual-phosphate from of ERK2 to efficiently phosphorylate Thr-38 on EtsΔ138. These data suggest that an efficient docking complex occurs between ERK2 and EtsΔ138 in the absence of active site interactions, however, the P+1 proline is required for efficient chemistry for the phosphorylation of Thr-38.

A



B

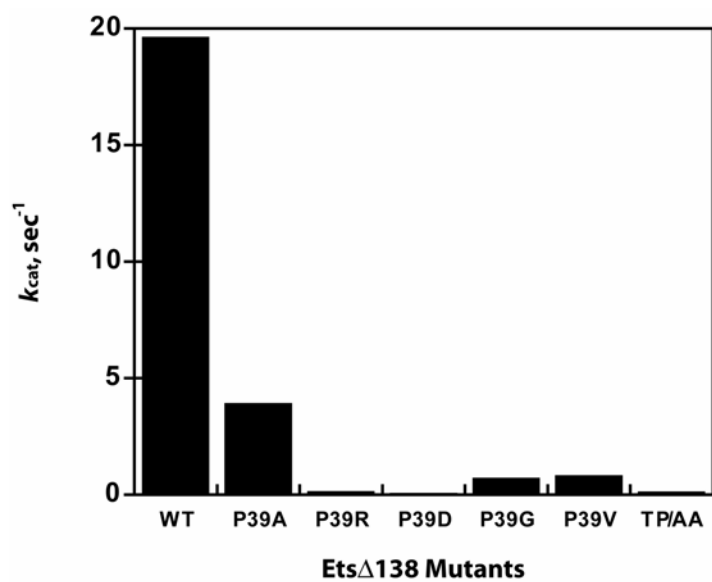


Figure 54. The P+1 proline of EtsΔ138 is not required for macromolecular substrate recognition by ERK2 but is required for catalysis. (A) The equilibrium dissociation constants (K_d) of several EtsΔ138 P+1 mutants were determined using a fluorescence anisotropy competition assay (Table 10). (B) The k_{cat} of each P+1 mutant was determined in Table 11.

MAGNESIUM CHLORIDE DECREASES THE AFFINITY OF ETSΔ138 AND ERK2

Mg^{2+} is required to stabilize negative charges on the ATP^{4-} so that it can bind in the active site of ERK2 as a MgATP^{2-} complex and is necessary for catalytic activity. Increasing concentrations of Mg^{2+} have been shown to increase the catalytic rate of ERK2 turnover of the EtsΔ138 substrate and increase the Henri-Michaelis-Menten constant (K_m) for EtsΔ138 phosphorylation by ERK2 [6]. However, the mechanism of magnesium's effects on ERK2 function is not fully understood. To test whether or not Mg^{2+} affects the affinity of ERK2 and EtsΔ138, fluorescence anisotropy experiments were carried out using both the unphosphorylated and dual-phosphate forms of ERK2 in the presence and absence of MgCl_2 .

The addition of 1-2 mM free MgCl_2 had less than a 2-fold affect on the affinity of the ERK2–EtsΔ138-F complex (Table 12) indicating that concentrations above free magnesium concentrations in mammalian cells (0.25-1 mM) [144] does not greatly affect the affinity of this complex. When carrying out steady state [7] and pre-steady state [44] phosphorylation assays we typically use 20 mM MgCl_2 so that MgATP^{2-} is saturating. The addition of 20 mM MgCl_2 led to an increase in the K_d for the ERK2–EtsΔ138-F complex for both the unphosphorylated (8-fold) and dual-phosphate (7-fold) forms of ERK2 as compared to the K_d in the absence of MgCl_2 (Table 12). These results indicate that high MgCl_2 concentrations are capable of decreasing the affinity of ERK2 and EtsΔ138-F for both phospho-forms of ERK2 suggesting that the MgCl_2 affect on binding is independent of the activation state of ERK2. These results are consistent with previous data suggesting that the K_m of EtsΔ138 increases as a function of increasing magnesium concentration [6]. The free magnesium concentration in cells can fluctuate based on cellular conditions such as growth, differentiation, proliferation, and senescence [145,

146] indicating that magnesium concentration fluctuation could regulate the activity of ERK2 and possibly other protein kinases through their ability to bind other proteins.

Dual-phosphate ERK2				
Free Mg²⁺, mM	AMP-PNP, mM	<i>r_f</i>	<i>r_b</i>	<i>K_d</i>, μM
20	-	0.106 ± 0.001	0.205 ± 0.009	17.2 ± 2.6 ⁿ⁼³
20	2	0.108 ± 0.001	0.192 ± 0.007	8.8 ± 1.2 ⁿ⁼³
2	-	0.113 ± 0.001	0.208 ± 0.002	2.6 ± 0.3 ⁿ⁼¹
2	2	0.112 ± 0.001	0.199 ± 0.006	4.5 ± 0.8 ⁿ⁼¹
1	-			
1	1	0.111 ± 0.001	0.188 ± 0.004	3.6 ± 0.6 ⁿ⁼¹
-	-	0.110 ± 0.000	0.203 ± 0.000	2.7 ± 0.1 ⁿ⁼²
Unphosphorylated ERK2				
20	-	0.107 ± 0.001	0.231 ± 0.003	6.0 ± 0.4 ⁿ⁼¹
20	2	0.106 ± 0.002	0.254 ± 0.003	3.9 ± 0.4 ⁿ⁼²
2	-	0.111 ± 0.001	0.253 ± 0.002	1.2 ± 0.1 ⁿ⁼¹
2	2	0.111 ± 0.001	0.253 ± 0.002	1.2 ± 0.1 ⁿ⁼¹
1	-	0.111 ± 0.002	0.256 ± 0.004	1.2 ± 0.2 ⁿ⁼¹
1	1	0.108 ± 0.001	0.224 ± 0.002	1.2 ± 0.1 ⁿ⁼¹
-	-	0.113 ± 0.000	0.247 ± 0.005	0.7 ± 0.1 ⁿ⁼³

Table 12. The affinity of ERK2 and EtsΔ138-F in the presence of MgCl₂ and AMP-PNP. Fluorescent anisotropy assays were carried out using several concentrations of dual-phosphorylated and unphosphorylated ERK2 and 100 nM EtsΔ138-F in the presence and absence of the concentrations of MgCl₂ and AMP-PNP shown using standard conditions. The hyperbolic curves generated were fit to Equation 9. All data are shown as a mean ± SE. The number of experiments for each are shown.

To further understand the role of Mg^{2+} in disrupting macromolecular recognition of EtsΔ138 by ERK2, several concentrations of MgCl_2 were added to two different concentrations of dual-phosphate ERK2 (9.55 and 4.8 μM) while using a fixed concentration of EtsΔ138-F (Figure 55a). As expected from the previous results, the apparent K_d increased with increasing concentrations of MgCl_2 . As magnesium concentrations increased, the affinity of ERK2 for EtsΔ138 decreased indicating that magnesium binding to ERK2 can compete with EtsΔ138-F binding.

If we assume that magnesium competes with EtsΔ138-F binding by binding directly to ERK2, we can use the same data from Figure 55a to determine the dissociation constant for Mg^{2+} binding to ERK2. When the data from Figure 55a was plotted as anisotropy versus MgCl_2 concentration, the K_d of Mg^{2+} for ERK2 was elucidated ($K_d^{\text{Mg}} \sim 3.3 \text{ mM}$ for both concentrations of ERK2 when r_f was fixed at a value of 0.110) (Figure 55b). These results are in close proximity to K_i values obtained for magnesium in kinetic studies with ERK2 [6].

From Figure 55a, equilibrium dissociation constants for the ERK2–EtsΔ138 complex can be estimated at each concentration of MgCl_2 and used to predict equilibrium dissociation constants at any give MgCl_2 concentration (data not shown). When the estimation of the dissociation constants are compared with the actual measured dissociation constants, the results are very consistent. For example, at 0 mM MgCl_2 it is estimated that the K_d of the ERK2–EtsΔ138-F complex should be $\sim 2 \mu\text{M}$ and the measured value was 2.7 μM (Table 12). At 20 mM MgCl_2 , the estimated K_d was $\sim 18 \mu\text{M}$ and the measured value was 17.2 μM (Table 12). We also carried out an ITC experiment to measure EtsΔ138 binding to ERK2 in 10 mM MgCl_2 (using similar assay conditions except that 0.1% 2-mercaptoethanol was used in place of 2 mM DTT) and found that the measured K_d was $21.4 \pm 3.2 \mu\text{M}$ ($n=2$) while the predicted dissociation

constant was $\sim 8.5 \mu\text{M}$ for the ERK2-Ets Δ 138-F complex. ITC experiments also suggested that the K_d for ERK2 and Ets Δ 138 was $7.1 \pm 0.3 \mu\text{M}$ ($n=2$) in the absence of magnesium chloride similar to the measured value using anisotropy ($K_d = 6.6 \mu\text{M}$).

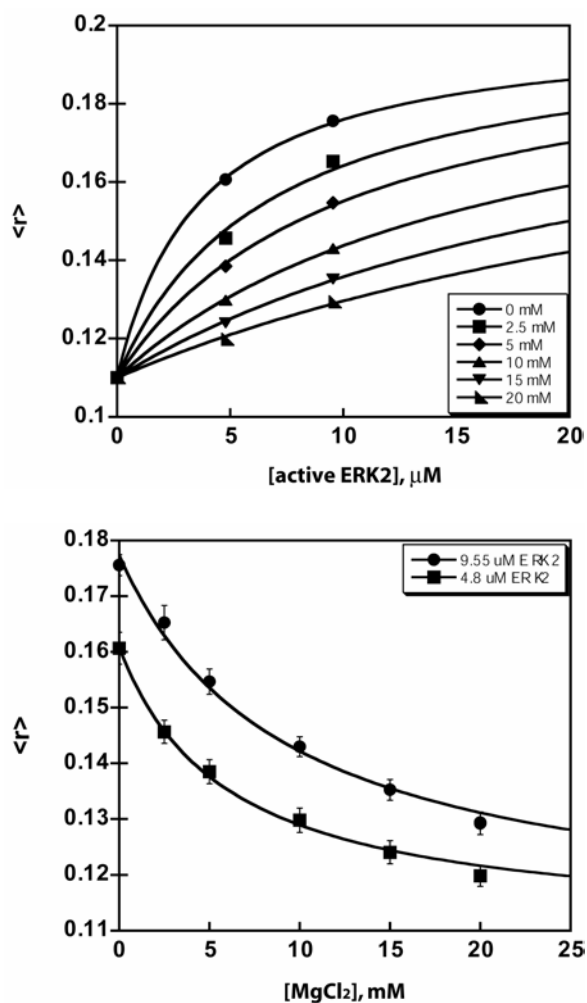
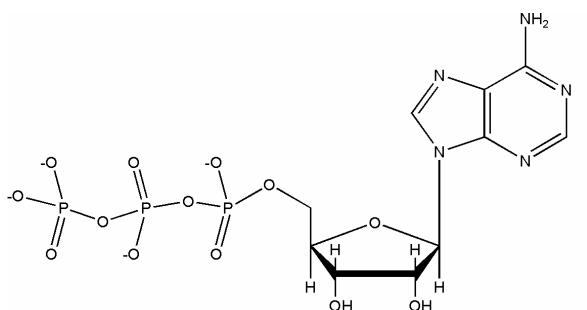


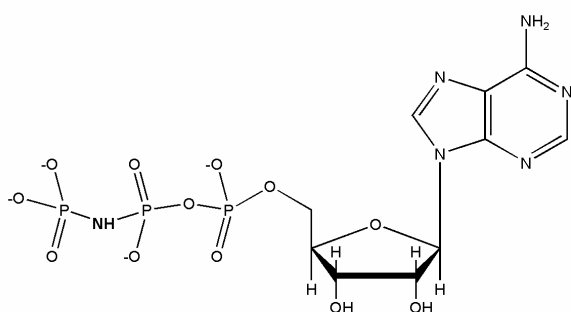
Figure 55. Mg^{2+} -dependence of the equilibrium dissociation constant of the ERK2–Ets138 complex. Fluorescence anisotropy was performed using 100 nM Ets Δ 138-F and varying concentrations of MgCl_2 using two concentrations of ERK2 (as shown above) using 25 mM Hepes, pH 7.5, 50 mM KCl, 40 $\mu\text{g/mL}$ BSA, 0.1 mM EDTA, 0.1 mM EGTA and 2 mM DTT.

MACROMOLECULAR SUBSTRATE RECOGNITION IN THE PRESENCE OF MAGNESIUM AND AN ATP-MIMIC

Analyses of protein kinase activity are carried out in the presence of both MgCl_2 and ATP, therefore, we were interested in the protein–protein binding events in the presence of MgATP^{2-} . Since the addition of ATP allows for the phosphorylation of Ets Δ 138-F by ERK2 to occur and disrupt the equilibrium of the binding assays, we measured the K_d in the presence of a non-hydrolyzable ATP mimic in which the oxygen bridging the β - and γ - phosphate group of ATP was replaced with a nitrogen (AMP-PNP, 5'-adenylylimidodiphosphate) (Figure 56). AMP-PNP has been used in several situations to mimic ATP binding in crystal structures of protein kinases [147-149] indicating that it binds sufficiently in the active site of several kinases and mimics ATP.



ATP



AMP-PNP

Figure 56. The structures of the nucleotide ATP and the non-hydrolyzable analog AMP-PNP. ATP and AMP-PNP are shown and differ by the linker between the β - and γ -phosphate where ATP contains a hydrolyzable oxygen and AMP-PNP contains a non-hydrolyzable nitrogen. AMP-PNP was used in fluorescence anisotropy binding assays in the presence of MgCl_2 to mimic the active ternary complex required for phosphorylation ($\text{Mg-ERK2-MgATP-Ets}\Delta 138$) [6].

Interestingly, the addition of 2 mM AMP-PNP led to an ~ 2.0 -fold decrease in the dissociation constant for Ets $\Delta 138$ -F and the unphosphorylated and dual-phosphate forms ERK2 as compared to the absence of nucleotide in the presence of 20 mM MgCl_2 (Table 12). Similarly, the addition of 2 mM ADP^{33} , a product of the phosphorylation reaction

³³ At 2 mM ADP and 20 mM MgCl_2 , the parameters were $r_f = 0.111 \pm 0.001$, $r_b = 0.193 \pm 0.015$, $K_d = 5.9 \pm 2.1 \mu\text{M}$ ($n=2$ association). A displacement assay under similar conditions gave values of $r_f = 0.110$ fixed, $r_b = 0.190 \pm 0.001$, and $K_d = 27.0 \pm 2.0 \mu\text{M}$ ($n=1$) for Ets $\Delta 138$ and values of $r_f = 0.110$ fixed, $r_b = 0.187 \pm 0.002$, and $K_d = 83.3 \pm 12.8 \mu\text{M}$ ($n=1$). $K_S^* \sim 0.5$.

that lacks a γ -phosphate group, led to a small 3-fold decrease in the K_d in the presence of 20 mM $MgCl_2$ indicating that the presence of a nucleotide has a small affect on the affinity of the docking complex. These results indicate that nucleotide binding to ERK2 ($MgAMP-PNP^{2-}$ and $MgADP^{1-}$) may have a small affect on stabilizing the docking complex between ERK2 and Ets Δ 138-F, however, the binding affinity was not as good as that seen in the absence of $MgCl_2$. At low concentrations of $MgCl_2$ (between 0-2 mM), the affinity of the docking complex was not largely altered by the addition of AMP-PNP (Table 12) which may be due to a poor affinity of the nucleotide for ERK2 at low magnesium concentrations [6]. These results suggest that nucleotide binding in the form of $MgAMP-PNP^{2-}$ and $MgADP^{1-}$ do not considerably stabilize the docking complex indicating the lack of strong active site binding affinity.

A MODEL FOR ETS Δ 138 SUBSTRATE RECOGNITION BY ERK2

We have determined the equilibrium dissociation constant for the ERK2–Ets Δ 138 complex and shown evidence that an Ets Δ 138 docking motif is required for efficient exosite interactions with ERK2 for macromolecular substrate recognition. In addition, we have shown that Ets Δ 138 residues that enter into the active site of ERK2 for phosphorylation (Thr-Pro site) are not required for macromolecular substrate recognition (Figure 54a) but are crucial for efficient catalysis (Figure 54b). Based on these data, we propose a two-step binding model leading towards the phosphorylation of Ets Δ 138 by the dual-phosphate form of ERK2 in which (1) an intermolecular binding step occurs to facilitate macromolecular substrate specificity followed by (2) intramolecular binding of the recognition motif in the active site leading to the active complex required for phosphorylation. We propose that intermolecular binding occurs between an ERK2

exosite and the EtsΔ138 docking motif independent of active site interactions (K_S). Once the exosite-tethered docking complex has formed, an intramolecular binding event allows the kinase active site to associate with the recognition motif of the substrate (K_{S^*}). Therefore, the K_d of the ERK2–EtsΔ138 docking complex measured using the fluorescence anisotropy assay was hypothesized to be an apparent equilibrium dissociation constant (K_d^{app}) that includes both K_S and K_{S^*} .

In order to determine the internal equilibrium dissociation constant (K_{S^*}) for ERK2 active site recognition of the substrate recognition motif, we must make a few assumptions. If we assume that K_d^{app} involves both the intermolecular and intramolecular binding steps of EtsΔ138, then the K_d of the ERK2–EtsΔ138 complex is indistinguishable from K_d^{app} . On the other hand, the T38A/P39A EtsΔ138 mutant has a docking motif for ERK2 recognition but lacks a recognition motif required for phosphorylation, therefore, we can assume that the K_d of the T38A/P39A mutant is indistinguishable from K_S and does not include K_{S^*} . If these assumptions are made, then the internal equilibrium dissociation constant (K_{S^*}) can be estimated using Equation 31.

$$\text{Equation 31} \quad K_d^{app} = \frac{K_S \times K_{S^*}}{K_{S^*} + 1}$$

Using Equation 31 and the K_d obtained from WT and T38A/P39A EtsΔ138 in the absence of $MgCl_2$, presence of 20 mM $MgCl_2$, and in the presence of 20 mM $MgCl_2$ and 2 mM AMP-PNP²⁻ (Table 13), were used to estimate the three internal equilibrium constants K_{S^*} , K_{S^*Mg} , and $K_{S^*A \cdot Mg}$ to be 1.5, 1.3, and 1.0, respectively. Each of the estimated internal equilibrium constants were not largely favorable (where $K_{S^*} \ll 1$) for the active conformation in which the recognition motif is bound in the enzymic active

site. We must also assume that the binding of AMP-PNP (catalytically inactive) is similar to that of ATP (catalytically active). These results suggest that neither magnesium nor the MgAMP-PNP^{2-} lead to a significant stabilization of the active ternary complex where the phospho-acceptor of Ets Δ 138 is in the active site consistent with the results that active site interactions for this E-S complex are weak. Since the active site interactions are not strong interactions, the mechanism of phosphoryl-transfer relies largely upon the docking complex mediated outside of the active site to ensure the fidelity of macromolecular recognition. The docking complex formed between Ets Δ 138 and ERK2 must exist long enough for a nucleotide substrate to bind (if not already bound to the enzyme) and for the phospho-acceptor of Ets Δ 138 to enter the active site in the absence of strong interactions. Certainly, a proline at the P+1 position to the phospho-acceptor helps to mediate efficient recognition and phosphorylation of this site by ERK2.

EtsΔ138		r_f	r_b	$K_d, \mu\text{M}$
Free Mg²⁺, mM	AMP-PNP, mM			
0	-	0.111 ± 0.002	0.209 ± 0.004	$6.6 \pm 1.2^{n=3}$
20	-	0.112 ± 0.001	0.184 ± 0.003	$29.0 \pm 12.8^{n=2}$
20	2	0.110^*	0.188 ± 0.001	$29.5 \pm 1.7^{n=1}$
T38A/P39A EtsΔ138				
Free Mg²⁺, mM	AMP-PNP, mM			
0	-	0.112 ± 0.002	0.209 ± 0.004	$11.0 \pm 0.8^{n=3}$
20	-	0.113 ± 0.001	0.189 ± 0.004	$50.9 \pm 4.2^{n=2}$
20	2	0.110^*	0.186 ± 0.002	$57.6 \pm 6.4^{n=1}$

Table 13. Competition anisotropy assays to determine the K_d of the ERK2–EtsΔ138 and ERK2–EtsΔ138(T38A/P39A) in the presence of MgCl₂ and AMP-PNP. A competition fluorescence anisotropy assay was carried out to determine the K_d of the ERK2–EtsΔ138 and ERK2–EtsΔ138(T38A/P39A) in the presence and absence of MgCl₂ and AMP-PNP. These data were used to estimate the docking complex dissociation constant (K_S) and the internal equilibrium constant (K_{S^*}) under conditions of no Mg²⁺, 20 mM free Mg, and 20 mM free Mg²⁺ and 2 mM AMP-PNP. Values of K_d^{app} were derived from the K_d of EtsΔ138. Values of K_S were derived from the K_d of T38A/P39A assuming that the K_{S^*} equilibrium does not occur for this mutant. K_{S^*} was estimated using Equation 31.

CONCLUSIONS

A mechanism of macromolecular substrate recognition by a post-translational modification enzyme as proposed here using exosite interactions to tether the enzyme–substrate interaction followed by intramolecular recognition of the recognition motif in the active site seems evolutionarily advantageous for cell signaling pathways utilizing covalent modifications such as phosphorylation, dephosphorylation, proteolysis, methylation, acetylation, and ubiquitination. Since the chemistry that occurs in the active

site of these enzymes are similar amongst family members, small changes of non-catalytic residues in the active site could be made to facilitate a subset of family-specific recognition motif sequences while excluding other non-family-specific recognition motifs. However, according to our data, these recognition motifs do not bind strongly in the active site even in the presence of magnesium and a nucleotide. Multiple isoforms of sub-family members with similar recognition motif preferences could evolve to have unique macromolecular substrate specificities by positively or negatively evolving exosites specific for new substrates bearing family-specific recognition motifs. We proposed that these exosite-docking motif interactions help to ensure the fidelity of cellular signal transduction mediated through post-translational modifications such as phosphorylation by ERK2 and other members of the MAPK family.

EXPERIMENTAL PROCEDURES

CONSTRUCTION OF SITE-SPECIFIC ETSΔ138 MUTANTS

A pET-28a bacterial expression vector encoding a hexa-histidine tag followed by the cDNA encoding murine Ets1 residues 1-138 (pET-28a EtsΔ138, a gift of L. P. McIntosh, University of British Columbia, Vancouver) was modified by PCR using site-directed mutagenesis to construct an *N*-terminal truncation mutant containing Ets1 residues 24-138 with an initial methionine (pET-28a EtsΔ24-138) and the EtsΔ138 mutants P35A, P39A, P39R, P39K, P39D, P39E, P39G, P39V. To construct the pET-28a EtsΔ24-138 and EtsΔ51-138 *N*-terminal truncation mutants, pET-28a EtsΔ138 was PCR amplified with a forward primer containing an *Nde*I site (underlined, encoding the initial methionine) followed by the codon encoding Phe-24 (5'-GG GAA TTC CAT ATG TTC CCT TCC CCG GAC ATG-3') or encoding Ala-51 (5'-GG GAA TTC CAT ATG GCT ACT TTC AGT GGT TTC ACA) and an outer reverse primer (5'-GCT AGT TAT TGC TCA GCG GTG G-3') using the following PCR conditions: 94 °C for 5 min to denature the complementary strands; 30 cycles of 55 °C for 30 sec to anneal the primers, extension for 1 min at 72 °C, followed by a denaturation step at 94 °C for 45 sec; complementary strands were extended a final 10 min at 72 °C. The *N*-terminal mutant PCR products were digested with *Nde*I and *Hind*III and ligated into *Nde*I-*Hind*III digested pET-28a.

Each EtsΔ138 construct and mutants were generated and purified essentially as described [42] and dialyzed into 1.25 mM Hepes, pH 7.5, 2.5 mM KCl, and 2 mM DTT. All proteins produced from the pET-28a vector have an *N*-terminal sequence of M-G-S-S-H-H-H-H-H-S-S-G-L-V-P-R-G-S-H- prior to the initial methionine encoded by the EtsΔ138 cDNA, however, usually the initial methionine is cleaved after production in

bacteria [42]. All EtsΔ138 constructs used here have an S26A mutation [44] unless otherwise denoted (* - P39A contains Ser-26).

For the EtsΔ138 point mutations, fragment A was PCR amplified with an outer forward primer (5'-GGT GAT GCC GGC CAC GAT GC) and an inner reverse primer containing the mutation for P35A (5'-AGT TAA CAG *CGC* GAC ATC TGC ACA-3'), P39A (5'-TC TTT GCT GCT *AGC* AGT TAA CAG CG-3'), P39R (5'-AT TTC TTT GCT GCT *ACG* AGT TAA CAG-3'), P39K (5'-TTC TTT GCT GCT *TTT* AGT TAA CAG CG-3'), P39D (5'-C TTT GCT GCT *ATC* AGT TAA CAG CGG -3'), P39E (5'-C TTT GCT GCT *TTC* AGT TAA CAG CGG -3'), P39G (5'-TTC TTT GCT GCT *GCC* AGT TAA CAG CGG-3'), P39V (5'-TC TTT GCT GCT *CAC* AGT TAA CAG CG-3') or F120A (5'-AT ATC CCC AAC *AGC* GTC TGG AGC CA-3'). Fragment B was amplified with an inner forward primer containing the mutation for P35A (5'-TGT GCA GAT GTC *GCG* CTG TTA ACT-3'), P39A (5'-CG CTG TTA ACT *GCT* AGC AGC AAA GA-3'), P39R (5'-CTG TTA ACT *CGT* AGC AGC AAA GAA AT-3'), P39K (5'-CG CTG TTA ACT *AAA* AGC AGC AAA GAA-3'), P39D (5'-CCG CTG TTA ACT *GAT* AGC AGC AAA G-3'), P39E (5'-CCG CTG TTA ACT *GAA* AGC AGC AAA G-3'), P39G (5'-CCG CTG TTA ACT *GGC* AGC AGC AAA GAA-3'), P39V (5'-CG CTG TTA ACT *GTG* AGC AGC AAA GA-3'), or F120A (5'-TG GCT CCA GAC *GCT* GTT GGG GAT AT-3') and an outer reverse primer (5'-GCT AGT TAT TGC TCA GCG GTG G-3'). Fragments A and B were purified and used as templates for a second round of PCR using the outer primers. Mutants containing two mutations were made using single mutant DNA as template and incorporating a second mutation. The mutant PCR products were digested with NdeI and HindIII and ligated into NdeI-HindIII digested pET28a. All mutations were verified by sequencing the DNA at UT core facilities using an Applied Biosystems automatic DNA sequencer.

CLEAVAGE OF THE HIS₆-TAG OF ETSΔ138

EtsΔ138 (5 mg) was subjected to thrombin proteolysis in a 5 mL reaction volume containing 7 units of thrombin (Novagen) in 20 mM Tris-HCl, pH 8.4, 1.5 M NaCl, and 25 mM CaCl₂ at 23 °C for 4 hours. The reaction was filtered with a 0.22 μm nylon filter (Pall) and applied to a Mono Q HR 10/10 anion exchange column pre-equilibrated in H1 buffer (20 mM Tris, pH 8.0, 0.1% 2-mercaptoethanol (v/v), 0.03% Brij-35 (w/v), 0.1 mM EDTA, and 0.1 mM EGTA) and eluted with a linear gradient of H2 buffer (H1 containing 0.25 M NaCl) over 80 min at a flow rate of 1.5 mL min⁻¹. The resulting EtsΔ138NoHis was dialyzed into 1.25 mM Hepes, pH 7.5, 2.5 mM KCl, and 2 mM DTT at 4 °C, concentrated, snap frozen in liquid nitrogen, and stored at -80 °C.

For mass spectrometry analysis, 1 mg of EtsΔ138NoHis was applied to a 250 mm × 4 mm Vydac RP column (218TP54) equilibrated with 0.1% trifluoroacetic acid (TFA) and eluted with a linear gradient of aqueous acetonitrile (99.9% v/v) containing 0.1% TFA at a flow rate of 0.7 mL min⁻¹ and collecting 0.7 mL fractions. All fractions from both major peaks were pooled as separate peaks, lyophilized, raised in 50% acetonitrile, lyophilized again, and raised in 200 μL of 50% acetonitrile. The solution was filtered in a 0.22 μm nylon filter (Pall), diluted 1:10, and analyzed by electrospray ionization as previously described [42]. The molecular mass of the second C18 peak was EtsΔ138NoHis (15 912 Da) while the first peak was devoid of protein.

KINETIC METHODS FOR ETSΔ138 PHOSPHORYLATION

Protein kinase assays were conducted as described previously by spotting 5 μ L aliquots of a 50 μ L reaction containing γ - 32 P-ATP (ICN) onto P81 paper as described [42]. Assays contained 0.5-1 nM ERK2, 25 mM Hepes pH 7.5, 50 mM KCl, 20 mM MgCl_2 , 0.1 mM EDTA, 0.1 mM EGTA, 40 μ g/mL BSA, and 2 mM DTT, while keeping ATP constant (2 mM) and varying EtsΔ138 (6.3-200 μ M) or while keeping EtsΔ138 constant (200 μ M) and varying ATP (31.3-1000 μ M). Initial rates were measured at each given concentration using at least 5 data points that lie in a straight line and saturation curves were fit to the Henri-Michaelis-Menten equation using Kaleidagraph (Synergy Software). Assays with P39A and P35/39A EtsΔ138 used 2 nM ERK2, those with P39R were 100 nM ERK2, and those with P39K, P39D, P39E EtsΔ138 were 200 nM ERK2.

PHOSPHOAMINO ACID ANALYSIS

Phosphoamino acid analysis was carried out essentially as described [103]. Radio-labeled EtsΔ138 was run on a 15% SDS-PAGE gel at 200V for 40 min, transferred to nitrocellulose in 25 mM Tris-HCl, 200 mM glycine, 20% methanol (v/v), and 0.1% SDS at 30 V for 12 h. The nitrocellulose was stained with 1% acetic acid (v/v) containing 0.1% Ponceau S to ensure the transfer occurred and to locate the target protein bands, destained in water 3×10 min, soaked in 100 mL of 0.1 M acetic acid containing 0.5% polyvinylpyrrolidone for 30 min at 37 °C. Bands containing EtsΔ138 were cut into small pieces with a razor blade, washed 3×1 mL with water, 2×1 mL with 25 mM ammonium carbonate, pH 8.5, raised in 200 μ L of ammonium carbonate with 10 μ g of sequencing grade trypsin (Roche), and shaken vigorously at 37 °C for 4 h. Another 10 μ g

of trypsin was added overnight. The digest was centrifuged for 10 min at 13,000 rpm and the supernatant containing the tryptic peptides was removed, dehydrated under vacuum, and raised in 0.1% TFA for reverse phase HPLC analysis. The sample was injected onto a reverse phase C18 column (Vydac 218TP54) in 0.1% TFA using a linear gradient of 0-99.9% acetonitrile over 100 min at a flow rate of 0.7 mL/min. Each 0.7 mL fraction was counted in the scintillation counter to locate radioactive samples. A peptide corresponding to phosphorylated EtsΔ138 eluted at 40% acetonitrile. The labeled peptide was hydrolyzed in 6 N HCl for 60 min at 110 °C and analyzed by phospho-amino acid analysis by electrophoresis of ~ 250-500 cpm on a 20 × 20 cm cellulose plate w/o fluorescent indicator using running buffer containing 5% acetic acid (v/v) and 0.5% pyridine (v/v), pH 3.5. Samples were electrophoresed at 250 V for 2 hours, the plate was dried, stained with 0.25% ninhydrin in acetone to expose the standard phosphorylated amino acids (P-Ser, P-Tyr, and P-Thr), exposed to film for 24 hours, and developed.

FLUORESCENCE ANISOTROPY BINDING ASSAY

The binding of EtsΔ138-F to ERK2 was monitored using fluorescence anisotropy. Fluorescence anisotropy, r , is defined in Equation 8 where I_{VH} is the intensity of the horizontal emission (second subscript) of the fluorescein moiety stimulated with vertically polarized light (first subscript), and G is the monochromator grating factor (I_{HV}/I_{HH}) to correct for emission components.

Equation 8

$$r = \frac{I_{VV} - (G \times I_{VH})}{I_{VV} + (2 \times G \times I_{VH})}$$

Various amounts of ERK2 were added to EtsΔ138-F, the fluorescence anisotropy of EtsΔ138-F signal increased and neared a saturating value indicating saturation of EtsΔ138-F binding to ERK2. All binding assays were carried out using 100 nM Fluorescein-EtsΔ138 (as measured by fluorescein concentration) in 25 mM Hepes, pH 7.5, 50 mM KCl, 0.1 mM EDTA, 0.1 mM EGTA, 40 μg/mL BSA, 2 mM DTT, 2% glycerol, and various concentrations of ERK2 in a 60 μL volume. Assays were made by adding a 5x concentration of ERK2 in 12 μL of S1 buffer (25 mM Hepes, pH 7.5, 50 mM KCl, 2 mM DTT, and 10% glycerol), a 10x concentration of EtsΔ138-F in 6 μL of S1 buffer lacking glycerol, 30 μL of Master Mix buffer (35 mM Hepes, pH 7.5, 70 mM KCl, 80 μg/mL BSA, 0.2 mM EDTA, 0.2 mM EGTA, and 2 mM DTT), followed by 12 μL of Competition buffer (1.25 mM Hepes, pH 7.5, 2.5 mM KCl, and 2 mM DTT) to make a final volume of 60 μL. AMP-PNP, ADP, and MgCl₂ were added at a 2x concentration in the Master Mix buffer.

Discontinuous assays were carried out by incubating separate reactions for 7 min at 27 °C, exciting the fluorescein moiety with both vertically and horizontally polarized light at 492 nm, and measuring the emission of polarized light at both the vertical and horizontal positions at 515 nm. Excitation and emission slit widths were set to 5 nm the integration time for each reading was 0.300 sec. The anisotropy of each assay point was measured every 15 sec for 3 min and the average anisotropy was calculated from the 12 data points. The G factor was near 0.75-0.76.

Anisotropy data were fit to Equation 9 to determine the equilibrium dissociation constant (K_d), where r_f and r_b are the anisotropy values of the free and bound EtsΔ138-F, respectively, and $[E_T]$ and $[S_T]$ are the total ERK2 and EtsΔ138-F concentration.

$$\text{Equation 9 } ^{34} \langle r \rangle = r_f + (r_b - r_f) \frac{K_d + [E_T] + [S_T] - \sqrt{(K_d + [E_T] + [S_T])^2 - 4[E_T][S_T]}}{2[S_T]}$$

COMPETITION ASSAY

Unlabeled EtsΔ138 and magnesium were used to compete with an EtsΔ138-F exosite on ERK2, the data was simultaneously fit to Equation 10 and Equation 11 using the program Scientist to determine the equilibrium dissociation constant (K_{d2}) of the unlabeled competitor and ERK2, where K_d is the equilibrium dissociation constant for EtsΔ138-F and ERK2 in the absence of competitor, $[C]$ is the concentration of the unlabeled competitor, and $[EC]$ is the concentration of the ERK2–EtsΔ138 or the ERK2– Mg^{2+} complex.

$$\text{Equation 10 } ^{34} \quad \langle r \rangle = r_f + \frac{(r_b - r_f)}{K_d \frac{[C] + K_{d2}}{K_{d2} \times [E_T]} + 1}$$

$$\text{Equation 11} \quad K_{d2} = \frac{[E_T] \times [C]}{[EC]}$$

Assays were made similar to above with the addition of ERK2 (5x), Master Mix buffer, the competitor (5x) in Competition buffer, followed by EtsΔ138-F (10x).

³⁴ If fluorescence yield of the bound and free forms of the labeled protein differ, as in the case of EtsΔ138-Fluorescein labeled at Cys-31 (the bound form has a fluorescence yield that is 50% of the unbound form), see “Equation Derivation” in Chapter 4.

ISOTHERMAL TITRATION CALORIMETRY

An MCS isothermal titration calorimeter (MicroCal Inc.) was used for titrations of Ets Δ 138 into ERK2 at 27 °C in 25 mM Hepes, pH 7.5, 50 mM KCl, 0.1 mM EDTA, 0.1 mM EGTA, and 0.1% 2-mercaptoethanol (v/v). The buffer was also used as the reference solution. Dual-phosphate ERK2 (30 μ M) was titrated with concentrated Ets Δ 138 (600 μ M) after overnight dialysis at 4 °C in the same buffer. Titrations were initiated with a 2 μ L injection followed by 30 \times 10 injections with a 5 s injection duration and a 120 s in between injections. Origin 2.3 data analysis software (MicroCal Inc.) was used for the integration of thermograms by fitting to a one-binding site model. Data fitting produced values for the binding stoichiometry (n), dissociation constant (K_d), and molar enthalpy change (ΔH). The change in molar entropy (ΔS) and the Gibbs free energy (ΔG) were calculated from the thermodynamic relationships. Experiments done with 10 mM MgCl₂ were carried out by dialyzing the proteins in buffer also containing MgCl₂; for these experiments the ERK2 concentration was 44 and 50 μ M in the presence of 600 and 800 μ M Ets Δ 138, respectively.

EQUATION DERIVATION

From Scheme 14

$$K_s = \frac{[E][S]}{[ES]} \text{ can be rearranged to } [ES] = \frac{[E][S]}{K_s}$$

$$K_{s^*} = \frac{[ES]}{[ES^*]} \text{ can be rearranged to } [ES^*] = \frac{[ES]}{K_{s^*}} \text{ and then to } [ES^*] = \frac{[E][S]}{K_s K_{s^*}}$$

$$E_T = [E] + [ES] + [ES^*]$$

The dissociation constant is defined as the free substrate concentration in which half of enzyme is bound to substrate and half is free. Therefore:

$$\frac{[E]}{[E_T]} = 0.5 = \frac{[E]}{[E] + [ES] + [ES^*]}$$

Divide by E to get:

$$0.5 = \frac{1}{1 + \frac{[ES]}{[E]} + \frac{[ES^*]}{[E]}}$$

Substitute [ES] and [ES*] in and solve for [S]

$$\text{Equation 31 } [S] = K_d^{app} = \frac{K_s K_{s^*}}{K_{s^*} + 1}$$

EXPERIMENTAL DATA

Table 10

EtsΔ138NoHis, Competition Fluorescence Anisotropy, 7/23/04 (ii)

[EtsΔ138NoHis], μM	<r>	
0	0.178	0.176
6.25	0.169	0.167
12.5	0.160	0.157
25	0.144	0.145
50	0.130	0.129
100	0.116	0.119
150	0.110	0.111
200	0.106	0.108

EtsΔ138, Competition Fluorescence Anisotropy, 1/26/04, 3/3/04, 4/22/04 (two different batches)

[EtsΔ138], μM	<r>		
0	0.170	0.178	0.175
6.25		0.171	0.166
12.5	0.154	0.160	0.157
25	0.136	0.148	0.144
50	0.127	0.133	0.129
100	0.121	0.124	0.122
200	0.118	0.115	0.119

EtsΔ24-138, Competition Fluorescence Anisotropy, 4/22/04 (ii – two different batches)

[EtsΔ24-138], μM	<r>
0	0.175
6.25	0.173
12.5	0.173
25	0.168
50	0.164
100	0.157
200	0.146

[EtsΔ24-138], μM	<r>
0	0.175
9.4	0.170
18.8	0.169
37.5	0.164
75	0.157
150	0.149
176	0.147

EtsΔ51-138, Competition Fluorescence Anisotropy, 1/30/04

[EtsΔ51-138], μM	<r>
0	0.169
12.5	0.169
25	0.166
50	0.163
100	0.157
200	0.149

F120A EtsΔ138, Competition Fluorescence Anisotropy, 3/5/04 (ii)

[F120A], μM	<r>	
0	0.175	0.176
6.25	0.172	0.173
12.5	0.173	0.171
25	0.169	0.167
50	0.163	0.160
100	0.154	0.152
200	0.143	0.143

P39A EtsΔ138, Competition Fluorescence Anisotropy, 1/27/04

[P39A], μM	<r>
0	0.169
12.5	0.154
25	0.144
50	0.133
100	0.125
200	0.119

P39D EtsΔ138, Competition Fluorescence Anisotropy, 1/27/04

[P39D], μM	<r>
0	0.169
12.5	0.154
25	0.145
50	0.134
100	0.125
200	0.121

P39G EtsΔ138, Competition Fluorescence Anisotropy, 5/1/04

[P39G], μM	<r>	
0	0.168	0.166
12.5	0.160	0.157
25	0.151	0.153
50	0.143	0.141
100	0.130	0.131
200	0.123	0.123

P39R EtsΔ138, Competition Fluorescence Anisotropy, 1/27/04, 3/3/04

[P39R], μM	<r>	
0	0.168	0.178
6.25		0.167
12.5	0.148	0.157
25	0.137	0.139
50	0.126	0.127
100	0.121	0.122
200	0.118	

P39V EtsΔ138, Competition Fluorescence Anisotropy, 5/1/04 (ii)

[P39V], μM	<r>	
0	0.165	0.162
6.25	0.160	0.158
12.5	0.151	0.149
25	0.143	0.140
50	0.128	0.129
100	0.121	0.121
200	0.116	0.115

T38A/P39A EtsΔ138, Competition Fluorescence Anisotropy, 1/30/04, 3/3/04 (ii)

[T38A/P39A], μM	<r>		
0	0.168	0.178	0.178
6.25	0.161	0.170	0.171
12.5	0.155	0.164	0.164
25	0.147	0.153	0.153
50	0.134	0.139	0.140
100		0.129	0.129
200		0.123	0.122
75	0.128		

Table 11

WT EtsΔ138 data can be found in Chapter 3, Experimental Data, n=12

P35A EtsΔ138

[P35A], μM	$k_{\text{obs}}, \text{s}^{-1}$			
	6/28/02	7/9/02	1/16/03	1/20/03
200	13.8	17.4	14.1	17.6
100	13.3	17.3	14.4	15.2
50	13.7	16.7	11.9	14.8
25	10.8	14.6	11.8	11.5
12.5	9.3	13.8	9.4	10.3
6.3	6.3	8.4	4.7	6.2

6/28/02 50 mM Hepes, pH 7.3, 100 mM KCl, 0.1 mM EDTA, 0.1 mM EGTA, 10 mM MgCl_2 , 2 mM ATP, 8 $\mu\text{g/mL}$ BSA

7/9/02, 50 mM Hepes, pH 7.3, 100 mM KCl, 10 mM MgCl_2 , 2 mM ATP, 8 $\mu\text{g/mL}$ BSA, 2.8 mM DTT

1/16/03 50 mM Hepes, pH 8.2, 100 mM KCl, 20 mM MgCl_2 , 2 mM ATP, 40 $\mu\text{g/mL}$ BSA, 2 mM DTT

1/20/03 50 mM Hepes, pH 8.2, 50 mM KCl, 20 mM MgCl_2 , 2 mM ATP, 40 $\mu\text{g/mL}$ BSA, 2 mM DTT

P39A EtsΔ138 containing Ser-26

[P39A], μM	k_{obs}, s^{-1}		
	5/11/03	1/30/03	1/30/03
200	2.3	4.0	4.5
100	2.1	3.8	3.7
50	1.5	2.9	2.6
25	1.0	1.9	1.7
12.5	0.7	1.4	1.1
6.3		1.0	0.6

5/11/03 25 mM Hepes, pH 7.3, 60 mM KCl, 20 mM MgCl₂, 2 mM ATP, 8 μg/mL BSA, 2 mM DTT

1/30/03 (ii) 50 mM Hepes, pH 8.2, 50 mM KCl, 20 mM MgCl₂, 2 mM ATP, 40 μg/mL BSA, 2 mM DTT

P39A EtsΔ138 lacking Ser-26 (S26A)

[P39A], μM	k_{obs}, s^{-1}					
	6/20/02	6/21/02	1/16/03	2/28/03	6/14/03	6/14/03
200	3.0	3.7	3.2	3.6	3.6	2.6
100	2.5	2.7	2.9	3.2	3.5	2.8
50	2.3	2.2	2.3	2.1	2.2	1.9
25	1.3	1.3	1.3	1.4	2.0	1.4
12.5	1.6	1.2	1.1	0.9	1.7	0.5
6.3	0.4	0.8		0.7	0.6	0.4

6/20/02 and 6/21/02 60 mM Hepes, pH 7.3, 120 mM KCl, 0.1 mM EDTA, 0.1 mM EGTA, 10 mM MgCl₂, 2 mM ATP, 8 μg/mL BSA, 2 mM DTT

1/16/03 and 2/28/03 50 mM Hepes, pH 8.2, 50 mM KCl, 20 mM MgCl₂, 2 mM ATP, 40 μg/mL BSA, 2 mM DTT

6/14/03 (ii) 25 mM Hepes, pH 7.5, 50 mM KCl, 20 mM MgCl₂, 2 mM ATP, 40 μg/mL BSA, 2 mM DTT

2 preps of P39A

P35/39A EtsΔ138

[P35/39A], μM	$k_{\text{obs}}, \text{s}^{-1}$			
	6/20/02	6/20/02	1/20/03	1/29/03
200	2.5	2.2	2.1	1.9
100	2.1	1.5	2.0	1.6
50	1.4	1.3	1.7	1.1
25	1.1	1.1	1.1	0.8
12.5	1.0	0.5	0.8	0.5
6.3	0.4		0.7	0.3

6/20/02 (ii) 60 mM Hepes, pH 7.3, 120 mM KCl, 0.1 mM EDTA, 0.1 mM EGTA, 10 mM MgCl₂, 2 mM ATP, 8 μg/mL BSA, 2 mM DTT

1/20/03 (ii) 50 mM Hepes, pH 8.2, 50 mM KCl, 20 mM MgCl₂, 2 mM ATP, 40 μg/mL BSA, 2 mM DTT

P39V and P39G EtsΔ138: initial rate data with 200 μM EtsΔ138

P39R EtsΔ138

[P39R], μM	$k_{\text{obs}}, \text{s}^{-1}$		
	1/8/04	12/11/03	12/11/03
200	0.098		0.081
150	0.094	0.116	0.072
100	0.081	0.093	0.064
75	0.074	0.090	0.063
50	0.058	0.085	0.050
25	0.047 0.040	0.042	0.034
12.5		0.031	

1/8/04, 12/11/03 (ii), 100 nM ERK2, 25 mM Hepes, pH 7.5, 50 mM KCl, 0.1 mM EDTA, 0.1 mM EGTA, 20 mM MgCl₂, 2 mM ATP, 40 μg/mL BSA, 2 mM DTT

P39K EtsΔ138

[P39K], μM	k_{obs}, S^{-1}	
	1/8/04	1/10/04
200	0.060	0.041
150	0.055	0.043
100	0.042	0.038
75	0.041	0.032
50	0.032	0.027
25	0.024 0.023	0.018

1/8/04, 1/10/04, 200 nM ERK2, 25 mM Hepes, pH 7.5, 50 mM KCl, 0.1 mM EDTA, 0.1 mM EGTA, 20 mM MgCl₂, 2 mM ATP, 40 μg/mL BSA, 2 mM DTT

P39D EtsΔ138

[P39D], μM	k_{obs}, S^{-1}				
	12/13/03	1/8/04	1/10/04	1/14/04	1/14/04
200	0.031	0.038	0.039	0.039	0.041
150	0.027	0.035	0.040	0.040	0.038
100	0.023	0.031	0.035	0.033	0.033
75	0.021	0.030	0.031	0.029	0.027
50	0.016	0.022	0.028	0.025	0.023
25	0.011	0.017 0.017	0.023	0.016	0.014

12/13/03, 1/8/04, 1/10/04, 1/14/04 (ii), 200 nM ERK2, 25 mM Hepes, pH 7.5, 50 mM KCl, 0.1 mM EDTA, 0.1 mM EGTA, 20 mM MgCl₂, 2 mM ATP, 40 μg/mL BSA, 2 mM DTT

P39E EtsΔ138

[P39E], μM	$k_{\text{obs}}, \text{s}^{-1}$	
	1/8/04	1/10/04
200	0.036	0.036
150	0.034	0.031
100	0.028	0.027
75	0.026	0.023
50	0.020	0.016
25	0.013	0.009
	0.016	

1/8/04, 1/10/04, 200 nM ERK2, 25 mM Hepes, pH 7.5, 50 mM KCl, 0.1 mM EDTA, 0.1 mM EGTA, 20 mM MgCl_2 , 2 mM ATP, 40 $\mu\text{g/mL}$ BSA, 2 mM DTT

Table 12

Dual-phosphate ERK2, 20 mM MgCl₂

[ERK2], μM	<r>	
	2/25/04	2/26/04
0	0.105	0.108
2.4	0.113	0.114
4.8	0.118	0.119
9.6	0.128	0.128
14.3	0.134	0.136
19.1	0.141	0.142

[ERK2], μM	<r>
	5/15/04
0	0.106
3.2	0.116
6.4	0.121
9.55	0.129
12.7	0.133
15.9	0.139
19.1	0.142

Dual-phosphate ERK2, 20 mM MgCl₂, 2 mM AMP-PNP

[ERK2], μM	<r>		
	3/6/04	7/21/04	7/21/04
0	0.106	0.108	0.108
3.2	0.122	0.122	0.123
6.4	0.131	0.132	0.127
9.55	0.136	0.137	0.139
12.7	0.142	0.145	0.142
15.9	0.146	0.148	0.148
19.1	0.151	0.155	0.152

Dual-phosphate ERK2, 2 mM MgCl₂

[ERK2], μM	<r>
	5/17/04
0	0.113
1.6	0.136
3.2	0.150
6.4	0.164
9.55	0.176
12.7	0.179
15.9	0.186
19.1	0.188

Dual-phosphate ERK2, 4 mM MgCl₂, 2 mM AMP-PNP, 2 mM free Mg²⁺

[ERK2], μM	<r>
	5/17/04
0	0.111
1.6	0.127
3.2	0.135
6.4	0.149
9.55	0.154
12.7	0.163
15.9	0.167
19.1	0.173

Dual-phosphate ERK2, 2 mM MgCl₂, 1 mM AMP-PNP, 1 mM free Mg²⁺

[ERK2], μ M	<r>
	4/23/04
0	0.109
0.96	0.122
1.9	0.126
2.4	0.131
4.8	0.141
7.2	0.149
9.6	0.154
19.1	0.168

Dual-phosphate ERK2, 0 mM MgCl₂

[ERK2], μ M	<r>	<r>
	2/26/04	1/26/04
0	0.110	0.110
0.96	0.123	
1.91	0.133	
2.4	0.141	0.140
4.8	0.154	0.154
7.2	0.163	0.164
9.6	0.170	0.170
14.3		0.179
19.1	0.183	0.183

Dual-phosphate ERK2, 20 mM MgCl₂, 2 mM ADP

[ERK2], μ M	<r>	
	6/16/04	6/16/04
0	0.110	0.109
1.6	0.123	0.125
3.2	0.129	0.131
6.4	0.140	0.142
9.6	0.146	0.144
12.7	0.153	0.152
15.9	0.160	0.155
19.1	0.166	0.162

Unphosphorylated ERK2, 20 mM MgCl₂

[ERK2], μM	<r>
	2/4/04
0	0.107
1.8	0.122
3.5	0.134
5.3	0.146
7	0.153
8.8	0.159
10.5	0.164
12.3	0.170
14	0.174
15.8	0.178
17.5	0.180

Unphosphorylated ERK2, 20 mM MgCl₂, 2 mM AMP-PNP

[ERK2], μM	<r>	
	4/27/04	5/15/04
0	0.106	0.108
0.45	0.113	
0.9	0.119	
1.3	0.125	
1.8	0.124	0.137
3.5	0.146	0.155
5.3	0.158	0.171
7	0.164	0.182
8.8	0.178	0.191
8.8	0.186	
10.5		0.195
12.3	0.201	0.200
14		0.204
15.8		0.209
17.5	0.207	0.213

4/27/04, data fit to $r_b \sim 0.254$ as the original r_b fit had a lot of error

Unphosphorylated ERK2, 2 mM MgCl₂

[ERK2], μM	<r>
	5/17/04
0	0.111
1	0.153
2	0.175
3	0.192
5	0.207
7	0.219
9	0.223

Unphosphorylated ERK2, 4 mM MgCl₂, 2 mM AMP-PNP, 2 mM Free Mg²⁺

[ERK2], μM	<r>
	5/17/04
0	0.111
1	0.153
2	0.175
3	0.192
5	0.207
7	0.219
9	0.223

Unphosphorylated ERK2, 1 mM MgCl₂

[ERK2], μM	<r>
	4/16/04
0	0.112
0.45	0.132
0.9	0.150
1.3	0.164
1.8	0.171
3.5	0.201
5.3	0.211
7	0.219
8.8	0.225

Unphosphorylated ERK2, 2 mM MgCl₂, 1 mM AMP-PNP, 1 mM Free Mg²⁺

[ERK2], μM	<r>
	4/23/04
0	0.109
0.45	0.124
0.9	0.138
1.3	0.149
1.8	0.157
3.6	0.177
5.3	0.187
7	0.193
8.8	0.199

Unphosphorylated (inactive) ERK2, 0 mM MgCl₂, data in Chapter 4

Table 13

T38A/P39A, Competition Fluorescence Anisotropy, Dual-phosphate ERK2, 9.55 μ M, 20 mM MgCl₂, K_d fit to 17.2 μ M

[T38A/P39A], μM	<r>	
	3/2/04	3/2/04
0	0.1290	0.1289
0	0.1281	
0	0.1277	
3.125	0.1277	
6.25	0.1279	0.1278
12.5	0.1265	0.1268
25	0.1242	0.1248
50	0.1214	0.1217
100	0.1190	0.1191
150	0.1172	0.1179
200	0.1165	0.1157
200	0.1169	

EtsΔ138, Competition Fluorescence Anisotropy, Dual-phosphate ERK2, 9.55 μ M, 20 mM MgCl₂, K_d fit to 17.2 μ M

[EtsΔ138], μM	<r>	
	3/2/04	3/2/04
0	0.1269	0.1269
6.25	0.1273	0.1276
6.25	0.1256	0.1242
12.5	0.1237	0.1244
25	0.1203	0.1216
50	0.1176	0.1203
100	0.1156	0.1162
150	0.1158	0.1156
200		0.1141

T38A/P39A, Competition Fluorescence Anisotropy, Dual-phosphate ERK2, 9.55 μ M, 20 mM MgCl₂, 2 mM ADP, K_d fit to 5.9 μ M

[T38A/P39A], μM	<r>
	6/16/04
0	0.1450
6.25	0.1426
12.5	0.1442
25	0.1394
50	0.1377
100	0.1311

Ets Δ 138, Competition Fluorescence Anisotropy, Dual-phosphate ERK2, 9.55 μ M, 20 mM MgCl₂, 2 mM ADP, K_d fit to 5.9 μ M

[EtsΔ138], μM	<r>
	6/16/04
0	0.1450
6.25	0.1435
12.5	0.1400
25	0.1365
50	0.1284
100	0.1222
200	0.1169

T38A/P39A, Competition Fluorescence Anisotropy, Dual-phosphate ERK2, 9.55 μ M, 20 mM MgCl₂, 2 mM AMP-PNP, K_d fit to 8.8 μ M

[T38A/P39A], μM	<r>
	7/21/04
0	0.1376
12.5	0.1345
25	0.1304
50	0.1265
100	0.1233
150	0.1206
200	0.1198

Ets Δ 138, Competition Fluorescence Anisotropy, Dual-phosphate ERK2, 9.55 μ M, 20 mM MgCl₂, 2 mM AMP-PNP, K_d fit to 8.8 μ M

[EtsΔ138], μM	<r>
	7/21/04
0	0.1376
12.5	0.1319
25	0.1288
50	0.1247
100	0.1190
150	0.1160
200	0.1153

ERK1 peptide (TGPLSPGPF), Competition Fluorescence Anisotropy, Dual-phosphate ERK2, 9.55 μ M, K_d fit to 2.7 μ M, r_f fit to 0.11

[peptide], μM	<r>	
0	0.166	0.166
80	0.164	0.164
160	0.167	0.166
320	0.163	0.162
640	0.164	0.164
3200	0.155	0.154

$r_b = 0.197 \pm 0.001$, $K_d = 4.7 \pm 0.2$ mM

BIBLIOGRAPHY

1. Marshall, C.J., *Specificity of receptor tyrosine kinase signaling: transient versus sustained extracellular signal-regulated kinase activation. Cell*, 1995. **80**(2): p. 179-85.
2. Lewis, T.S., P.S. Shapiro, and N.G. Ahn, *Signal transduction through MAP kinase cascades. Adv Cancer Res*, 1998. **74**: p. 49-139.
3. Chen, Z., et al., *MAP kinases. Chem Rev*, 2001. **101**(8): p. 2449-76.
4. Canagarajah, B.J., et al., *Activation mechanism of the MAP kinase ERK2 by dual phosphorylation. Cell*, 1997. **90**(5): p. 859-69.
5. Prowse, C.N. and J. Lew, *Mechanism of Activation of ERK2 by Dual Phosphorylation. J. Biol. Chem.*, 2001. **276**(1): p. 99-103.
6. Waas, W.F. and K.N. Dalby, *Physiological concentrations of divalent magnesium ion activate the serine/threonine specific protein kinase ERK2. Biochemistry*, 2003. **42**(10): p. 2960-70.
7. Waas, W.F. and K.N. Dalby, *Transient protein-protein interactions and a random-ordered kinetic mechanism for the phosphorylation of a transcription factor by extracellular-regulated protein kinase 2. J Biol Chem*, 2002. **277**(15): p. 12532-40.
8. Songyang, Z., et al., *Use of an oriented peptide library to determine the optimal substrates of protein kinases. Curr Biol*, 1994. **4**(11): p. 973-82.
9. Gonzalez, F.A., D.L. Raden, and R.J. Davis, *Identification of substrate recognition determinants for human ERK1 and ERK2 protein kinases. J Biol Chem*, 1991. **266**(33): p. 22159-63.
10. Caffrey, D.R., L.A. O'Neill, and D.C. Shields, *A method to predict residues conferring functional differences between related proteins: application to MAP kinase pathways. Protein Sci*, 2000. **9**(4): p. 655-70.
11. Tanoue, T., et al., *Identification of a docking groove on ERK and p38 MAP kinases that regulates the specificity of docking interactions. Embo J*, 2001. **20**(3): p. 466-79.
12. Robinson, F.L., et al., *Identification of Novel Point Mutations in ERK2 That Selectively Disrupt Binding to MEK1. J. Biol. Chem.*, 2002. **277**(17): p. 14844-14852.
13. Chou, F.L., et al., *PEA-15 binding to ERK1/2 MAPKs is required for its modulation of integrin activation. J Biol Chem*, 2003. **278**(52): p. 52587-97.
14. Zhang, J., et al., *A bipartite mechanism for ERK2 recognition by its cognate regulators and substrates. J Biol Chem*, 2003.
15. Brunner, D., et al., *A gain-of-function mutation in Drosophila MAP kinase activates multiple receptor tyrosine kinase signaling pathways. Cell*, 1994. **76**(5): p. 875-88.

16. Bott, C.M., S.G. Thorneycroft, and C.J. Marshall, *The sevenmaker gain-of-function mutation in p42 MAP kinase leads to enhanced signalling and reduced sensitivity to dual specificity phosphatase action. FEBS Lett*, 1994. **352**(2): p. 201-5.
17. Tanoue, T., et al., *A conserved docking motif in MAP kinases common to substrates, activators and regulators. Nat Cell Biol*, 2000. **2**(2): p. 110-6.
18. Jacobs, D., et al., *Gain-of-Function Mutations in the Caenorhabditis elegans lin-1 ETS Gene Identify a C-Terminal Regulatory Domain Phosphorylated by ERK MAP Kinase. Genetics*, 1998. **149**(4): p. 1809-1822.
19. Jacobs, D., et al., *Multiple docking sites on substrate proteins form a modular system that mediates recognition by ERK MAP kinase. Genes Dev.*, 1999. **13**(2): p. 163-175.
20. Fields, S. and O. Song, *A novel genetic system to detect protein-protein interactions. Nature*, 1989. **340**(6230): p. 245-6.
21. Choi, K.Y., et al., *Ste5 tethers multiple protein kinases in the MAP kinase cascade required for mating in S. cerevisiae. Cell*, 1994. **78**(3): p. 499-512.
22. Zanke, B.W., et al., *Mammalian mitogen-activated protein kinase pathways are regulated through formation of specific kinase-activator complexes. J Biol Chem*, 1996. **271**(47): p. 29876-81.
23. Purcell, N.H., et al., *Extracellular signal-regulated kinase 2 interacts with and is negatively regulated by the LIM-only protein FHL2 in cardiomyocytes. Mol Cell Biol*, 2004. **24**(3): p. 1081-95.
24. Zhang, S., et al., *A new ERK2 binding protein, Naf1, attenuates the EGF/ERK2 nuclear signaling. Biochem Biophys Res Commun*, 2002. **297**(1): p. 17-23.
25. McDonald, P.H., et al., *Beta-arrestin 2: a receptor-regulated MAPK scaffold for the activation of JNK3. Science*, 2000. **290**(5496): p. 1574-7.
26. Slack, D.N., et al., *Distinct binding determinants for ERK2/p38alpha and JNK map kinases mediate catalytic activation and substrate selectivity of map kinase phosphatase-1. J Biol Chem*, 2001. **276**(19): p. 16491-500.
27. Chang, C.I., et al., *Crystal structures of MAP kinase p38 complexed to the docking sites on its nuclear substrate MEF2A and activator MKK3b. Mol Cell*, 2002. **9**(6): p. 1241-9.
28. Lee, T., et al., *Docking motif interactions in MAP kinases revealed by hydrogen exchange mass spectrometry. Mol Cell*, 2004. **14**(1): p. 43-55.
29. Yang, S.-H., et al., *The Elk-1 ETS-Domain Transcription Factor Contains a Mitogen-Activated Protein Kinase Targeting Motif. Mol. Cell. Biol.*, 1998. **18**(2): p. 710-720.
30. Hoofnagle, A.N., et al., *Changes in protein conformational mobility upon activation of extracellular regulated protein kinase-2 as detected by hydrogen exchange. Proc Natl Acad Sci U S A*, 2001. **98**(3): p. 956-61.
31. Hill, J.M., et al., *Recognition of ERK MAP kinase by PEA-15 reveals a common docking site within the death domain and death effector domain. Embo J*, 2002. **21**(23): p. 6494-504.

32. Farooq, A., et al., Solution structure of ERK2 binding domain of MAPK phosphatase MKP-3: structural insights into MKP-3 activation by ERK2. *Mol Cell*, 2001. 7(2): p. 387-99.
33. Camps, M., et al., Catalytic Activation of the Phosphatase MKP-3 by ERK2 Mitogen-Activated Protein Kinase. *Science*, 1998. 280(5367): p. 1262-1265.
34. Silverman, J.A. and P.B. Harbury, Rapid mapping of protein structure, interactions, and ligand binding by misincorporation proton-alkyl exchange. *J Biol Chem*, 2002. 277(34): p. 30968-75.
35. Zhou, B., et al., Multiple regions of MAP kinase phosphatase 3 are involved in its recognition and activation by ERK2. *J Biol Chem*, 2001. 276(9): p. 6506-15.
36. Fox, T., et al., A single amino acid substitution makes ERK2 susceptible to pyridinyl imidazole inhibitors of p38 MAP kinase. *Protein Sci*, 1998. 7(11): p. 2249-55.
37. Young, P.R., et al., Pyridinyl imidazole inhibitors of p38 mitogen-activated protein kinase bind in the ATP site. *J Biol Chem*, 1997. 272(18): p. 12116-21.
38. Barr, R.K., T.S. Kendrick, and M.A. Bogoyevitch, Identification of the critical features of a small peptide inhibitor of JNK activity. *J Biol Chem*, 2002. 277(13): p. 10987-97.
39. LoGrasso, P.V., et al., Kinetic mechanism for p38 MAP kinase. *Biochemistry*, 1997. 36(34): p. 10422-7.
40. Kelemen, B.R., K. Hsiao, and S.A. Goueli, Selective in vivo inhibition of mitogen-activated protein kinase activation using cell-permeable peptides. *J Biol Chem*, 2002. 277(10): p. 8741-8.
41. Fowler, A., et al., An evaluation of fluorescence polarization and lifetime discriminated polarization for high throughput screening of serine/threonine kinases. *Anal Biochem*, 2002. 308(2): p. 223-31.
42. Waas, W.F. and K.N. Dalby, Purification of a model substrate for transcription factor phosphorylation by ERK2. *Protein Expr Purif*, 2001. 23(1): p. 191-7.
43. Chen, G., et al., Kinetic mechanism of the p38- α MAP kinase: phosphoryl transfer to synthetic peptides. *Biochemistry*, 2000. 39(8): p. 2079-87.
44. Waas, W.F., et al., Two rate-limiting steps in the kinetic mechanism of the serine/threonine specific protein kinase ERK2: a case of fast phosphorylation followed by fast product release. *Biochemistry*, 2003. 42(42): p. 12273-86.
45. Kallunki, T., et al., JNK2 contains a specificity-determining region responsible for efficient c-Jun binding and phosphorylation. *Genes Dev*, 1994. 8(24): p. 2996-3007.
46. Knighton, D.R., et al., Structure of a peptide inhibitor bound to the catalytic subunit of cyclic adenosine monophosphate-dependent protein kinase. *Science*, 1991. 253(5018): p. 414-20.
47. Rubinfeld, H., T. Hanoch, and R. Seger, Identification of a cytoplasmic-retention sequence in ERK2. *J Biol Chem*, 1999. 274(43): p. 30349-52.
48. Xu, B., et al., Hydrophobic as well as charged residues in both MEK1 and ERK2 are important for their proper docking. *J Biol Chem*, 2001. 276(28): p. 26509-15.

49. Gum, R.J. and P.R. Young, Identification of two distinct regions of p38 MAPK required for substrate binding and phosphorylation. *Biochem Biophys Res Commun*, 1999. **266**(1): p. 284-9.
50. Dai, T., et al., Stress-activated protein kinases bind directly to the delta domain of c-Jun in resting cells: implications for repression of c-Jun function. *Oncogene*, 1995. **10**(5): p. 849-55.
51. Kallunki, T., et al., c-Jun can recruit JNK to phosphorylate dimerization partners via specific docking interactions. *Cell*, 1996. **87**(5): p. 929-39.
52. Seidel, J.J. and B.J. Graves, An ERK2 docking site in the Pointed domain distinguishes a subset of ETS transcription factors. *Genes Dev.*, 2002. **16**(1): p. 127-137.
53. Pulido, R., A. Zuniga, and A. Ullrich, PTP-SL and STEP protein tyrosine phosphatases regulate the activation of the extracellular signal-regulated kinases ERK1 and ERK2 by association through a kinase interaction motif. *Embo J*, 1998. **17**(24): p. 7337-50.
54. Bardwell, A.J., M. Abdollahi, and L. Bardwell, Docking sites on mitogen-activated protein kinase (MAPK) kinases, MAPK phosphatases and the Elk-1 transcription factor compete for MAPK binding and are crucial for enzymic activity. *Biochem J*, 2003. **370**(Pt 3): p. 1077-85.
55. Smith, J.A., et al., Identification of an extracellular signal-regulated kinase (ERK) docking site in ribosomal S6 kinase, a sequence critical for activation by ERK in vivo. *J Biol Chem*, 1999. **274**(5): p. 2893-8.
56. Gavin, A.C. and A.R. Nebreda, A MAP kinase docking site is required for phosphorylation and activation of p90(rsk)/MAPKAP kinase-1. *Curr Biol*, 1999. **9**(5): p. 281-4.
57. Roux, P.P., S.A. Richards, and J. Blenis, Phosphorylation of p90 Ribosomal S6 Kinase (RSK) Regulates Extracellular Signal-Regulated Kinase Docking and RSK Activity. *Mol. Cell. Biol.*, 2003. **23**(14): p. 4796-4804.
58. Smith, J.A., et al., Creation of a stress-activated p90 ribosomal S6 kinase. The carboxyl-terminal tail of the MAPK-activated protein kinases dictates the signal transduction pathway in which they function. *J Biol Chem*, 2000. **275**(41): p. 31588-93.
59. Zhan, X.L. and K.L. Guan, A specific protein-protein interaction accounts for the in vivo substrate selectivity of Ptp3 towards the Fus3 MAP kinase. *Genes Dev*, 1999. **13**(21): p. 2811-27.
60. Xu, B., et al., The N-terminal ERK-binding site of MEK1 is required for efficient feedback phosphorylation by ERK2 in vitro and ERK activation in vivo. *J Biol Chem*, 1999. **274**(48): p. 34029-35.
61. Sharrocks, A.D., S.H. Yang, and A. Galanis, Docking domains and substrate-specificity determination for MAP kinases. *Trends Biochem Sci*, 2000. **25**(9): p. 448-53.
62. Ouwens, D.M., et al., Growth factors can activate ATF2 via a two-step mechanism: phosphorylation of Thr71 through the Ras-MEK-ERK pathway and of Thr69 through RalGDS-Src-p38. *EMBO J.*, 2002. **21**(14): p. 3782-3793.

63. Hibi, M., et al., Identification of an oncoprotein- and UV-responsive protein kinase that binds and potentiates the c-Jun activation domain. *Genes Dev*, 1993. **7**(11): p. 2135-48.
64. Waskiewicz, A.J., et al., Mitogen-activated protein kinases activate the serine/threonine kinases Mnk1 and Mnk2. *EMBO J.*, 1997. **16**(8): p. 1909-1920.
65. Hsiao, K.M., et al., Evidence that inactive p42 mitogen-activated protein kinase and inactive Rsk exist as a heterodimer in vivo. *Proc Natl Acad Sci U S A*, 1994. **91**(12): p. 5480-4.
66. Fukuda, M., Y. Gotoh, and E. Nishida, Interaction of MAP kinase with MAP kinase kinase: its possible role in the control of nucleocytoplasmic transport of MAP kinase. *Embo J*, 1997. **16**(8): p. 1901-8.
67. Blanco-Aparicio, C., J. Torres, and R. Pulido, A novel regulatory mechanism of MAP kinases activation and nuclear translocation mediated by PKA and the PTP-SL tyrosine phosphatase. *J Cell Biol*, 1999. **147**(6): p. 1129-36.
68. Garcia, J., et al., IEX-1: a new ERK substrate involved in both ERK survival activity and ERK activation. *Embo J*, 2002. **21**(19): p. 5151-63.
69. Duesbery, N.S., et al., Proteolytic inactivation of MAP-kinase-kinase by anthrax lethal factor. *Science*, 1998. **280**(5364): p. 734-7.
70. Zhang, F., et al., Atomic structure of the MAP kinase ERK2 at 2.3 Å resolution. *Nature*, 1994. **367**(6465): p. 704-11.
71. Weiwad, M., et al., Evidence that the substrate backbone conformation is critical to phosphorylation by p42 MAP kinase. *FEBS Lett*, 2000. **478**(1-2): p. 39-42.
72. Bardwell, L., et al., Signaling in the yeast pheromone response pathway: specific and high- affinity interaction of the mitogen-activated protein (MAP) kinases Kss1 and Fus3 with the upstream MAP kinase kinase Ste7. *Mol. Cell. Biol.*, 1996. **16**(7): p. 3637-3650.
73. Bardwell, A.J., et al., A conserved docking site in MEKs mediates high-affinity binding to MAP kinases and cooperates with a scaffold protein to enhance signal transmission. *J Biol Chem*, 2001. **276**(13): p. 10374-86.
74. Camps, M., A. Nichols, and S. Arkinstall, Dual specificity phosphatases: a gene family for control of MAP kinase function. *Faseb J*, 2000. **14**(1): p. 6-16.
75. Formstecher, E., et al., PEA-15 mediates cytoplasmic sequestration of ERK MAP kinase. *Dev Cell*, 2001. **1**(2): p. 239-50.
76. Smith GP, S.J., Libraries of peptides and proteins displayed on filamentous phage. *Methods Enzymol*, 1993. **217**: p. 228-57.
77. Cobb, M.H., et al., The mitogen-activated protein kinases, ERK1 and ERK2. *Semin Cancer Biol*, 1994. **5**(4): p. 261-8.
78. de Azevedo, W.F., Jr., et al., Structural basis for specificity and potency of a flavonoid inhibitor of human CDK2, a cell cycle kinase. *PNAS*, 1996. **93**(7): p. 2735-2740.
79. Engh, R.A., et al., Crystal structures of catalytic subunit of cAMP-dependent protein kinase in complex with isoquinolinesulfonyl protein kinase inhibitors H7, H8, and H89. Structural implications for selectivity. *J Biol Chem*, 1996. **271**(42): p. 26157-64.

80. Xu, R.-M., et al., *Structural basis for selectivity of the isoquinoline sulfonamide family of protein kinase inhibitors*. PNAS, 1996. **93**(13): p. 6308-6313.
81. Tong, L., et al., *A highly specific inhibitor of human p38 MAP kinase binds in the ATP pocket*. Nat Struct Biol, 1997. **4**(4): p. 311-6.
82. Wilson, K.P., et al., *The structural basis for the specificity of pyridinylimidazole inhibitors of p38 MAP kinase*. Chem Biol, 1997. **4**(6): p. 423-31.
83. Davies, S.P., et al., *Specificity and mechanism of action of some commonly used protein kinase inhibitors*. Biochem J, 2000. **351**(Pt 1): p. 95-105.
84. Traut, T.W., *Physiological concentrations of purines and pyrimidines*. Mol Cell Biochem, 1994. **140**(1): p. 1-22.
85. Parang, K., et al., *Mechanism-based design of a protein kinase inhibitor*. Nat Struct Biol, 2001. **8**(1): p. 37-41.
86. Schulman, B.A., D.L. Lindstrom, and E. Harlow, *Substrate recruitment to cyclin-dependent kinase 2 by a multipurpose docking site on cyclin A*. Proc Natl Acad Sci U S A, 1998. **95**(18): p. 10453-8.
87. Takeda, D.Y., J.A. Wohlschlegel, and A. Dutta, *A Bipartite Substrate Recognition Motif for Cyclin-dependent Kinases*. J. Biol. Chem., 2001. **276**(3): p. 1993-1997.
88. Lowman HB, B.S., Simpson N, Wells JA, *Selecting high-affinity binding proteins by monovalent phage display*. Biochemistry, 1991. **30**(45): p. 10832-8.
89. Koivunen E, G.D., Ruoslahti E, *Selection of peptides binding to the alpha 5 beta 1 integrin from phage display library*. J Biol Chem, 1993. **268**(27): p. 20205-10.
90. Giebel LB, C.R., Milligan DL, Young DC, Arze R, Johnson CR, *Screening of cyclic peptide phage libraries identifies ligands that bind streptavidin with high affinities*. Biochemistry, 1995. **34**(47): p. 15430-5.
91. Fernandez, A. and H.A. Scheraga, *Insufficiently dehydrated hydrogen bonds as determinants of protein interactions*. Proc Natl Acad Sci U S A, 2003. **100**(1): p. 113-8.
92. Scott JK, S.G., *Searching for peptide ligands with an epitope library*. Science, 1990. **249**(4967): p. 386-90.
93. Zwick, M.B., et al., *The maltose-binding protein as a scaffold for monovalent display of peptides derived from phage libraries*. Anal Biochem, 1998. **264**(1): p. 87-97.
94. Khokhlatchev, A., et al., *Reconstitution of Mitogen-activated Protein Kinase Phosphorylation Cascades in Bacteria*. EFFICIENT SYNTHESIS OF ACTIVE PROTEIN KINASES. J. Biol. Chem., 1997. **272**(17): p. 11057-11062.
95. Robinson MJ, H.P., Zhang J, Baer R, Haycock JW, Cobb MH, Goldsmith EJ, *Mutation of position 52 in ERK2 creates a nonproductive binding mode for adenosine 5'-triphosphate*. Biochemistry, 1996. **35**(18): p. 5641-6.
96. Wang B, Y.H., Liu YC, Jelinek T, Zhang L, Ruoslahti E, Fu H, *Isolation of high-affinity peptide antagonists of 14-3-3 proteins by phage display*. Biochemistry, 1999. **38**(38): p. 12499-504.
97. Luzzago A, F.F., Tramontano A, Pessi A, Cortese R, *Mimicking of discontinuous epitopes by phage-displayed peptides, I. Epitope mapping of human H ferritin using a phage library of constrained peptides*. Gene, 1993. **128**(1): p. 51-7.

98. McLafferty MA, K.R., Ladner RC, Markland W, M13 bacteriophage displaying disulfide-constrained microproteins. *Gene*, 1993. **128**(1): p. 29-36.
99. Sidhu, S.S., et al., Phage display for selection of novel binding peptides. *Methods Enzymol*, 2000. **328**: p. 333-63.
100. Barrett RW, C.S., Ackerman MS, Olson AM, Peters EA, Dower WJ, Selective enrichment and characterization of high affinity ligands from collections of random peptides on filamentous phage. *Anal Biochem*, 1992. **204**(2): p. 357-64.
101. Engvall, E. and P. Perlman, Enzyme-linked immunosorbent assay (ELISA). Quantitative assay of immunoglobulin G. *Immunochemistry*, 1971. **8**(9): p. 871-4.
102. Khokhlatchev, A.V., et al., Phosphorylation of the MAP kinase ERK2 promotes its homodimerization and nuclear translocation. *Cell*, 1998. **93**(4): p. 605-15.
103. Waas, W.F., H.H. Lo, and K.N. Dalby, The kinetic mechanism of the dual phosphorylation of the ATF2 transcription factor by p38 mitogen-activated protein (MAP) kinase alpha. Implications for signal/response profiles of MAP kinase pathways. *J Biol Chem*, 2001. **276**(8): p. 5676-84.
104. Tartof, K.D. and C.A. Hobbs, Improved media for growing plasmid and cosmid clones. *Bethesda Res. Lab. Focus*, 1987. **9**(12).
105. Annis I, H.B., Barany G, Disulfide bond formation in peptides. *Methods Enzymol*, 1997. **289**: p. 198-221.
106. Gill, S.C.v.H., P H, Calculation of protein extinction coefficients from amino acid sequence data. *Analytical Biochemistry*, 1989. **182**(2): p. 319-326.
107. Bradford, M.M., A rapid and sensitive method for the quantitation of microgram quantities of protein utilizing the principle of protein-dye binding. *Anal Biochem*, 1976. **72**: p. 248-54.
108. Sefton, B.M. and T. Hunter, Protein Phosphorylation. 1998.
109. Chu, Y., et al., The mitogen-activated protein kinase phosphatases PAC1, MKP-1, and MKP-2 have unique substrate specificities and reduced activity in vivo toward the ERK2 sevenmaker mutation. *J Biol Chem*, 1996. **271**(11): p. 6497-501.
110. Yung, Y., et al., Altered regulation of ERK1b by MEK1 and PTP-SL and modified Elk1 phosphorylation by ERK1b are caused by abrogation of the regulatory C-terminal sequence of ERKs. *J Biol Chem*, 2001. **276**(38): p. 35280-9.
111. Brill, J.A., E.A. Elion, and G.R. Fink, A role for autophosphorylation revealed by activated alleles of FUS3, the yeast MAP kinase homolog. *Mol Biol Cell*, 1994. **5**(3): p. 297-312.
112. Cook, P.F., et al., Adenosine cyclic 3',5'-monophosphate dependent protein kinase: kinetic mechanism for the bovine skeletal muscle catalytic subunit. *Biochemistry*, 1982. **21**(23): p. 5794-9.
113. Espanel, X., et al., Mapping of synergistic components of weakly interacting protein-protein motifs using arrays of paired peptides. *J Biol Chem*, 2003. **278**(17): p. 15162-7.
114. Slupsky, C.M., et al., Structure of the Ets-1 pointed domain and mitogen-activated protein kinase phosphorylation site. *PNAS*, 1998. **95**(21): p. 12129-12134.
115. Fantz, D.A., et al., Docking sites on substrate proteins direct extracellular signal-regulated kinase to phosphorylate specific residues. *J Biol Chem*, 2001. **276**(29): p. 27256-65.

116. Galanis, A., S.H. Yang, and A.D. Sharrocks, Selective targeting of MAPKs to the ETS domain transcription factor SAP-1. *J Biol Chem*, 2001. **276**(2): p. 965-73.
117. Murphy, L.O., et al., Molecular interpretation of ERK signal duration by immediate early gene products. *Nat Cell Biol*, 2002. **4**(8): p. 556-64.
118. MacKenzie, S.J., et al., ERK2 Mitogen-activated Protein Kinase Binding, Phosphorylation, and Regulation of the PDE4D cAMP-specific Phosphodiesterases. THE INVOLVEMENT OF COOH-TERMINAL DOCKING SITES AND NH2-TERMINAL UCR REGIONS. *J. Biol. Chem.*, 2000. **275**(22): p. 16609-16617.
119. Gill, S.C. and P.H. von Hippel, Calculation of protein extinction coefficients from amino acid sequence data. *Anal Biochem*, 1989. **182**(2): p. 319-26.
120. Chen, J.H., Cloning, sequencing, and expression of mouse c-ets-1 cDNA in baculovirus expression system. *Oncogene Res*, 1990. **5**(4): p. 277-85.
121. O'Neill, E.M., et al., The activities of two Ets-related transcription factors required for Drosophila eye development are modulated by the Ras/MAPK pathway. *Cell*, 1994. **78**(1): p. 137-47.
122. Yang, S.H., et al., Differential targeting of MAP kinases to the ETS-domain transcription factor Elk-1. *Embo J*, 1998. **17**(6): p. 1740-9.
123. Araujo, H., et al., Characterization of PEA-15, a major substrate for protein kinase C in astrocytes. *J Biol Chem*, 1993. **268**(8): p. 5911-20.
124. Ramos, J.W., et al., The death effector domain of PEA-15 is involved in its regulation of integrin activation. *J Biol Chem*, 1998. **273**(51): p. 33897-900.
125. Kubes, M., et al., Endothelin induces a calcium-dependent phosphorylation of PEA-15 in intact astrocytes: identification of Ser104 and Ser116 phosphorylated, respectively, by protein kinase C and calcium/calmodulin kinase II in vitro. *J Neurochem*, 1998. **71**(3): p. 1307-14.
126. Ohkuma, S. and B. Poole, Fluorescence probe measurement of the intralysosomal pH in living cells and the perturbation of pH by various agents. *Proc Natl Acad Sci U S A*, 1978. **75**(7): p. 3327-31.
127. Vinson, V.K., et al., Interactions of Acanthamoeba profilin with actin and nucleotides bound to actin. *Biochemistry*, 1998. **37**(31): p. 10871-80.
128. Manning, G., et al., The protein kinase complement of the human genome. *Science*, 2002. **298**(5600): p. 1912-34.
129. Kemp, B.E., et al., Substrate specificity of the cyclic AMP-dependent protein kinase. *Proc Natl Acad Sci U S A*, 1975. **72**(9): p. 3448-52.
130. Zetterqvist, O., et al., The minimum substrate of cyclic AMP-stimulated protein kinase, as studied by synthetic peptides representing the phosphorylatable site of pyruvate kinase (type L) of rat liver. *Biochem Biophys Res Commun*, 1976. **70**(3): p. 696-703.
131. Obata, T., et al., Peptide and protein library screening defines optimal substrate motifs for AKT/PKB. *J Biol Chem*, 2000. **275**(46): p. 36108-15.
132. Clark-Lewis, I., J.S. Sanghera, and S.L. Pelech, Definition of a consensus sequence for peptide substrate recognition by p44mpk, the meiosis-activated myelin basic protein kinase. *J Biol Chem*, 1991. **266**(23): p. 15180-4.

133. Songyang, Z., et al., *A structural basis for substrate specificities of protein Ser/Thr kinases: primary sequence preference of casein kinases I and II, NIMA, phosphorylase kinase, calmodulin-dependent kinase II, CDK5, and Erk1*. *Mol Cell Biol*, 1996. **16**(11): p. 6486-93.
134. Alvarez, E., et al., *Pro-Leu-Ser/Thr-Pro is a consensus primary sequence for substrate protein phosphorylation. Characterization of the phosphorylation of c-myc and c-jun proteins by an epidermal growth factor receptor threonine 669 protein kinase*. *J Biol Chem*, 1991. **266**(23): p. 15277-85.
135. Marin, O., et al., *The consensus sequences for cdc2 kinase and for casein kinase-2 are mutually incompatible. A study with peptides derived from the beta-subunit of casein kinase-2*. *FEBS Lett*, 1992. **301**(1): p. 111-4.
136. Marin, O., et al., *Site specificity of casein kinase-2 (TS) from rat liver cytosol. A study with model peptide substrates*. *Eur J Biochem*, 1986. **160**(2): p. 239-44.
137. Pinna, L.A. and M. Ruzzene, *How do protein kinases recognize their substrates?* *Biochim Biophys Acta*, 1996. **1314**(3): p. 191-225.
138. Hawkins, J., et al., *p38 map kinase substrate specificity differs greatly for protein and peptide substrates*. *Arch Biochem Biophys*, 2000. **382**(2): p. 310-3.
139. Bergstrom, R.C., et al., *Binding of nonphysiological protein and peptide substrates to proteases: differences between urokinase-type plasminogen activator and trypsin and contributions to the evolution of regulated proteolysis*. *Biochemistry*, 2003. **42**(18): p. 5395-402.
140. Rudolph, J., et al., *Specificity of natural and artificial substrates for human Cdc25A*. *Anal Biochem*, 2001. **289**(1): p. 43-51.
141. Boskovic, D.S. and S. Krishnaswamy, *Exosite binding tethers the macromolecular substrate to the prothrombinase complex and directs cleavage at two spatially distinct sites*. *J Biol Chem*, 2000. **275**(49): p. 38561-70.
142. Haycock, J.W., et al., *ERK1 and ERK2, two microtubule-associated protein 2 kinases, mediate the phosphorylation of tyrosine hydroxylase at serine-31 in situ*. *Proc Natl Acad Sci U S A*, 1992. **89**(6): p. 2365-9.
143. Brondello, J.M., J. Pouyssegur, and F.R. McKenzie, *Reduced MAP kinase phosphatase-1 degradation after p42/p44MAPK-dependent phosphorylation*. *Science*, 1999. **286**(5449): p. 2514-7.
144. Grubbs, R.D., *Intracellular magnesium and magnesium buffering*. *Biometals*, 2002. **15**(3): p. 251-9.
145. Waas, W.F., et al., *A kinetic approach towards understanding substrate interactions and the catalytic mechanism of the serine/threonine protein kinase ERK2: identifying a potential regulatory role for divalent magnesium*. *Biochim Biophys Acta*, 2004. **1697**(1-2): p. 81-7.
146. Walker, G.M. and J.H. Duffus, *Magnesium ions and the control of the cell cycle in yeast*. *J Cell Sci*, 1980. **42**: p. 329-56.
147. Yang, J., et al., *Crystal structure of an activated Akt/protein kinase B ternary complex with GSK3-peptide and AMP-PNP*. *Nat Struct Biol*, 2002. **9**(12): p. 940-4.
148. Xie, X., et al., *Crystal structure of JNK3: a kinase implicated in neuronal apoptosis*. *Structure*, 1998. **6**(8): p. 983-91.

149. Brown, N.R., et al., *The structural basis for specificity of substrate and recruitment peptides for cyclin-dependent kinases. Nat Cell Biol*, 1999. **1**(7): p. 438-43.

VITA

Mark Allan Rainey was born in Vancouver, Washington on February 19, 1975, the son of Norman Wayne Rainey and Donna Jean Rainey. After attending Mt. View High School in Vancouver, WA, he attended the University of Washington, Seattle in 1993 and received his Bachelors of Science degree in Cellular and Molecular Biology in 1997. In 1997 he began doing undergraduate research in the laboratory of Dr. Richard Palmiter at the University of Washington, Seattle. In 1998 he entered Graduate School at the University of Texas, Austin under the supervision of Kevin N. Dalby. His publications include:

Waas WF, Rainey MA, Szafranska AE, Cox K, Dalby KN (2004) A kinetic approach towards understanding substrate interactions and the catalytic mechanism of the serine/threonine protein kinase ERK2: identifying a potential regulatory role for divalent magnesium. *Biochem Biophys Acta* 1697: 81-7

Rainey MA, Linse KD, Dalby KN (2004) Phage display identifies novel peptides that bind extracellular-regulated protein kinase 2 to compete with transcription factor binding. *Journal of Physical Organic Chemistry* 17:1-11

Waas WF, Rainey MA, Szafranska AE, Dalby KN (2003) Two rate-limiting steps in the kinetic mechanism of the serine/threonine specific protein kinase ERK2: a case of fast phosphorylation followed by fast product release. *Biochemistry* 42:12273-86

Szczyпка MS, Rainey MA, Palmiter RD (2000) Dopamine is required for hyperphagia in Lep (ob/ob) mice. *Nat Genet* 25:102-4

Szczyпка MS, Rainey MA, Kim DS, Alaynick WA, Marck BT, Matsumoto AM, Palmiter RD (1999) Feeding behavior in dopamine-deficient mice. *Proc Natl Acad Sci USA* 96:12138-43

Permanent Address: 5505 Helen St. #106, Austin, TX, 78751

This dissertation was typed by the author.